Investigations of Combined Strategies to reverse P-glycoprotein- and BCRP-mediated Multidrug Resistance in Human Ovarian Cancer Cells and Xenograft Tumors

Dissertation

zur Erlangung des Doktorgrades (Dr. rer. nat.)

der Mathematisch-Naturwissenschaftlichen Fakultät

der Rheinischen Friedrich-Wilhelms-Universität Bonn

vorgelegt von

VERONIKA JEKERLE

aus Kassel

Bonn 2006

1. Referent: Prof. Dr. M. Wiese

2. Referent: Prof. Dr. M. Piquette-Miller

Tag der Promotion: 02 Juni 2006

Für meine Eltern

„Die Wissenschaft muss auf Magie verzichten

und trotzdem an Wunder glauben"

George Bernard Shaw (1856-1950)

A2780/Adr   Adriamycin (=doxorubicin) resistant human ovarian cancer cell line

A2780/wt   Wild-type human ovarian cancer cell line

ABC   ATP-binding cassette (transporter family)

ALT   Alanin Aminotransferase

AML   Acute Myeloid Leukemia

AS   Antisense

ATP   Adenosine triphosphate

AU   Arbitrary units

AUC   Area under the curve

BA   Bioavailability

Bcl-2   B-cell lymphoma-2

BCRP   Breast cancer resistance protein

bp   Base pair

BSA   Bovine serum albumine

BSO   Buthionine sulfoximine

Caco-2   Human colon cancer cell line

CCRF-CEM   Human lymphoma cell line

CD^- Hematopoetic stem cells

cDNA   Complementary DNA

5-CFDA   5-Carboxy fluorescein diacetate

CMV   Cytomegalo Virus

cpm   Counts per minute

CS   Chemosensitivity

CyA   Cyclosporin A

DAPI   4',6-Diamidino-2-phenylindole

DEPC   Diethyl pyrocarbonate

DMSO   Dimethyl sulfoxide

dNTP   Deoxyribonucleotide triphosphate

DNA   Desoxyribose Nucleic Acid

DNR   Daunorubicin

DOX   Doxorubicin

DTPA   Diethylene triamine pentaacetate

EC_{50} Effective concentration (50% reduction of the measured effect)

e.g.   Exempli gratia

ETP   Etoposide

FACS   Fluorescence assorted cell sorter

FCS   Fetale calf serum

FDA   Food and Drug Administration

FITC   Fluorescein isothiocyanate

GapDH   Glyzerinaldehyd-3-phosphat Dehydrogenase

GR   Gene ruler

GST   Glutathione S-transferase

H&E   Hematoxylin and Eosion

HeLa   Human cervix carcinoma cells

HepG2   Human hepatoma cell line

ID   Injected dose

IgG   Immunoglobulin G

Ind   Indomethacin

i.p.   intra peritoneally

i.v.   intra venously

ITLC   Instant Thin Layer Chromatography

kDA   Kilo Dalton

L   Intracellular loop

LRP   Lung resistance protein

MCF7/mx   Mitoxantrone resistant human breast cancer cell line

MCF7/wt   Wild-type human breast cancer cell line

MDCK   Madin-Darby Canine Kidney cell line

MDA435/LCC6^{MDR1} Selectively transfected human breast cancer cell

MDR   Multidrug resistance

MDR1   Multidrug resistance gene 1

MIBI ^{99m}Tc-Sestamibi

mRNA   Messenger RNA

MRP   Multidrug resistance associated protein

MSD   Membrane spanning domain

MTT   3-(4,5-Dimethylthiazol-2-yl)-2,5-diphenyltetrazoliumbromid

MITX   Mitoxantrone

NADH   Nicotinamid-Adenin Dinucleotid

NBF   Nucleotide binding fold

NCI   National Cancer Institute

Nvb   Novobiocin

ODNs   Oligodeoxynucleotides

p53   Tumor suppressor gene

PBS   Phosphate buffered saline

PCR   Polymerase chain reaction

Ph*   Photoaffinity labeling

Pgp   P-glycoprotein

PK   Pharmacokinetic

PTX   Paclitaxel

R*   Radiolabeled

RF   Resistance factor

RNA   Ribonucleic acid

RNAse H   Ribonuclease H

ROI   Regions of Interest

RT   Room temperature

RT-PCR   Reverse Transcription Polymerase Chain Reaction

s.c.   Sub cutaneously

SCLC   Small Cell Lung Cancer

SKOV 3   Human ovarian carcinoma cell line

S.D.   Standard deviation

S.F.   Sensitizing factor

siRNA   Short interfering RNA

^{99m}Tc   Metastable Technetium-99

TGH   Toronto General Hospital

TM   Transmembrane domain

TAX   Taxol

TOX   Toxicity

TPC   Topotecan

UHN   University Health Network

UV   Ultraviolette light

VCR   Vincristine

VNB   Vinblastine

Vrp   Verapamil

1   Introduction

1.1   Multidrug Resistance

Multidrug resistance (MDR) is a major obstacle in the chemotherapeutic treatment of cancer (Gottesman, 1993). An MDR tumor is characterized by the ability to simultaneously exhibit resistance towards a large number of structurally unrelated chemotherapeutic drugs. Consequently, chemotherapeutic agents fail to target the MDR tumor, thus the cancer becomes untreatable by chemotherapy. MDR can be either intrinsic (*de novo*) or acquired by exposure of malignant cells to chemotherapeutic agents (Fojo, 1987; Dalton, 1989).

In the clinical reality, MDR is a multifactoral and complex condition. Various cellular and non-cellular mechanisms are involved in clinical MDR (Fojo, 2003). Although the focus of this thesis is on transporter-mediated MDR phenotypes, other cellular mechanisms of MDR will be introduced. Cellular mechanisms can be further classified as non-classical and transporter-based MDR mechanisms.

1.1.1   Cellular MDR mechanisms

Cellular mechanisms of MDR arise in the tumor cell as a response to cytotoxic challenge. In the course of chemotherapeutic treatment, some tumors can adapt to a toxic environment by altering the expression of key genes, which help the tumor cell to escape the toxic effects of the chemotherapeutic drug.

1.1.1.1   Non-classical MDR mechanisms

The term, "non-classical MDR mechanisms", summarizes all non-transporter-based MDR mechanisms. These types of resistance include enzyme–mediated (e.g.

Glutathione-S-transferase, topoisomerase) and apoptosis-derived mechanisms (e.g. tumor suppressor gene p53).

Glutathione S-transferase enzyme system

The Glutathione S-transferase (GST) enzyme system is involved in the biotransformation of drugs and xenobiotics (Lewis, 1989). Furthermore, it protects cells from damage resulting from reactive epoxides (Kuzmich, 1991) and free radicals (Ketterer, 1990). In many resistant tumor cell lines, the GST system has been found to be overexpressed (Lewis, 1989). It is believed that the GST system, when expressed at a high level, can protect the cell from chemotherapeutic agents. For instance, when an isoform of GST gene was selectively transfected into yeast cells, an 8-fold increase in resistance towards the cytotoxic drug chlorambucil was obtained (Black, 1990). However, the GST resistance mechanism appears to be specific only for some chemotherapeutic drugs. There has been evidence that an induced GST activity is not a resistance mechanism for doxorubicin (Moscow, 1989).

Topoisomerase enzymes

Topoisomerase type I and II enzymes are involved in DNA replication processes. Topoisomerase I assists to alter DNA topology via single strand breaks, whereas Topoisomerase II causes transient double strand breaks of the DNA molecule. Some chemotherapeutic agents such as doxorubicin, etoposide or campothecin target topoisomerase enzymes by stabilizing the enzyme DNA complex and thus preventing the two DNA fragments from rejoining (Ross, 1984; Kunimoto, 1978). The resulting DNA strand breaks are thought to trigger apoptosis, which may lead to tumor death (Roy, 1992). Tumor cells can develop resistance mechanisms against topoisomerase inhibitors by either downregulating the expression of the topoisomerase enzymes or by gene mutations within the topoisomerase gene (Drake, 1987). Resistance against Topoisomerase II is often synchronized with the overexpression of P-glycoprotein (Kunikane, 1990).

Tumor suppressor gene p53

In cases of DNA damage, incurred by stress stimuli like irradiation or hypoxia, the tumor suppressor gene p53 mediates a growth suppressive response through the activation of pathways involved in cell cycle arrest, DNA repair, apoptosis and angiogenesis (El-Deiry, 2003). A loss of p53 function is often associated with the formation of aggressive tumors. Some anticancer drugs are active against tumor cells by inducing DNA damage and triggering apoptosis via p53. Therefore, downregulation or mutations of the p53 gene hinders chemotherapeutic agents from inducing apoptosis and protects the tumor cell against the treatment (Lowe, 1993a). Furthermore, p53 regulates the expression of a downstream gene, B-cell lymphoma-2 (bcl-2) (Lowe, 1993b). The anti-apoptotic protein bcl-2 inhibits the apoptosis pathway through a regulation of the mitochondrial pathway prior to caspase activation (Kaufmann, 2003). Bcl-2 is involved in the cellular protection from cell death stimuli including gamma radiation, UV and tumor necrosis factor (Reed, 1995). Increased expression levels of bcl-2 have been associated with cellular resistance towards a number of cytotoxic agents including doxorubicin, taxol and mitoxantrone.

1.1.1.2   Classical MDR mechanisms

The term "classical MDR mechanisms" refers to transporter-based resistance mechanisms and describes the generally accepted primary mechanism of drug resistance. The transporters involved in MDR mainly belong to the family of ATP-binding cassette (ABC) transporters. ABC transporters actively expel cytotoxic drugs out of the tumor cell and maintain an intracellular drug level below effective concentrations (Bodó, 2002). This mechanism of resistance appears to be most relevant to drugs which enter cells by passive diffusion such as most natural chemotherapeutic agents including doxorubicin or paclitaxel.

An important characteristic of MDR transporters is their wide substrate acceptance. In contrasts to other mammalian transporters, the ABC-proteins are highly promiscuous transporters and recognize a wide range of structurally diverse substrates (Bodó, 2002). This is of clinical importance: a tumor which develops an MDR transporter-based resistance mechanism as a result of treatment with one

cytotoxic drug will likely be resistant towards most other chemotherapeutic agents. Genes encoding for ABC transporters are often overexpressed in MDR tumors (Krishna, 2000).

The family of ABC transporters and their most relevant members will be introduced in detail in chapter 1.2.

1.1.2   Non-cellular MDR mechanisms

Although less obvious, non-cellular mechanisms can contribute to an environment, in which the tumor protects itself from the chemotherapeutic drug. Non-cellular mechanisms of MDR arise during the formation of tumor tissue, and are associated with the physiological environment and the surrounding tissue of the tumor. These mechanisms mainly occur in solid tumors and hinder anticancer drugs from accessing their sites of action.

Several different mechanisms can lead to non-cellular-based resistance. In some solid tumors, for example, the interstitial fluid pressure is increased. This can be due to either a higher vascular permeability or the absence of a functional lymphatic system (Jain, 1987). As a consequence, the tissue is vascularized but poorly circulated and this prevents the chemotherapeutic drug from being transported into the tumor region.

Tumor regions are often deficient in nutrition and oxygen. This creates an environment of unfavorable physicochemical conditions for many chemotherapeutic drugs. In these tumor areas, lactic acid generation and hypoxia lead to conditions, in which drugs can be protonated (Demant, 1990). As many drugs are weak bases, protonation will introduce an ionic force, which might impair their ability to cross biological membranes and enter the tumor cell.

1.2   ABC-transporter family

The family of ABC transporters is a large gene family of structurally related transmembrane proteins. Close to 50 members of the ABC transporter family in humans have been discovered to date (Sarkadi, 2004). All ABC transporters contain a distinct DNA signature which includes the ATP-binding domain (Klein, 1999). ABC transporters are phylogenetically ancient and evolutionary conserved from bacteria to men. Homologues of human ABC transporters were found in microorganisms such as bacteria and yeast where they were shown to be involved in conferring resistance to antibiotics (Van Veen, 1998b). The human *MDR1*/Pgp transporter, for example, has a similar antineoplastic profile to, and can be substituted by, LmrA, the multidrug transporter from Lactococcis lactis (Van Veen, 1998a).

In eukaryotic organisms, ABC transporters are ubiquitary present. Human members of the ABC family are widely expressed throughout the body and take part in such diverse functions as transport across membranes or cell signaling (Holland, 1999). Functionally, ABC transporters move their substrates across biomembranes in an energy-dependent manner. The ATPase activity necessary for this transport follows classical Michaelis-Menten kinetics (Ambudkar, 2003).

The main physiological role of these transporters is the protection of the body against xenobiotics and toxic endogenous substrates. Therefore, ABC transporters can be found in important pharmacological barriers or organs of excretion including the liver and the kidney. ABC transporters are all characterized by a broad substrate acceptance which makes them clinically important as the majority of the current drugs on the market are substrates of the ABC-transporters (Beringer, 2005). Thus, their ubiquitous expression and diverse affinity brings about many drug-to-drug interactions and pharmacokinetic alterations.

In resistant tumor cells, ABC transporters are highly overexpressed and primarily involved in MDR mechanisms (see chapter 1.1.1.2). Among the various ABC-transporters the following members have been recognized as the most significant for clinical MDR: P-glycoprotein (Pgp, ABCB1), the breast cancer resistance protein (BCRP, ABCG2) and the multidrug resistance associated proteins (MRPs, ABCC family) (Fojo, 2003; Tan, 2000; Bodó, 2002). These transporters shall be described in the following chapters.

1.2.1   P-glycoprotein (Pgp, ABCB1)

Pgp was discovered and first characterized by Ling and co-workers (Ling, 1974; Juliano, 1976) using multidrug resistant Chinese hamster ovary cells. To date, Pgp, also termed ABCB1, is the most intensively studied and possibly the most prevalent of the ABC-transporters in cancer cells.   The 170 kDa protein is a membrane-bound, energy-dependent drug transporter (Ling, 1995).   By actively effluxing its substrates, Pgp reduces intracellular concentrations to subtherapeutic levels, thereby conferring resistance to a broad range of cytotoxic drugs.   These substrates are of such large structural diversity, that common features are difficult to discover.   Indeed the only common features for Pgp substrates appear to be hydrophobicity and a molecular mass of 300 – 2000 Da (Ford, 1990).   Anionic structures are not transported by Pgp. Substrates for Pgp include many cytotoxic drugs used in cancer treatment such as the anthracyclines, *Vinca* alkaloids and taxanes as well as commonly prescribed drugs such as the calcium channel blockers and antiviral protease inhibitors.

Pgp is encoded by the *MDR1* gene in humans and by the *mdr1a* and *mdr1b* genes in rodents. Together, *mdr1a-* and *mdr1b*-type Pgps fulfil the same function as the single human Pgp (Schinkel, 1997). The human protein consists of 1280 amino acids and spans the biomembrane with 12 transmembrane domains (Figure 1.1). The protein is folded into two similar parts, each containing six transmembrane segments and one ATP binding domain. The gene sequences of these two halves of the molecule share about 43 % of homology. Pgp contains three glycosylation sites (see figure 1.2) on an extracytoplasmic domain (Chen, 1986).

MSD_1 MSD_2

extracellular

cytoplasma

NH_2

ATP   ATP   COOH

Figure 1.1   Topological model of Pgp

The organization of Pgp is depicted with two membrane spanning domains (MSD) and two intracellular ATP-binding sites located between the MSD and at the C-terminus.

Mechanisms of transport

Different theories on the mechanism by which Pgp transports its substrates across biomembranes have been developed. In the "Flippase" model, Higgins and Gottesman postulate that substrates congregate with Pgp at the inner leaflet of the plasma membrane. There, Pgp flips the substrates into the outer leaflet, from which they diffuse into the extracellular area (Higgins, 1992).

A second model by Gottesman and Pastan describes Pgp as a "hydrophobic vacuum cleaner" (Gottesman, 1993). According to the model, substrates of Pgp passively diffuse into the inner layer of the plasma membrane. There, Pgp recognizes the substrates and directly pumps them out. In figure 1.2, the two postulated routes of transport are illustrated.
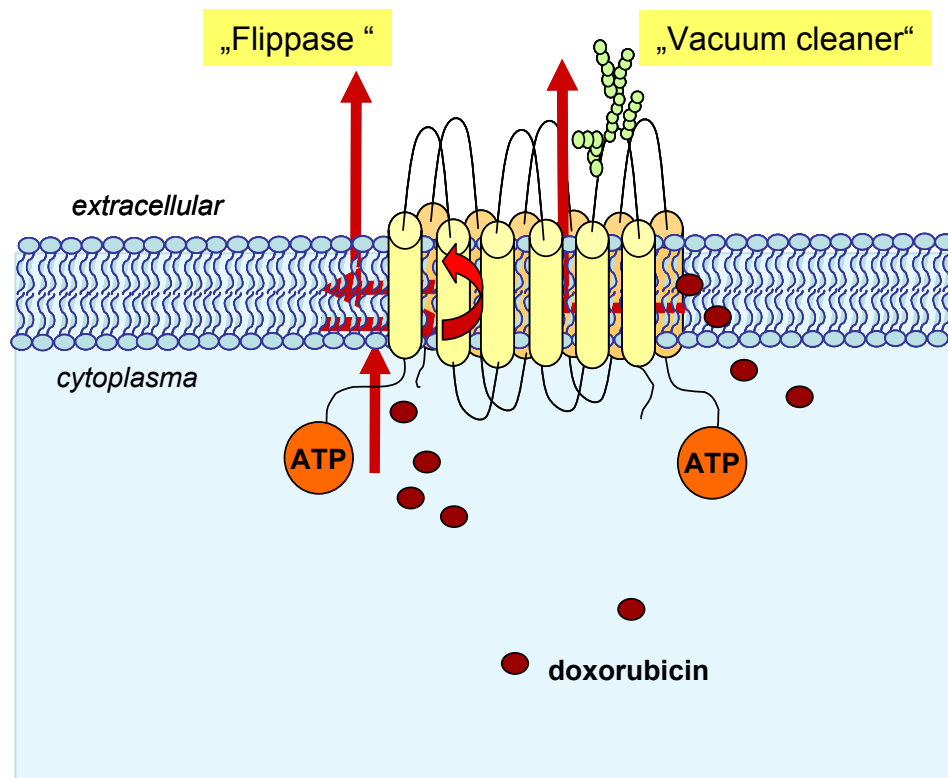
Figure 1.2   Mechanisms of Pgp transport

Two proposed routes of efflux ("Flippase model" and "Vacuum cleaner model") are illustrated for doxorubicin.

Multiple binding sites

The binding parameters and putative binding sites on the molecule have been extensively characterized in the past using radio- or fluorescent-labeled probes. Evidence for a vinblastine binding site could be generated using the photoactive analogue of vinblastine, N-(*p*-azido-)-[3-^{125}I]-salicyl)-N´-ß-amino vindesine, in membrane vesicles obtained from MDR Chinese hamster lung cells. As binding could be inhibited by the addition of vincristine and daunorubicin, competitive binding characteristics were concluded (Cornwell, 1986).

The presence of multiple binding sites was proposed when additional Pgp substrates, including colchicine and actinomycin D, were discovered.   These substrates did not compete for the vinblastine binding site (Akiyama, 1988). Studies

in models of purified and reconstituted Pgp in liposomes demonstrated a direct transport of the Pgp substrate Hoechst 33342 (Shapiro, 1995). These investigations supported the "hydrophobic vacuum cleaner" transport model.

Using fluorescent probes in a model of reconstituted Pgp in membrane vesicles, Shapiro and Ling could demonstrate the presence of at least two distinct binding sites, which they named the H site and the R site (R for rhodamine 123, H for Hoechst 33342). According to their model, the two binding sites interact in a positively cooperative manner (Shapiro, 1997). Further studies of the R and H site by Pajeva and coworkers revealed that both binding sites, the H and the R site, switch their orientation between two functional states characterized as nucleotide-free and nucleotide-bound (Pajeva, 2004). The described conformational change is thought to mediate the transport of the substrate from the membrane to the inner pore.

By classifying drugs that interact with Pgp either as substrates or modulators, Martin and coworkers developed a model of Pgp's transport mechanisms, in which they postulate a minimum of four drug binding sites. These binding sites switch between high and low affinity binding and belong to two categories of either transport or regulatory function (Martin, 2000).

The localization of drug-binding sites on the Pgp molecule was further investigated using photoaffinity analogues. Results from these studies have been summarized by Ambudkar and coworkers (Ambudkar, 2003). Ambudkar suggests that several transmembrane domains (TM) are involved in substrate binding and that different substrates possess multiple and potentially overlapping binding sites.

Loo and Clarke have developed another model of substrate binding to Pgp (Loo, 2002). This model is based on extensive investigations using cystein scanning mutagenesis and crosslinking experiments. According to the authors, the protein contains one common binding site, folded like a pocket, involving eight different TM domains. This 'pocket' allows diverse substrates to create their own binding sites in such a way that the substrates use a combination of residues from the different TM involved. The binding pocket is thought to be mobile, however, when binding of the substrate occurs, the binding pocket stabilizes.

Very recently, Safa has developed a model of several binding sites on the Pgp molecule. The model is based on data obtained from photoaffinity-labeled substrates and postulates seven different binding sites which account for distinct binding of vinblastine, taxol, Hoechst 33342, prazosin, bepridil, flupentixol and dihydropyridine calcium channel blockers (Safa, 2004).

These reports exemplify the large number of sophisticated models, which have been developed to explain the enigma of Pgp's broad function and efficacy. However, the exact mechanism of binding as well as structure activity relationships of substrates and modulators have not been entirely resolved to date.

Physiological expression

Pgp is widely expressed throughout the body with a concentration in excreting organs and physiological barriers. In the intestine, liver and kidney, Pgp is localized in transporting tissues such as the brush border membrane of intestinal cells or the biliary canalicular membrane of the hepatocytes. This indicates an involvement of Pgp in the transepithelial secretion of substrates into bile, urine or intestinal lumen.

Pgp can also be found in barrier tissues such as the placenta or the testis. In the brain, Pgp is expressed in endothelial cells of the brain capillaries and the choroid plexus, both major components of the blood-brain barrier (Borst, 2000; Rao, 1999). Hence, Pgp plays an important role in the excretion and the protection of various tissues against toxic xenobiotics (Borst, 1996; Smit, 1999). Studies in *MDR1* knock out mouse models elegantly confirmed the physiological implications of Pgp (Schinkel, 1997). Whereas the viability of mice lacking MDR1 transporters was not altered, these animals demonstrated a hypersensitivity to xenobiotics with altered excretion and distribution parameters.

Involvement in MDR tumors

Pgp is highly overexpressed in the majority of MDR tumor cells of leukemic and solid tumors (Ambudkar, 2003). The MDR phenotype could be selected *in vitro* using natural product anticancer agents such as vinblastine, doxorubicin and

paclitaxel. These tumor cells then displayed cross resistance to other structurally diverse compounds (Ling, 1995).

In the clinical setting, Pgp has been associated with the development of MDR tumors. Leith and coworkers have reported Pgp expression in 30 % of acute myelogenous leukemia patients at first diagnosis. In patients with disease relapse, overexpression of Pgp was detected in over 50 % of the patients. The degree of Pgp expression in tumors from these patients was comparable to the Pgp expression seen in MDR resistant tumor cells selected through *in vitro* assays (Leith, 1999).

1.2.2   Breast Cancer Resistance Protein (BCRP, ABCG2)

BCRP was first discovered and isolated from the doxorubicin resistant breast cancer cell line MCF7 AdVp3000, which did not possess detectable levels of Pgp or MRP1 (Doyle, 1998). Doyle and coworkers named this new transport protein the breast cancer resistance protein (BCRP), as they derived it from a resistant breast cancer cell line.

BCRP is a 72 kDa ABC-half transporter composed of 655 amino acids. It is thought to function as a homodimer, thus requiring a second molecule for activity. The two halves are bridged by a disulfide bond (Doyle, 2003). The BCRP peptide sequence reveals a single ATP binding domain and an ABC signature motif within the relatively hydrophobic amino terminal domain. Furthermore, BCRP possesses six transmembrane domains and four potential N-glycosilation sites (Doyle, 1998). BCRP is similar to one half of the Pgp or MRP1 molecule with the exception that the ATP binding domain is located at the amino-terminus of the peptide and not at the carboxyl-terminus (Figure 1.3). Of note, members of the ABCG subfamily are the only human ABC transporters discovered in which the ABC signature domain precedes the transmembrane region.
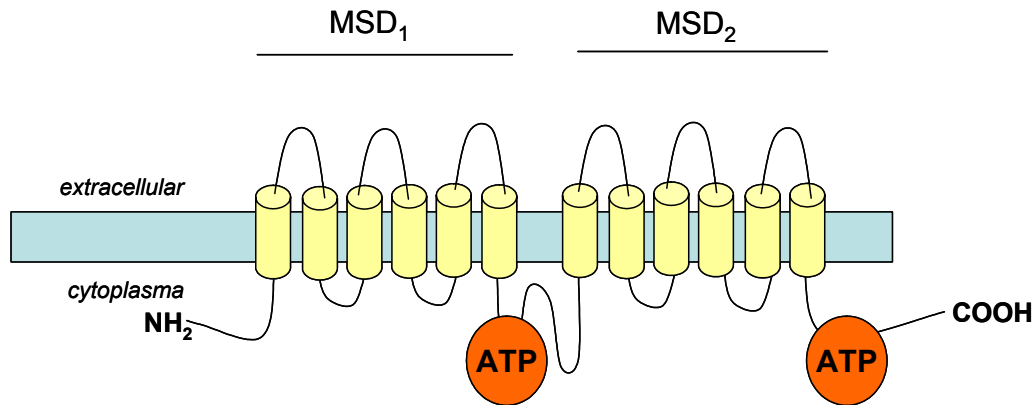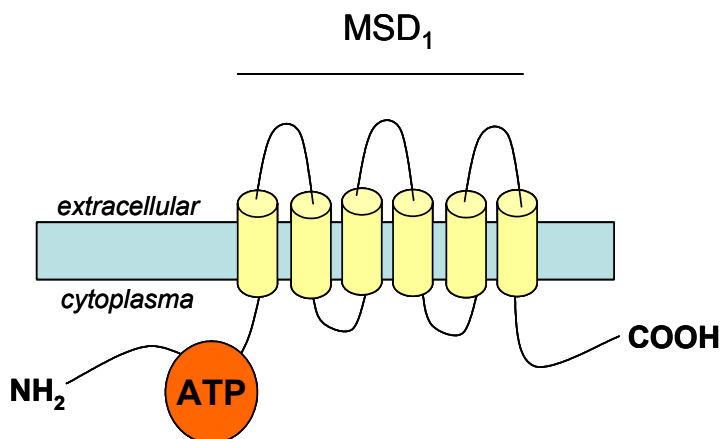
Figure 1.3 Topological model of BCRP

The organization of BCRP is depicted with one membrane spanning domain (MSD1) and the intracellular ATP-binding domain at the N-terminus.

In humans, the BCRP gene is located on chromosome 4, a gene site where no other ABC transporter is located. Analyses of the phylogenetic relationships showed that BCRP is only distantly related to Pgp. However, Pgp is closely related to ABCG1, another member of the G subfamily of the ABC transporters (Chen, 1996) which regulates the macrophage cholesterol and phospholipid transport.

Though different in structure and genetic background, Pgp and BCRP share many common substrates. Both actively transport various structurally diverse substrates out of the cell. Substrates of BCRP include the anticancer drugs mitoxantrone, camptothecin-based topoisomease I inhibitors, methotrexate and flavopiridol (Bates, 2001). BCRP mutated at codon 482, can also transport anthracyclines (Doyle, 2003). Most Pgp inhibitors including PSC 833 and LY335979 do not inhibit BCRP. Some other Pgp inhibitors have been reported to also interact with BCRP (Doyle, 2003), such as GF120918 (Maliepaard, 2001) and Cyclosporin A (Qadir, 2005). Other selective inhibitors for BCRP include fumitremorgin C (Doyle, 2003) and novobiocin (Shiozawa, 2004). More recently a non-toxic, synthetic analog of fumitremorgin C, Ko143, has been identified as a potent and selective inhibitor of BCRP (Allen, 2002).

Physiological expression

Immunohistochemical studies have confirmed the predominant localization of BCRP in the plasma membrane (Rocchi, 2000). This is of importance, as almost all other known half-transporters are localized within the intracellular membranes of the mitochondria or the endoplasmatic reticulum.

Similarly to Pgp, BCRP is widely expressed throughout the body, but with the highest concentration in the placenta. These findings suggest that BCRP plays a protective role for the fetus preventing potentially harmful substances from entering the uterus (Jonker, 2000). Moreover, BCRP expression is found in many other organs and tissues including the liver, ovaries, colon, kidneys and brain microvessels (Doyle, 2003). Tissue distribution studies have demonstrated an extensive overlap between BCRP and Pgp, suggesting that BCRP plays a similar physiological role in providing protection from xenobiotics. Indeed, BCRP regulates the distribution of xenobiotics to various tissues like the liver, intestine and placenta (Allen, 2002).

Interestingly, BCRP has been found to be highly expressed in stem cell subpopulations, such as hematopoetic stem cells (CD⁻) (Zhou, 2001) or embryonic kidney cells (Scharenberg, 2002). These findings imply that BCRP might be involved in the general regulation and protection of stem cells.

Involvement in MDR tumors

Immunohistochemical investigations of various tumors have revealed that BCRP is expressed in over 40 % of solid tumors (Diestra, 2002). BCRP overexpression was detected in tumor specimens obtained from colon, endometrium, lung and melanoma. Thus, BCRP has a substantial involvement in the development of MDR tumors.

BCRP is believed to play a role in recurrent tumors. High BCRP expression was found to be correlated with disease relapse and poor prognosis in acute myeloid leukemia. Furthermore, BCRP expression was verified in premature stem cells of various different tissues. These findings suggest that BCRP might be involved in the protection of cancer stem cell subpopulations where it is believed to offer survival advantages, particularly under hypoxic conditions (Sarkadi, 2004).

1.2.3 Multidrug Resistance Associated Proteins (MRP, ABCC)

The multidrug resistance associated protein (MRP) family or ABCC family, is another distinct class of ABC drug efflux transporters with at least nine members. MRP proteins actively transport structurally diverse lipophilic anions across the biomembrane. The members MRP1, MRP2 and MRP3 were found to play a role in the MDR phenotype of resistant tumors (Borst, 2000; Kruh, 2003). In figure 1.4, the topological models of MRP1, MRP2 and MRP3 are compared. As specified in the following, all three proteins are of almost equal size and organization. They contain three membrane spanning domains, two intracellular loops and two nucleotide folding domains for ATP binding.

	MSD_0	L_0	MSD_1	NBF_1	L_1	MSD_2	NBF_2	C	amino acids
MRP1									1531
MRP2									1545
MRP3									1527
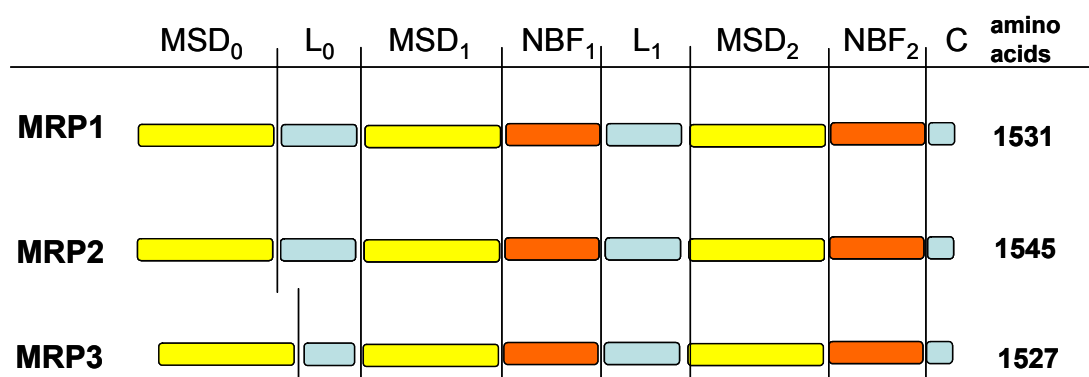
Figure 1.4   Topology of MRP1, MRP2 and MRP3

The organization of protein domains is schematically illustrated. Regions are indicated as follows: Yellow, membrane-spanning domains; blue, cytoplasmic loops; orange, ATP binding domains.

MSD: membrane spanning domain; **L**: intracellular loop; **NBF**: nucleotide-binding fold; **C**: C-terminus

Multidrug Resistance associated Protein 1

MRP1 is a 190 kDa basolateral efflux pump, which transports glutathione-S-conjugates of anionic compounds directly or in cotransport with glutathione. Substrates of MRP1 include chemotherapeutic agents like mitoxantrone, anthracyclines and Vinca alkaloids. Despite its partly overlapping resistance profile

with Pgp, the amino-acid sequence of MRP1 resembles Pgp to a small extent of only 15 %. The structure of MRP1 contains a central 'core' region and a third membrane spanning domain. The additional domain (MSD_0) contains five transmembrane helices, and an extracellular loop with the N-terminus located on the outside of the cell (Bakos, 1996). Two membrane spanning domains as well as two ATP-binding domains are situated (see Figure 1.5) within the 'core' region.
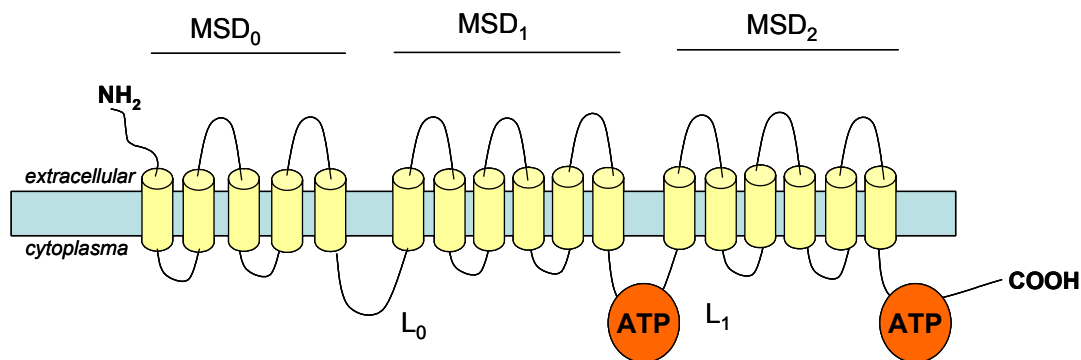
Figure 1.5   Topological model of MRP1

The organization of MRP1 is depicted with three membrane spanning domains (MSD), the intracellular loops (L), two ATP-binding domains and an extracellular N-terminus. This model resembles MRP2 and MRP3.

MRP1 expression is found in the adrenal gland, breast, lung, kidney, heart, blood-brain barrier and endocrine tissue. Studies in *mrp1 -/-* knockout mice have indicated that MRP1 is a transporter functioning as a resistance factor for some mucosal tissues and bone marrow. Furthermore, MRP1 is involved in the physiological barrier for the protection of the testis and the choroids (Kruh, 2003). In contrast to Pgp, MRP1 is expressed on the basolateral site of epithelial cells. Thus, MRP1 transports its substrates away from the luminal surface (e.g. intestinal lumen, bile duct) into the tissue beneath it (Evers, 1996).

Due to its strong affinity for glutathione and glucuronate conjugates, both products from the phase II cellular detoxification of hydrophobic compounds

(Ishikawa, 1992), MRP1 holds an important role in the physiological detoxification system. MRP1 also transports unmodified lipophilic anions, such as many cytotoxic agents, in co-transport with glutathione. Consequently, MRP1-based resistance mechanisms can be inhibited by agents, which block the synthesis of glutathione (Schneider, 1995). Such an inhibitor is buthionine sulfoximine (BSO). Other inhibitors of MRP1 include indomethacin and nifedipine (Draper, 1997; Cullen, 2001).

Multidrug Resistance associated Protein 2

MRP2 is another glutathione efflux pump for amphipathic anions. The protein is composed of 1545 amino acids and its topological organization, as presented in figure 1.4 and 1.5, is closely related to MRP1. Even though the substrate-specificity of MRP2 is very similar to that of MRP1, its physiological function is completely different.

MRP2 has a distinct expression pattern and subcellular polarity. In contrast to MRP1, MRP2 is expressed on the apical site of polarized cells. In the liver, MRP2 is localized in canaliculi cells where it mediates the extrusion of lipophilic anions into the bile. MRP2 is an important component in the biliary excretion of bilirudin glucuronates, which are conjugated end products of heme degradation (Jedlitschky, 1997). Families with hereditary deficiencies of MRP2 have an increased disposition for pathological liver conditions. A lack of MRP2 is associated with defects in hepatobiliary excretion of anionic compounds, which leads to the Dubin-Johnson syndrome, a clinical manifestation of jaundice (Dubin, 1954).

To a lesser extent, MRP2 is expressed in renal proximal tubules, enterocytes of the intestine and brain capillaries (Kruh, 2003). The functional overlap with Pgp is evident as both transporters are involved in the excretion of cytotoxic compounds and the protection of tissue through barrier formation.

With a similar resistance profile as MRP1, MRP2 confers resistance to a variety of natural chemotherapeutics such as anthracyclines, vinca alkaloids and epipodophyllotoxines. Like MRP1, MRP2 needs glutathione for their transport. The affinity to these substrates, however, is slightly weaker as in the case of MRP1. Importantly, MRP2 overexpression was detected in cisplatin resistant cell lines. This

suggests that MRP2 might confer resistance to cisplatin, a substance that forms toxic glutathione-conjugates in the cell (Tanigutchi, 1996). Of note, other ABC transporters such as Pgp or BCRP are not involved in resistance mechanisms against cisplatin.

Multidrug Resistance associated Protein 3

Among the MRP transporters, MRP3 is structurally most closely related to MRP1 with a homology of 58 %. Likewise, MRP3 contains a third membrane spanning domain with an extracellular loop and the N-terminus on the extracellular side (see figure 1.4 and 1.5). MRP3 functions as a transporter of glutathione and glucuronate-conjugated compounds. Its affinity to these conjugates, however, is significantly lower than that of MRP1. Contrary to MRP1 and MRP2, MRP3 does not require glutathione for transport of its substrates, thus, the MRP1 inhibitor BSO cannot attenuate MRP3-mediated transport (Zelcer, 2001).

Although it was shown that MRP3 mediates resistance to some cytotoxic agents such as etoposide and teniposide (Kool, 1999), its involvement in MDR tumors appears to be much smaller compared to MRP1 or MRP2.

MRP3 can be found in a variety of different tissues. In the liver, MRP3 is expressed at the basolateral membrane of bile duct cells, where it extrudes monoanionic bile acids such as glycocholate and taurocholate. During cholestatic liver conditions, MRP3 is highly upregulated and helps to detoxify the hepatocyte by transporting toxic bile acids into the blood (Hirohashi, 1998). In addition to the liver, MRP3 is expressed in the intestine, kidney, pancreas and gall bladder (Belinsky, 1998).

1.3   Modulation of Multidrug Resistance

Conventional chemotherapy has succeeded in many different cancers and saved the lives of millions of patients. At the same time, however, conventional chemotherapy has failed to cure cancer numerous times, unable to reverse the progress of the disease. While some oncologists argue that the efficacy of conventional chemotherapy is limited; others state that resistance mechanisms hamper their potential (Fojo, 2003). If the latter is true, resistance mechanisms, namely those outlined in chapter 1.1.1, could be inhibited and the chemotherapeutic activity restored. Motivated by this argument, many researchers have investigated strategies to overcome MDR in untreatable tumors. The strategies involving ABC transporters are introduced in the following chapters.

1.3.1   P-glycoprotein inhibitors

Development of chemosensitizing modulators which inhibit the function of Pgp thereby reversing MDR has been pursued extensively for the past 20 years. In the early 1980s, the calcium channel blocker verapamil was discovered to reverse Pgp-mediated MDR *in vitro* (Tsuruo, 1981). Other first generation modulators of Pgp belonged to various therapeutic classes. Among them are the class I antiarrythmic agent quinidine and the immunosuppressant cyclosporin A. These agents are required at relatively high concentrations to effectively inhibit Pgp. However, at these concentrations unacceptable *in vivo* toxicities and interactions with numerous physiological tissues and transporters occur. Heart block with subsequent heart failure was observed, when verapamil was combined with doxorubicin (Ozols, 1987). Among the first generation modulators, the immunosuppressant cyclosporin A remains one of the most effective and best studied.

Development of the second generation Pgp modulators was driven with the intension of improving the affinity to Pgp while reducing clinical toxicities. These compounds were all derivatives of the first generation modulators, however, less toxic and without the main pharmacological effects of their templates. The non-immunosuppressive analog of cyclosporin A, PSC 833 (see figure 1.6), demonstrated a 10-fold more potent MDR reversal activity *in vitro* than cyclosporin A

(Krishna, 1997).   PSC 833 (Valspodar) has been used extensively in tumor xenografts and clinical trials (Oza, 2002; Fracasso, 2000).   As preclinical evidence suggested that serum protein binding would decrease the effectiveness of PSC 833 (Lehnert, 1996), the compound was administered at doses, which in retrospect were much too high.   At these concentrations major pharmacokinetic interactions were reported.   In a clinical trial using PSC 833 and doxorubicin, a 10-fold increase in doxorubicin blood levels was detected, which substantially increased hematological toxicities (Giaccone, 1997).

PSC 833   Cyclosporin A
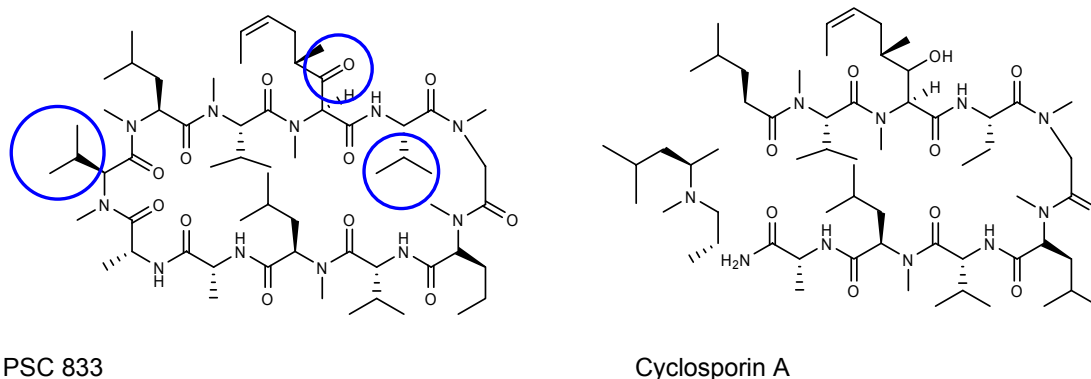
Figure 1.6   Chemical structure of cyclosporin A and PSC 833 (Valspodar)

Chemical structures of PSC 833 and Cyclosporin A are depicted; chemical variations of PSC 833 are indicated by a blue circle.

Lessons learned from second generation Pgp inhibitors resulted in more sophisticated approaches with aims to develop specific inhibitors, which would not interact with other targets.   Pharmacophore models with efforts to explain Pgp's broad substrate acceptance have been developed (Pajeva, 2002).   Furthermore, structure-activity relationships and combinatorial chemistry techniques have been elaborated and used to synthezise promising third generation Pgp modulators. These modulators demonstrated increased specificity for Pgp with an inhibition in the nanomolar range and reduced *in vivo* toxicities (Tan, 2000; Fojo, 2003).

Some examples of third generation Pgp modulators are presented in figure 1.7.   These compounds include XR9576 (Tariquidar: Dale, 1998), LY335979 (Dantzig, 1996; Kemper, 2004), OC144-093 (Newman, 2000) and GF120918 (Hyafil, 1993) and are currently referred to as the state of the art.
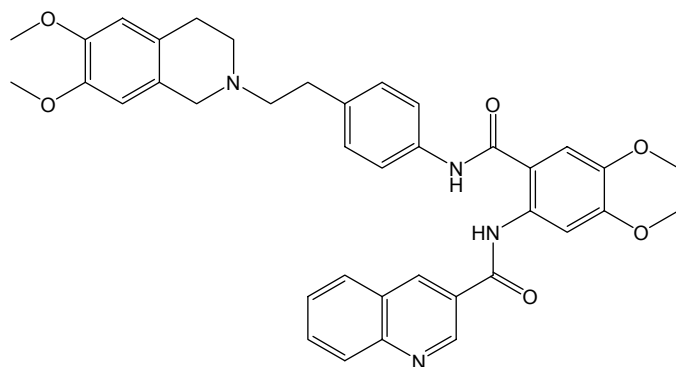
XR 9576 (Tariquidar)
Mr: 647
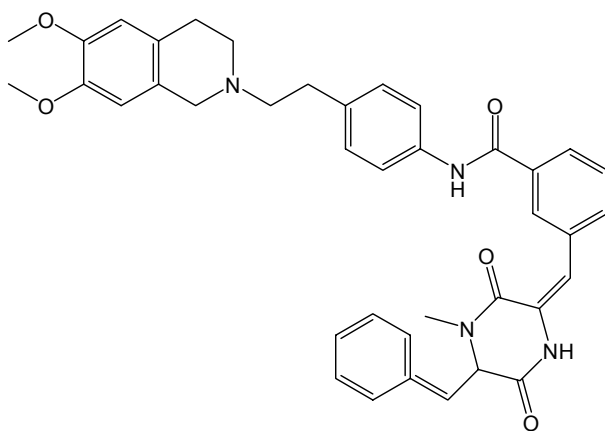
XR 9051
Mr: 645
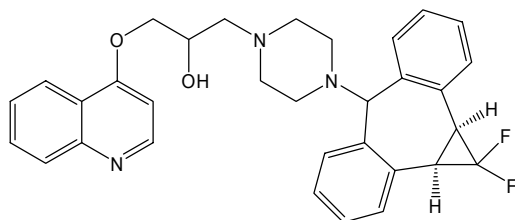
LY 335979 (Zosuquidar)

Mr: 526
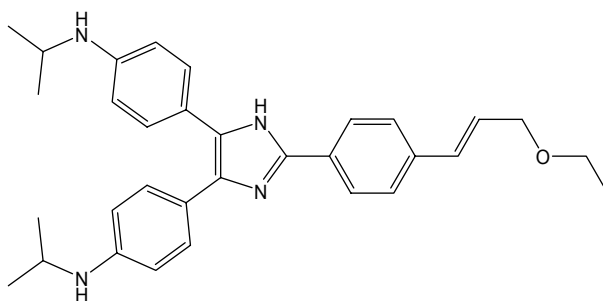
OC 144-093 (ONT-093)

Mr: 495
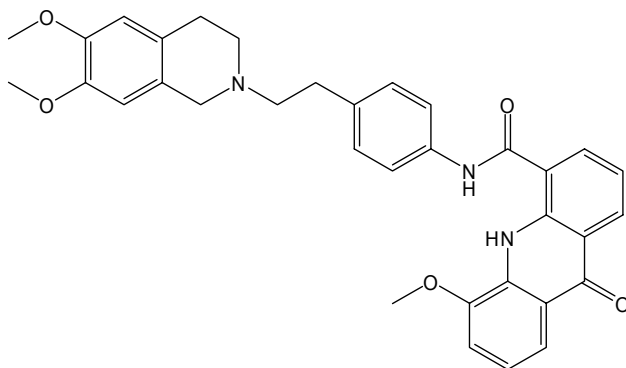
GF 120918 (Elacridar)

Mr: 564

Figure 1.7   Chemical structures of selected third generation Pgp inhibitors

Various second- and third-generation modulators have been evaluated in clinical trials with partly encouraging, partly conflicting results (Tan, 2000). Their drawbacks in clinical applications resulted from alterations in the pharmacokinetic profile of coadministered cytotoxic agents. Additionally, clinical toxicities by and lack of efficacy of MDR inhibitors were observed. These complications were presumably caused by the existence of multiple and redundant cellular mechanisms of resistance (Fisher, 1996). Despite tremendous efforts and many encouraging reports published in this field, no Pgp inhibitor has received a market authorization to date.

1.3.2   Multi targeted MDR inhibitors

The first generation Pgp inhibitor, cyclosporin A, has proven sufficient efficacy in clinical trials to reverse MDR in acute myelomic lymphoma (AML) (Smeets, 2001; List, 2001). Interestingly, cyclosporin A was later found to inhibit not only Pgp but also BCRP, MRP1 and the lung resistance protein (LRP), another transporter involved in the transport of cytotoxic agents (Qadir, 2005). Whereas third generation Pgp inhibitors are being developed to increase specificity for Pgp with means to prevent *in vivo* toxicities and pharmacokinetic interactions (Tan, 2000; Fojo, 2003), the concept of broad-spectrum MDR modulation has recently attracted much attention. Most complicated MDR-protected tumors such as acute leukemia are protected by multiple and redundant cellular mechanisms of resistance (Ross, 2000; Urasaki, 1996). Thus, modulation of more than one ABC-transporter-mediated mechanism appears to be a promising approach.

Recently, some groups including Minderman and coworkers have developed MDR inhibitors targeted against more than one ABC transporter. The synthetic taxane derivative BAY 59-8862 (Ortataxel) was found to simultaneously inhibit the function of Pgp, BCRP and MRP1 (Minderman, 2004) and is currently under investigation in Phase I clinical trials (Ramnath, 2004). VX-710 (Biricodar), a pipecolinate derivative, is another multi targeted MDR inhibitor with modulating properties of Pgp, BCRP and MRP1 (Minderman, 2004), currently under investigation in Phase II clinical trails (see figure 1.8).
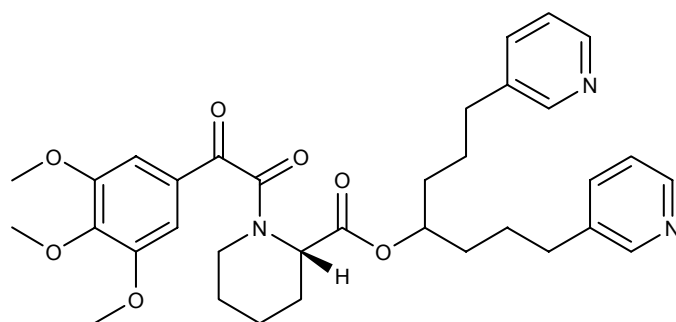
VX-710 (Biricodar)

Mr: 604
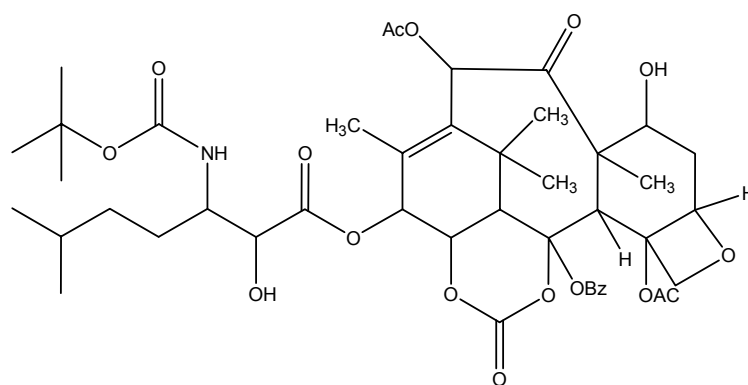
BAY 59-8862 (Ortataxel)

Mr: 855

Figure 1.8   Chemical structure of VX-710 and BAY 59-8862

1.3.3   Antisense Therapy

While modulation using small molecule inhibitors has been the main focus to circumvent MDR, other strategies including gene regulation approaches have been investigated. Among them are synthetic DNA oligomers, the conventional antisense oligodeoxynucleotides (ODNs).   ODNs directed against the *MDR1* gene can specifically inhibit the expression of Pgp.

Antisense ODNs are powerful tools for the selective and sequence-specific regulation of gene expression (Benett, 1999; Galderisi, 1999). The synthetic DNA molecules can be specifically designed for each target and are susceptible to degradation. To produce oligonucleotides suitable for *in vivo* applications, chemical modifications of oligonucleotides have been described in efforts to increase their stability and specificity. Most experience with *in vivo* application has been generated with phosphorothioate oligonucleotides (Eckstein, 2000) which contain a sulphur atom replacing a single oxygen atom at each phosphate group. Phosphorothioation makes ODNs relatively nuclease resistant (Stein, 1988). Although associated with non-specific binding and toxic side effects *in vivo* (Levin, 1999), a phosphorothioated antisense-based drug against CMV, Vitravene[TM] (De Smet, 1999), receive market authorization in 1998.

Antisense molecules hybridize to their target mRNA in the cytosole, where they recruit the endonuclease RNAse H. The enzyme destroys the target mRNA and releases the antisense molecule.   The released antisense molecule can hybridise to another target mRNA strand. In this way, the degradation of target mRNA prevents the translation of the protein. The mode of action is illustrated in figure 1.9.
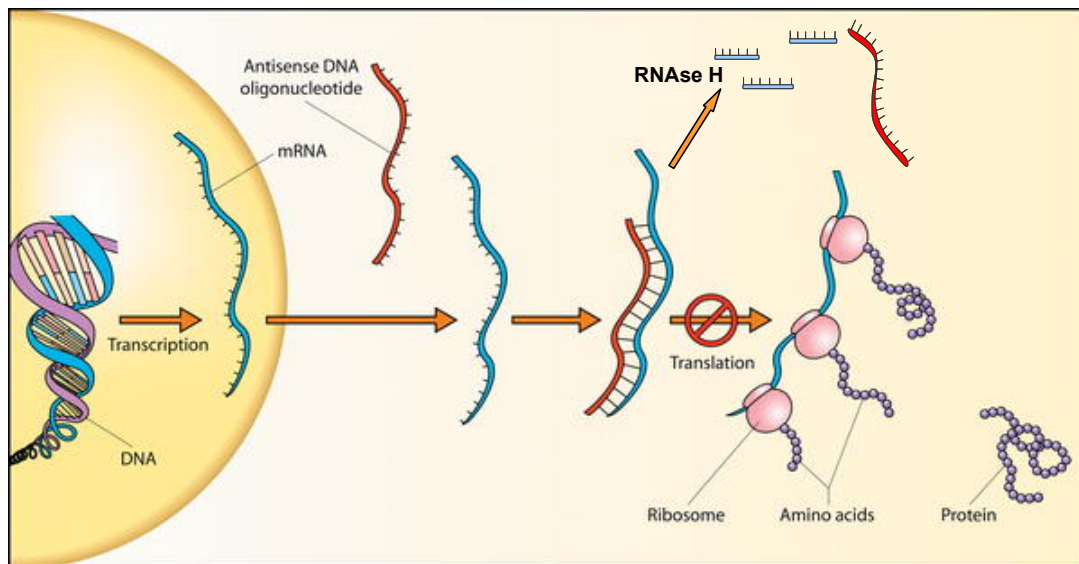
Figure 1.9   Mechanism of protein-synthesis inhibition by antisense ODNs

In the cyctoplasma, antisense ODNs hybridize to target mRNA. This process recruits RNAse H enzyme, which degradates mRNA and releases the antisense strand. Lack of mRNA, inhibits the translation of the protein. (Picture taken from Robinson, PLoS 2004;2:18-20)

Antisense oligodeoxynucleotides directed against the *MDR1* gene have been widely used to inhibit the translation of *MDR1* mRNA and downregulate the expression of Pgp (Alahari, 1996; Dassow, 2000). ODNs, designed mostly against the region of the initiation codon of *MDR1*, have been reported to inhibit the Pgp-mediated multidrug resistant phenotype *in vitro* in cell culture (Alahari, 1998) and *in vivo* in human tumor xenografts (Ramachandran, 2003).

Other antisense strategies used to downregulate Pgp include various chemically modified antisense oligonucleotides (e.g. locked nucleic acids), hammerhead ribozymes and siRNA (Kurreck, 2003).

1.4   Imaging of Multidrug Resistance

Non-invasive methods to examine the multidrug resistant status of tumors before therapy are valuable tools to select the most effective combination of chemotherapy for treatment. Detection of Pgp expression is commonly performed using immunohistochemical or immunofluorescence techniques (Beck, 1996). These techniques, however, may also detect altered or functionally impaired Pgp and are therefore of limited prediction. Furthermore, their routine use in a clinical setting is laborious, expensive and rather complicated.

Imaging of Pgp function with the cardioimaging tool ^{99m}Tc-Sestamibi (see chapter 3.3.6.1 and 3.3.7, methods) is a technique used to non-invasively evaluate Pgp activity in tumors (Piwnica-Worms, 1993). The synthetic gamma-emitting organotechnetium complex, ^{99m}Tc-Sestamibi, is a Pgp substrate and has been approved by the Food and Drug Administration (FDA) for the use as a radiotracer.

^{99m}Tc-Sestamibi accumulation is directly correlated to physiological Pgp expression; it is inversely proportional to the degree of Pgp expression. Other ABC transporters do not interfere with ^{99m}Tc-Sestamibi transport. MRP1 has a much lower affinity and the radiopharmaceutical does not interact with BCRP (Chen, 2000). Thus the detection of ^{99m}Tc-Sestamibi accumulation permits to selectively trace and map Pgp function. Del Vecchio and coworkers have performed imaging studies in breast cancer patients using ^{99m}Tc-Sestamibi (Del Vecchio, 2004). In Pgp overexpressing tumors, efflux of ^{99m}Tc-Sestamibi was increased over 2-fold compared to tumors with basal levels of Pgp expression. Tumor response to chemotherapy has also been correlated with intratumoral ^{99m}Tc-Sestamibi accumulation. In a study by Ciarmiello (Ciarmiello, 1998), the response rate of breast tumors to neoadjuvant chemotherapy was markedly decreased in tumors, which rapidly effluxed ^{99m}Tc-Sestamibi. In human tumor xenograft models, ^{99m}Tc-Sestamibi imaging has been successfully used to monitor the effectiveness of novel Pgp inhibitors (Marián, 2003; Hendrikse, 1999). Through detectable changes in the distribution and accumulation of ^{99m}Tc-Sestamibi, the technique further permits to evaluate interaction of Pgp inhibitors with physiological Pgp expressed in various organs and barriers (Zhou, 2001).

2 Rational

2.1 Rational and hypothesis

Clinical MDR remains a major obstacle in the successful chemotherapeutic treatment of cancer. In many recurring and untreatable tumors the machinery of MDR contributes to the fatal progress of the disease. Over the past years, different therapeutic strategies, including those targeting Pgp by small molecule inhibitors or RNA inhibition, have been extensively investigated in cell culture, animal models and in cancer patients. Yet a medication against the condition of "multidrug resistant cancer" could not be developed to a level of marketing authorization.

The disparity between research effort and outcome in the sense of a therapeutic strategy suggests that MDR is a phenomenon more multifaceted than originally thought. Consequently, its resolution will likely be more involved. A combinational treatment designed to target more than one MDR mechanism simultaneously might be a solution to master MDR in its complexity.

Two hypotheses of combinational treatment strategies are being formulated:

- Different mechanisms of MDR are targeted simultaneously

- The same mechanism is targeted by more than one approach

To address these hypotheses, I have investigated two different treatment strategies for their effectiveness and feasibility in reversing MDR in human tumors. The two treatment strategies were studied both separately and in combination using *in vitro* and *in vivo* experimental techniques:

I. **Novel multi-targeted MDR inhibitors** (Tetrahydroisoquinolin-ethyl-phenyl amine-based MDR inhibitors developed in Prof. Dr. M. Wiese's laboratory at the University of Bonn)

II. **Transcriptional downregulation by *MDR1* antisense ODNs** (in combination with an MDR inhibitor)

Hypothesis

(**I.**) In line with recent discoveries that several ABC-transporters coexist in many tumors, multi-targeted MDR inhibitors are thought to reverse the ABC-transporter-mediated multidrug resistant phenotype more effectively than selective inhibition of just one ABC-transporter (e.g. Pgp). The novel tetrahydroisoquinolin-ethyl-phenyl amine-based MDR inhibitors were characterized as potential multi-targeted MDR inhibitors.

(**II.**) Moreover, a combination of transcriptional suppression and functional inhibition of the *MDR1* gene and functional Pgp, respectively, is an interesting approach, which has not been investigated before. The combined treatment using antisense ODNs together with a Pgp inhibitor is though to be more effective in comparison to the single treatments as it allows the simultaneous targeting of the function and formation of the protein.

2.2   Aim and experimental outline

To address the two above-mentioned hypotheses, the two outlined treatment strategies (**I.** and **II.**, see chapter 2.1) were implemented in a series of *in vitro* and *in vivo* studies using a tumor model of human ovarian cancer:

In vitro

- Novel MDR inhibitors were tested for their ability to inhibit transport function of relevant members of the ABC-transporter family, involved in MDR: Pgp, BCRP and MRP1-3.

- Potential *in vitro* toxicities of novel MDR inhibitors and *MDR1* antisense ODNs were investigated in several cell lines.

- The potency and specificity of novel MDR inhibitors to reverse Pgp and BCRP-mediated resistance towards chemotherapeutic agents were studied in multidrug resistant cell lines.

- The effectiveness of *MDR1* antisense ODNs to downregulate the surface expression of Pgp was studied in a Pgp overexpressing cell line.

- The MDR-reversing properties of *MDR1* antisense ODNs were investigated by studying inhibition of Pgp-mediated transport and resistance towards a chemotherapeutic drug.

Among the novel MDR inhibitors, the most promising candidate, WK-X-34, was selected for further in vivo investigations.

In vivo

- Potential *in vivo* toxicity including hepatotoxicity of the selected MDR inhibitor, WK-X-34, was studied in mice.

- The ability to reverse the MDR phenotype by WK-X-34 *in vivo* was studied in tumor xenograft models of resistant human ovarian cancer using ^{99m}Tc-Sestamibi imaging techniques.

- Potential interactions of WK-X-34 with physiological Pgp and pharmacokinetic alterations of the Pgp substrate ^{99m}Tc-Sestamibi were examined in nude mice.

- The effectiveness of *MDR1* antisense ODNs to downregulate *MDR1*/Pgp mRNA and protein expression were studied in tumor xenograft models of multidrug resistant human ovarian cancer.

- The MDR-reversing ability of antisense treatments alone and in combination with the selected MDR inhibitor, WK-X-34, was investigated in a human MDR solid tumor xenograft models using ^{99m}Tc-Sestamibi imaging techniques.

2.3   Justification of experimental methods

2.3.1   Choice of Pgp inhibitors

The novel tetrahydroisoquinolin-ethyl-phenylamine-based MDR inhibitors WK-X-34, WK-X-50 and WK-X-84 (Figure 3.1) were designed and synthesized by W. Klinkhammer in Prof. Dr. M. Wiese's laboratory at the Pharmaceutical Institute, University of Bonn, Germany. Based on initial functional *in vitro* assays, including the MTT assay and the Calcein AM and daunorubicin transport assays performed by H. Mueller and K. Breitbach, these compounds were selected as the most promising candidates for further *in vitro* and *in vivo* characterization. Increased amounts of these compounds were synthesized by W. Klinkhammer and sent to the laboratory of Dr. Piquette-Miller at the University of Toronto.

In vitro assays were conducted using verapamil and cyclosporin A as reference substances. Verapamil is the oldest and most prominent amongst the Pgp inhibitors (Tsuruo, 1981). To date, the first generation Pgp inhibitor cyclosporin A is the only inhibitor to perform convincingly in clinical applications. Cyclosporin A demonstrated efficacy in clinical trials reversing MDR in acute myelomic lymphoma (AML) patients (Smeets, 2001; List, 2001). One can argue, that the more effective and more potent third generation Pgp inhibitors such as GF120918 (Hyafil, 1993) or XR9576 (Mistry, 1999) are the current state of the art Pgp inhibitors. Despite extensive research and clinical development, these compounds have not yet received market authorization. As the successful clinical application is the main motivation for the development of MDR inhibitors, cyclosporin A was used as the reference compound.

2.3.2   Cell model

The multidrug resistant human ovarian cancer cell line A2780/Adr and its sensitive counterpart A2780/wt were used for the *in vitro* and *in vivo* investigations of Pgp. These cell lines were initially isolated from a drug sensitive patient with ovary tumors. Through selection with adriamycin, a multidrug resistant phenotype with cross resistance characteristics was obtained (Louie, 1986; Sasaki, 1991). Over the

past decades, resistant A2780/Adr cells have proven to be a suitable model to study Pgp-mediated MDR in solid tumors. They have been widely used both in cell culture (e.g. Sasaki, 1991; Plumb, 1990; Mueller, 2004) and xenograft models (e.g. Caffrey, 1998; De Cesare, 2001). Therefore, this well-established cell model was chosen and applied in this thesis.

Resistant A2780/Adr cells tend to loose their phenotype over a span of 10-20 passages by the development of two subpopulations, in which the sensitive fraction keeps increasing and the resistant fraction keeps decreasing. To guarantee a high and constant expression of Pgp, adriamycin (10 μM) needed to be added to these cells every 10 passages. To monitor and verify a constant Pgp expression, *MDR1* and Pgp expression was routinely examined by RT-PCR and protein staining techniques.

2.3.3   *MDR1* antisense ODN treatments

I wanted to compare Pgp inhibition caused by small-molecule inhibitors to *MDR1* antisense treatment, which downregulates the expression of functional Pgp. For this purpose, conventional phosphorothioated antisense ODNs directed against the start codon of the human *MDR1* gene were used. The ODN sequence was taken from reports by Alahari *et al.* (Alahari, 1998). The anti-MDR activity of these sequences has been previously verified *in vitro* (Brigui, 2003) and *in vivo* (Ramachandran, 2003). Among the DNA-based antisense tools, phosphorothioated antisense ODNs are the oldest and best characterized. Indeed Vitravene^{TM} (Fomivirsen), a phosphorothioated antisense inhibitor of CMV replication (De Smet, 1999; Naesens, 2001), developed by ISIS Pharmaceuticals is the only antisense-based drug ever to get a marketing authorization. As I was primarily interested in using a basic antisense tool, rather than optimizing antisense-targeted therapy in MDR cancer, I decided to utilize conventional phosphorothioated antisense ODNs. Moreover, I evaluated *in vitro*, whether the inhibitory effects were due to antisense effects and not simple toxic effects. FITC-labeled *MDR1* antisense ODNs were used to investigate the uptake path of antisense ODNs. Fluorescent microscopy permitted to study whether antisense *MDR1* ODNs actually accumulated in the nucleus. Interestingly, these studies demonstrated that the delivery of antisense molecule is

increased when formulated as a double-stranded antisense and sense duplex. These results have been published (Jekerle, 2005), however, they are only partly contained in this PhD thesis.

For *in vivo* antisense treatments, I also used conventional phosphorothioated antisense ODNs for the same reasons: 1) much experience has been generated with *in vivo* applications using phosphorothioated antisense ODNs; 2) the rational of my thesis asked for a functional comparison of antisense strategy to Pgp modulation, rather than the optimization of different *in vivo* applications. I designed the treatment regiments according to previously published antisense applications (Kuss, 2002). The *in vivo* experiments were conducted as proof of principle approaches. Therefore, the most direct route of application was chosen, an intra tumoral injection. By using this route of application, additional *in vivo* effects and complications resulting from unequal *in vivo* stability, distribution and delivery to the site of action could be minimized.

2.3.4   Choice of *in vitro* functional assays for Pgp

To evaluate *in vitro* inhibition of Pgp, a combination of chemosensitivity assays and transport assays were utilized. Chemosensitivity assays investigate the effects of inhibition on the Pgp-mediated MDR phenotype. The increased sensitivity of the multidrug resistant tumor cell towards chemotherapeutic agents such as the anthracyclines (e.g. daunorubicin) can be directly measured. EC_{50} values allow the quantification and comparison of inhibitory effects by different modulators.

A series of transport assays investigating both increases in intracellular accumulation and decreases in the efflux rate of Pgp substrates were utilized. Three different Pgp transport assays were chosen for these studies: 1) ^{99m}Tc-Sestamibi accumulation assay; 2) Daunorubicin accumulation assay; and 3) Daunorubicin efflux assay. This combination of transport assays included two different Pgp substrates and two different transport parameters (basic accumulation and efflux). Studies comparing the usefulness of the substrates ^{99m}Tc-Sestamibi and daunorubicin in Pgp transport assays have also indicated differences between these two assays. Muzzammil and coworkers stated that sufficient sensitivity to distinguish

wild-type from resistant cell variants was given for both substrates (Muzzammil, 2001). A greater sensitivity with more reliable conclusions, however, was detected for ^{99m}Tc-Sestamibi-based transport assays. These differences were explained by additional MDR factors (see chapter 1.1, introduction) unequally affecting ^{99m}Tc-Sestamibi and anthracyclines. Hence, combined results from both assays allow a more predictive and reliable evaluation of Pgp inhibition.

2.3.5   Choice of *in vitro* functional assays for BCRP and MRPs

To examine potential interactions with the MRP proteins, a conventional 5-CFDA efflux assay was used. The MRP family of ABC transporters has currently up to seven members and is constantly growing. As outlined in the introduction, solely MRP1, MRP2 and MRP3 were found to be implicated in the MDR phenotype of resistant tumors (Borst, 2000; Kruh, 2003). Therefore, I decided to examine potential effects of novel MDR inhibitors on these three MRP transporters. Selectively transfected cell lines were used for these studies. In selectively transfected cell lines, the actual human protein of a defined sequence has been artificially engineered into the cell. This has an advantage over selected resistant cell lines which might contain different mutants of a protein together with other resistance mechanisms. Every cell line expresses basal levels of other ABC transporters. The protein of interest, however, is relatively overexpressed in selectively transfected cell lines. Results obtained from these cell lines can thus provide fairly accurate information about the transport properties of the transfected protein.

As selectively transfected cell lines for BCRP have not yet been generated, I used the BCRP overexpressing cell line MCF7/mx, a mitoxantrone selected human breast cancer cell line in a previously established and commonly applied flow cytometry-based efflux assay (Minderman, 2002).

2.3.6   Tumor xenograft model

To investigate the *in vivo* performance of WK-X-34 and antisense treatments, a suitable *in vivo* model needed to be developed. Numerous rodent models have been actualized to simulate the development of ovarian cancer *in vivo* and to aid in the research of human ovarian cancer. Rodent models of ovarian cancer include the chemical/hormonal induced model, the genetic knockout and transgenic model, the syngeneic model and the xenograft model (Stakleff, 2003).

In chemically or hormonally induced tumor models, the tumors are specifically induced by a chemical trigger and display all stages of tumorgenesis. These models can therefore proceed through all stages of neoplasia from the initiation and promotion to the actual development of the tumor. The chemical/hormonal induced model, however, is difficult to apply in praxis as tumors are not selectively induced only in the ovaries. The model furthermore lacks consistency and reproducibility (Silva, 1997; Nishida, 1998).

Genetic knockout and transgenic models are generated in genetically altered mice. These models are used when the impact of genetic alterations in oncogenes or tumor suppressor genes is investigated (Orsulic, 2002; Wang, 1999).

In syngeneic models, tumors are derived from animal tissues by *in vitro* transformation and re-injected into the same animal species (Rose, 1996). Although this model allows a good evaluation of host-tumor interactions, the development of the primary tumor occurs *in vitro* and does not represent physiological conditions.

In xenograft models, human tumor specimens are implanted into immunocomprimised nude mice, which lack functional T lymphocytes (Croy, 2001). In this way, the xenograft model permits the growth of human tumor specimens (Massazza, 1989; Elkas, 2002). The cell lines can be manipulated *in vitro* before being injected into the animal. In xenografts, multidrug resistant and/or sensitive tumors can be selectively generated in the same model (Bradley, 1989). The lack of immune response in the animals, however, does not allow the direct translation into clinical reality.

The xenograft model appeared to be the most suitable for my purposes and was used for the *in vivo* ^{99m}Tc-Sestamibi imaging and biodistribution studies. The

same A2780/Adr and A2780/wt cells which were already used for *in vitro* investigation could be inoculated s.c. into the back flank of immunocomprimised mice. Thus, the tumors grew on each back flank of the animals. This was important as imaging studies necessitated a model in which the tumors were localized away from all the inner organs (Picture 5, Appendix) to avoid overlap of ^{99m}Tc-Sestamibi levels between organs and tumors. Furthermore, the tumor models could be generated in such a way that each animal bore one multidrug resistant A2780/Adr and one sensitive A2780/wt on each back flank. This design allowed the comparison of the treatments on each tumor simultaneously and within the same animal.

A literature study based on data from the National Cancer Institute (NCI) compared the clinical predictive value of preclinical cancer models including *in vitro* cell lines and human xenografts for different tumors (Voskoglou-Nomikos, 2003). In this study, the human xenograft model turned out to be predictive for non-small lung cancer and for ovarian cancer (Johnson, 2001; Taetle, 1987), but not for breast or colon cancer. Overall, the human xenograft models were rated useful in predicting the Phase II clinical performance of cancer drugs (Voskoglou-Nomikos, 2003).

2.3.7 ^{99m}Tc-Sestamibi imaging and biodistribution

To study *in vivo* applications of Pgp inhibitors and antisense therapy, an *in vivo* imaging approach combined with a biodistribution analysis using ^{99m}Tc-Sestamibi was chosen. As previously mentioned in the introduction, the gamma-emitting complex ^{99m}Tc-Sestamibi has been discovered to be a Pgp substrate. Therefore, ^{99m}Tc-Sestamibi can non-invasively map Pgp expression and functionality through changes in organ accumulations (Piwnica-Worms, 1993). ^{99m}Tc-Sestamibi imaging is widely used to detect multidrug resistant tumors (Zhou, 2001) and to monitor the effectiveness of novel Pgp inhibitors in cancer patients (Agrawal, 2003) and human tumor xenograft models (Lorke, 2001; Muzzamil, 1999; Ballinger, 2000). Moreover, the technique of ^{99m}Tc-Sestamibi imaging has been approved by the FDA for rapid evaluation of the effectiveness of anti-MDR therapies in clinical trials. ^{99m}Tc-Sestamibi imaging was used to test the third generation Pgp inhibitor XR9576 in clinical trials Phase II and pivotal Phase III clinical trials (Menefee, 2005). Other ^{99m}Tc-labeled lipophilic cationic complexes such as ^{99m}Tc-tetrofosmin and [99m]Tc-

Q12, both myocardial infusion agents (Bernard, 1998; Utsunomiya, 2000), have also been evaluated for the use in *in vitro* and *in vivo* imaging studies. A study comparing the suitability of these three ^{99m}Tc-labeled imaging agents came to the conclusion that ^{99m}Tc-Sestamibi is the most appropriate agent for tumor imaging due to advantages in tumor uptake (Bernard, 1998).

Therefore, ^{99m}Tc-Sestamibi was chosen as the Pgp substrate and detector for the imaging and biodistribution studies. These studies, however, are rather expensive and time-consuming, involving the generation of an animal model as well as conducting the actual imaging experiments. Time and resources only permitted the testing of the most promising candidate among the MDR inhibitors developed in Prof. Dr. M. Wiese's laboratory, WK-X-34.

[99m]Tc-Sestamibi imaging enabled to non-invasively monitor the impact of WK-X-34 on Pgp activity in multidrug resistant and sensitive tumors as well as on physiologically expressed Pgp in excreting organs and barrier tissue. Hence, potential interactions and organ toxicities resulting from Pgp inhibition by WK-X-34 could be evaluated. Results from ^{99m}Tc-Sestamibi imaging were correlated with biodistribution studies to verify, whether the detected levels of radioactivity in the regions of interest of the selected organs corresponded to the actual ^{99m}Tc-Sestamibi uptake in these organs.

3 Materials and Methods

3.1 Materials

3.1.1 Chemicals, Reagents and Materials

Agarose	Bio-Rad Laboratories, Mississauga, ON, Canada
ALT (Alanin Aminotransferase assay)	ThermoDMA, Arlington, TX, USA

Antibodies

FITC-labeled anti-human Pgp monoclonal antibody	BD Biosciences, San Diego, CA, USA
Primary anti-human BCRP monoclonal BXP-21 antibody	Abcam Inc, Cambridge, MA, USA
Fluorescein-labeled sheep anti-mouse Ig antibody	Amersham Biosciences, Piscataway, NJ, USA
Bicarbonate buffer (pH 7.5)	Dept. of Radiopharmacy, TGH, Toronto, ON, Canada
Bio P-2 gel (45-90 μm)	Bio-Rad, Mississauga, ON, Canada
Bovine serum albumine (BSA) solution	Sigma-Aldrich, Steinheim, Germany
Bovine serum albumin (BSA) powder	Sigma, Oakville, ON, Canada
Bradford protein assay	Bio-Rad, Hercules, CA, USA
Casy® ton isotonic NaCl solution	Schärfe-Systems, Reutlingen, Germany
Cellstar Vials (15 ml)	Greiner Labortechnik, Frickenhausen, Germany
Cellstar Vials (50 ml)	Greiner Labortechnik, Frickenhausen, Germany
Cellstar Culture Flasks 25 cm^2	Greiner Labortechnik, Frickenhausen, Germany
Cellstar Culture Flasks 75 cm^2	Greiner Labortechnik, Frickenhausen, Germany

Cellstar Culture Flasks 175 cm^2	Greiner Labortechnik, Frickenhausen, Germany
Cell scraper	Greiner Labortechnik, Frickenhausen, Germany
5-CFDA	Sigma, Oakville, ON, Canada
Chloroform	Merck, Darmstadt, Germany
Cover slips for microscope slides	CR Scientific, Lebanon, NJ, USA
Cremophor EL	Sigma Chem. Co, St Louis, MO, USA
Cryovials	Greiner Labortechnik, Frickenhausen, Germany
Cyclosporin A	Sigma-Aldrich, Steinheim, Germany
Daunorubicin	Sigma, Oakville, ON, Canada
DEPC water	Invitrogen, Carlsbad, CA, USA
Dimethylsulfoxide	Promochem GmbH, Wesel, Germany
Disodium hydrogen phosphate x 2 H$_2$O	Merck, Darmstadt, Germany
DMEM-Medium with Glutamax	Sigma-Aldrich, Steinheim, Germany
DMEM-Medium with high Glucose	Sigma-Aldrich, Steinheim, Germany
Doxorubicin	Sigma, Oakville, ON, Canada
Eosin Y	Sigma, Oakville, ON, Canada
Ethanol 96-100 % (V/V)	Merck, Darmstadt, Germany
FACS Flow	Becton-Dickinson, Heidelberg, Germany
FACS Clean	Becton-Dickinson, Heidelberg, Germany
Fetal Calf Serum (FCS)	Sigma, Oakville, ON, Canada
First Strand cDNA synthesis kit	MBI Fermentas, Flamborough, ON, Canada
Fluorescein isothiocyanate (FITC)	Molecular Probes, Invitrogen Canada Inc. Burlington, ON, Canada
Gene Ruler^{TM} (100 bp)	Invitrogen, Carlsbad, CA, USA
Haematoxylin	Fisher Scientific, Nepean, Ontario, Canada
Halothane	MTC Pharmaceuticals, Cambridge, ON, Canada
Heparin	Organo Teknica, Toronto, ON, Canada
Human *MDR1* antisense and random phosphorothioated oligodeoxynucleotides with aminohexyl modifications (5'-end)	Invitrogen, Carlsbad, CA, USA

Hydrochloric acid 37 % (m/V)	Merck, Darmstadt, Germany
Indomethacin	Sigma, Oakville, ON, Canada
Insulin Syringe (1ml) with permanently attached 29g x ½" Ultra-fine Needle (U-100)	BD Canada, Oakville, ON, Canada
Isopropanol 100 %	Merck, Darmstadt, Germany
ITLC-Silica Gel	Gelman, Ann Arbor, MI, USA
Ketamine	Parke-Davis, Scarborough, ON, Canada
L-Glutamin	Sigma-Aldrich, Steinheim, Germany
Mitoxantrone	Sigma, Oakville, ON, Canada
Methanol	Merck, Darmstadt, Germany
MTT (3-(4,5-Dimethylthiazol-2-yl) -2,5-diphenyltetrazoliumbromid)	Sigma-Aldrich, Steinheim, Germany
Novobiocin	Sigma, Oakville, ON, Canada
Nuclease-free purified water	Invitrogen, Carlsbad, CA, USA
PCR primers	DNA synthesis facility, Sick Kids Hospital, Toronto, ON, Canada
Penicillin-Streptomycin-solution Conc. Penicillin: 10000 I.U./ ml	Sigma-Aldrich, Steinheim, Germany
Potassium dihydrogen phosphate	Merck, Darmstadt, Germany
Potassium chloride	Merck, Darmstadt, Germany
Purelab Plus water	USF Reinstwassersysteme, Ransbach-Baumbach, Germany
RPMI 1640-Medium	Sigma-Aldrich, Steinheim, Germany
RPMI 1640-Medium phenolred-free	Sigma-Aldrich, Steinheim, Germany
Sodium acetate buffer (1M)	Dept. of Radiopharmacy, TGH, Toronto, ON, Canada
Sodium azide	Merck, Darmstadt, Germany
Sodium chloride	Merck, Darmstadt, Germany
Sodium citrate buffer (100 mM, pH 5.0)	Dept. of Radiopharmacy, TGH, Toronto, ON, Canada
SuperFect®	Qiagen, Mississauga, ON, Canada
SYBR Gold nucleic acid stain	Molecular Probes, Eugene, OR, USA
Taq polymerase®	MBI Fermentas Inc, Burlington, ON, Canada

[99m]Tc-Sestamibi (Cardiolite[®])	Bristol-Meyers Squibb Medical Imaging, N. Billerica, MA, USA
TRIzol	GIBCO-BR Life Technologies, Gaithersburg, MD,USA
Trypsin-EDTA	Sigma-Aldrich, Steinheim, Germany
Tween 40	Sigma, Oakville, ON, Canada
Verapamil	Sigma-Aldrich, Steinheim, Germany
6-well culture plates (clear)	Greiner Labortechnik, Frickenhausen, Germany
24-well culture plates (clear)	Greiner Labortechnik, Frickenhausen, Germany
96-well culture plates (clear)	Greiner Labortechnik, Frickenhausen, Germany
96-well culture plates (black)	Greiner Labortechnik, Frickenhausen, Germany
WK-X-34, WK-X-50, WK-X-84, XR9577	synthesized by W. Klinkhammer, Laboratory Prof. Dr. M. Wiese, Pharmaceutical Institute, University of Bonn, Bonn, Germany
Xylazine 100 mg/ml	Bayer Inc., Agriculture Division–Animal Health, Etobicoke, ON, Canada

3.1.2   Buffers and Solutions

Blocking-buffer (10 %)

BSA	5 g
Tween 40	50 µl
PBS	ad 50 ml

Cell Culture media

A2780/Adr; A2780/wt

RPMI 1640-Medium	500 ml
FCS	50 ml
Penicillin/Streptomycin	5 ml

MDCK/wt; MDCK-MRP2, MDCK-MRP3, MCF7/wt

DMEM-Medium with Glutamax	500 ml
FCS	50 ml
Penicillin/Streptomycin	5 ml

Hela-MRP1

DMEM-Medium with high Glucose	500 ml
FCS	50 ml
Geniticine	400µg/ ml

MCF7/mx

DMEM-Medium with high Glucose	500 ml
Heat inactivated FCS	50 ml
Penicillin/Streptomycin	5 ml

Dilution Buffer

BSA powder	1 g
PBS	ad 50 ml

Formaldehyde-solution (10 %)

Formaldehyde	5 ml
PBS	ad 50 ml

Isopropanol / HCL-solution

Isopropanol 100 %	50 ml
Hydrochloric Acid 37 %	165 µl

Methanol-solution (90 %)

Methanol	45 ml
PBS	5 ml

MTT-solution

MTT	100.0 mg
PBS-solution	ad 20.0 ml

PBS-(phosphate-buffered-saline) Buffer

Sodium chloride	8.0 g
Disodium hydrogen phosphate	1.14 g
Potassium dihydrogen phosphate	0.2 g
Potassium chloride	0.2 g
Purelab Plus Water	ad 1000 ml

Staining-buffer

Sodium azide	100 mg
BSA powder	500 mg
PBS-solution	ad 100.0 ml

Washing-buffer I

BSA powder	500 mg
PBS-solution	ad 100.0 ml

Washing-buffer II

Tween 20	10 µl
PBS-solution	ad 100 ml

3.1.3   Instruments and Software

ADAC TransCam gamma-camera	ADAC Laboratories Inc, Milpitas, CA
Beckmann Microfuge® Lite Centrifuge	Beckmann Coulter, Fullerton, USA
BioRad Gel Doc system	Bio-Rad Laboratories, Mississauga, ON, Canada
Casy® 1 cellcounter (Model TT)	Schärfe System, Reutlingen, Germany
Cell incubator	WTC Labortechnik, Truttlingen, Germany
Cell Quest Pro™ Software	Becton-Dickinson Bioscience, Heidelberg, Germany
Centrifuge Allegra® 21 R	Beckmann Coulter, Fullerton, USA
DS1D Scientific Imaging software	Eastman Kodak Company, Rochester, New York, USA
FACSCalibur	Becton-Dickinson, Heidelberg, Germany
GeneAmp 2400 thermocycler	Perkin-Elmer, Mississauga, ON, Canada
GraphPad Prism 3.0	San Diego, CA, USA
Kodak DC120 camera	Eastman Kodak Company, Rochester, New York, USA
Laminar-Air-flow workbench	Heraeus, Hanau, Germany
Nikon Eclipse E400 microscope	Nikon, Mississauga, ON, Canada
Packard Cobra® II Series Auto-Gamma Counting Systems	Model 5003, Packard Instrument Company, Meridien, CT, USA
Pegasys™ X, Version 4.2 software	ADAC Laboratories Inc, Milpitas, CA, USA
Polarstar Galaxy Microplate reader	BMG-LABTECH GmbH, Offenburg, Germany

Polytron homogenizer	Kinematica, Littau, Switzerland
Purelab Plus water preparation facility	USF Reinstwassersysteme, Ransbach-Baumbach, Germany
Spectra MAX^{TM} Gemini XS spectrofluorometer	Molecular Devices, Sunnyvale, CA, USA
Ultrasound bath	Bandelin, Berlin, Germany
UV/VIS-spectrometer UltroSpec 2100 pro	Amersham Pharmacia Biotech, Uppsala, Sweden
Vortexer	Vortex, Würzburg, Germany
Waterbath Büchi 461	Büchi, Switzerland
Win MDI software	Verity Software House Inc., Topsham, ME, USA
Zeiss Axiovert 200 Objective LD ACHROPLAN 100x, 63X	CarlZeiss AG, Oberkochen,Germany

3.1.4   MDR inhibitors, chemicals and formulations

The novel MDR inhibitors WK-X-34, WK-X-50 and WK-X-84 (Figure 3.1) were designed in Prof. Dr. M. Wiese's laboratory at the Pharmaceutical Institute, University of Bonn, Germany and synthesized by W. Klinkhammer. All compounds posses a tetrahydroisoquinolin-ethyl-phenyl amine partial structure but differ in the rest of the structure.   WK-X-34, (N-(2-(4-(2-(6,7-dimethoxy-3,4-dihydroisoquinolin-2(1H)-yl)ethyl)   phenylcarbanoyl)phenyl)-3,4-dimethoxybenzamide),   contains   a anthranilic   acid   linker.   WK-X-50   (N-(2-(3-(4-(2-(3,4-dihydroisoquinolin-2(1H)-yl)ethyl)phenyl)ureido) phenyl) quinoline-3-carboxamide) is a diaminobenzene derivative.   WK-X-84   (N-(2-(2-(4-(2-(6,7-dimethoxy-3,4-dihydroisoquinolin-2(1H)-yl)ethyl)phenylamino)-2-oxoethoxy)phenyl)-3,4-dimethoxybenzamide)   is   a   2-(2-aminophenoxy)acetic acid derivative.   These compounds have been kindly made available for this thesis.

XR9577 was synthesized according to the literature (Roe, 1999) by W. Klinkhammer.   Stock solutions (10 mM) of verapamil, XR9577 and the WK-X-compounds were prepared in DMSO and cyclosporin A was prepared in methanol. Stock solutions were further diluted in PBS.

[99m]Tc-Sestamibi was freshly prepared by the Radiopharmacy Department at Toronto General Hospital (UHN, Toronto, Canada) using the reconstituting kits (Cardiolite[®]) and radiochemical purity was routinely determined by thin layer chromatography to be greater than 93 %.

Human *MDR1* antisense and random phosphorothioate oligodeoxynucleotides with aminohexyl modifications at the 5'-end were reconstituted in purified nuclease free water up to a concentration of 1 mg/ml and further diluted in PBS.
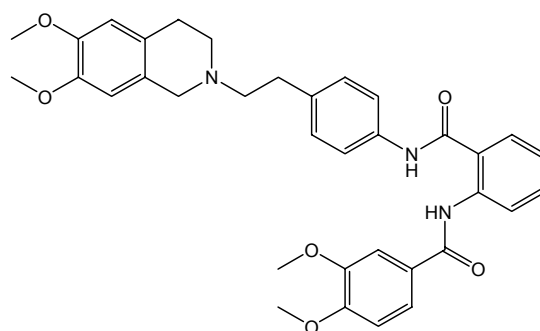
WK-X-34
Mr: 596
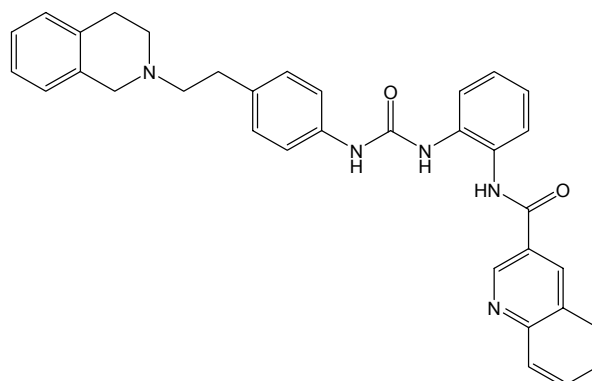
WK-X-50
Mr: 542
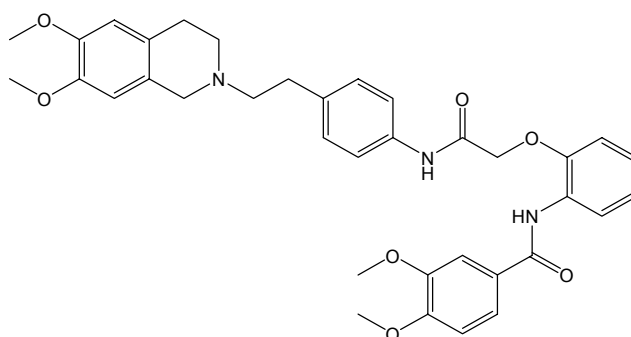
WK-X-84
Mr: 626
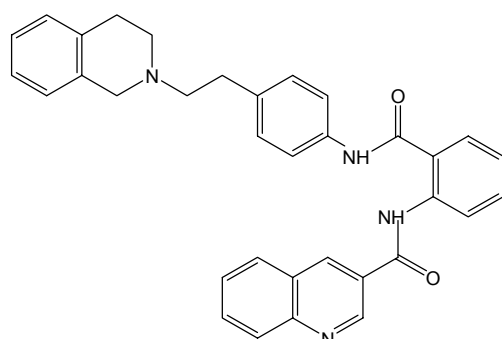
XR9577
Mr: 526

Figure 3.1   Chemical Structures of novel tetrahydroisoquinolin-ethyl-phenylamine-based MDR inhibitors

3.2   Cell culture

3.2.1   Cell lines

Several different wild-type, resistant or transfected tumor cell lines of human or dog origin were used in this thesis. Human ovarian cancer cell line A2780/wt was originally obtained from a drug-sensitive patient with a tumor on one ovary. The Pgp overexpressing and doxorubicin-resistant (= Adriamycin, Adr) variant A2780/Adr had been generated through step-wise selection from its sensitive parental cell line A2780/wt using doxorubicin (see description of cell line at ECACC). Therefore, doxorubicin (10 µM) needed to be added to the media of A2780/Adr cells for one passage every 10 passages in order to prevent cells from losing their high Pgp expression levels. Both cell lines were purchased from ECACC, UK.

The BCRP-overexpressing MCF7/mx cell line was generated by mitoxantrone selection and kindly provided by Dr. E. Schneider, Wadsworth Center, Albany, NY, USA. Human breast cancer cell line MCF7/wt was originally selected from the mammary epithelial tissue of a Caucasian woman with adenocarcinoma.

HeLa cells transfected with human MRP1 were kindly provided by Dr. S. Cole, Queen's University, Kingston, ON, Canada. HeLa cells originate from a cervix carcinoma isolated from a patient named Henrietta Lachs.

MRP2- and MRP3- transfected MDCK (Madin-Darby Canine Kidney) epithelial cells from dog origin were engineered by transfecting them with human MRP2 or MRP3 plasmid. These cells were generated and kindly provided by Dr. P. Borst, the Netherlands Cancer Institute, Amsterdam, Netherlands.

3.2.2   Growing and subculturing of cells

All cell lines used in this thesis are adherent cells, which grow in monolayers. Thus, ordinary culture flasks were utilized. Cells were cultivated in an incubator, which constantly maintained an atmosphere of 37°C and 5 % CO_2. Medium needed to be replaced when the indicator phenolred changed its color from red to yellow,

which occurred about every three days, depending on the density of plated cells and the growth rate of the particular cell line. Cells needed to be subcultured, when the flask was entirely covered with cells (100 % confluency). For subculturing cells were washed once with PBS to remove floating cells and the additives fetal bovine serum and antibiotics. Two ml of trypsin were then added and cells were incubated at 37°C until they separated from each other. Cells were washed off the culture dish and placed into a 15 ml tube. Cells were now separated from trypsin-containing medium by centrifugation (1200 x g, 4 min and 4°C) and resuspended in 10 ml fresh growth medium. One to three ml of cell suspension depending on the cell line were placed into a new culture flask containing fresh growth medium.

3.2.3   Counting cells

20 µl of cell suspension were pipetted into 10 ml of sterile Casy®ton solution and analyzed with the Casy® 1 cell counter. Based on the techniques of a "coulter-counter", this instrument measures the cell number together with the mean cell diameter and can thus provide information on the status and integrity of the analyzed cell population.

3.2.4   Storing, freezing and defrosting cells

To generate long-lasting backups, trypsinized cells from a confluent T75 flask were centrifuged and redissolved in 1 ml growth medium containing 10 % of DMSO. The cell suspension was pipetted into a cryovial. The cryovials were kept in the -80°C freezer for one week and then transferred into a liquid nitrogen tank (-190°C) for storage. Under these conditions, cells can be stored for some years. To re-culture frozen cells, vials were carefully warmed in a 37°C waterbath until cells were defrosted. Cells were then quickly transferred into T25 or T75 culture flasks filled with warm (37°C) fresh growth medium and placed into the incubator. The next day, growth medium was replaced and floating cells were removed.

3.3   *In vitro* methods

3.3.1   RT-PCR analysis

For RT-PCR analysis, RNA needed to be isolated from all cell lines. Total RNA was isolated from a confluent 10 cm^2 Petri dish of cells using the TRIzol extraction kit. Growth medium was removed and one ml of TRIzol was added onto the cells. After 5 min of incubation cells were scraped off the dish and lysed by pipeting up and down. The cell lysates were placed into an eppendorf cap and 0.2 ml of chloroform was added. Caps were shaken and incubated at RT for 10 min. Tubes were then centrifuged at 12000 x g for 15 min and at 4˚C. The upper aquaeous phase containing the RNA was transferred into a clean cap and 0.5 ml of isopropyl alcohol was added. Samples were incubated for 10 min at RT and then centrifuged for 10 min at 12000 x g and 4˚C. At this step, RNA precipitated and formed a gel-like pellet. The supernatant was removed and the pellet was washed with ethanol (75 %). Ethanol was removed by centrifugation at 7500 x g and RNA pellet was air-dried before redissolving it in demineralised autoclaved water containing DEPC. RNA samples were stored at -20˚C.

RNA was quantified using UV-spectrophotometry at 260 nm. 1 µl of RNA-solution was dissolved in 49 µl of DEPC water and RNA concentration in µg/µl was quantified in a UV/VIS-spectrometer UltroSpec 2100 pro at 260 nm. The ratio of RNA/protein (260/280 nm) was furthermore determined and served as an indicator of the quality of the RNA isolation. An RNA quality with a ratio of above 1.5 was accepted for RT-PCR. Ratios between above 1.8 are commonly obtained for highly purified DNA; however the obtained value is strongly dependant on the pH of the solution buffer (Wilfinger, 1997).

MDR1 expression was examined by RT-PCR analysis (Lee, 2001). A quantitative RT-PCR assay was used based on previously reported methods (Hartmann, 2001; Sukhai, 2001). mRNA levels of human *MDR1* were determined and *GapDH* served as a housekeeping gene to normalize *MDR1* expression. Primer sequences and PCR conditions can be found in table 3.1. Reverse transcription of 0.5 µg of RNA was performed using the First Strand cDNA Synthesis kit in a total

volume of 20 µl. One µl of reverse transcription product (see standard curve in chapter 4.1.1.1) was used for amplification of specific DNA sequences in the presence of 1 mM MgCl2, 200 µM dNTP, and 50 pmol of each primer in a total volume of 100 µl DEPC water using a GeneAmp 2400® thermocycler. The reaction was initiated by addition of 2.5 units of Taq polymerase® and amplification proceeded through different cycle numbers, depending on relative expression levels of the genes. The parameters are summarized in table. 3.1.

PCR products were separated on 2 % agarose gels by electrophoresis (150 V, 500 mA, 45 min). Gels were stained with PBS containing SYBR Gold nucleic acid stain (1:10000) and visualized by UV light. DNA band sizes were confirmed using the Gene Ruler 100 bp DNA ladder. Optical densities of bands obtained from agarose gels were quantified on gel pictures taken with a Kodak DC120 camera and DS1D Scientific Imaging software. Linear conditions were established from standard curves. For the generation of standard curves, dilutions containing 5, 2.5, 1.25, 0.625, 0.313, 0.156, 0.078 or 0.039 µl cDNA were prepared and ran using the conditions in table 3.1. Optical densities of bands obtained from the PCR products were plotted against the amount of cDNA template and a cDNA amount within the linear range was chosen for RNA quantifications. Levels of mRNA expression are reported as percentages of normalized values, as compared to control values. Optical densities were normalized to *GapDH* band intensities and calculated as ratios: (OD *MDR1* mRNA) / (OD *GapDH* mRNA). Standard PCR curves were generated for each PCR product to establish linearity of the RT-PCR reaction and determine optimal template concentrations.

The expression of the *MRP1*, *MRP2* and *MRP3* transporters in selectively transfected cell lines was verified by RT-PCR analysis. Likewise, *BCRP* expression in MCF7/mx and lack of *BCRP* expression in MCF7/wt, A2780/Adr and A2780/wt were examined. Primer sequences and PCR conditions for all transporters are given in table 3.1.

Gene name	Primer Sequence	Product size	# cycle	PCR cycle
MDR1	fwd: 5'-GTA CCC ATC ATT GCA ATA GC-3' rev: 5'-CAA ACT TCT GCT CCT GAG TC-3'	237 bp	28 Xen 29	95°C (45 sec) 55°C (120 sec) 72°C (60 sec)
GapDH	fwd: 5'-TCC CAC CAC CCT GTT GCT GTA-3' rev: 5'-TCC CAC CAC CCT GTT GCT GTA-3'	450 bp	26	95°C (60 sec) 54°C (120 sec) 72°C (90 sec)
MRP1	fwd: 5'-AGG TGG ACC TGT TTC GTG AC-3' rev: 5'-ACC CTG TGA TCC ACC AGA AG-3'	183 bp	30	95°C (60 sec) 52°C (120 sec) 72°C (90 sec)
MRP2	fwd: 5'-CTG CCT CTT CAG AAT CTT AG-3' rev: 5'-CCC AAG TTG CAG GCT GGC C-3'	220 bp	28	95°C (60 sec) 54°C (120 sec) 72°C (90 sec)
MRP3	fwd: 5'-GCC ATC GAC CTG GAG ACT GA-3' rev: 5'-GAC CCT GGT GTA GTC CAT GAT AGT-3'	117 bp	30-33	94°C (30 sec) 55°C (30 sec) 72°C (60 sec)
BCRP	fwd: 5'-GGC CTC AGG AAG ACT TAT GT-3' rev: 5'-AAG GAG GTG GTG TAG CTG AT-3'	342 bp	27	94°C (45 sec) 55°C (30 sec) 72°C (90 sec)
18S	fwd: 5'-GTC TGT GAT GCC CTT AGA TG-3' rev: 5'-AGC TTA TGA CCC GCA CTT AC-3'	185 bp	Xen 20	94°C (45 sec) 55°C (30 sec) 72°C (45 sec)

Table 3.1 Primer sequences and parameters for PCR analysis

Fwd: forward primer, Rev: reverse primer. The cycle numbers refer to cell material, unless otherwise indicated (Xen = tumor xenograft).

The primer sequences were based on the following references:

MDR1: Lingya, Chinese Med J 2001; 114:929-932

MRP3: Ros, J of Pathol 2003; 200: 553-560

BCRP: Krishnamurthy, J Bio Chem 2004; 279:24218-24225

All other primer sequences were obtained using the GenBank cDNA sequences and PRIMER3 online software at: http://www-genome.wi.mit.edu/cgi-bin/primer/primer3_www.cgi

3.3.2   Protein expression analysis

P-glycoprotein surface expression in A2780/Adr and A2780/wt control cells before and after antisense treatments was analyzed using an FITC-conjugated mouse anti-human monoclonal Pgp antibody in an assay with flow cytometry detection. The antibody is a 17F9 clone and binds to the surface of the viable, unfixed multidrug resistant cell. The 17F9 epitope is located on the outside of the cell, therefore cells can be analyzed directly without preceding permeabilization.

Attached cells were washed three times with PBS. Two ml of trypsin were added and cells were washed off with growth medium 10 min later. Cells were then counted (see chapter 3.2.3) and aliquots of 10^6 cells were sampled into 15 ml flasks. Samples were washed with 1 ml of washing buffer I (for preparation of buffers and solutions see chapter 3.1.2). Samples were then dissolved in 1 ml of staining buffer and 20 µl of the FITC-labeled anti-human monoclonal Pgp antibody were carefully added to each sample. Tubes were quickly protected from light and incubated on ice for 40 min. To terminate incubation period, cells were washed with 1 ml of ice-cold staining buffer. Unbound antibody was removed from the cell suspension and cells were resuspended in washing buffer I. The amount of antibody-bound FITC on the cell surface per cell was analyzed on the FACSCalibur using an excitation wavelength of 488 nm. Emitted light signals were collected through a 530/15 nm band pass filter for FITC (FL1-H). Acquisition was set to 10,000 events and fluorescence intensities were collected while gating on physical parameters (forward and side scatter) to exclude cell debris. The number of events within the gate for intact cells remained consistently well above 75 % for all measurements. Autofluorescence of A2780/Adr and A2780/wt cells were tested to be identical.

BCRP expression in MCF7/mx and MCF7/wt control cells was analyzed using the primary anti-human BCRP antibody BXP-21 together with a secondary anti-mouse Ig fluorescein-linked whole antibody (Minderman, 2002). The BCRP-specific BXP-21 antibody, a mouse IgG antibody, reacts with an internal epitope of BCRP, therefore, cells needed to be fixed and permeabilized. As previously described, attached cells were trypsinized, counted and aliquots of 10^6 cells in PBS sampled into 15 ml flasks. Cells were then fixed in formaldehyde-solution (10 %) for 10 min at RT and subsequently incubated with an ice-cold methanol-solution (90 %) for

10 min.   After washing with washing-buffer II, cells were incubated with blocking-buffer (10 %) for 1 h at RT.   After thoroughly washing the cells three times with washing-buffer II, 100 μl of a 1:100 dilution of the primary monoclonal antibody BXP-21 (final concentration 2.5 μg/ml) in dilution-buffer were added onto the cells and tubes were placed on ice for 60 min.   To terminate incubation period, cells were washed with 1 ml of ice-cold washing buffer II so that unbound primary antibody was removed from the cell suspension.   100 μl of a 1:50 dilution of the fluorescein-linked anti-mouse IgG antibody in washing-buffer II were added onto the cells.   Tubes were protected from light and incubated for 20 min on ice.   The secondary antibody was removed by washing.   Cells were resuspended in washing buffer II and stored on ice until flow cytometry analysis. The amount of cell-bound fluorescein on the cell surface was detected as previously described for Pgp.   Autofluorescence of MCF7/mx and MCF7/wt cells were tested to be identical.

As A2780/Adr and A2780/wt cell lines do not express BCRP, non-specific binding to the BCRP binding antibody BXP-21 was used to evaluate unspecific binding.   Likewise, as MCF7/mx and MCF/wt cell lines do not express Pgp, non-specific binding to the FITC-labeled anti-human Pgp antibody was used to measure unspecific binding. Minimal non-specific binding was detected for all four cell lines and no differences in fluorescence intensities were detected between the resistant and wild-type cell lines.

3.3.3   Transfections with *MDR1* antisense ODNs

The expression of P-glycoprotein can be specifically inhibited by transient transfection using human *MDR1* antisense oligodeoxynucleotides. Sequences of phosphorothioated oligodeoxynucleotides with aminohexyl modifications at the 5'-end against the promoter region of the human *MDR1* gene were as follows:

Antisense: Aminohexyl-5'-CCA TCC CGA CCT CGC GCT CC-3'

Random: Aminohexyl -5'-GCT CCC CCA CGC GCC TCC AT-3'

(Sequence taken from Alahari et al. 1998 (sequence: ISIS 13758)).

Experiments were carried out with ODN concentrations of 50, 100 and 200 nM according to previously published methods (Jekerle, 2005). For ODN treatments, A2780/Adr and A2780/wt cells were plated onto 6-well plates at a concentration of 33,000 cells per well and allowed to attach and recover for 24 h. Treatment mixtures of different concentrations (50 nM-200 nM) of AS and random ODNs were prepared in 100 μl of growth medium without the additives fetal calf serum and antibiotics. Growth medium without any additives was used for controls. SuperFect® and DNA were then added according to manufacturer's instructions in such a way that the ratio between SuperFect® was 12 μl per 1 μg of DNA. Transfection mixtures were thoroughly vortexted and incubated at RT for 10 min to allow formation of transfection complex. The transfection mixture was added drop-wise onto the cells and plates were placed into the incubator. After 6 h, the transfection medium was removed, cells were washed and fresh growth medium was added. Cells were treated daily on three consecutive days so that the total transfection period was 72 h. After final ODN treatments, nonviable, floating cells were removed by several PBS washing steps. Only viable, attached cells were used for further experiments including antibody staining.

ODN stability, as routinely examined in 37°C tempered PBS containing bovine serum albumin (Takei, 2002), did not detect reduction in stability over a 24 h time period. All samples remained stable under these conditions and no degradation products were detected. As fresh ODN were replaced in the media every 24 h during the treatment periods, this implies that stable ODNs were present over the entire span of the transfection period.

3.3.4   FITC-labeling of *MDR1* antisense ODNs

To evaluate the efficacy of ODN uptake into A2780/Adr and A2780/wt cells during transient transfection, antisense ODNs needed to be labeled with a fluorescent tracer. Fluorescence-labeled ODNs permit to visualize the uptake and intracellular distribution of ODNs. For FITC-labeling of AS ODNs, a 1 mg/ml fluorescein-isothiocyanate solution was prepared in 100 mM sodium bicarbonate buffer (pH 9). 50 μg of aminohexyl-modified antisense ODNs were incubated with

300 μl of fluorescein-isothiocyanate solution (total ratio aminohexyl-group to FITC ratio: 1:100) for 30 min at room temperature in the dark. To separate FITC-labeled ODNs from unbound FITC, ODN material was purified by size-exclusion chromatography on a P-2 column.

Bio P-2 gel consists of fine porous polyacrylamid beads with a grain size between 45 and 90 μm. To prepare the P-2 column, a small piece of glass wool was placed into a Pasteur pipette to seal the bottom. The Pasteur pipette was now filled with P-2 gel, soaked in sodium chloride solution (1 M) for 2 h and washed with 2 ml of saline.

20 μl of ODN solution was loaded onto the P-2 column and saline was slowly added. 17 fractions of 100 μl volume each were collected. The absorbance of the eluated fractions was detected at 495 nm (FITC-chromophore) and 260 nm (DNA) and fractions 10-13, containing the FITC-labeled antisense molecules were pooled and used for uptake experiments (see figure 3.2)
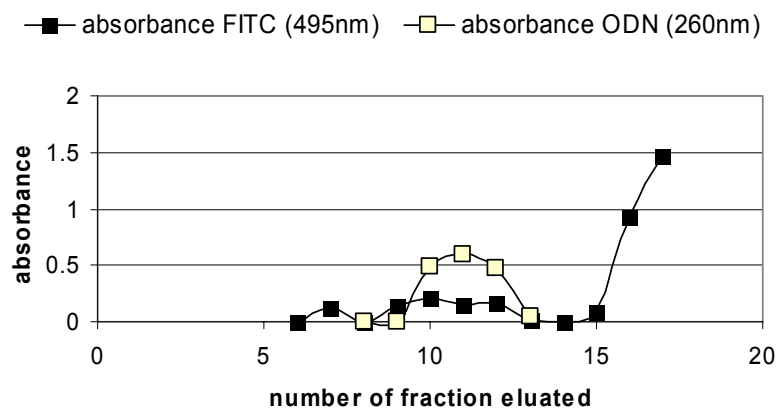
Figure 3.2   P-2 separation of FITC-labeled ODNs from unbound FITC

FITC-labeled ODN material was placed on a P-2 column and eluated in different fractions. The absorbance of the collected fractions was detected at 495 nm (fluorescein-chromophore) and at 260 nm (DNA). The fractions 10 to 13 contain FITC-labeled ODNs as overlapping local maxima can be detected for both curves. Free FITC is eluated after fraction 15.

3.3.5   MTT viability assay

Cellular toxicities of all inhibitors and oligodeoxynucleotides were analyzed in A2780/Adr, A2780/wt and in MCF7/wt and MCF7/mx cells using the methylthiazolyldiphenyl-tetrazolium bromide (MTT) cell viability assay. This assay measures the viability status of the cell after a specific treatment. In viable cells, MTT is reduced by mitochondrial dehydrogenases to the blue formazan precipitate (Figure 3.3). Formazan can be visualized as blue crystals with a light microscope. When solubilized, formazan can also be detected and quantified by absorption measurements at 595 nm.
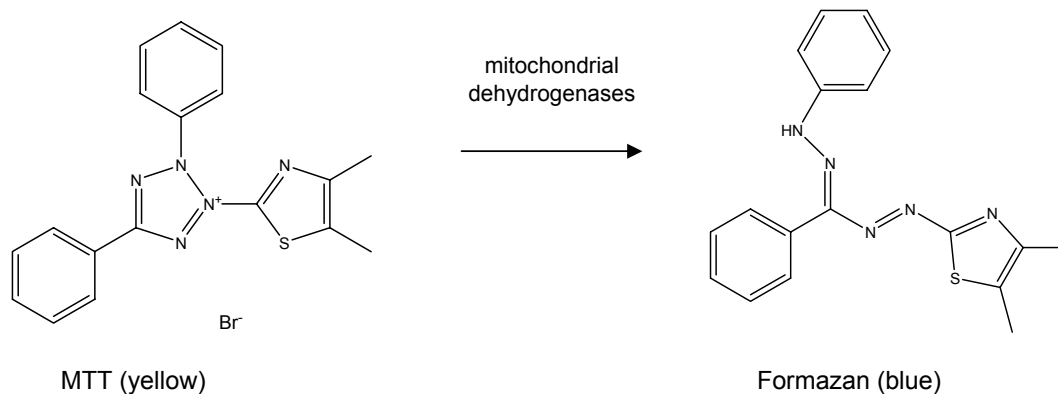
Figure 3.3   Chemical reaction of the MTT assay

Experiments were performed according to previously established methods from our laboratory (Mueller, 2004). Cells were plated onto 96-well plates at a consistent density of 3 x 10^4 cells/well and in a volume of 90 μl. At this initial plating density, cells remained in the exponential growth phase over the entire span of the incubation period (72 h). 10 μl of different concentrations (100 nM-10 mM) of the inhibitor prepared in PBS were added to a total volume of 100 μl and plates were incubated at 37°C and 5 % CO_2 for 72 h. 20 μl of a 5 mg/ml MTT solution (for preparation see chapter 3.1.2) were added to each well. After an incubation period of about 1 h the formation of blue formazan needles became detectable under the light microscope. Cells were then solubilized by adding 150 μl of an isopropanol-HCl

solution and plates were placed into the Polarstar Galaxy Microplate reader. The absorption of solubilized formazan in each well was detected at 595 nm. Values were corrected for background absorbance at 690±6 nm. Cell viability was calculated as a percentage of controls treated only with PBS. EC_{50} values (effective concentration= concentration that produced a 50 % reduction of cell viability) were derived by nonlinear regression analysis, assuming a sigmoidal concentration-response curve using Prism 3.0 software as described in statistical analysis (see chapter 3.3.11). Three independent experiments were performed and the mean value ± S.D. was calculated.

3.3.6   Pgp transport assays

In transport assays the impact of MDR inhibitors on Pgp transport function was studied. Two transport assays with different substrates of Pgp were used. Substrate efflux and substrate accumulation were both examined in the Pgp-overexpressing A2780/Adr cell line in comparison to the drug sensitive A2780/wt cell line.

3.3.6.1 ^{99m}Tc-Sestamibi accumulation assay

^{99m}Tc-Sestamibi (Figure 3.4) is a gamma imaging complex and a substrate of Pgp. The molecule ^{99m}Tc-Sestamibi (^{99m}Tc-hexakis(2-methoxy-isobutylisonitrile) consists of technetium in the 1+ oxidation state bound to six alkyl isonitrile groups in an octahedral geometry (Jones, 1984). In Pgp overexpressing cells, the cellular accumulation of ^{99m}Tc-Sestamibi is depending on the degree of Pgp inhibition and can be easily quantified by gamma counting.

CH$_3$

H$_3$C —— C —— CH$_3$

CH$_2$

N

C

RNC   1+   CNR

Tc

RNC   CNR

CNR

R = CH$_2$C(CH$_3$)$_2$OCH$_3$
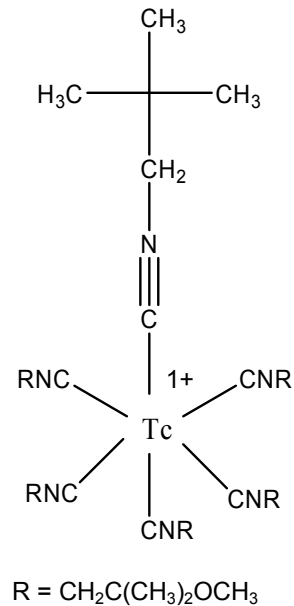
Figure 3.4   Chemical structures of ^{99m}Tc-Sestamibi

The ^{99m}Tc-Sestamibi accumulation assay was carried out according to previously described methods (Utsunomiya, 2000). A2780/Adr and A2780/wt cells were plated into 24-well plates at a constant density of 200,000 cells/well and grown until confluency.   Cells were preincubated with different concentrations of the inhibitors. After 60 min, 15 µl (= 8.25 kBq) of a ^{99m}Tc-Sestamibi solution in PBS (specific activity: 0.55 MBq/ml) were added to each well. ^{99m}Tc-Sestamibi uptake was terminated at different time points (0, 15, 30, 60 min) by washing the cells and subsequently trypsinizing them with 200 µl trypsin. Media and cells were carefully and quantitatively collected and samples were distributed into three 300 µl PCR tubes. Tubes were placed into the Packard Cobra® II gamma counter and counted along with a Cardiolite® standard of known activity.   The relative cellular accumulation (Acc_{Cell}) of ^{99m}Tc-Sestamibi was determined for each well of confluent cells according to *E1*:

$$Acc_{Cell} = \frac{cpm_{cells} \cdot 100}{cpm_{medium}}$$

E1

Furthermore, EC_{50} values for each inhibitor were determined using ^{99m}Tc-Sestamibi accumulation. For determination of EC_{50} values, the transport assay was terminated at 1 h and levels of relative intracellular ^{99m}Tc-Sestamibi were measured. Relative amounts of intracellular ^{99m}Tc-Sestamibi were plotted against the logarithm of the inhibitor concentration and EC_{50} values were derived by nonlinear regression analysis, assuming a sigmoidal concentration-response curve as described in statistical analysis.

Protein content from cell lysates was determined using the Bradford assay. 2 μl of cell lysates were added to 1 ml of Bio-Rad-Protein Assay (1:5 in demineralised water), incubated for 10 min and absorbance at 595 nm was detected in the UV spectrophotometer. Three aliquots of each sample were measured. A BSA standard (1 mg/ml) was prepared in PBS and different amounts of BSA standard (0, 0.5, 1, 2, 4, 8 and 16 μl) were dissolved in 1 ml of Bio-Rad-Protein Assay, incubated for 10 min and absorbance measured. Protein amounts did not differ significantly between wells as confluent wells were used for experiments.

To confirm no involvement of BCRP in ^{99m}Tc-Sestamibi transport across cellular membranes as previously published (Chen, 2000), ^{99m}Tc-Sestamibi accumulation studies were performed in the BCRP expressing MCF7/mx cells.

3.3.6.2   Daunorubicin efflux assay

Efflux assays permit to measure the efflux component separately from all other transport processes. The assay was performed according to previously described methods (Brooks, 2003). A2780/Adr or A2780/wt cells were harvested, counted and 10^6 cells were placed into 15 ml flasks. Cells were washed and incubated in 1 ml phenolred-free RPMI medium containing 3 μM of daunorubicin at 37°C in a shaking waterbath. Brooks and coworkers choose an uptake period of 30 min and an efflux period of 90 min. Using these time intervals, a detection window, sensitive enough to detect significant differences between daunorubicin levels after efflux was confirmed for controls and treated cells (see figure 4.20). Thus, after a 30 min uptake the probe was washed twice with ice-cold PBS to remove free daunorubicin and incubated in fresh and daunorubicin-free medium in

the presence of 0.1, 1 and 10 μM of each inhibitor. After 90 min, efflux was terminated by washing the samples and storing them protected from light on ice. The amount of intracellular daunorubicin per cell after 90 min of efflux was quantified. Daunorubicin levels were measured with the FACSCalibur using an excitation wavelength of 488 nm with detection in the FL-2 channel (585/22 band pass filter). Each data point represents an average of the gated, viable cell population of a total of 5000 cells. Three aliquots were measured per sample and experiments were performed on three separate occasions. Changes in the efflux of daunorubicin which reflects inhibition of Pgp are expressed as the relative amount of Pgp ihibition, calculated as the I_{Pgp} according to *E2*. A derivation of *E2* is described for mitoxantrone efflux in chapter 3.3.7.

$$I_{Pgp} = \frac{\ln\left(c_t\right)_{Mod}}{\ln\left(c_t\right)_{Control}}$$

<div align="right">*E2*</div>

I_{Pgp} = relative inhibition of Pgp

C_t = Intracellular concentration of daunorubicin at time t (90 min)

3.3.6.3   Daunorubicin accumulation assay

In contrast to the efflux assay, the accumulation assay measures the retained amount of daunorubicin in the cell and is depending on uptake and efflux parameters. The assay was performed as previously described and published (Jekerle, 2006a). Likewise, aliquots of 10^6 A2780/Adr or A2780/wt cells were placed into 15 ml flasks, washed and preincubated in 1 ml phenolred-free RPMI medium containing different concentrations (10 nM-0.1 mM) of inhibitor. After 15 min, 3 μM of daunorubicin were added to each sample and tubes were placed in a tempered (37°C) shaking waterbath. When steady state was reached at 180 min, samples were washed and analyzed on a FACSCalibur. The amount of intracellular daunorubicin per cell was quantified using an excitation wavelength of 488 nm with

detection in the FL-2 channel (585/22 band pass filter) and EC_{50} values were determined using GraphPad Prism 3.0 software by nonlinear regression analysis. Data are expressed as the calculated mean value ± S.D. as indicated. The analysis was repeated three times to confirm reproducibility of the obtained value.

3.3.7   BCRP-mediated transport assay

Inhibition of BCRP activity was examined using the BCRP substrate mitoxantrone in a flow cytometry-based efflux assay. The BCRP-overexpressing MCF7/mx cell line (Figure 3.5) was used according to previously published methods (Minderman, 2002).
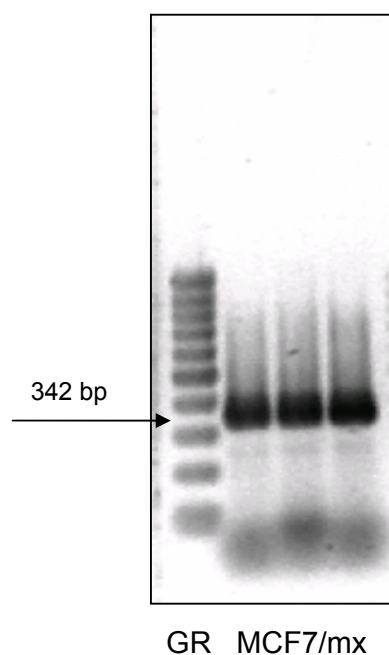
GR   MCF7/mx

Figure 3.5   BCRP expression in MCF7/mx cells

RT-PCR analyses were performed to confirm expression of *BCRP* in mitoxantrone selected MCF7/mx cells. A representative PCR gel is depicted and bands for *BCRP* are visible. The product size of 342 bp was verified using the 100 bp gene ruler (GR).

To evaluate specificity for BCRP, mitoxantrone accumulation was examined in the non-expressing wild-type MCF7/wt cell line. Furthermore, the overexpression of BCRP mRNA and protein and the absence of Pgp were verified using RT-PCR (see chapter 3.3.1) and protein staining (see chapter 3.3.2). MCF7/mx and MCF7/wt cells were harvested, counted and 10^6 cells were sampled into 15 ml flasks with 1 ml of media containing 3 μM of mitoxantrone. Flasks were incubated in a tempered (37ºC), shaking waterbath for 30 min. After mitoxantrone uptake was terminated, an aliquot per each tube was collected. To remove unbound mitoxantrone, cells were washed with ice-cold PBS and media were replaced with mitoxantrone-free media in the presence and absence of various concentrations of the inhibitors (1-1000 μM). The well-established BCRP inhibitor novobiocin (Shiozawa, 2004; Yang, 2003) was used as a positive control. Efflux was terminated after 90 min; cells were washed and redissolved in ice-cold PBS. The amount of intracellular accumulated mitoxantrone after 90 min of efflux was quantified on a FACSCalibur using an excitation wavelength of 488 nm with detection in the FL-4 channel (633 nm). A base fluorescence of fewer than 5 % of all values detected in the presence of mitoxantrone, was measured for all MDR inhibitors. A total of 5000 events per sample were acquired and results were gated for the viable cell population in the forward and side scatter plot. Three aliquots were studied per sample and experiments were performed on three separate occasions. The relative concentration of mitoxantrone retained after 90 min of efflux was calculated using *E6,* which was derived from a basic transport function *E3*:

$$ c_t = c_0 \cdot e^{-k \cdot t} \qquad \longrightarrow \qquad \ln \frac{c_0}{c_t} = k \cdot t \qquad\qquad E3 $$

c_t = intracellular mitoxantrone concentration at time t (y= 90 min)

c_0 = intracellular mitoxantrone concentration at time t_0 (y= 0 min)

k = transport constant (velocity of transport)

t = time of efflux

Transport across the plasma membrane is influenced by two independent determinants: passive diffusion (k_D) and active transport via BCRP (k_a). Hence, the transport constant k is actually the sum of passive diffusion and active transport via BCRP (*E4*). Whereas passive diffusion is thought to be equal in control and treated cells, BCRP-mediated active transport (k_a) is depending on the degree of BCRP inhibition.

$$k = k_a + k_D$$
<div align="right">*E4*</div>

k_a = "active" BCRP-mediated transport

k_D = passive transport via diffusion

By insertion of *E4* into *E3* for control and modulator (Mod) treatment the following equation is obtained (*E5*).

$$\frac{\ln\left(\dfrac{c_0}{c_t}\right)_{Mod}}{\ln\left(\dfrac{c_0}{c_t}\right)_{Control}} = \frac{k_D + k_a \cdot f}{k_D + k_a}$$
<div align="right">*E5*</div>

$f \leq 1$

The factor f indicates the degree of inhibition of mitoxantrone efflux which reflects BCRP-mediated active transport k_a. The smaller f the greater is the inhibition of BCRP activity. As C_0 values could not be measured with reasonable accuracy, C_0 was removed from the equation, assuming an unknown but constant starting concentration, and *E6* was obtained. Results were calculated according to *E6* and the data is expressed as the delogarithmized value of I_{BCRP} for the different MDR inhibitors.

$$I_{BCRP} = \frac{\ln\left(c_t\right)_{Mod}}{\ln\left(c_t\right)_{Control}} \qquad\qquad I_{BCRP} = \frac{k_D + k_a \cdot f}{k_D \cdot k_a}$$
<div align="right">*E6*</div>

3.3.8   MRP-mediated transport assay

5-CFDA (5-carboxyfluorescein diacetate) can be used to quantify effects on MRP-mediated transport. After entering the cells by rapid passive diffusion, the nonfluorescent ester 5-CFDA is hydrolysed by intracellular carboxylesterases and forms the fluorescent moiety 5-CF, which is a specific substrate of the MRP transporters (Figure 3.6).

5-carboxyfluorescein diacetate (5-CFDA)   5-carboxyfluorescein (5-CF)
non-fluorescent   fluorescent anion and MRP substrate
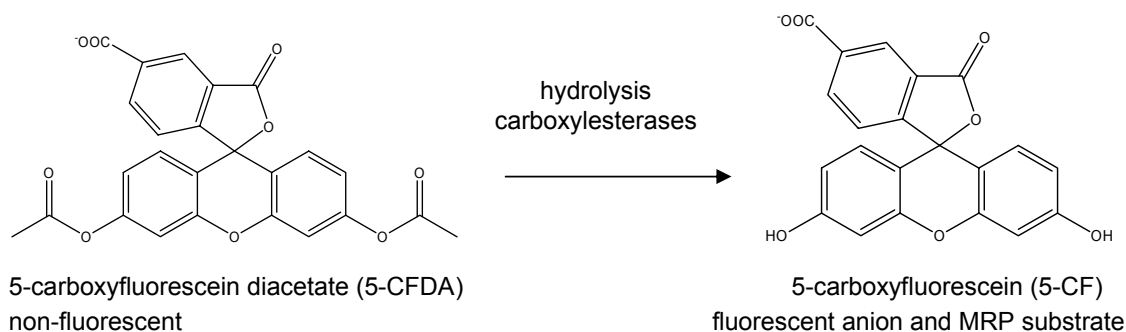
Figure 3.6   Chemical reaction of the 5-CFDA assay

For the 5-CFDA assay selectively transfected HeLa-MRP1 cells and MDCK-MRP2 and –MRP3 cells were used. Wild-type MDCK cells served as a negative control and the WK-X-compounds, XR9577, verapamil and cyclosporine A were examined. The assay was performed according to previously described methods (Lee 2001). Confluent cells were preloaded with 4 µM of 5-CFDA for 30 min. Cells were then washed and 5-CFDA containing medium was replaced with 5-CFDA-free media in the presence and absence of the inhibitors (10 or 200 µM). As selectively transfected cell lines were used, the concentration necessary to obtain significant MRP inhibition for MRP1, MRP2 and MRP3 was relatively high. To date, no highly effective and multi-functional MRP inhibitors could be identified. Therefore, the well-established but fairly unspecific MRP inhibitor indomethacin was used at commonly-used concentration of 200 μM (Draper, 1997) in order to obtain sufficient inhibition to characterize all three MRP subtypes. Therefore, the concentrations of the MDR inhibitors needed to be adjusted to 10 and 200 μM.

Efflux was terminated after 5 min; incubation medium was removed and cells were washed two times with ice-cold PBS. Cells were then lysed with 1 ml of 1 % Triton solution. Three aliquots of cell-lysates per well were sampled (200 μl) into individual wells of a black 96-well plate and plates were protected from light. 5-carboxyfluorescein (5-CF) fluorescence per well was detected with the Spectra MAX^{TM} Gemini XS spectrofluorometer at an excitation wavelength of 490 nm and an emission wavelength of 540 nm. Values were normalized for background fluorescence and calculated as mean values ± S.D.

The selective expression of human MRP1, MRP2 and MRP3 in each genetically engineered cell line was verified by RT-PCR analysis. Conditions are presented in table 3.1. As presented in figure 3.7, the presence of the artificially introduced human genes *MRP1, 2* or *3* were confirmed in the respective transfected cell lines

183 bp

HeLa-MRP1   GR   **A.**

240 bp

117 bp

MDCK-MRP3   GR   MDCK-MRP2

B.
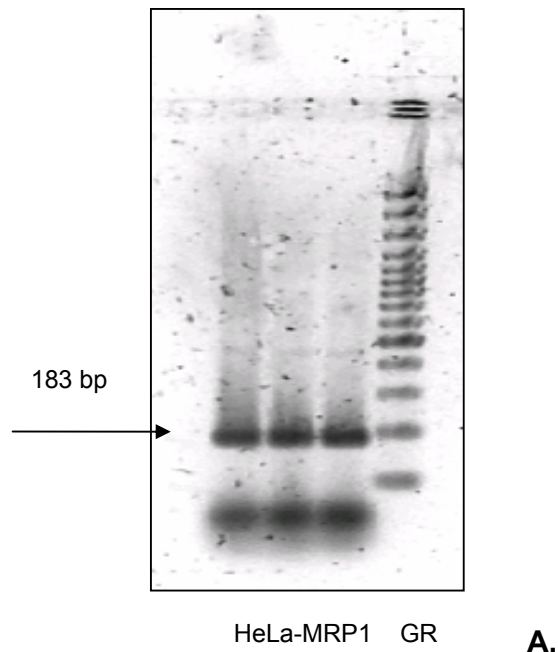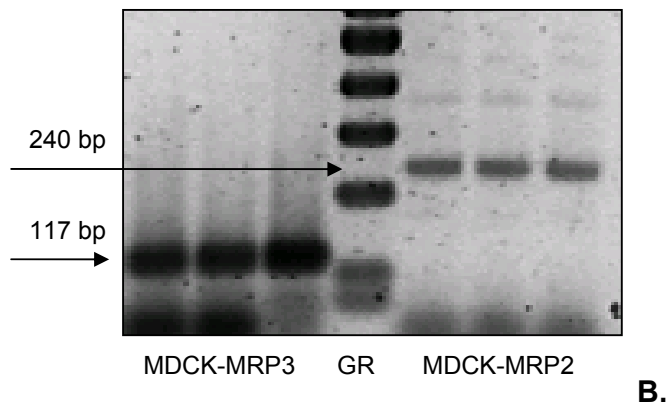
Figure 3.7   MRP1, MRP2 and MRP3 expression in HeLa-MRP1, MDCK-MRP2 and -MRP3 cells.

RT-PCR analyses were performed to confirm expression of MRP1 in HeLa-MRP1 cells **(A)** and MRP2 and MRP3 in MDCK-MRP2 and MDCK-MRP3 cells, respectively **(B)**. Experiments were performed as specified in 3.3.1. Representative PCR gels show bands for MRP1 (183 bp), MRP2 (220 bp) and MRP3 (117 bp). Product sizes were confirmed using the 100 bp gene ruler (GR).

3.3.9   Chemosensitivity assay

In contrast to transport assays, chemosensitivity assays are a measurement of the overall MDR phenotype towards the examined chemotherapeutic drug such as daunorubicin or mitoxantrone.

Chemosensitivity assays were used to characterize the degree of resistance of the MDR cell lines towards the chemotherapeutic agents used to select the MDR phenotype.   Hence, Pgp-overexpressing A2780/Adr cells, initially selected using doxorubicin, were tested for sensitivity towards doxorubicin and BCRP-overexpressing MCF7/mx cells, select in the presence of mitoxantrone, were tested for sensitivity towards mitoxantrone (Jekerle, 2006b).   The degree of resistance towards these selecting agents was quantified for the MDR cell line and the parental cell. EC_{50} value, derived by nonlinear regression analysis (see chapter 3.3.11), permitted to calculate a resistance factor (RF) using equation $E7$:

$$RF = \frac{EC_{50}\ (MDR)}{EC_{50}\ (sensitive)}$$

E7

RF = Resistance factor

Chemosensitivity assays were used as a functional assay to examine the ability to reverse MDR by different MDR inhibitors. The A2780/Adr, A2780/wt and MCF7/mx with MCF7/wt cells were employed to investigate inhibition of the MDR phenotype by WK-X inhibitors. Cells were harvested, counted and 3×10^{4} cells/well were plated into 96-well plates. Cells were preincubated in a total volume of 90 μl of media containing 10 μM of the inhibitor or PBS for one hour. 10 μl of different concentrations of daunorubicin or mitoxantrone (100 nM-10 mM) were added to the cells and plates were stored in the incubator. After 72 h, the assay was continued according to the MTT assay as described in chapter 3.3.5. From MTT results, EC_{50} values were derived by plotting the absorption values against the logarithm of the daunorubicin or mitoxantrone concentration. Nonlinear regression analyses were performed with sigmoidal concentration-response curve using GraphPad Prism 3.0 Software. EC_{50} concentrations for sensitivity towards daunorubicin were expressed in micromole (μM) and EC_{50} concentrations for sensitivity towards mitoxantrone were expressed in nanomole (nM). A sensitizing factor (S.F.) was calculated by dividing the EC_{50} obtained in the presence of inhibitor by the EC_{50} in the absence of inhibitor (control) for each cell line. The sensitizing factor (S.F.) describes the factor by which the chemosensitivity of the specific cell line towards daunorubicin/ mitoxantrone increases in the presence of 10 μM of inhibitor. A ratio of sensitizing factors (S.F.$_{Adr/wt}$; S.F.$_{mx/wt}$) was calculated in order to normalize for Pgp- or BCRP-specific effects, respectively. S.F.$_{Adr/wt}$; S.F.$_{mx/wt}$ were calculated by dividing the S.F. of the Pgp- or BCRP-expressing cell line by the S.F. of the non-expressing wild type cell line. All experiments were performed at least in triplicates on three independent occasions.

3.3.10   Cellular examinations with fluorescence microscopy

Uptake of fluorescence-labeled ODNs on the one hand and daunorubicin in the presence or absence of inhibitor or antisense treatment on the other hand were examined by fluorescence microscopy.

Glass supports were placed into 6-well plates, and A2780/wt and A2780/Adr cells were grown on these glass supports. At 60 % confluency, cells were treated with 200 nM of FITC-labeled *MDR1* antisense ODNs for three hours. For nuclear morphology analysis, cells were additionally incubated with a 1 μg/ml DAPI (4'-6-Diamidino-2-phenylindole) solution in PBS for 5 min. DAPI forms a fluorescent complex with natural double-stranded DNA. Therefore, DAPI is commonly used to visualize cell nuclei. Cells were washed and examined in the FITC, DAPI and light channel under a 100x1.30 oil immersion objective using the Nikon Eclipse E400 microscope. Exposure time for fluorescent light pictures was set to 8 seconds.

Functional inhibition of Pgp-mediated efflux of daunorubicin (3 μM) was visualized both, in the presence of 10 μM of WK-X-34 and in *MDR1* antisense (200 nM) treated cells, by fluorescence microscopy. Cells analyzed under the microscope were treated as described in chapter 3.3.6.3 ("Daunorubicin accumulation assay") and chapter 3.3.3 ("Transfection with *MDR1* antisense ODNs"). Antisense and WK-X-34 treated cells were incubated with 3 μM of daunorubicin for 60 min. Finally, cells were washed with ice-cold PBS to remove unbound daunorubicin and redissolved in PBS. Samples were protected from light and stored on ice. 5 μl of the cell suspension were pipetted onto a microscopy glass support, covered with a glass cover plate and placed under a Zeiss Axiovert 200 fluorescence microscope. Cells were examined at an excitation wavelength of 485 nm using an oil immersion 63x objective.

3.3.11   Statistical analysis

All *in vitro* cell accumulation and efflux studies were performed at least in triplicate on three separate occasions. Data are reported as mean values ± S.D. and calculated with Microsoft Excel® software. For cell experiments the unpaired two-tailed Student's *t*-test was used for statistical comparison between the treatment

group and the control group. A p-level of $\alpha < 0.05$ was considered statistically significant and is indicated by *; a p-level of $\alpha < 0.01$ is indicated by **.

EC_{50} values (=effective concentration for 50 % of the measured effect) were calculated for results obtained from the Pgp transport assays (^{99m}Tc-Sestamibi accumulation and daunorubicin accumulation) and for the BCRP-mediated mitoxantrone efflux assay. Moreover, data obtained from MTT viability assays such as *in vitro* toxicity and chemosensitivity data was expressed as EC_{50} values. EC_{50} is the concentration required to reduce the measured effect. The measured effect can be either a transport function (e.g. Pgp efflux or accumulation) or a reduction in cell viability caused by a cytotoxic drug (e.g. MTT assay, chemosensitivity assay). In MTT assays, EC_{50} is the concentration required to reduce the cell viability (e.g. cell proliferation) by 50 %. EC_{50} values were generated according to the mathematical model of concentration-response relationships by nonlinear regression using GraphPad Prism 3.0 Software. Classical concentration-response relationships apply to agonist-receptor binding phenomenons and can be extended for other biological binding events such as transporter binding. Standard concentration-response curves are defined by four parameters: the baseline response (Bottom), the maximum response (Top), the slope (Hill slope) and the drug concentration that provokes 50 % of the maximum response (EC_{50}). For nonlinear regression analysis, these parameters are incorporated in the so called "Four parameter logistic equation", which is derived from the Hill equation (*E8*):

$$Y = Bottom + \frac{Top - Bottom}{1 + 10^{\log EC_{50} - \log X \cdot HillSlope}} \qquad\qquad E8$$

Bottom =baseline response

Top =maximum response

Hill Slope = slope at the turning point

EC_{50} = drug concentration, that provokes 50 % of the maximum response

As experiments were conducted on three separate occasions, three EC_{50} values were obtained. The data is expressed as mean values ± S.D. Concentration-

response curves were normalized to top and bottom values for inhibition of Pgp- or BCRP-mediated transport activity and to top values only for MTT assays.

3.4   *In vivo* methods

3.4.1   Experimental setup of ^{99m}Tc-Sestamibi imaging studies

The effects of WK-X-34 and *MDR1* antisense ODN treatments on the accumulation of the Pgp substrate ^{99m}Tc-Sestamibi in multidrug resistant and sensitive tumor xenograft models were evaluated in two separate sets of imaging experiments.

3.4.1.1   WK-X-34 imaging

In a series of studies, the impact of the novel 3rd generation Pgp inhibitor WK-X-34 on the accumulation of ^{99m}Tc-Sestamibi was evaluated in resistant and sensitive tumors. Furthermore, the potential inhibition of physiological Pgp in the organs liver, kidney, brain, intestine and heart was investigated. The experimental design of this study is depicted in figure 3.8. Human ovarian cancer xenografts were developed in such a way that mice were bearing a sensitive (A2780/wt) tumor on the left flank and a Pgp overexpressing resistant (A2780/Adr) tumor on the right flank. The same animal was injected with ^{99m}Tc-Sestamibi and imaged twice on two consecutive days. On Day 1, mice were preinjected with vehicle (control) 1 h prior to the injection and imaging of ^{99m}Tc-Sestamibi. On Day 2, mice were preinjected with 20 mg/kg of WK-X-34 prior to the injection and imaging of ^{99m}Tc-Sestamibi. This way, the changes in ^{99m}Tc-Sestamibi accumulation between control and WK-X-34 treatments could be directly compared in the same tumors and tissues of the same animal. Animals were imaged 15 min, 30 min, 1 h, 2 h and 4 h postinjection. After imaging experiments mice were sacrificed and tissues isolated for biodistribution analysis and examinations of *MDR1* mRNA and Pgp expression.
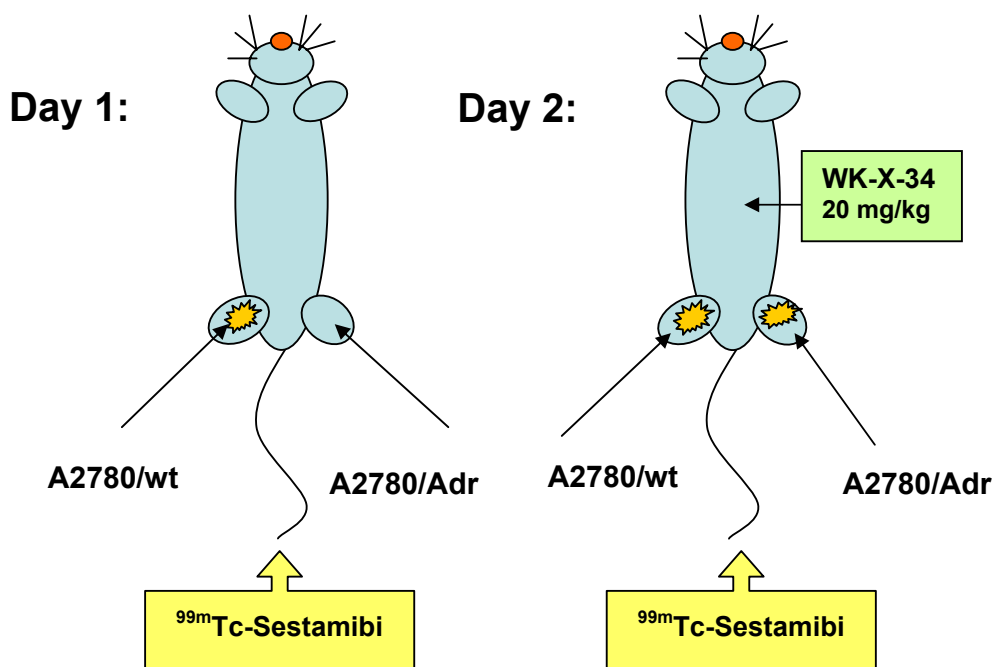
Figure 3.8   Schematic presentation of experimental design for ^{99m}Tc-Sestamibi imaging of "WK-X-34 imaging studies" in the absence (Day 1) and presence (Day 2) of WK-X-34.

3.4.1.2   WK-X-34 + antisense imaging

The impact of Pgp downregulation caused by antisense treatments alone and in combination with WK-X-34 was examined by determining the tissue uptake of ^{99m}Tc-Sestamibi into the resistant and sensitive tumor xenografts. The experimental design of this study is depicted in figure 3.9. Here, human ovarian cancer xenografts were developed in such a way that mice were bearing two resistant (A2780/Adr) tumor on each back flank. One tumor of each animal was randomly selected for antisense treatment. The selected tumor was treated with 200 μg of human *MDR1* antisense ODNs intratumorally on three consecutive days. The animals were then randomly divided into two groups: a verum and a control group. After antisense treatments, the control group received an i.p. injection of vehicle (control) 1 h prior to the injection and imaging of ^{99m}Tc-Sestamibi. Animals in the WK-X-34 group were preinjected with 20 mg/kg of WK-X-34 prior to the injection and imaging of ^{99m}Tc-Sestamibi. Animals were imaged 15 min and 1 h postinjection. After imaging

experiments were terminated mice were sacrificed and tissues were isolated for biodistribution analysis and examinations of *MDR1* mRNA and Pgp expression.

Day 4:
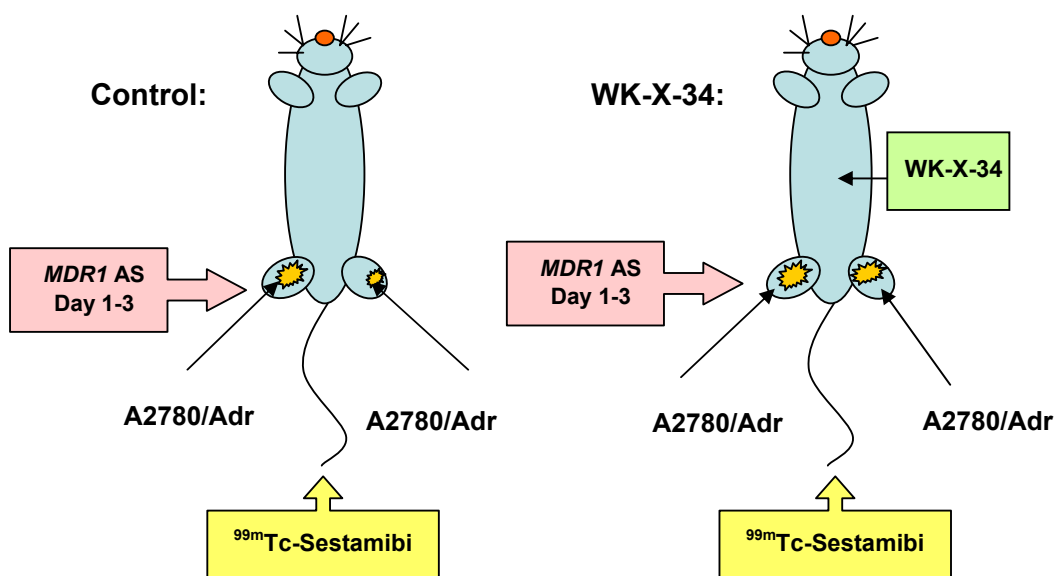
Figure 3.9   Schematic presentation of experimental design for ^{99m}Tc-Sestamibi imaging of "WK-X-34 + antisense imaging studies". In all animals, one of two A2780/Adr tumors on the back flanks was treated with *MDR1* antisense (AS) ODNs for three days prior to imaging experiments. Imaging was performed on Day 4 in the absence (Control) and presence (WK-X-34) of WK-X-34.

3.4.2   Animals

All animal studies were conducted in accordance with the guidelines of the Canadian Council on Animal Care. Eight-week-old male CD1 mice (25-35 g) and five week old female BalbC nu/nu mice (20-25 g) were supplied by Charles River (St. Constant, QC, Canada).

The coat-color white albino CD1 mice originate from a non-inbred stock in the laboratory of Dr. de Coulon, Centre Anticancereux Romand, Lausanne, Switzerland and were imported into the United States to the Rockefeller Institute in 1926.

BalbC nu/nu immunodeficient mice have initially been developed at Charles River Japan. The mice are hairless and have albino background. The inbred

animals lack a thymus and are T-cell deficient. Five-week old male CD1 nu/nu mice (20-25 g) were obtained from the breeding colony, established by breeding pairs of homozygous male CD1 nu/nu mice and heterozygous female CD1 nu/wt (Charles River, St. Constant, QC) mice. This breeding colony was initiated by Prof. Dr. M Piquette-Miller at the Department of Comparative Medicine at the Faculty of Medicine, University of Toronto. The colony was developed and maintained by V. Vassileva from the Department of Pharmaceutical Sciences, University of Toronto.

In vivo work using wild-type CD-1 mice was carried out in the animal facility at the Leslie Dan Faculty of Pharmacy, University of Toronto, Canada. Immunocomprimized BalbC nu/nu and CD1 nu/nu mice were maintained in a pathogen-free environment using sterile working techniques only. These studies were carried out at the Department of Comparative Medicine at the Faculty of Medicine, University of Toronto and at the Animal Facility of the Toronto General Hospital, UHN, Toronto.

3.4.3   Xenograft model

For "WK-X-34 imaging studies" (see chapter 3.4.1.1) drug resistant and drug sensitive xenografts were established in the right and left flank regions of BalbC nu/nu mice by subcutaneous implantation of A2780/Adr and A2780/wt cells, respectively (see 1. in figure 3.10). Cell injections were prepared with an amount of 5×10^6 cells in an injection volume of 100 µl. Cells were harvested, counted and washed two times using PBS. The pellets were resuspended in 100 µl of RPMI medium without FCS and antibiotics. After cleaning the skin with alcohol, tumor cell suspensions were injected s.c. using a 1 ml insulin syringe. Mice were injected randomly to avoid any errors resulting from inconsistencies during cell harvesting etc. Animals were monitored daily and tumor weights estimated by calliper measurements (*E9*):

$$Tumor\ weight = (length \times width^2) / 2 \qquad\qquad E9$$

For "WK-X-34 + antisense imaging studies" (see chapter 3.4.1.2), murine xenograft models were established in the right and left flank region of male CD1 nu/nu mice (see 2. in figure 3.10). 5×10^6 A2780/Adr cells in an injection volume of 100 µl were subcutaneously implanted into each back flank. For tumor inoculations and development of tumors see Pictures 1, Appendix.

1. WK-X-34 imaging:	A2780/wt	A2780/Adr	(BalbC nu/nu mice)
2. Antisense ODN			
+ WK-X-34 imaging:	A2780/Adr	A2780/Adr	(CD1 nu/nu mice)
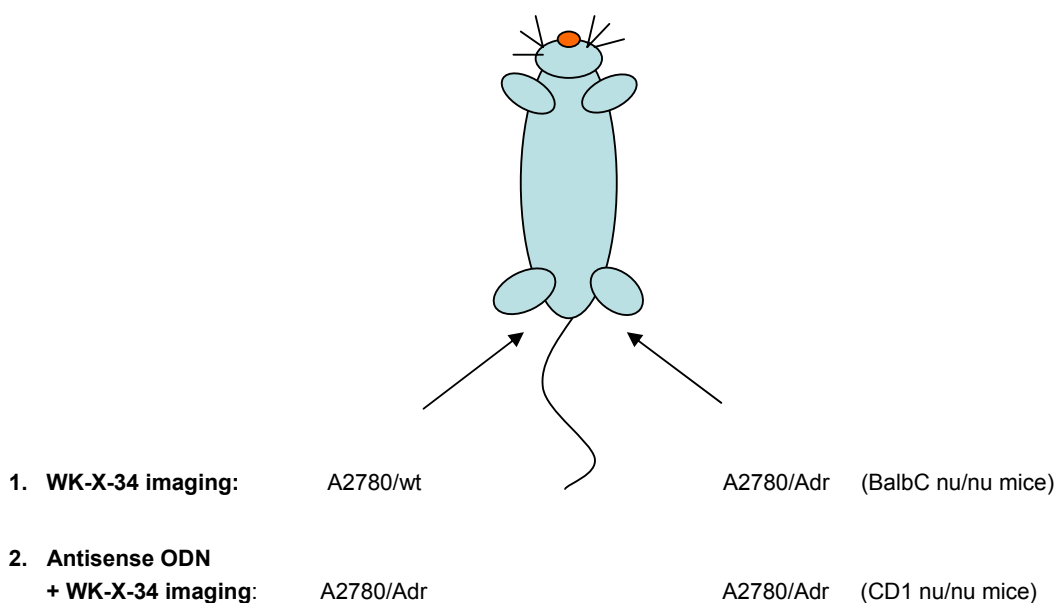
Figure 3.10   Experimental setup for A2780/Adr and A2780/wt xenografts

3.4.4   Formulation and toxicity of WK-X-34

For the *in vivo* application of WK-X-34, a formulation in Cremophor EL was chosen. Cremophor EL is a white viscous liquid with an approximate molecular weight of 3000 Da. It is produced by a reaction of castor oil with ethylene oxide at a molecular ratio of 1:35. Castor oil, a yellowish fixed oil, can be obtained from the seeds of *Ricinus Communis* (Euphorbiacea). The poly-hydroxylated castor oil has a highly variable composition of mainly oxyethylated triglycerides of ricinoleic acid (Van Zuylen, 2001) (Figure 3.11). Cremophor EL is commonly used to solubilize highly

hydrophobic compounds such as paclitaxel for *in vivo* use and clinical applications. However, Cremophor EL is associated with some toxic effects and hepatotoxicity in animals (Le Garrec, 2004) and humans (e.g. hyperlipidemia, peripheral neuropathy) (Gelderblom, 2001; Jie, 2005).

$$CH_2\text{-}O\text{-}(CH_2\text{-}CH_2\text{-}O)_x\text{-}CO\text{-}(CH_2)_7\text{-}CH=CH\text{-}CH_2\text{-}CHOH\text{-}(CH_2)_5\text{-}CH_3$$

$$CH\text{-}O\text{-}(CH_2\text{-}CH_2\text{-}O)_y\text{-}CO\text{-}(CH_2)_7\text{-}CH=CH\text{-}CH_2\text{-}CHOH\text{-}(CH_2)_5\text{-}CH_3$$

$$CH_2\text{-}O\text{-}(CH_2\text{-}CH_2\text{-}O)_z\text{-}CO\text{-}(CH_2)_7\text{-}CH=CH\text{-}CH_2\text{-}CHOH\text{-}(CH_2)_5\text{-}CH_3$$

$$(x + y + z \sim 35)$$
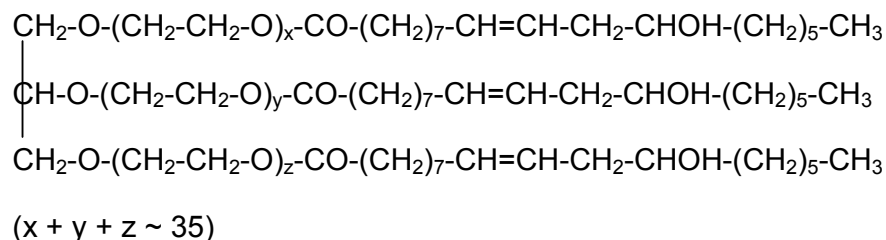
Figure 3.11   Chemical structure of the major component of Cremophor EL

Therefore, WK-X-34 in a formulation with Cremophor EL had to be carefully examined for potential toxic effects in mice. For toxicity evaluations, doses of 20 and 50 mg/kg of WK-X-34 in a total injection volume of 100 μl were prepared. A stock solution of 0.025 mg/μl in a 1:1 mixture of Cremophor EL ethanol was made. Mice were weighted, marked and amounts of WK-X-34 stock solution for each animal receiving either 20 mg/kg or 50 mg/kg were calculated. Amounts of WK-X-34 – Cremophor EL ethanol (1:1) stock solutions for each mouse were further diluted in saline to a final treatment volume of 100 μl. For example, a mouse in the 50 mg/kg treatment group with a body weight of 20.5 g received a dose of 41 μl WK-X-34 stock solution further diluted by 59 μl of saline. Control animals received Cremophor EL ethanol (1:1) dilution in saline only. In the 20 mg/kg WK-X-34 preparation as well as in the vehicle formulation, the amount of Cremophor EL ethanol (1:1) was increased so that animals in all treatment groups received the same amount Cremophor EL ethanol (1:1).

In vivo toxicities of the WK-X-34 formulations in Cremophor EL ethanol (1:1) were studied in 8-week old male CD1 mice. The animals were injected i.p. daily with a 100 µl containing a dose of 20 or 50 mg/kg of WK-X-34; control mice received the vehicle.   Mice   were   examined   for   general   toxicities   using   common   toxicity

measurements including behavioural observations and weight recordings (Delaney, 2002).

The widely applied alanin aminotransferase (ALT) assay was used to study potential hepatotoxicity of WK-X-34. The ALT test is a blood test that measures levels of alanin aminotransferase, a liver enzyme that is produced in higher amounts when the liver is inflamed. The reaction is initiated by the addition of α-ketoglutarat as a second reagent (ALT reagent). The concentration of NADH is measured by its absorbance at 340 nm, and the rate of absorbance decrease is proportional to the ALT activity. High levels of ALT due to acute hepatitis, for example, are indicated by a rapid transformation of the ALT reagent. Thus, a loss in absorption can be detected.

Animals were monitored daily, behaviour was observed and body weights were recorded. On day 14, mice were sacrificed by cervical dislocation and blood samples were obtained by heart puncture using a needle pretreated with heparin. Blood plasma was obtained by centrifuging the blood samples immediately at 6000 G at 4°C for 10 min. The plasma in the supernatant was carefully removed and cooled on ice. 50 µl of blood plasma were incubated in 450 µl of 37°C warm ALT reagent for 1 min. Samples were quickly transferred into the UV-spectrophotometer and absorption was detected at 340 nm at 0 sec, 30 sec and 60 sec. The absorption was plotted against the time and the loss of absorption over time. A significantly stronger loss of absorption expressed as the negative slope in the treatment groups versus controls indicates hepatotoxicity of the treatment.

3.4.5   Treatment of xenografts with WK-X-34

On Day 2 of the "WK-X-34 imaging studies" (see chapter 3.4.1.1) and on Day 4 of the "WK-X-34 + antisense imaging studies" (see chapter 3.4.1.2), animals were treated with a dose of 20 mg/kg WK-X-34 in the formulation with Cremophor EL-ethanol 1 h prior to the injection of ^{99m}Tc-Sestamibi. Control mice received the vehicle containing Cremophor EL-ethanol. For preparation of the doses, the mice were weighted. Doses of 20 mg/kg of WK-X-34 in a total injection volume of 100 µl were prepared. Amounts of WK-X-34 in Cremophor EL ethanol (1:1) stock solutions

for each mouse were further diluted with saline up to the final injection volume of 100 μl. Mice had a fairly constant weight of around 15 g; therefore doses ranged around 0.3 mg WK-X-34 per animal. A stock solution of 3 mg WK-X-34 was prepared in a total volume of 200 μl. 20 μl of stock solution were then further diluted in 80 μl of saline to obtain a total injection volume of 100 μl. WK-X-34 formulations were freshly prepared before each animal experiment.

3.4.6   Treatment of xenografts with antisense ODNs

For "WK-X-34 + antisense imaging studies" (see chapter 3.4.1.2), animals were treated with antisense ODNs on three consecutive days. On Day 4, imaging experiments were performed.

When tumor xenografts reached a weight of approximately 0.5 g, one tumor per animal was randomly selected for antisense treatments. Lyophilised antisense ODNs were dissolved in saline to a final concentration of 2 μg/μl.   On three consecutive days at the same time of the day, tumors were locally injected with 100 μl (200 μg) of antisense ODN-solution, containing 200 μg of DNA or vehicle as previously described (Kuss, 2002).

3.4.7 ^{99m}Tc-Sestamibi imaging

^{99m}Tc-Sestamibi imaging studies were performed according to previously reported methods (Muzzammil, 1999). Mice were injected with 5 MBq of ^{99m}Tc-Sestamibi into one of the lateral tail veins (see picture 2, Appendix). The animals were subsequently anaesthetized with an i.p. injection of a mixture of ketamine and xylazine. When the animal needed additional anaesthetic in order to keep it in deep anaesthesia, a tube containing a tissue soaked with halothane was prepared and opened in front of the animal's head for occasional inhalation.   For picture acquisition, the animal was placed on the imaging counter in such a way, that all legs were stretched away from the torso. Dorsal views were obtained at 15 min, 30 min, 1 h, 2 h, and 4 h post-injection ("WK-X-34 imaging studies"; see chapter 3.4.1.1) or 15 min and 1 h post-injection ("WK-X-34 + antisense imaging studies"; see chapter

3.4.1.2) of the radiopharmaceutical using a small field-of-view gamma-camera ADAC TransCam™ equipped with a pinhole collimator (4 mm aperture). Static images were acquired for 5 minutes at earlier imaging time points and up to 20 minutes for later time points. At later time points, the radioactivity of ^{99m}Technetium was reduced, due to its relatively short half life of about 6 h. Therefore, acquisition time needed to be extended at later imaging time points in order to obtain images with the same number of total counts. Images were acquired into a 256 × 256 matrix with a 32 keV (22.8 %) window set around the 140 keV photopeak of ^{99m}Technetium.

As described in chapter 3.4.1.1, the design of the "WK-X-34 imaging studies" required injection of ^{99m}Tc-Sestamibi and imaging on two consecutive days. Although ^{99m}Tc-Sestamibi is rapidly eliminated from the system, whole body images were acquired prior to the second dose of ^{99m}Tc-Sestamibi to ensure minimal contribution of residual radioactivity. ^{99m}Tc-Sestamibi levels detected on Day 2 were less than 2 % of the original dose see picture 4, Appendix. After completion of imaging experiments, mice were sacrificed by cervical dislocation and dissected. Tumors were used for biodistribution studies and kept for immunohistochemistry and RT-PCR analysis.

3.4.8   Analysis of ^{99m}Tc-Sestamibi images

All images were analyzed with Pegasys™ X, Version 4.2 software. In "WK-X-34 imaging studies" (see chapter 3.4.1.1) regions of interest were drawn around the whole body, brain, heart, liver, right kidney, intestine, and both tumors (Picture 5, Appendix). In "WK-X-34 +antisense imaging studies" (see chapter 3.4.1.2) regions of interest were drawn around the whole body and both tumors. Organ regions (e.g. heart) were identified by varying the radio intensity. ^{99m}Tc-Sestamibi organ uptake (Up_{Tc}) from each region was expressed as counts/pixel/acquisition time in seconds (cts/pix/sec) and then normalized to the region of the whole body and corrected for background radiation (Wang, 2005). The total amount of administered ^{99m}Tc-Sestamibi is represented in the whole body region. Additional corrections were made for radioactive decay (At) at every imaging time point (t_{min}) using equation *E10* and *E11*:

$$A_t = A_0 \cdot e^{(Dc \cdot t)}$$

E10

A_t = Activity at time t

A_0 = Activity at time 0 min

e = base of natural logarithm

t = elapsed time

D_c = Decay constant

$$Dc = \frac{(\ln 2)}{t^{\frac{1}{2}}}$$

E11

$\ln 2$ = natural logarithm of 2 (=0.693)

$t^{1/2}$ = half-life of the radioisotope

This correction was necessary in order to plot the radioactivity form each individual organ against all timepoints. The values for the AUC between all time points were calculated using equation *E12*:

$$AUC_{t1\text{-}t2} = (cpm1 + cpm2) \times (t_2\text{-}t_1) / 2$$

E12

The AUC values for each organ in the presence and absence of WK-X-34 were calculated and the mean values ± S.D. were compared. Radioactive intensities obtained from these images correlated with results obtained from ^{99m}Tc-Sestamibi biodistribution studies.

3.4.9 ^{99m}Tc-Sestamibi biodistribution

Biodistribution studies were performed for both experimental designs described in chapters 3.4.1.1 and 3.4.1.2. For biodistribution studies mice were sacrificed by cervical dislocation four hours (chapter 3.4.1.1) and two hours (chapter 3.4.1.2) after ^{99m}Tc-Sestamibi injection. Blood samples were obtained by heart puncture using a needle previously treated with heparin. The different tissues of interest (e.g. tumors, brain, heart, liver, kidney and intestine) were carefully isolated and weighted (see picture 3, Appendix). Tissues and blood were then gamma-counted along with a Cardiolite$^{®}$ standard of known activity using the Packard Cobra$^{®}$ II Series Auto-Gamma Counting System. Relative tissue accumulation of ^{99m}Tc-Sestamibi was calculated as a % dose/gram of tissue. The relative injected dose (D_{rel}) was calculated by subtracting the remaining amount of radioactivity in the needle after injection (D_{rem}) from the absolute dose (D_{abs}) according to *E13*:

$$D_{rel} = D_{abs} - D_{rem} \qquad\qquad E13$$

D_{rel} = relative injected dose

D_{abs} = absolute injected dose

D_{rem} = remaining amount of radioactivity in the needle after injection

The detected counts per 1 kBq (Cts_{1kBq}) of the Cardiolite$^{®}$ standard allowed the transformation of the corresponding counts (Cts_{corr}) of the relative injected dose (D_{rel}) using *E14*:

$$Cts_{corr} = D_{rel} \cdot Cts_{1kBq} \qquad\qquad E14$$

Cts_{corr} = corresponding counts (e.g. 5.33 MBq = 55879187 cpm)

D_{rel} = relative injected dose

Cts_{1kBq} = counts per 1 kBq of Cardiolite$^{®}$ Standard

The % dose/gram of tissue ($\%~D_{rel}/g_{tis}$) was calculated from counts per minute detected per gram of tissue (cpm/g_{tis}) in *E15*:

$$\%~D_{rel}~/~g_{tis} = \frac{cpm~/~g_{tis}~\cdot~100}{Cts_{corr}}$$

E15

$\%~D_{rel}/g_{tis}$ = % dose/ gram of tissue

cpm/g_{tis} = counts per minute detected per gram of tissue

Cts_{corr} = corresponding counts

[99m]Tc-Sestamibi organ levels were strongly depending on the quality of the tail vein injection and the excretion parameters for ^{99m}Tc-Sestamibi. Thus, ^{99m}Tc-Sestamibi organ and tumor levels were normalized to an internal factor such as blood and muscle. Results were calculated as tissue to blood and tissue to muscle ratios. Results normalized to the non-Pgp expressing deep tissue muscle were more consistent than blood levels. Blood levels change with time and are strongly influenced by the extent of ^{99m}Tc-Sestamibi excretion and metabolism. Therefore the tissue/muscle ratios were used for presentation and discussion of biodistribution data.

3.4.10   Immunohistochemical and RT-PCR analyses of tumors

Following gamma counting (< 1 h after tissue isolation), tumors obtained from both experimental designs described in chapters 3.4.1.1 and 3.4.1.2 were divided into two parts and snap-frozen in liquid nitrogen for RNA isolation or fixed in saline containing 5 % of formaldehyde for immunohistochemistry.

For RNA isolation, about 50 mg of tumor tissue per sample were used. Tissues were homogenized for 60 min using the Polytron tissue homogenizer. Total RNA was isolated from tumor tissue using the TRIzol extraction kit and cDNA synthesized according to table 3.1. mRNA levels of human *MDR1* were determined

by semi-quantitative RT-PCR and normalized to human 18S. Primer sequences and PCR conditions were used as indicated in table 3.1.

Tumor tissue sections were prepared using the routine stain of hematoxylin and eosion (H and E). Hematoxylin, the oxidized product of the logwood tree, has an affinity to the nucleic acids of the cell nucleus. Eosin is an acidic dye with an affinity for cytoplasmic components of the cell. The fixed tumor tissue was paraffin embedded and 5 μm sections were cut and stained with hematoxylin and eosin as follows. Paraffin slides were washed in water and placed in filtered hematoxylin for 5 min. After washing with water, slides were rinsed with 1 % of acid alcohol for a few seconds and washed. Slides were then placed in a 1 % eosin solution in water for 5 min. Slides were finally washed in tap water and dried.

Immunohistochemical staining was prepared by Kelvin So at the Department of Pathology, Toronto General Hospital, UHN. Expression of Pgp was visualized on paraffin-embedded tissue slides applying the FITC-linked monoclonal Pgp antibody (1:500 dilutions) for 18 h at 21°C. Slides were examined under a 40x/0.65 oil immersion objective using a Nikon Eclipse E400 fluorescence microscope. Pictures were acquired under fluorescent light from the FITC channel with an acquisition time of 8 seconds. For negative controls, A2780/Adr slides were incubated in the absence of antibody. To distinguish false-positive responses from non-specific binding of the FITC-labeled antibody, A2780/wt slides were incubated in the presence of FITC-labeled monoclonal Pgp antibody and examined.

3.4.11   Statistical analysis

A paired, two-tailed Student's *t*-test was used to compare *in vivo* imaging of ^{99m}Tc-Sestamibi within the same tumor of one animal. A difference in mean values with a p-level of $\alpha < 0.05$ was considered statistically significant (p-levels: * $\alpha < 0.05$; ** $\alpha < 0.01$).

^{99m}Tc-Sestamibi imaging and biodistribution experiments in xenografts treated with *MDR1* antisense and vehicle were performed in groups of 4 animals for WK-X-34 treatments and controls. For these experiments an unpaired, two-tailed Student's *t*-test was used to compare ^{99m}Tc-Sestamibi uptake between two tumors in two

different animals. A difference in mean values with a p-level of $\alpha < 0.05$ was considered statistically significant (p-levels: * $\alpha < 0.05$; ** $\alpha < 0.01$).

For *MDR1* mRNA quantification of tumors, 4 tumors from 4 animals per group were used. Statistical analysis of mRNA expression was performed using an unpaired, two-tailed Student's *t*-test. Likewise, a difference in mean values with a p-level of $\alpha < 0.05$ was considered statistically significant (p-levels: * $\alpha < 0.05$; ** $\alpha < 0.01$).

4   Results – *in vitro*

4.1   Characterization of cell models

The Pgp-overexpressing human ovarian cancer cells, A2780/Adr, and the non Pgp-expressing wild-type cells, A2780/wt, were used for *in vitro* and *in vivo* investigations.   To study interactions with BCRP and the MRPs in transport and chemosensitivity assays, BCRP-overexpressing MCF7/mx and wild-type MCF7/wt cells and selectively transfected cell lines such as Hela-MRP1 were used.   To characterize these cell lines, different biomolecular techniques were applied. These techniques include analyses of gene expression using RT-PCR and protein expression using antibody staining techniques with flow cytometry detection. Moreover, chemosensitivity assays were used to examine the degree of resistance towards cytotoxic drugs.

4.1.1   RT-PCR analyses

Pgp-overexpressing A2780/Adr cells were used as a model of human multidrug resistant cancer. Results generated in A2780/Adr cells were compared to those obtained from the non Pgp-expressing wild-type cell line A2780/wt. Therefore, *MDR1* overexpression and lack of *MDR1* expression was confirmed in A2780/Adr and A2780/wt, respectively.   For quantification of mRNA results (e.g. *MDR1* expression in tumor xenografts), a standard curve needed to be generated.

4.1.1.1   Standard curve for the human *MDR1* gene

A standard curve enables one to determine the linear range at which the relative amount of PCR product, detected on the PCR gel directly, corresponds to the relative amount of template present in the probe.   Standard curves were

generated using the conditions described in chapter 3.3.1.   In figure 4.1, a representative standard curve is depicted.   The linear range for the PCR reaction at a cycle number of 28 was found to be at amounts of cDNA template of up to 1.25 μl. Thus, a template amount of 1 μl was chosen for further *MDR1* mRNA quantifications.
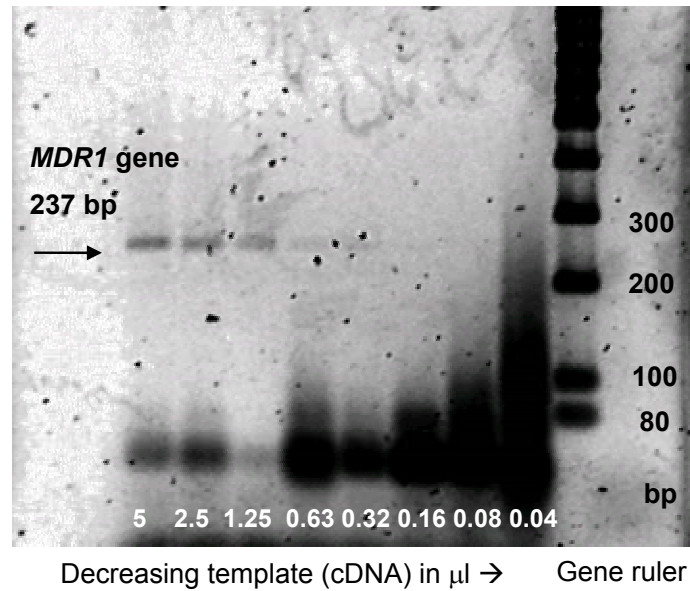
A.
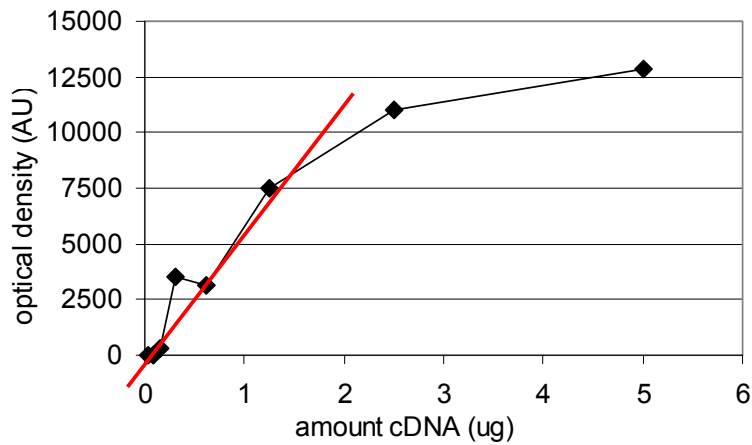
B.

Figure 4.1   Standard curve for *MDR1* mRNA expression

Gel electrophoresis for different amounts of cDNA template (5.0-0.04 μl).   PCR products (size: 237 bp) were separated by gel electrophoresis **(A)**.   Optical densities of PCR bands were determined (in arbitrary units (AU)) and plotted against the amount of cDNA template **(B).**   The linear range (red line) was found to be up to 1.25 μl of template at a cycle number of 28.

4.1.1.2   *MDR1* mRNA expression in A2780/Adr and A2780/wt

Expression of human *MDR1* mRNA in A2780/Adr and A2780/wt cells was examined by RT-PCR analysis as specified in chapter 3.3.1.   As derived from standard curves (see above), 1 μl of template was used for the PCR reaction. Results confirm high expression levels of *MDR1* mRNA in A2780/Adr cells but no detectable levels in wild-type A2780/wt cells (Figure 4.2)
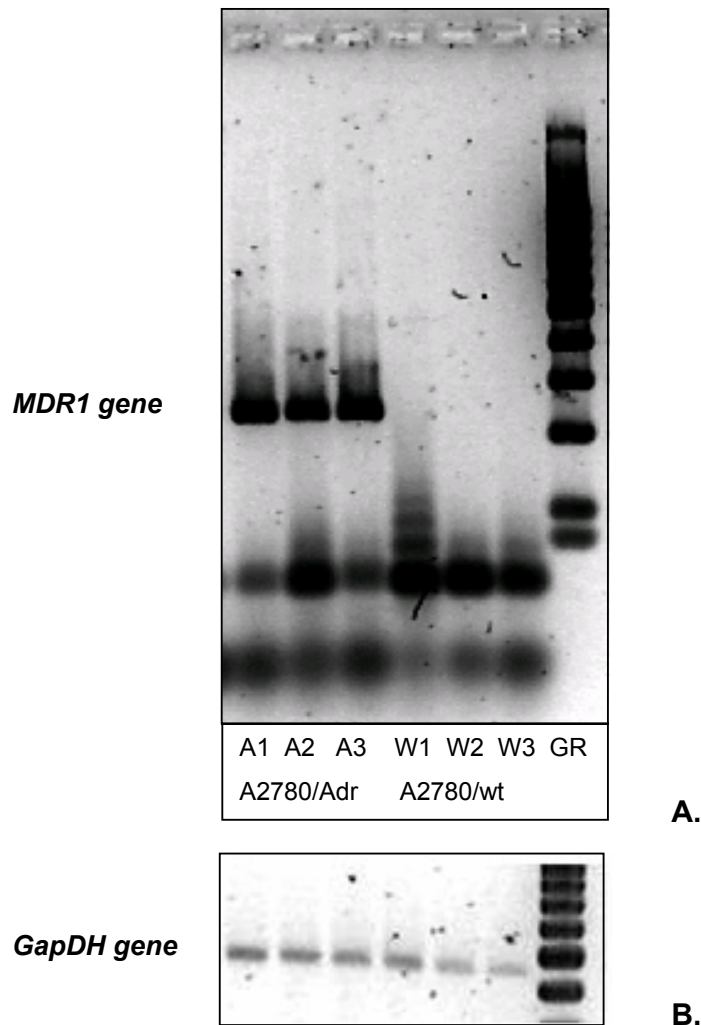
Figure 4.2   *MDR1* mRNA expression in A2780/Adr and A2780/wt

MDR1 mRNA expression in A2780/Adr (A1-3) and lack of *MDR1* mRNA expression in A2780/wt (W1-3) cells is depicted on a representative RT-PCR gel **(A)**. The gene ruler (GR) confirms the PCR product size of 237 bp for the *MDR1* gene. Quality and amount of template were verified by the housekeeping gene *GapDH* **(B)**.

4.1.1.3   *MRP* and *BCRP* mRNA expression in A2780/Adr and /wt

Expression levels of other ABC transporters including *MRP1*, *MRP2*, *MRP3* and *BCRP* in A2780/Adr and A2780/wt were examined in order to evaluate potential interactions of Pgp substrates with these transporters. Primer sequences and PCR conditions for these PCR reactions are presented in table 3.1.   A basal and increased expression of *MRP1* was detectable in both, A2780/wt and A2780/Adr cells. No mRNA expression of *MRP2* was visible in both, A2780/Adr and A2780/wt cells, and only basal levels of *MRP3* could be measured for both cell lines (Figure 4.3).   Likewise, no *BCRP* mRNA expression could be detected in A2780/Adr and A27807wt cell lines (Figure 4.4). Taken together, MRP1 was identified as the only transporter with expression levels high enough to interfere with Pgp functionality in A2780/Adr cells. The relative amount of *MRP1* mRNA was under 10 % of mRNA levels detected for Pgp. *MRP1* expression present in A2780/wt and A2780/Adr cells showed interactions or interferences in some of the functional assays which were based on Pgp and MRP1 substrates (e.g. daunorubicin).   In the daunorubicin chemosensitivity assay using A2780/wt cells (see chapter 4.3.5.1.), for example, MRP1 effects could be detected for verapamil.
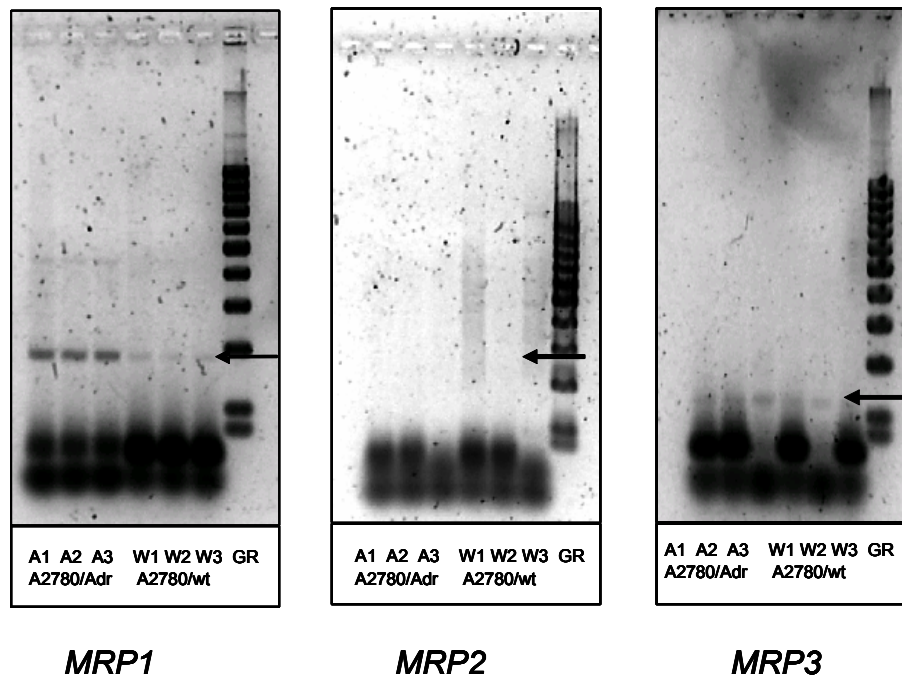
Figure 4.3   *MRP1, MRP2* and *MRP3* mRNA expression in A2780/Adr and A2780/wt

Expression of *MRP1* and *MRP3* mRNA and non-expression of *MRP2* in A2780/Adr (A1-3) and A2780/wt (W1-3) cells is depicted on representative RT-PCR gels. The gene ruler (GR) confirms the PCR product size of 183 bp (black arrow) for the *MRP1* gene and 117 for the *MRP3* gene. Quality and amount of template, confirmed by *GapDH* expression, were similar in all probes.
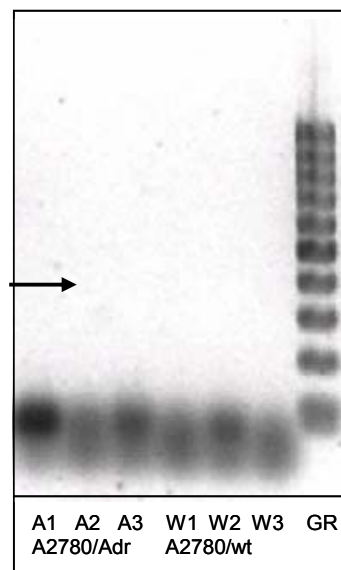
Figure 4.4   Lack of *BCRP* mRNA expression in A2780/Adr and A2780/wt

Lack of *BCRP* mRNA expression in A2780/Adr (A1-3) and in A2780/wt (W1-3) cells. The gene ruler (GR) confirms the PCR product size of 342 bp (black arrow) for the *BCRP* gene. The quality and amount of template, confirmed by *GapDH* expression, were similar in all probes.

4.1.2   Protein analyses

4.1.2.1   Pgp expression in A2780/Adr and A2780/wt

Pgp surface expression was analyzed directly using the FITC-labeled anti-human Pgp antibody with detection on a FACSCalibur. Corresponding to mRNA results, high expression levels of Pgp were seen in the multidrug resistant A2780/Adr cells but not in A2780/wt cells (Figure 4.5). Thus, these cell lines served as a model of Pgp-overexpressing and non-expressing tumors and were utilized for examinations of Pgp functionality as well as for *in vivo* tumor xenograft models in immunocomprimised mice.
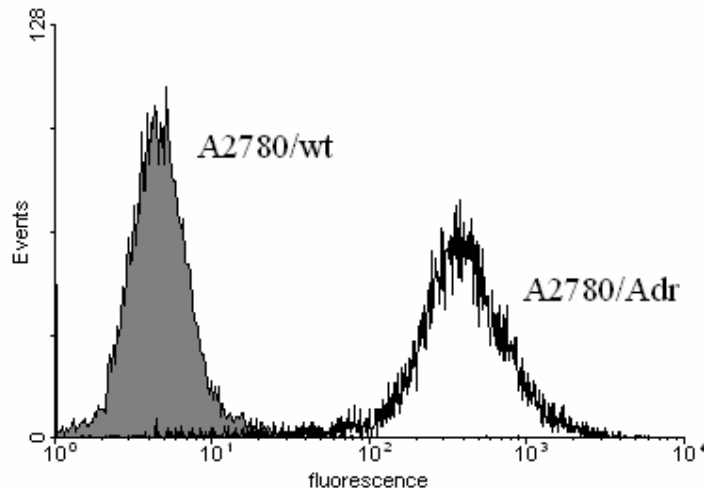
Figure 4.5   P-glycoprotein overexpression in A2780/Adr

Pgp expression in A2780/wt and A2780/Adr. Levels of surface Pgp were detected with a FITC-labeled anti-human Pgp antibody using the FL-1 channel of the FACSCalibur. The fluorescence intensity of cellular bound FITC is plotted against the cell number (= events). Geometric means were: A2780/Adr 402; A2780/wt 23.

Pgp levels were strongly increased in those A2780/Adr cells which were routinely treated with doxorubicin every 10 passages as indicated in chapter 3.2.1. To demonstrate the magnitude in overexpression of Pgp in doxorubicin treated A2780/Adr cells, Pgp surface expression was examined in several different cell lines. As presented in figure 4.6, doxorubicin treated A2780/Adr cells (A2780/Adr*D) showed a considerably higher overexpression than untreated A2780/Adr cells. Pgp

expression levels in other MDR cell lines including HepG2 and Caco-2 were marginal in comparison to A2780/Adr cells.
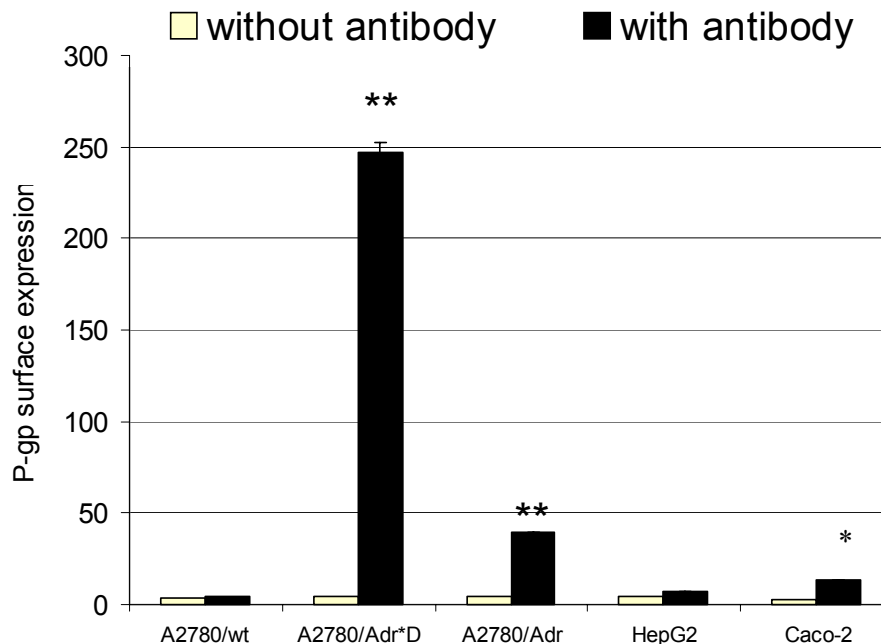
Figure 4.6   Relative P-glycoprotein expression in several cell lines

Pgp expression in several cell lines compared to non-Pgp expressing A2780/wt cells.   Doxorubicin treated A2780/Adr are indicated as **A2780/Adr*D**. Results are expressed as relative Pgp surface expression, detected as geometric means of the FITC fluorescence and ** indicates a p-level of < 0.01 as determined using an unpaired, two-tailed *t*-test.   Some arrow bars were too small to be depicted in some samples.

4.1.2.2   Lack of Pgp expression in MCF7/mx

Many substrates or inhibitors of Pgp also interact with BCRP. Therefore, it is necessary to verify that the cell line used for BCRP-specific assays does not express considerable levels of Pgp. A lack of Pgp expression was confirmed for MCF7/mx cells, which were used for BCRP functional assays (Mitoxantrone transport and chemosensitivity assays; see chapters 4.3.3 and 4.3.5.2). The experiments were performed as described in chapter 3.3.2.

Indeed, MCF7/mx cells did not display any detectable levels of Pgp. In A2780/Adr cells, high levels of surface Pgp were measured in contrast to MCF7/mx

and A2780/wt, which both did not express detectable levels of Pgp. The histogram obtained from MCF7/mx cells overlapped with the histogram obtained from the non Pgp-expressing A2780/wt cells, however, showed no overlap with the histogram obtained from A2780/Adr cells (Figure 4.7).

A.   **B.**
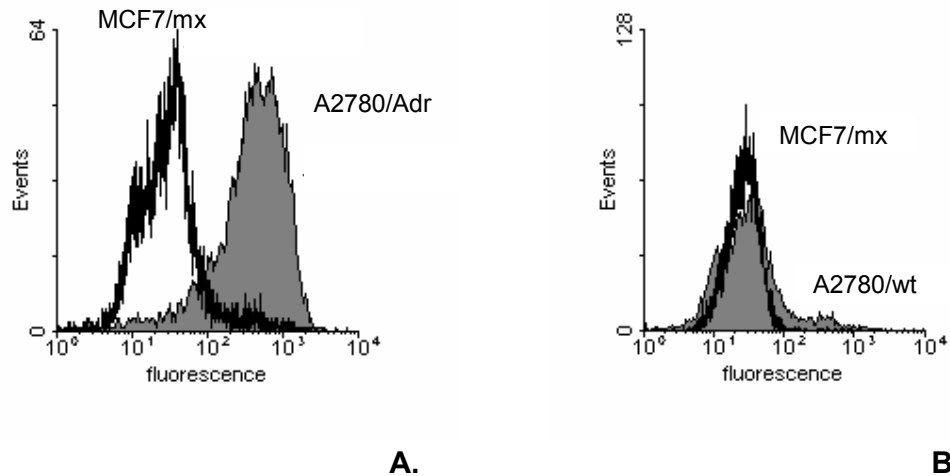
Figure 4.7   Lack of P-glycoprotein surface expression in MCF7/mx

Pgp surface expression in MCF7/mx in comparison to A2780/wt **(A)** and A2780/Adr **(B)**. Levels of surface Pgp are visualized using a FITC-labeled anti-human Pgp antibody with detection in the FL-1 channel of the FACSCalibur. The fluorescence intensity of FITC bound to the cell (in arbitrary units) is plotted against the cell number (= events). Geometric means are: A2780/Adr 406; A2780/wt 24; MCF7/mx 27.

4.1.2.3   BCRP overexpression in MCF7/mx

Overexpression of BCRP was confirmed in MCF7/mx cells, before using them for BCRP functional assays. The detection was based on protein staining techniques using a primary anti-human BCRP monoclonal BXP-21 antibody together with a secondary fluorescein-conjugated antibody. The amount of cellular-bound fluorescein was quantified using flow cytometry techniques as outlined in chapter 3.3.2. In comparison to wild-type MCF7/wt and A2780/Adr cells, BCRP was overexpressed in MCF7/mx cells (Figure 4.8). These results agree with results obtained from *BCRP* mRNA expression analysis (see chapter 4.1.1.3).

A.   **B.**
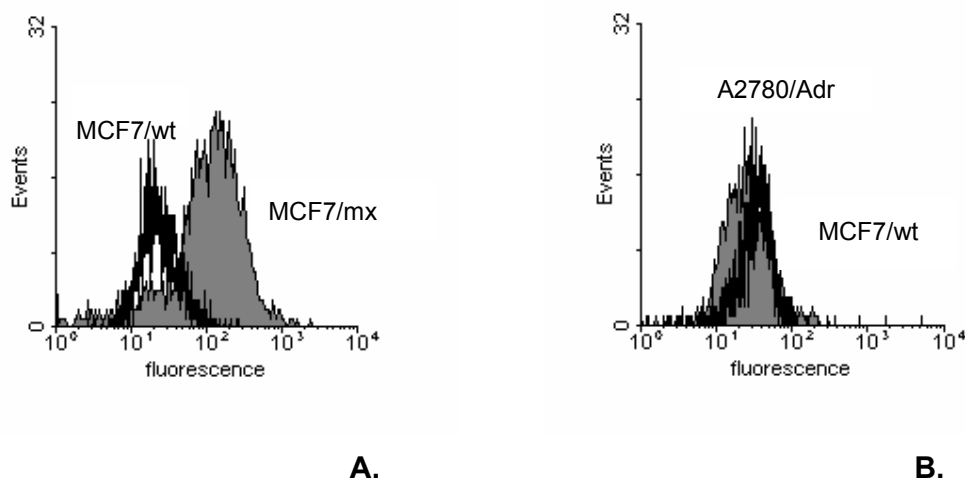
Figure 4.8   BCRP overexpression in MCF7/mx

BCRP expression in MCF7/mx **(A)** and A2780/Adr **(B)** in comparison to wild-type MCF7/wt cells. Protein levels were detected in the FL-1 channel of the FACSCalibur using the monoclonal BCRP antibody BXP-21 and a fluorescein-conjugated secondary antibody. The fluorescence intensity of cellular-bound fluorescein is plotted against the cell number (= events). Geometric means were: MCF7/mx 117; MCF7/wt 23; A2780/Adr 33.

4.1.3   Chemosensitivity in MDR cell lines

Chemosensitivity towards the chemotherapeutic agent, which was used to select the multidrug resistant cell line from its sensitive parental cell line, is a characteristic commonly used to determine the degree of resistance. Chemosensitivity was determined in multidrug resistant and sensitive cell lines. An MTT-based chemosensitivity assay was applied as described in chapter 3.3.9. The degree of chemosensitivity is expressed as an EC_{50} value.

4.1.3.1   Chemosensitivity towards doxorubicin in A2780/Adr

Chemosensitivity towards the anthracycline doxorubicin was measured in the A2780/Adr and to sensitive A2780/wt. In figure 4.9, dose-effect curves are shown from which EC_{50} values were derived as described in chapter 3.3.11.
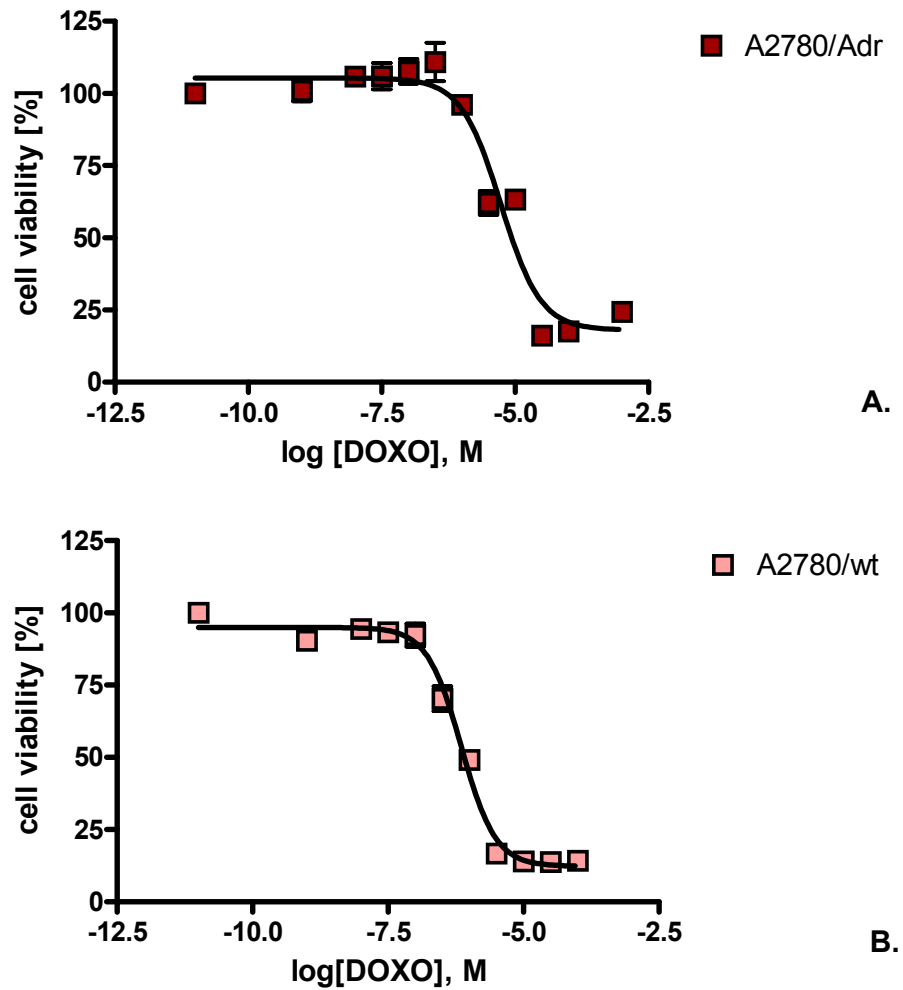
Figure 4.9   Chemosensitivity towards doxorubicin

EC_{50} values of doxorubicin (DOXO) were determined for A2780/Adr **(A)** and A2780/wt **(B)** cells using the MTT assay. EC_{50} values, as derived from nonlinear regression analysis, were 5.4 μM (log EC_{50}: -5.27 ± 0.1; Hill slope: -1.16) for A2780/Adr and 713 nM (log EC_{50}: -6.15 ± 0.04; Hill slope: -1.37) for A2780/wt cells. Some error bars are smaller than data symbols.

EC_{50} values of 5.4 μM and 713 nM were calculated for doxorubicin in A2780/Adr and A2780/wt cells, respectively. A degree of resistance of A2780/Adr towards A2780/wt of 7.5 was obtained.

4.1.3.2 Chemosensitivity towards mitoxantrone in MCF7/mx

The BCRP-overexpressing MCF7/mx cells were initially generated by selection using mitoxantrone. Therefore, the degree of chemosensitivity towards mitoxantrone was determined for MCF7/mx and the parental MCF7/wt cells (see chapter 3.3.9). According to figure 4.10, EC_{50} values of 26 µM and 317 nM were obtained for MCF7/mx and MCF7/wt cells, respectively. The calculated degree of resistance of MCF7/mx towards MCF7/wt was 82.

A.

B.
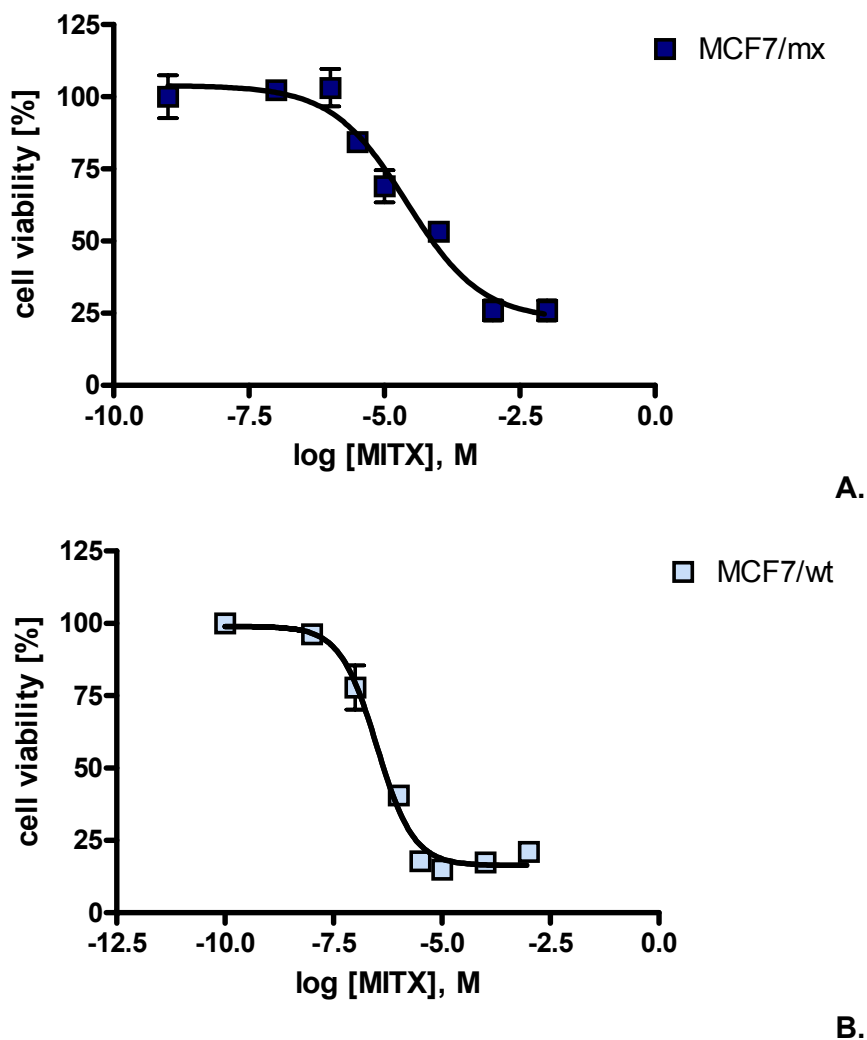
Figure 4.10 Chemosensitivity towards mitoxantrone

EC_{50} values of mitoxantrone were determined for MCF7/mx **(A)** and MCF7/wt **(B)** cells using the MTT assay. EC_{50} values, as derived from nonlinear regression analysis, were 26 µM (log EC_{50}: -4.6 ± 0.2; Hill slope: -0.62) for MCF7/mx and 317 nM (log EC_{50}: -6.5 ± 0.1; Hill slope: -1.03) for MCF7/wt cells. Some error bars are smaller than data symbols.

4.2   Characterization of *MDR1* antisense ODNs

Antisense oligodeoxynucleotides (ODNs) are a commonly used tool to transcriptionally downregulate the expression of the target gene *MDR1* and thus prevent the translation into the gene product Pgp. The antisense sequence used in this study (see chapter 3.3.3) has been previously shown to downregulate the expression of *MDR1* mRNA in cell culture (Alahari, 1998) and xenograft models (Brigui, 2003). In order to apply these sequences to the human ovarian cancer model used in the present work, the antisense sequences and transfection conditions needed to be evaluated *in vitro* in A2780/Adr cells. Their effectiveness in downregulating Pgp expression and functionality was investigated using Pgp surface expression analysis and functional transport assays. Cellular uptake and distribution were examined with FITC-labeled antisense ODNs. Finally, potential toxic effects were evaluated using cell proliferation assays.

4.2.1   Downregulation of Pgp expression

Downregulation of Pgp expression after antisense treatments (see chapter 3.3.3) was examined by surface protein staining according to chapter 3.3.2.

A significant downregulation of Pgp expression upon treatments with *MDR1* antisense ODNs for 72 h was detected in A2780/Adr cells (Figure 4.11). As the half life of Pgp is 14 h, this corresponds to treatment periods of three to five Pgp half lives (Aleman, 2003). The downregulation was dose-dependent with reductions to about 82 %, 67 % and 55 % of control levels in the presence of 50 nM, 100 nM and 200 nM of *MDR1* antisense ODNs, respectively. Furthermore, even low antisense concentrations of 50 nM resulted in a significant downregulation of Pgp by about 20 %. Antisense effects appeared to be specific as treatments with random controls did not induce any alterations of Pgp expression.
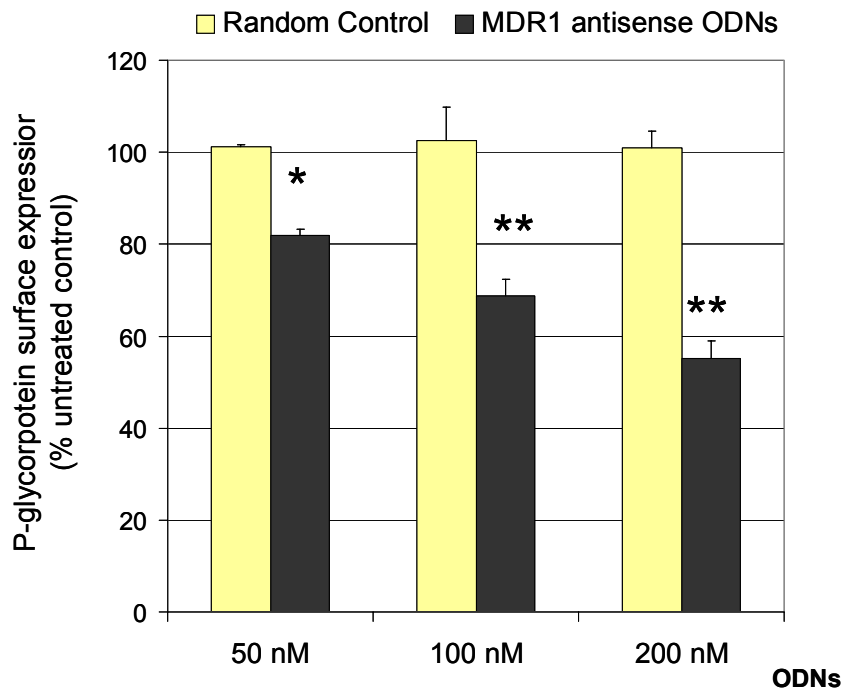
Figure 4.11   Pgp downregulation by *MDR1* antisense ODNs

A2780/Adr cells have been treated with different concentrations of ODNs. Pgp surface expression in antisense and random treated cells was detected using the FITC-labeled anti-human Pgp monoclonal antibody. Results are normalized to untreated controls. * and ** indicate p-level of $\alpha < 0.05$ and $\alpha < 0.01$, respectively, as determined by an unpaired, two-tailed *t*-test.

4.2.2   Downregulation of Pgp functionality

Decreases in Pgp expression by antisense treatments resulted in a reduced Pgp functionality. This could be identified in A2780/Adr cells via a reduced efflux of the substrate or increased sensitivity towards the cytotoxic drug. An increased accumulation of daunorubicin due to impaired efflux was detected in *MDR1* antisense pretreated A2780/Adr cells as compared to control A2780/Adr. In figure 4.12-A, the increased intracellular fluorescence of accumulated daunorubicin could be nicely visualized by fluorescence microscopy. Likewise, increased daunorubicin levels in *MDR1* antisense treated A2780/Adr cells were detected using flow cytometry-based transport assays (Figure 4.12-B).
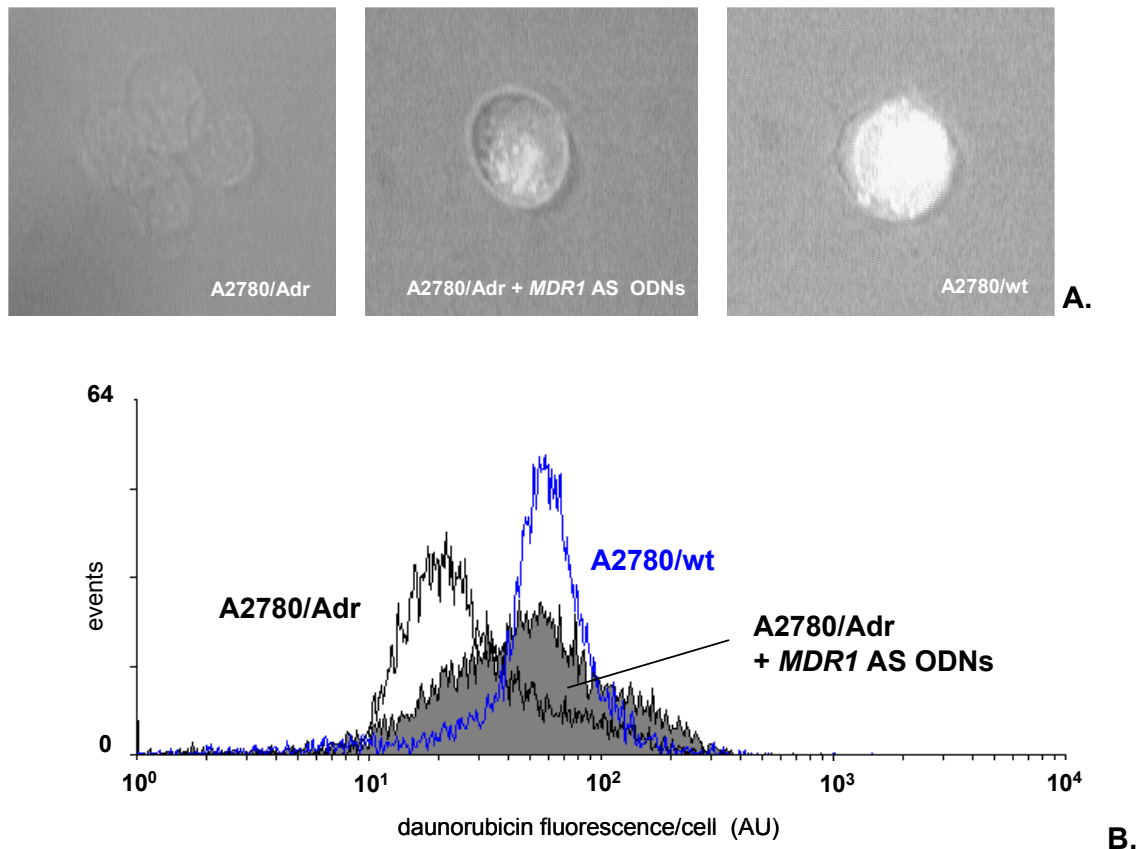
Figure 4.12   Increased daunorubicin accumulation in antisense treated A2780/Adr

Daunorubicin uptake in *MDR1* antisense pretreated A2780/Adr (solid grey), control A2780/Adr (black) and A2780/wt (blue) is visualized by fluorescence microscopy (on a 63x objective) **(A)** and flow cytometry **(B)** In the FACS histogram **(B)**, the fluorescence of daunorubicin in arbitrary units (AU) was detected in the FL-2 channel and is plotted against the cell number (= events). Cells were incubated with 3 μM of daunorubicin for 60 min. Geometric means as determined by flow cytometry in the FL-2 channel were: A2780/Adr control 26; A2780/wt control 57; A2780/Adr + *MDR1* AS ODN 68.

Decreases in Pgp expression and functionality by antisense treatments resulted in a diminution of the Pgp-mediated MDR phenotype. This was detectable as a stronger cellular sensitivity of A2780/Adr cells towards the cytotoxic drug daunorubicin in chemosensitivity assays (see chapter 3.3.9). The sensitivity towards daunorubicin in A2780/Adr cells was significantly and dose-dependently increased upon antisense treatments.   In table 4.1, EC_{50} values for different antisense concentrations are summarized. The daunorubicin concentration tolerated by 50 % of the cell population decreased with treatments of *MDR1* antisense ODNs in a dose-dependent manner.

Table 4.1   Daunorubicin chemosensitivity after *MDR1* antisense ODN treatments in A2780/Adr

	$EC_{50} \pm$ S.D. / μM			
Treatments (dose)	**0 nM**	**50 nM**	**100 nM**	**200 nM**
MDR1 AS ODNs		$19{,}0 \pm 0{,}8$*	$9{,}7 \pm 0{,}9$*	$7{,}7 \pm 0{,}9$*
Controls	$37{,}9 \pm 0{,}8$			

Table 4.1   A2780/Adr pretreated with 50 nM, 100 nM or 200 nM of *MDR1* antisense ODNs or PBS (controls) were incubated with different concentrations of daunorubicin for 72 h. Cell viability after ODN treatments was analyzed with the MTT-assay. EC_{50} values were calculated and results represent the mean of six samples in two separate experiments. * indicates a p-level of $\alpha < 0.05$ versus control treatment

4.2.3   Cellular uptake of FITC-labeled *MDR1* antisense ODNs

Cellular uptake and distribution of FITC-labeled *MDR1* antisense ODNs were further examined by fluorescence microscopy. ODNs enter the cells via endocytosis and accumulate in vesicles in the cytoplasm (Jensen, 2002). In figure 4.13, the cellular uptake and retention of FITC-labeled antisense was greater in A2780/Adr (A), as compared to the non-Pgp expressing A2780/wt cells (B). Furthermore, accumulation of fluorescein in vesicles was detectable on both pictures.
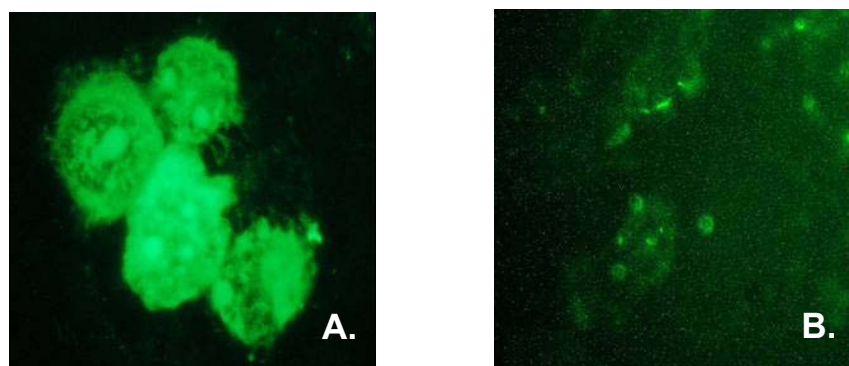
Figure 4.13   Fluorescence microscopy of intracellular ODN delivery

FITC-fluorescence microscopy analysis was compared in A2780/Adr **(A)** and A2780/wt **(B)** cells.   Cells were transfected with *MDR1* antisense ODNs for 3 h.

According to Jensen and coworkers (Jensen, 2003), two hours following uptake and accumulation in cytosolic vesicles, oligonucleotides begin to leave the vesicles and escape into the cytosole, from which they enter the nucleus. To examine whether FITC-labeled *MDR1* antisense ODNs, used in this work, penetrated into the nucleus, phase-contrast, DAPI and FITC microscopic pictures of A2780/Adr cells after uptake of FITC-labeled antisense ODNs were acquired.   As DAPI selectively stains the cell nucleus, overlapping DAPI (see chapter 3.3.10) and FITC-marked regions indicate nuclear localization.   According to fluorescence microscopy analysis (Figure 4.14), antisense ODNs were distributed within cells and also accumulated in the nucleus.
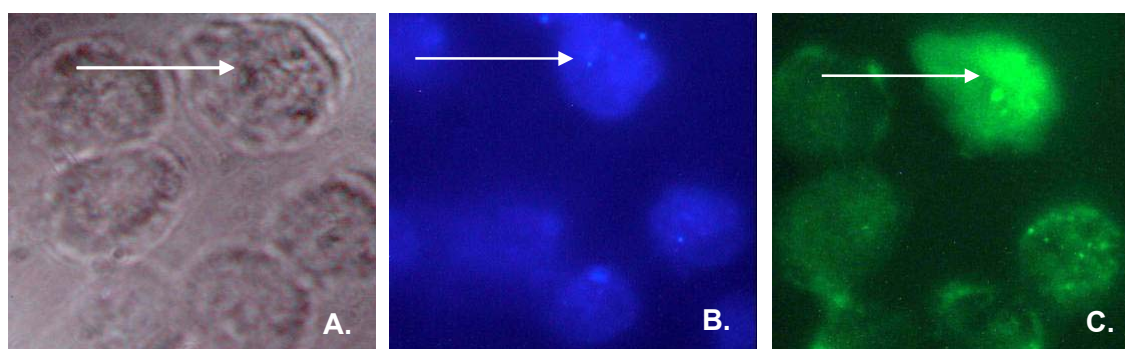
Figure 4.14   Fluorescence microscopy of nuclear ODN delivery

For nuclear localization analysis, phases contrast **(A, grey)**, DAPI nuclear stain **(B, blue)** and FITC-fluorescence **(C, green)** microscopy images were acquired for antisense uptake in A2780/Adr cells.   Overlapping stains in B and C (white arrows) indicate nuclear localization of FITC-labeled ODNs.

4.2.4 Toxicity of *MDR1* antisense transfections

Cellular toxicity has been associated with the exposure to phosphorothioated ODNs (Kurreck, 2003) and remains a major challenge in antisense applications. Furthermore, the transfection agent Superfect itself possibly has some toxic effects on cells (Axel, 2000). Therefore, the potential toxicity of the *MDR1* antisense ODN Superfect preparation compared to untreated controls was examined. The number of cells proliferated over 72 h was measured using the Casy 1$^{®}$ cell counter (see chapter 3.2.3). The cell number was dose-dependently decreased up to about 23 % for the treatment with 200 nM of ODNs (Figure 4.15), as a result of reduced cell proliferation over the span of the transfection.
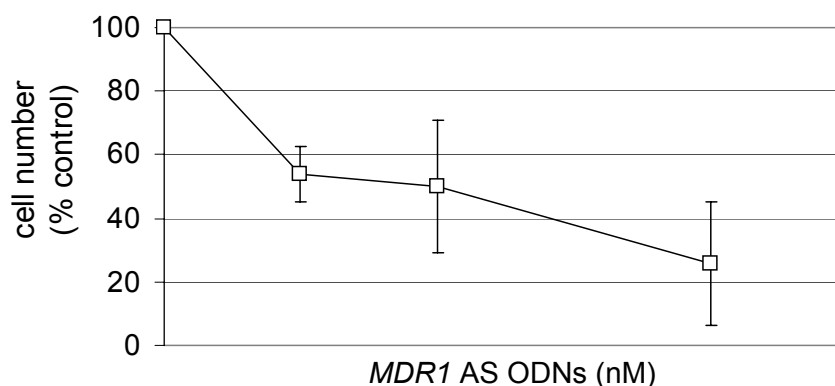
Figure 4.15   Reduced cell number after 72 h of antisense treatments

Effects of different concentrations of *MDR1* antisense ODNs on the number of proliferated A2780/Adr cells after 72 h of transfection. To evaluate toxicity of ODN preparations with SuperFect, untreated A2780/Adr cells were used as controls. Cell numbers were quantified using the Casy1$^{®}$ cell counter and are expressed as the means $\pm$ S.D. of three data points and normalized to untreated controls. Similar results were obtained in three individual experiments.

Significant reductions in cell number occurred during the course of antisense treatments due to reduced proliferation rates. For protein staining experiments, only viable cells were harvested; dead cells were washed off. All aliquots contained the same cell number for protein staining. Thus, differences in cell number after transfection regiments did not impact the quality of the protein measurements. During FACS measurements, the number of events within the gate for intact cells remained consistently well above 75 % for all treatment groups.

4.3   Characterization of novel MDR inhibitors

MDR mechanisms can be functionally modulated by specific MDR inhibitors which inhibit the activity of ABC transporters involved in MDR.   Whereas the overexpression of Pgp is the best characterized and most prevalent MDR mechanism, others such as MRP- or BCRP-mediated MDR mechanisms are often coexpressed in tumor cells. Therefore, Pgp, MRP and BCRP-functional assays were included in the *in vitro* characterization of the novel MDR inhibitors.   First of all, general toxicities of the novel compounds were examined in comparison to cyclosporin A and verapamil.

4.3.1   Toxicity of MDR inhibitors

The cellular toxicity of all inhibitors was analyzed in A2780/Adr, A2780/wt, MCF7/wt and MCF7/mx cells using the MTT viability assay. Cells were incubated with increasing concentrations of the inhibitors and EC_{50} values were derived. EC_{50} values were well above 10 μM for all compounds with the exception of cyclosporin A (Table 4.2). Here, the EC_{50} values obtained for A2780/wt, MCF7/wt and MCF7/mx were between 1 μM and 10 μM. Thus, concentrations of 10 μM, which were used for transport and chemosensitivity assays, did not severely impact the cell viability. Solely cyclosporin A imposed additional toxic effects at concentrations used in the transport assays.

Table 4.2   Effects of MDR inhibitors on cell viability in different cell lines

EC$_{50}$ MTT ± S.D.(µM)	A2780/wt	A2780/Adr	MCF7/wt	MCF7/mx
XR9577	48.6 ± 12	77 ± 12	25 ± 0.3	444 ± 84
WK-X-34	124 ± 28	221 ± 37	24 ± 3	50 ± 6
WK-X-50	36 ± 19	256 ± 153	26 ± 4	76 ± 6
WK-X-84	53 ± 18	50.6 ± 19	77 ± 23	43 ± 15
Cyclosporin A	7 ± 0.6	27 ± 7	4 ± 0.3	2 ± 0.8
Verapamil	294 ± 192	182 ± 6	28 ± 3	42 ± 3

Table 4.2. Toxicity of WK-X-compounds, XR9577, cyclosporin A and verapamil was evaluated in different cell lines using the MTT viability assay and expressed as an EC$_{50}$ value. Experiments were performed in triplicates on three separate occasions and results are expressed as means ± S.D.

4.3.2   Pgp-mediated transport assays

To examine potential inhibition of Pgp-mediated transport, three different Pgp transport assays were chosen (see chapter 2.3.4), the ^{99m}Tc-Sestamibi accumulation, the daunorubicin accumulation and the daunorubicin efflux assay.

4.3.2.1 ^{99m}Tc-Sestamibi accumulation assay

Cellular accumulation studies of ^{99m}Tc-Sestamibi were performed using A2780/Adr and A2780/wt cells (see chapter 3.3.6.1). RT-PCR analysis confirmed high Pgp-overexpression in A2780/Adr cells and lack of Pgp-expression in A2780/wt cells (see chapters 4.1.1.2 and 4.1.2.1). Considerably lower levels of *MRP1* and a

lack of *BCRP* were detected in both A2780/Adr and A2780/wt cells (see chapter 4.1.1.3). The gamma emitter and Pgp substrate ^{99m}Tc-Sestamibi served as a direct tracer of Pgp transport activity. As ^{99m}Tc-Sestamibi is actively effluxed by Pgp, intracellular accumulation levels of ^{99m}Tc-Sestamibi were inversely proportional to the Pgp transport capacity.

In figure 4.16, the uptake kinetics of ^{99m}Tc-Sestamibi into untreated A2780/Adr and A2780/wt cells are shown. Furthermore, effects of WK-X-34 in comparison to cyclosporin A and verapamil are depicted. A2780/Adr cells have been pretreated with 10 μM of either WK-X-34, cyclosporin A or verapamil and were compared to vehicle treated A2780/Adr or wild-type A2780/wt.
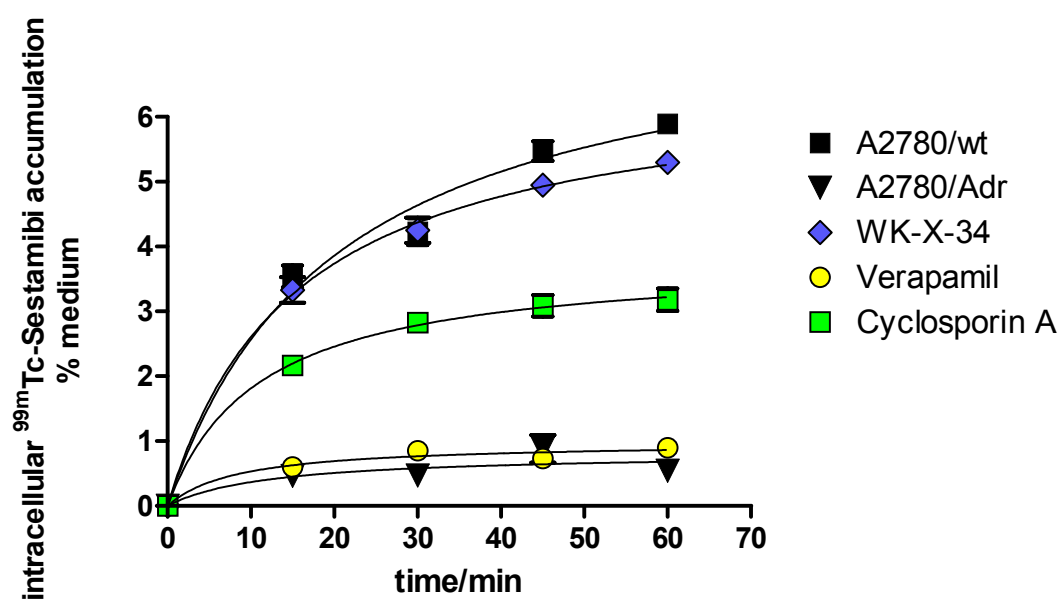
Figure 4.16   Impact of WK-X-34, cyclosporin A and verapamil on ^{99m}Tc-Sestamibi uptake

Effects of WK-X-34, verapamil and cyclosporin A on the uptake kinetics of ^{99m}Tc-Sestamibi in A2780/Adr in comparison to A2780/wt cells. Cells have been preincubated with 10 μM of inhibitor or vehicle for 1 h. Results represent means of three samples ± S.D. Similar results were obtained in three independent experiments.

10 μM of WK-X-34 completely inhibited Pgp functionality and increased intracellular retention of ^{99m}Tc-Sestamibi to levels in A2780/wt cells for all examined time points (15 min – 60 min). Smaller effects were seen for cyclosporin A and no inhibition could be detected for verapamil. The effects of all other inhibitors at a

tested concentration of 10 μM and after 60 min of uptake are presented in figure 4.17. XR9577 and WK-X-34 completely reversed the Pgp-mediated ^{99m}Tc-Sestamibi efflux and led to accumulation levels seen in A2780/wt cells. All other inhibitors did not show any significant effects on Pgp inhibition with the exception of cyclosporin A.
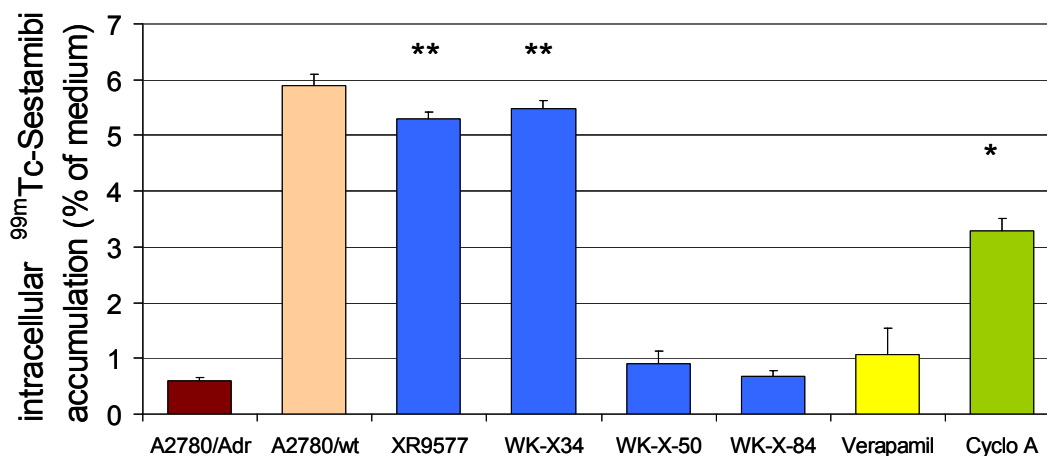
Figure 4.17   Impact on ^{99m}Tc-Sestamibi accumulation – overview

Effects of WK-X-compounds, XR9577, verapamil and cyclosporin A (10 μM, 60 min uptake) on ^{99m}Tc-Sestamibi accumulation in A2780/Adr. Results are expressed in relative ^{99m}Tc-Sestamibi accumulation (in % of medium) and compared to levels obtained in A2780/wt and represent means of three samples± S.D. Similar results were obtained in three independent experiments.

Based on the results in figure 4.17, dose-response analyses of ^{99m}Tc-Sestamibi accumulation were performed for XR9577, WK-X-34 and cyclosporin A (Figure 4.18). EC$_{50}$ values were obtained in the nanomolar range for XR9577 (300 nM) and WK-X-34 (416 nM) and in the lower micromolar range for cyclosporin A (5.5 μM).
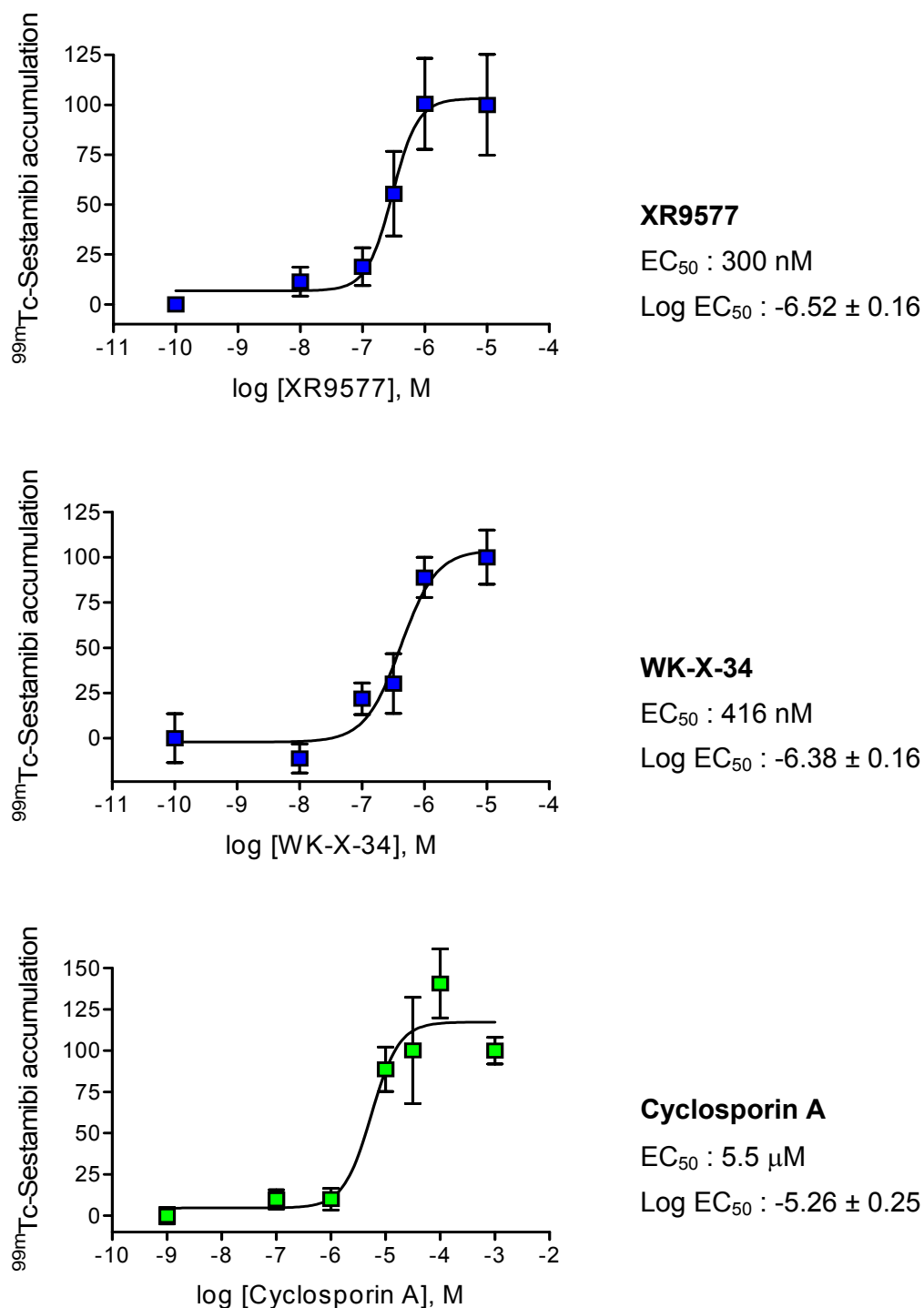
Figure 4.18   EC$_{50}$ values of Pgp inhibition using the ^{99m}Tc-Sestamibi accumulation assay

A2780/Adr cells were preincubated with concentrations of 10 nM to 100 μM of XR9577, WK-X-34 and 10 nM to 1 μM of cyclosporin A. ^{99m}Tc-Sestamibi accumulation levels were determined after 60 min of uptake and plotted against the logarithm of the inhibitor concentration in molarity. EC$_{50}$ values were determined by nonlinear regression analysis. Results are expressed as means ± S.D. and normalized to top and bottom values; some error bars are smaller than the data symbols.

For *in vivo* characterizations of WK-X-34 and *MDR1* antisense ODNs, an imaging approach was chosen based on the accumulation of ^{99m}Tc-Sestamibi in resistant and sensitive tumor xenografts (see chapter 3.4.1). As BCRP and Pgp are often coexpressed in different tissues and tumors (Doyle, 2003), potential contributions of BCRP in the efflux of ^{99m}Tc-Sestamibi were investigated. Studies in the MCF7/mx cells did not detect any contribution of BCRP to the cellular accumulation of ^{99m}Tc-Sestamibi (Figure 4.19). If ^{99m}Tc-Sestamibi was a substrate of BCRP, intracellular ^{99m}Tc-Sestamibi levels would be elevated in novobiocin treated MCF7/mx and MCF7/wt as compared to MCF7/mx. Novobiocin-treated MCF7/mx and MCF7/wt have no functional BCRP, thus no potential transport activity. However, MCF7/mx cells possessing functional BCRP do not decrease ^{99m}Tc-Sestamibi levels. Therefore, ^{99m}Tc-Sestamibi cannot be a substrate for BCRP. Intracellular ^{99m}Tc-Sestamibi levels were slightly increased in MCF7/mx, which can be explained by the lack of novobiocin in competition for uptake processes. As previously published (Chen, 2000), the results confirm no involvement of BCRP in ^{99m}Tc-Sestamibi transport across cellular membranes.
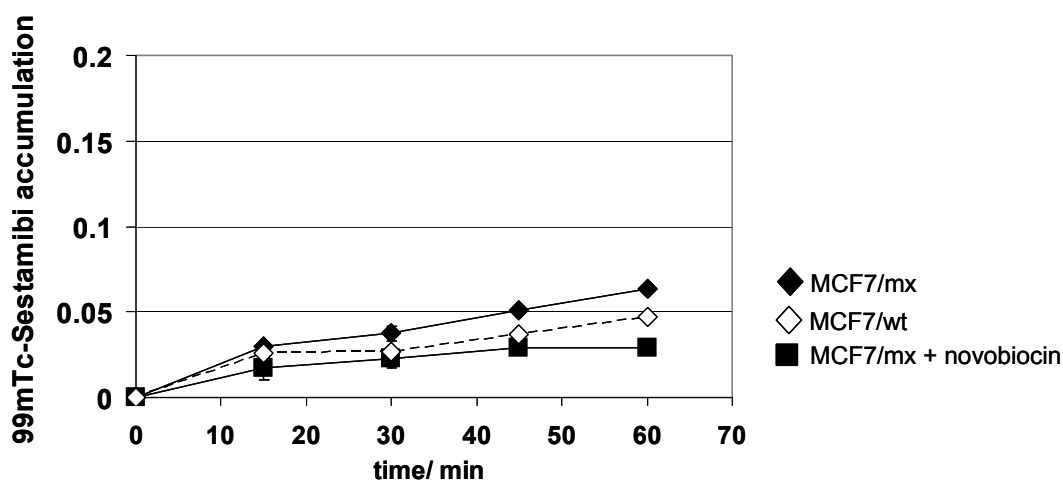
Figure 4.19   ^{99m}Tc-Sestamibi accumulation in MCF7/mx and MCF7/wt

Time-dependent cellular accumulation of ^{99m}Tc-Sestamibi is shown in BCRP-expressing MCF7/mx and non-BCRP-expressing MCF7/wt cells. MCF7/mx cells have been additionally treated with 200 µM of the BCRP inhibitor novobiocin. Cells have been pretreated with novobiocin or vehicle for 1 h prior to addition of ^{99m}Tc-Sestamibi as specified above. Results represent the means ± S.D. of three independent experiments. Some error bars are smaller than the data symbols.

4.3.2.2   Daunorubicin efflux assay

The daunorubicin efflux assay was performed in A2780/Adr as described in chapter 3.3.6.2. As daunorubicin is also a weak substrate of BCRP and MRP1, RT-PCR analyses were performed to examine the mRNA expression of those MDR transporters. As summarized in chapter 4.1.1.3, A2780/Adr displayed no detectable levels of *BCRP* and only very low levels of *MRP1*. Cells were incubated in the presence of daunorubicin and the amount of intracellularly retained daunorubicin after 90 min of efflux was measured by flow cytometry

Results from the daunorubicin efflux assay (Figure 4.20) partly corresponded to results from the ^{99m}Tc-Sestamibi efflux assay.
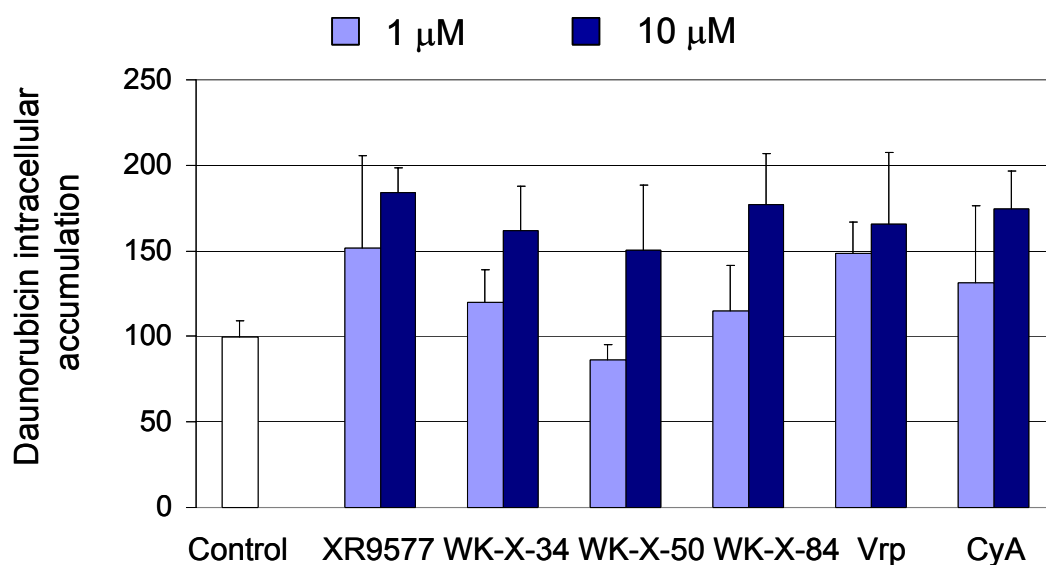
Figure 4.20   Inhibition of Pgp-mediated daunorubicin efflux

Effects of WK-X-compounds, XR9577, verapamil and cyclosporin A (10, 1 μM) on Pgp-mediated daunorubicin efflux were detected by flow cytometry. Values are normalized to 100 % of controls and values above 100% indicate Pgp-inhibition. Results represent means ± S.D. Similar results were obtained in three independent experiments.

Likewise, the compounds XR9577, WK-X-34 and cyclosporin A significantly inhibited daunorubicin efflux at both tested concentrations of 10 and 1 μM. In contrast to results from the ^{99m}Tc-Sestamibi accumulation assay, concentrations of

10 μM of verapamil and WK-X-84 also demonstrated some Pgp inhibition. Studies comparing the reliability of the substrates ^{99m}Tc-Sestamibi or anthracyclines (e.g. doxorubicin, daunorubicin) for Pgp transport assays have indicated differences between these two assays (see chapter 2.3.4). Thus, a combination of both assays allows for a more predictive analysis of Pgp inhibition.

4.3.2.3   Daunorubicin accumulation assay

Daunorubicin accumulation after a 180 min incubation period in the presence and absence of inhibitors could be quantified as an indicator of Pgp-mediated transport. In this assay, the intracellular daunorubicin concentration was inversely proportional to the activity and expression of Pgp. The assay was performed as outlined in chapter 3.3.6.3. To visualize these effects, microscopy pictures of daunorubicin accumulation in A2780/Adr cells pretreated with 1 and 10 μM of WK-X-34 were acquired and are depicted in figure 4.21-A. Furthermore, the daunorubicin uptake in A2780/Adr was compared to untreated A2780/wt cells (Figure 4.21-Aiiii). The modulating effects on daunorubicin accumulation could also be detected by flow cytometry (Figure 4.21-B).

untreated   1 μM WK-X-34   10 μM WK-X-34   untreated

A2780/Adr   A2780/Adr   A2780/Adr   A2780/wt
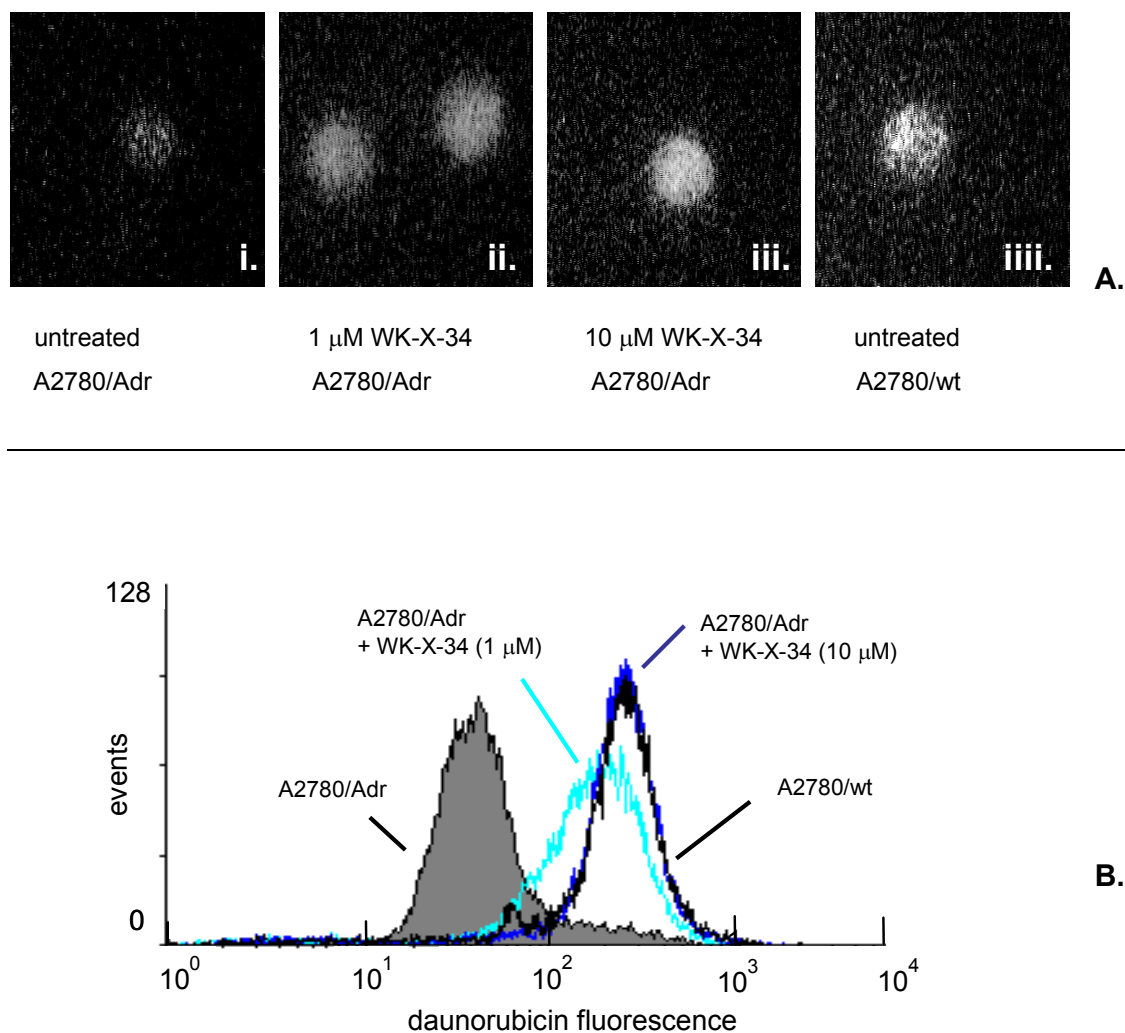
Figure 4.21   Impact of WK-X-34 on daunorubicin accumulation

A2780/Adr and A2780/wt cells were pretreated with 1 and 10 μM of WK-X-34, incubated with daunorubicin (3 μM) (for 60 min **(A)** and 180 min **(B)**) and examined by fluorescence microscopy (on a 63x objective) **(A)** and flow cytometry **(B)**. As compared to untreated A2780/Adr **(Ai)** and A2780/wt **(Aiiii)** cells, daunorubicin uptake was dose-dependently increased in A2780/Adr treated with 1 μM WK-X-34 **(Aii)** and 10 μM WK-X-34 **(Aiii)**. Daunorubicin uptake in WK-X-34-treated A2780/Adr was detectable on FACS histograms **(B)**. Cells were gated for the intact cell population using forward and side scatter dot plots and 10000 events were acquired per sample. Geometric means as determined by flow cytometry in the FL-2 channel were: A2780/Adr control 44; + WK-X-34 (1 μM) 170; + WK-X-34 (10 μM) 235; A2780/wt 234.

For EC_{50} determination, the daunorubicin accumulation assay has been extensively used in our laboratory. A2780/Adr cells were preincubated with different concentrations of inhibitors and daunorubicin accumulation after 180 min was quantified. EC_{50} and log EC_{50} values were derived by nonlinear regression analysis.

These experiments were performed by Kerstin Breitbach and are the subject of her PhD thesis. A representative curve of the characterization of WK-X-34 is depicted in figure 4.22.

WK-X-34
logEC$_{50}$: -7.09 ± 0.03
EC$_{50}$: 82.1 ± 6.2 nM
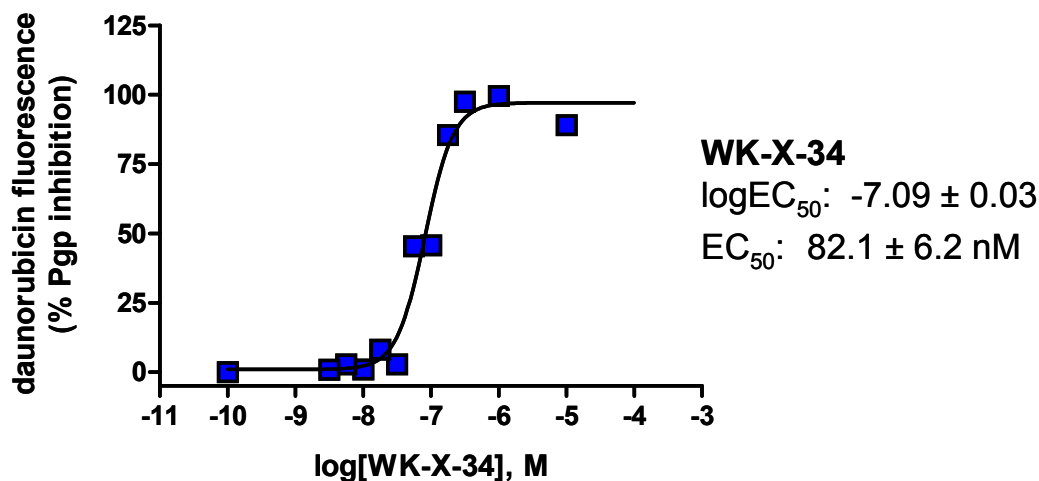
Figure 4.22   EC$_{50}$ determination of Pgp inhibition using daunorubicin accumulation

Representative EC$_{50}$ determination of WK-X-34 in A2780/Adr cells as determined by daunorubicin accumulation. Results represent means of three samples ± S.D. and are normalized to top and bottom values. Error bars are smaller than the data symbols. Three independent experiments were performed. (The data and graph were kindly provided by K. Breitbach)

EC$_{50}$ values were determined for all the other MDR inhibitors. The following values were obtained: **XR9577** (EC$_{50}$: 136 nM; log EC$_{50}$: -6.87 ± 0.01); **WK-X-50** (EC$_{50}$: 1.55 µM; log EC$_{50}$: -5.81 ± 0.02); **WK-X-84** (EC$_{50}$: 1.06 µM; log EC$_{50}$: -5.98 ± 0.01); **verapamil** (EC$_{50}$: 4.77 µM; log EC$_{50}$: -5.32 ± 0.03) and **cyclosporin A** (EC$_{50}$: 2.47 µM; log EC$_{50}$: -5.61 ± 0.01).

4.3.2.4   Summary of Pgp transport assays

The MDR inhibitors were characterized for Pgp-mediated transport by three different Pgp transport assays: the ^{99m}Tc-Sestamibi accumulation assay; the daunorubicin efflux assay and the daunorubicin accumulation assay. These assays combine two different Pgp substrates and two different transport parameters (accumulation and efflux). Results from these three different assays are not

consistent. Thus, the results need to be interpreted in conjunction and discrepancies noted. Table 4.3 presents an overview of the results.

Table 4.3   Summary of Pgp transport assays

Inhibitor	Pgp Transport Assays		
	^{99m}Tc-Sestamibi accum.	Daunorubicin efflux	Daunorubicin accum.
XR9577	++ (EC$_{50}$: 300 nM)	++	++ (EC$_{50}$: 136 nM)
WK-X-34	++ (EC$_{50}$: 416 nM)	+	++ (EC$_{50}$: 82 nM)
WK-X-50	-	-	+ (EC$_{50}$: 1.55 μM)
WK-X-84	-	+	+ (EC$_{50}$: 1.06 μM)
Verapamil	-	++	+ (EC$_{50}$: 4.77 μM)
Cyclosporin A	+ (EC$_{50}$: 5.5 μM)	+	+ (EC$_{50}$: 2.47 μM)

Table 4.3. Results from three different Pgp transport assays are summarized. A significant and strong inhibition at a 1 μM concentration or with an EC$_{50}$ value in the nanomolar range is indicated by ++; a weaker but yet significant inhibition at a 10 μM concentration or with an EC$_{50}$ value in the micromolar range is indicated by +.

XR9577 and WK-X-34 showed substantial and significant Pgp inhibition in all three transport assays. The effects of cyclosporin A were weaker, yet significantly detectable in all three assays. Consistently, WK-X-50 showed no effects in all three assays. For all other MDR inhibitors, results of Pgp inhibition were rather inconsistent between the three assays. This was particularly seen for verapamil. Whereas verapamil showed no effects in the ^{99m}Tc-Sestamibi assay, a significant Pgp inhibition with an EC$_{50}$ value in the lower micromolar range was detected in the daunorubicin accumulation assay. This was likely due to unspecific MDR inhibition and interaction with other transporters such as MRP1. As the resistant A2780/Adr cells were selected through continuous exposure to doxorubicin, other cellular non-classical mechanisms (see chapter 1.1.1.1) might be present in these cells and could contribute to unspecific MDR inhibition (also see results from daunorubicin chemosensitivity assays, chapter 4.3.5.1).

4.3.3 BCRP-mediated transport assays

Inhibition of BCRP-mediated transport of the BCRP substrate mitoxantrone was examined in MCF7/mx cells. The cell model was confirmed to overexpress BCRP but to lack detectable expression of Pgp (see chapter 4.1.2). Overexpression of BCRP led to a MDR phenotype towards mitoxantrone, detectable as a strong mitoxantrone efflux in MCF7/mx (Figure 4.23-A) but not in MCF7/wt cells (Figure 4.23-B).

A. MCF7/mx   **B. MCF7/wt**
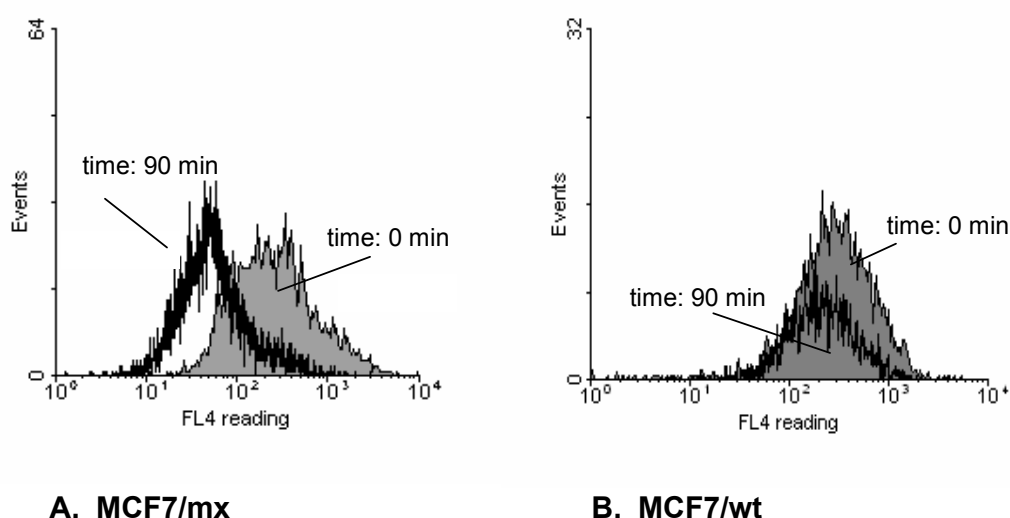
Figure 4.23   BCRP-mediated efflux of mitoxantrone in MCF7/mx

Representative histograms demonstrating mitoxantrone intracellular levels after 90 min efflux in MCF7/mx **(A)** in comparison to MCF7/wt **(B)** cells. Intracellular mitoxantrone levels after 180 min incubation with 3 μM of mitoxantrone were detected on a FACSCalibur in the FL4 channel. Geometric means as determined by flow cytometry were: MCF7/mx (0 min) 230; MCF7/mx (90 min) 89; MCF7/wt (0 min) 243; MCF7/wt (90 min) 215.

Inhibition of BCRP-mediated mitoxantrone efflux was tested for all compounds at a concentration of 10 and 200 μM. WK-X-34 and XR9577 were found to be the most potent inhibitors in this assay. At both tested concentrations, these compounds significantly retained intracellular mitoxantrone with a potency that was comparable to that of the well-established BCRP inhibitor novobiocin (Figure 4.24). BCRP inhibition with a comparable potency was detectable for WK-X-50 and WK-X-84, yet a comparable level of significance could not be reached due to a higher variability

between the individual experiments. No major interactions with BCRP were seen in the verapamil and cyclosporin A treated cells.
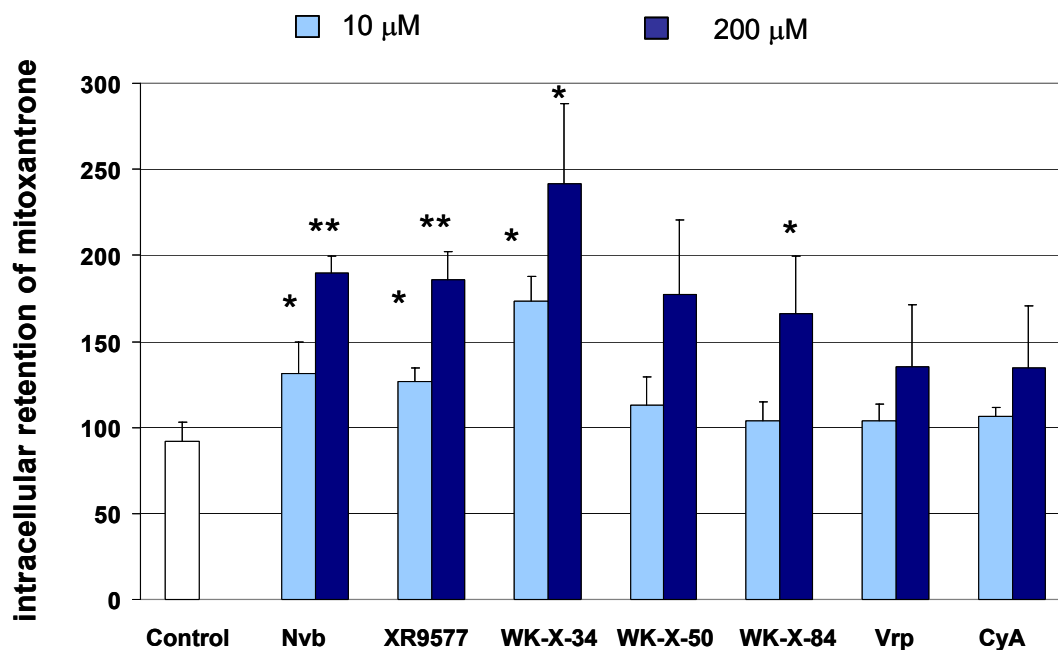
Figure 4.24   Inhibition of BCRP-mediated mitoxantrone efflux

Inhibition of mitoxantrone efflux in the presence of 10 and 200 μM of novobiocin (Nvb), XR9577, WK-X-34, -50, -84, verapamil (Vrp) and cyclosporin A (CyA). Retained mitoxantrone accumulation after 90 min of efflux was detected by flow cytometry. Data was calculated as described in methods and are expressed as a percent of control with a control value of 100 %. Results represent mean values ± S.D. of three individual experiments with p-levels of * α = 0.05 and ** α = 0.01.

For quantification and comparison of BCRP inhibitors, EC_{50} values were derived by quantifying the mitoxantrone efflux in MCF7/mx cells in the presence of various concentrations (1-1000 μM) of MDR inhibitors. Novobiocin was included as a positive control (Shiozawa, 2004; Yang, 2003). Apparent EC_{50} values of BCRP inhibition (Figure 4.25) were calculated for novobiocin and each MDR inhibitor.

Novobiocin

EC_{50} : 25 µM

Log EC_{50} : -4.60 ± 0.03

XR9577

EC_{50} : 21 µM

Log EC_{50} : -4.68 ± 0.05

WK-X-34

EC_{50} : 27 µM

Log EC_{50} : -4.57 ± 0.1
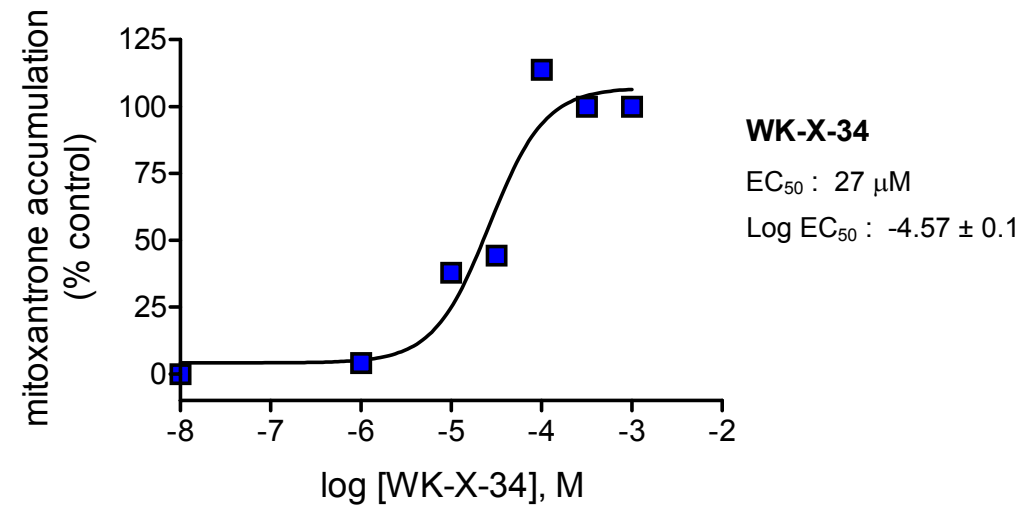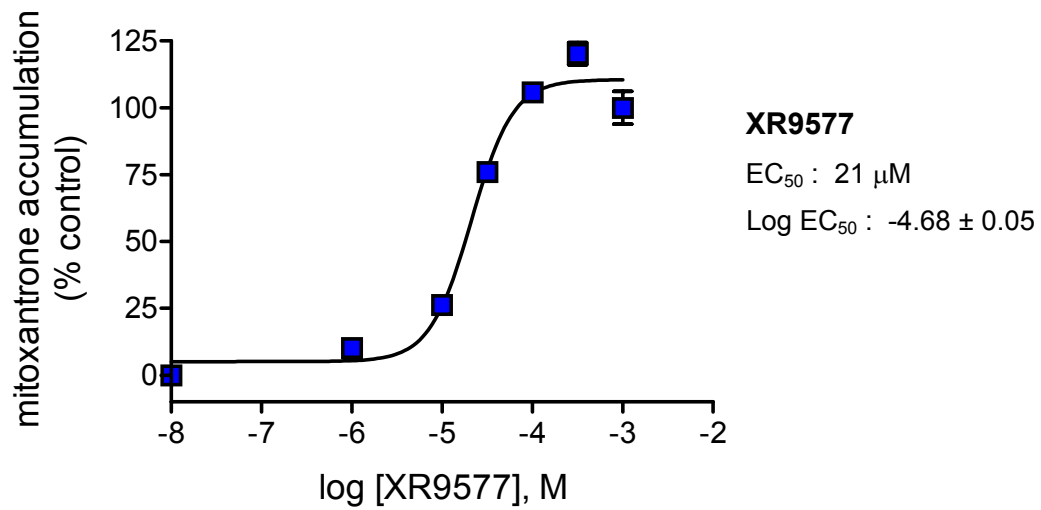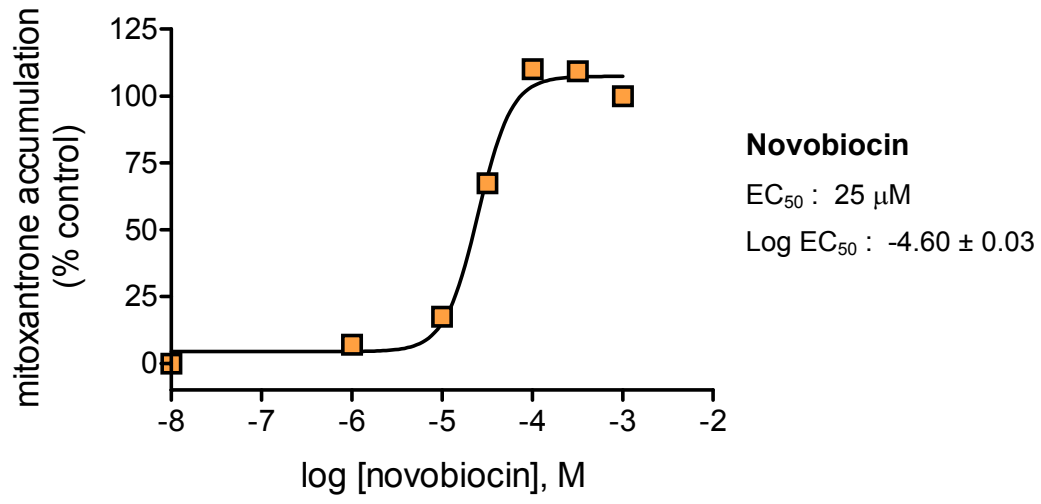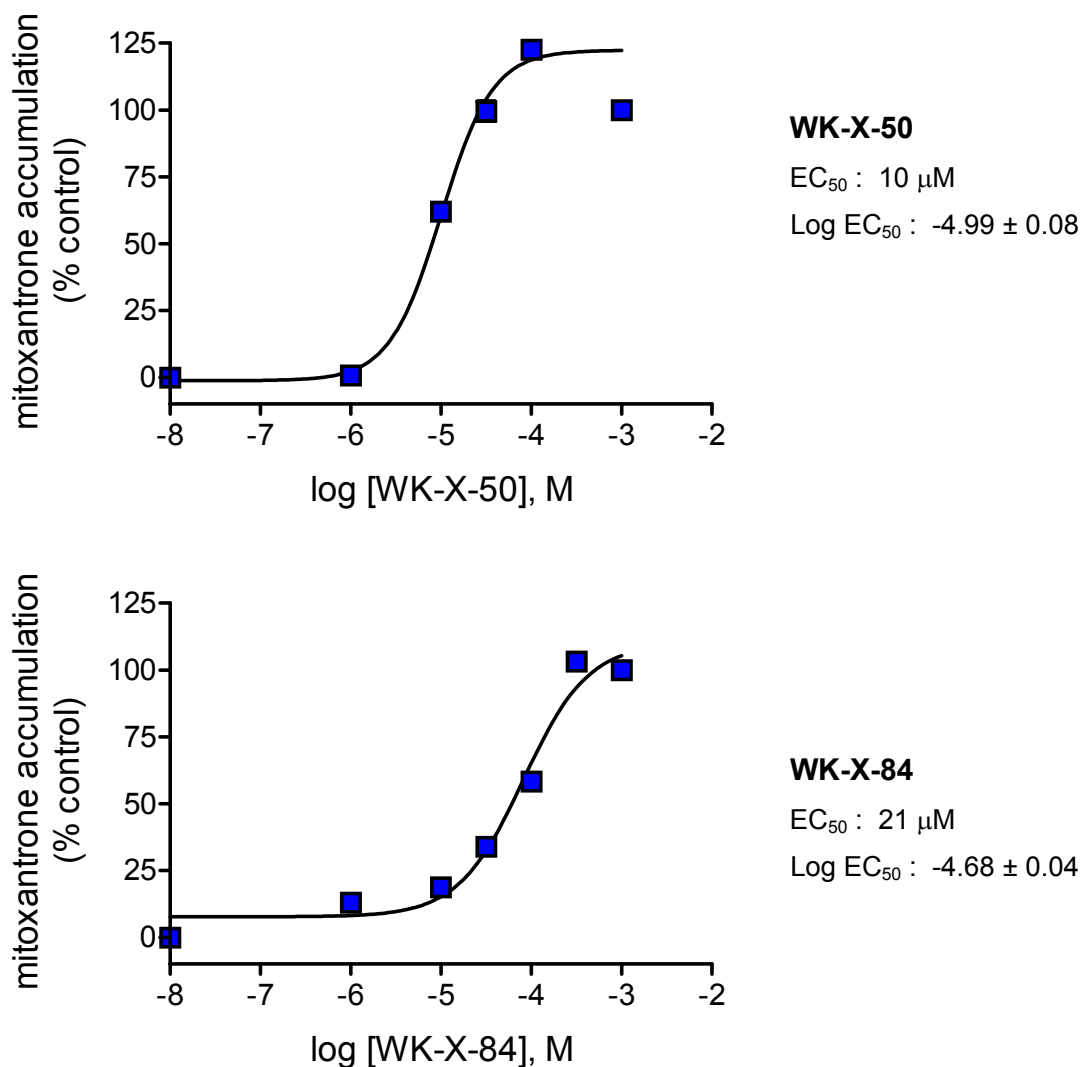
Figure 4.25   EC$_{50}$ values of BCRP inhibition

MCF7/mx cells were preincubated with mitoxantrone and different concentrations of novobiocin, XR9577, WK-X-34, -50 and -84. Retained mitoxantrone accumulation was measured after 90 min efflux by flow cytometry and plotted against the inhibitor concentration. EC$_{50}$s were determined by nonlinear regression from data normalized to top and bottom values and represent mean values ± S.D. of three independent experiments. Error bars can be smaller than data symbols.

As expected from results in figure 4.24, EC$_{50}$ values in the same range were obtained for XR9577 and WK-X-34 in comparison to novobiocin. Unexpectedly, WK-X-50 and WK-X-84 displayed EC$_{50}$ values which were comparable to those of WK-X-34 and novobiocin. Results from mitoxantrone efflux assays as presented in figure

4.24, however, indicated a comparable inhibition for WK-X-50 and WK-X-84 as compared to XR9577, for instance. These results, however, did not reach significance due to the higher variability between the different runs of the assay. In summary, all three WK-X-compounds appear to inhibit BCRP-mediated mitoxantrone efflux with a potency comparable to that of novobiocin.

4.3.4   MRP-mediated transport assays

Interactions of the WK-X-compounds, XR9577, verapamil and cyclosporin A with the MRP transporters were examined using the 5-CFDA efflux assay in selectively transfected cell lines, HeLa-MRP1 and MDCK-MRP2 and -MRP3 (see chapter 3.3.8).

4.3.4.1   Interaction with MRP1

In comparison to the MRP inhibitor indomethacin, the effects of most compounds on MRP1 inhibition were weak and only significant at high concentrations of 200 μM (Figure 4.26). Interestingly, cyclosporin A, even though fairly weak at 200 μM, already showed a highly significant MRP1 inhibition at 10 μM. Potent inhibition of the MRP transporters, particularly MRP1, has previously been reported for cyclosporin A (Quadir, 2005).
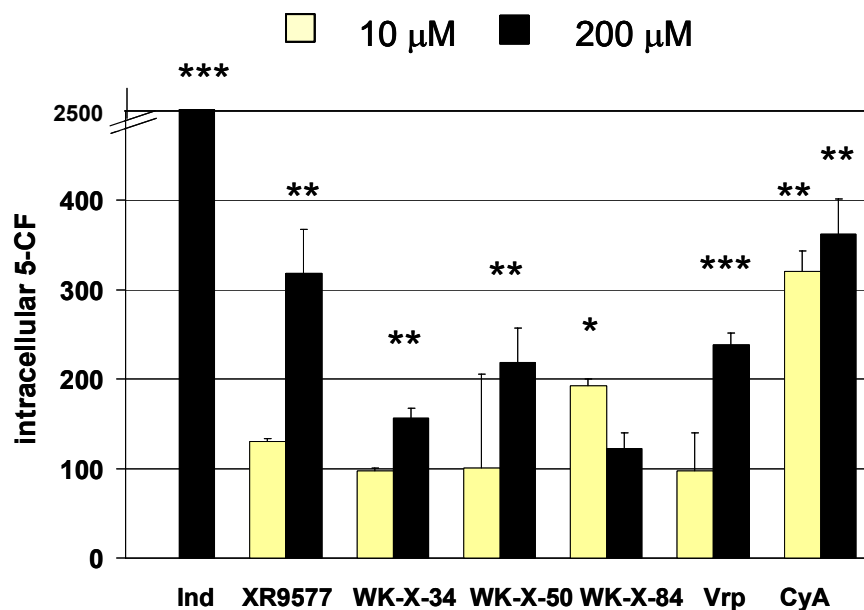
Figure 4.26   Interaction with MRP1 activity

Effects of 10 μM and 200 μM of WK-X-compounds, XR9577, verapamil (Ver) or cyclosporin A (CyA) on MRP1-mediated efflux of 5-CF were analyzed in HeLa-MRP1 cells. Indomethacin (Ind) (200 μM) was used as a positive control. The cellular bound 5-CF after efflux was measured. Results are calculated as a % of control and represent means ± S.D. with p-levels of α= * < 0.05;** <0.01; * < 0.001 as determined using an unpaired *t*-test. Similar results were obtained in three separate experiments.

4.3.4.2   Interaction with MRP2

MRP2-mediated efflux in MDCK-MRP2 cells was significantly inhibited by WK-X-50 at 10 and 200 μM whereas other WK-X-compounds showed no effects on MRP2 (Figure 4.27). These results identify WK-X-50 as an MRP2 inhibitor. Solely verapamil showed some significant but weak MRP2 interactions at concentrations of 200 μM. The MRP inhibitor indomethacin displayed only very weak inhibition of MRP2 when compared to MRP1 inhibition, for example.
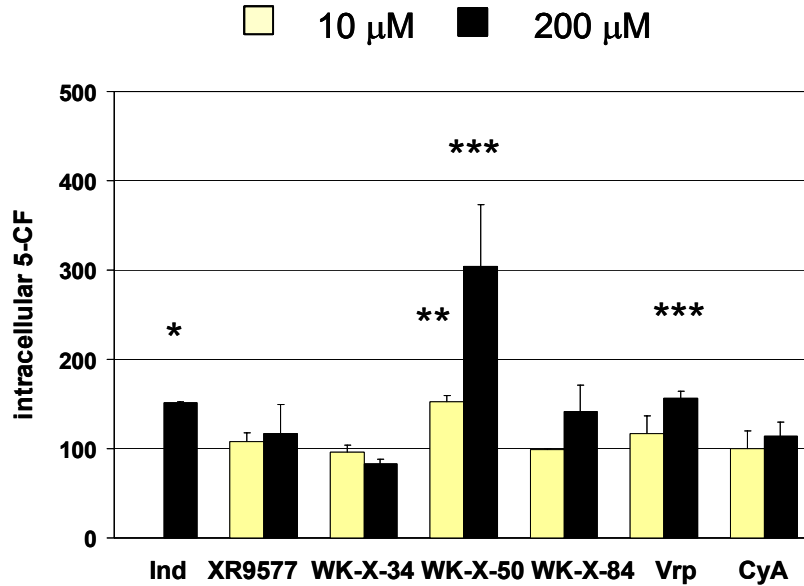
Figure 4.27   Interaction with MRP2 activity

Effects of 10 μM and 200 μM of WK-X-compounds, XR9577, verapamil (Vrp) or cyclosporin A (CyA) on MRP2-mediated efflux of 5-CF were analyzed in MDCK-MRP2 cells. Indomethacin (Ind) (200 μM) was used as a positive control. The cellular bound 5-CF was quantified after efflux. Results are calculated as a % of control and represent means ±S.D. with p-levels of α= * < 0.05;** <0.01; * < 0.001 as determined using an unpaired *t*-test. Similar results were obtained in three separate experiments.

4.3.4.3   Interaction with MRP3

In comparison to indomethacin, cyclosporin A showed potent MRP3 inhibition at concentrations of 200 μM in MDCK-MRP3 cells (Figure 4.28). No MRP3 inhibition was detected for the other MDR inhibitors with the exception of some weak but significant effects of verapamil at concentrations of 200 μM.
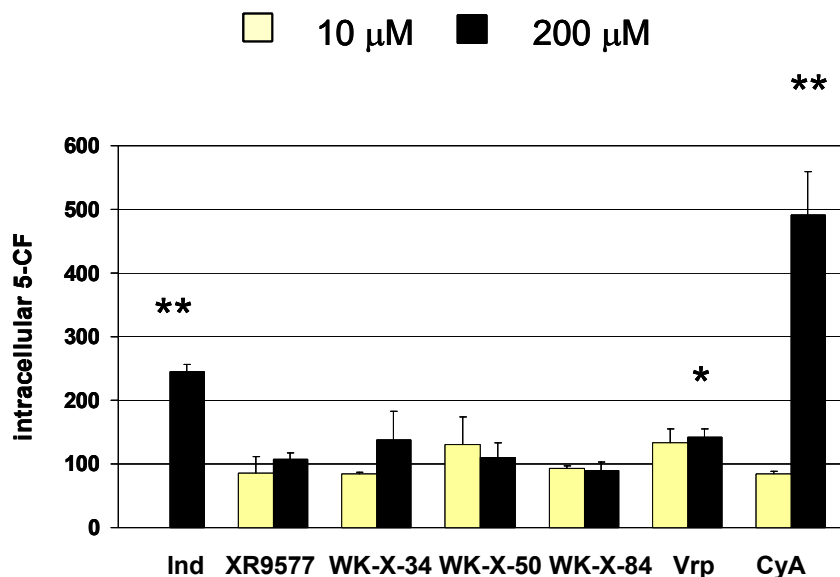
Figure 4.28   Interaction with MRP3 activity

Effects of 10 μM and 200 μM of WK-X-compounds, XR9577, verapamil (Vrp) or cyclosporin A (CyA) on MRP3-mediated efflux of 5-CF were analyzed in MDCK-MRP3 cells. Indomethacin (Ind) (200 μM) was used as a positive control. The cellular bound 5-CF after efflux was measured. Results are calculated as a % of controls and represent means ±S.D. with p-levels of α= * < 0.05;** <0.01; *** < 0.001 as determined using an unpaired *t*-test. Similar results were obtained in three separate experiments.

4.3.4.4   Summary of MRP-mediated transport assays

The MDR inhibitors XR9577, WK-X-34 and -84 showed no interactions with the MRP inhibitors, with the exception of some high dose MRP1 effects. The specificity for Pgp and BCRP inhibition appeared to be enhanced for XR9577, WK-X-34 and -84 in comparison to the first generation Pgp inhibitors cyclosporin A and verapamil, which demonstrated substantial unspecific MRP interactions. Of note, WK-X-50 was identified as a weak MRP2 inhibitor.

4.3.5   Chemosensitivity Assays

Corresponding to results presented in chapter 4.2.2, decreased Pgp functionality by treatments with MDR inhibitors resulted in both, a weakened Pgp- and BCRP-mediated MDR phenotype. The cellular sensitivity towards the cytotoxic drugs daunorubicin and mitoxantrone, as detected in chemosensitivity assays (see chapter 3.3.9), was significantly altered in the presence of some of the novel MDR inhibitors.

Chemosensitivity assays were performed in A2780/Adr and A2780/wt for daunorubicin and in MCF7/wt and MCF7/mx for mitoxantrone, respectively (Table 4.4 and 4.5). As outlined in chapter 3.3.9, the sensitizing factor (S.F.) describes the factor by which the chemosensitivity of the specific cell line towards daunorubicin/ mitoxantrone increases in the presence of 10 µM of inhibitor. Since the effect of an inhibitor is not solely dependent on the expression of Pgp/BCRP, both Pgp/BCRP expressing and non-expressing cell lines were examined. The non-specific MDR inhibitor verapamil (see chapter 4.3.4) was included as an unspecific control. For example, an increased sensitivity towards daunorubicin was detected for verapamil in non-Pgp expressing A2780/wt (S.F. 6.8), likely due to partial MRP inhibition (see table 4.4). The $S.F._{Adr/wt}$ or $S.F._{mx/wt}$ give a normalized value. A ration of $S.F._{Adr/wt}$ and $S.F._{mx/wt}$ was calculated by dividing the S.F. obtained for the Pgp/BCRP expressing (Adr, mx) cell line by the S.F. of the wild-type (wt) cell line.

4.3.5.1   Daunorubicin chemosensitivity in A2780/Adr

The chemosensitivity towards daunorubicin was increased in the presence of 10 µM of WK-X-34, WK-X-84 and XR9577, as sensitizing factors ($S.F._{Adr/wt}$) above 7 were calculated for these treatment groups (Table 4.4). These $S.F._{Adr/wt}$ were higher than the $S.F._{Adr/wt}$ for verapamil ($S.F._{Adr/wt}$: 4.1) and cyclosporin A ($S.F._{Adr/wt}$: 3.2). Unspecific effects were detectable for verapamil and cyclosporin A as treatment of A2780/wt cells with verapamil or cyclosporin A also showed significant induction of chemosensitivity. This can be explained by an unspecific interaction of these compounds with other MDR mechanisms particularly MRP1, which was expressed at detectable levels in A2780/Adr and A2780/wt cells. The same effects were not

detectable upon treatments with the MRP2 inhibitor WK-X-50. This seems plausible as A2780/Adr and A2780/wt cells did not have any levels of MRP2 as presented in figure 4.3.

Table 4.4   Daunorubicin chemosensitivity in A2780/Adr and A2780/wt

EC_{50} MTT / **µM ± S.D**. (S.F.: control/treatment)	**A2780/wt**	**A2780/Adr**	**S.F.$_{Adr/wt}$**
Control	**1.29 ± 0.1**	**40.4 ± 9.8**	*(R.F. 31)*
XR9577	0.99 ± 0.1 (1.3)	3.8 ± 0.9 (10.5)*	**8.1**
WK-X-34	1.06 ± 0.1 (1.2)	4.5 ± 0.7 (8.9)*	**7.4**
WK-X-50	1.13 ± 0.06 (1.1)	18.5 ± 0.9 (2.2)	**2**
WK-X-84	1.18 ± 0.03 (1.1)	5.1 ± 12.1 (7.9)*	**7.1**
Verapamil	0.19 ± 0.08 (6.8)**	1.5 ± 0.2 (28)*	**4.1**
Cyclosporin A	0.18 ± 0.16 (7.3)*	1.7 ± 0.3 (24)*	**3.2**

Table 4.4. Different concentrations of daunorubicin were added to cells preincubated with 10 µM of different inhibitors as indicated. Cell viability was examined after 72 h with MTT assays and EC_{50} values were calculated by nonlinear regression (with hill slopes ranging between -10 and -3.5 for A2780/wt and -4 for A2780/Adr cells, respectively). Chemosensitivity was expressed as a sensitizing factor (S.F.) and normalized for effects not related to Pgp overexpression in A2780/Adr cells (S.F.$_{Adr/wt}$). Experiments were performed in triplicates on three individual occasions. EC_{50} results represent means ± S.D. and p-levels (* $\alpha < 0.05$, ** $\alpha < 0.01$) were determined between drug treatment and controls within one cell line.

4.3.5.2   Mitoxantrone chemosensitivity in MCF7/mx

Sensitivity towards mitoxantrone was substantially higher in MCF7/wt (EC_{50}: 107 ± 13 nM) than in MCF7/mx (EC_{50}: 22 ± 4 µM) cells (Table 4.5). In MCF7/wt cells, none of the inhibitors showed any detectable effects and all S.F. control/treatment factors were close to 1. 10 µM of WK-X-34, XR9577 and

novobiocin were able to restore sensitivity towards mitoxantrone to levels of MCF7/wt with S.F.$_{mx/wt}$ of 298, 385 and 423, respectively.   Sensitivity towards mitoxantrone in MCF7/mx was increased to a lesser extent, yet significantly in the presence of WK-X-50 (by 48-fold) and WK-X-84 (by 109-fold).

Table 4.5   Mitoxantrone chemosensitivity in MCF7/mx and MCF7/wt

EC$_{50}$ MTT / **nM ± S.D**. (S.F.: control/treatment)	**MCF7/wt**	**MCF7/mx**	**S.F.$_{mx/wt}$**
Control	**104 ± 13**	**22000 ± 4000**	*(R.F. 211)*
XR9577	85 ± 6 (1.2)	62 ± 40 (357)*	**298**
WK-X-34	81 ± 8 (1.3)	44 ± 8 (506)*	**389**
WK-X-50	83 ± 3 (1.3)	460 ± 300 (48)*	**37**
WK-X-84	87 ± 11 (1.2)	202 ± 190 (109)*	**91**
Verapamil	83 ± 5 (1.3)	22500 ± 14000 (0,9)	**0.7**
Cyclosporin A	98 ± 6 (1.1)	86000 ± 21000 (0.26)	**0.24**
Novobiocin	81 ± 7 (1.3)	40 ± 18 (550)*	**423**

Table 4.5. Different concentrations of mitoxantrone were added to cells preincubated with 10 µM of different inhibitors as indicated. Cell viability was examined after 72 h with MTT assays and EC$_{50}$ values were calculated by nonlinear regression (with hill slopes ranging around -7). Chemosensitivity was expressed as a sensitizing factor (S.F.) and normalized to effects not related to BCRP overexpression (S.F.$_{mx/wt}$). Experiments were performed in triplicates on three individual occasions. EC$_{50}$ results represent means ± S.D. and p-levels (*α <0.05, ** α <0.01) were determined between drug treatment and controls within one cell line.

5   Discussion - *in vitro*

In the following chapter, *in vitro* results presented in chapter four will be discussed. The two MDR-reversing strategies outlined in "Rational and hypothesis", transcriptional downregulation by *MDR1* antisense ODNs and MDR inhibition using small molecule multi-targeted inhibitors (see chapter 2.1), will be evaluated and compared to each other.

5.1   Cell model A2780/Adr

The characterization of the cell model is of importance for every *in vitro* and *in vivo* investigation. In particular, the differential expression of genes and proteins involved in MDR mechanisms between the multidrug resistant and the sensitive variant exemplify the "pathological condition" of resistance. In comparison to other Pgp expressing cell lines such as Caco-2 and HepG2 cells, A2780/Adr cells showed considerably higher Pgp levels. When A2780/Adr cells were challenged with doxorubicin, their Pgp expression was even higher (chapter 4.1.2.1). Hence, the detection window for Pgp expression (see figure 4.5 and 4.6) and Pgp-mediated effects was greatest between doxorubicin challenged A2780/Adr and wild-type A2780/wt cells. A resistance factor of 7.5 for doxorubicin and 31 for daunorubicin was obtained for this cell pair. This was important in order to sensitively detect Pgp inhibition *in vitro,* and particularly *in vivo* in the tumor xenografts. Moreover, as such highly overexpressed levels are common in multidrug resistant solid tumors (Leith, 1999); this cell model reflects conditions, which might occur in clinically untreatable tumors.

The ovarian cancer cells A2780/Adr are sourced from a human solid tumor. To obtain a multidrug resistant phenotype, these cells have been selected with the chemotherapeutic agent doxorubicin. *In vitro* data indicates that the multidrug resistant phenotype is mainly characterized by Pgp overexpression. However, other

cellular mechanisms of resistance (see chapter 1.1) are likely to be involved (Vikhanskaya, 1997) as RT-PCR analyses have confirmed expression of MRP1 in A2780/Adr cells (see figure 4.3).

Although concurrent resistance mechanisms might interfere with investigations of the Pgp phenotype, chemoselected, rather than transfected, cells are favored by most researchers when studying the MDR phenotype. In contrast to genetically engineered cell lines, chemoselected cells more closely mimic a situation in which a tumor develops an MDR phenotype as a response to chemotherapeutic treatment. In clinical reality, multidrug resistant tumors are characterized by a predominant mechanism of resistance in concert with a variety of other non-cellular and cellular MDR mechanisms (Fojo, 2003). Hence, the clinical relevance is increased when experiments can be conducted in chemoselected, rather than transfected cell lines. In the present thesis, the chemoselected cell lines A2780/Adr and MCF7/mx were used in line with most *in vitro* and *in vivo* studies characterizing or targeting the MDR phenotype (see table 5.2).

5.2   *MDR1* antisense ODNs

MDR1 antisense ODNs have been previously used by different researchers to inhibit the expression of Pgp in cell culture and animal models. Results from the *in vitro* characterization of antisense ODNs are discussed in the following. To begin with, results from delivery and toxicity studies will be discussed.

5.2.1   Intracellular uptake and toxicity

Cellular uptake and distribution, as examined using FITC-labeled antisense ODNs, were greater in A2780/Adr, when compared to the non-Pgp expressing A2780/wt cells (see chapter 4.2.3). This was likely due to an increased retention of the *MDR1* antisense ODNs in cells, which offer a higher availability of target RNA. Cellular uptake of DNA is generally thought to occur through receptor-mediated endocytosis. A temperature–dependent, saturable transport process across plasma

membranes was described for oligonucleotides (Loke, 1989). Once inside the cells, antisense molecules leave their transfection complex and are distributed within the cytoplasm. In the cytoplasm they hybridize to their target mRNA (Jensen, 2001). As A2780/wt cells do not express detectable levels of *MDR1* (see chapter 4.1.1.2), these cells do not possess the target mRNA for *MDR1* antisense molecules. In A2780/Adr cells, however, high levels of *MDR1* mRNA are available for binding. Therefore, antisense molecules are more likely to be retained in these cells.

The FITC-labeled ODNs were also able to penetrate into the nucleus. This observation is in agreement with previously published reports (Chin, 1990; Fisher, 1993; Lorenz, 1998).

Cellular toxicity has been associated with the exposure to phosphorothioated ODNs and remains a major challenge in antisense application (Kurreck, 2003). Results in chapter 4.2.4 demonstrate a substantial suppression of the proliferation capacity of A2780/Adr cells upon antisense treatments. The effects were dose-dependent and decreased the proliferation rate of A2780/Adr cells by over to 70 % (see figure 4.15). These results point to a major impact of antisense treatments on cell viability and are in accordance with reports of ODN-related toxicities upon treatments with phosphorothioated ODNs (Galderisi, 1999).

The transfection agent SuperFect contributes to the overall toxicity. In MTT-based viability assays, SuperFect was found to also reduce mitochondrial activity (Axel, 2000). Thus, the observed toxic effects were likely due to a combination of the transfection reagent and the antisense molecules. As 'naked' antisense molecules are not easily being incorporated into cells (Axel, 2000) the use of a transfection reagent like SuperFect is essential for activity. Hence, SuperFect-related toxicities cannot be avoided. Antisense-associated toxicities represent a disadvantage and uncertainty linked to their experimental and potential therapeutic use.

5.2.2 Pgp expression and functionality

Antisense ODNs directed against *MDR1* (Alahari, 1998) were effective in downregulating Pgp expression and functionality in A2780/Adr cells (see figure

4.11). Changes in Pgp surface expression resulted in an impaired MDR phenotype which was detectable by investigations of daunorubicin chemosensitivity and intracellular accumulation. The degree of Pgp downregulation, however, was limited to about 50 % of controls. Lower Pgp levels could not be achieved even with the highest tolerated concentration.

Daunorubicin accumulation and chemosensitivity are depending on the degree of Pgp expression (Coley, 2002; Marks, 1992). Results confirmed that decreasing levels of Pgp expression lead to a decrease of Pgp activity, which was detectable as a reduced daunorubicin efflux. Thus, higher intracellular levels of daunorubicin were seen in antisense treated cells (see chapter 4.2.2). This relationship was dose-dependent and translated into an increased chemosensitivity towards daunorubicin, as determined using the MTT assay (see table 4.1). Likewise, a saturation of the anti-MDR effect against daunorubicin was detectable by MTT assays. The antisense concentration of 200 nM versus 100 nM caused a smaller increase in daunorubicin chemosensitivity than 100 nM versus 50 nM (compare EC_{50} values for 50nM, 100 nM and 200 nM in table 4.1) pointing to a saturation of the downregulating effect. The saturable effect might result from limitations in ODN uptake. This seems plausible as reports have indicated an energy-dependant saturable uptake process for ODNs (Loke, 1989) (see chapter 5.2.1).

To evaluate the usefulness of antisense treatments, Pgp inhibition caused by a functional inhibitor like WK-X-34 was compared to that caused by *MDR1* antisense ODNs. These two treatment strategies are based on totally different mechanisms of action. In antisense treated cells, two events leading to the inhibition of Pgp take place: 1. Antisense molecules target and downregulate the expression of *MDR1* mRNA. 2. Reductions in *MDR1* mRNA levels are then being translated into reduced Pgp surface expression, which leads to a reduced Pgp activity. Therefore, Pgp is indirectly targeted by antisense ODNs. In contrast, WK-X-34 directly interacts with surface Pgp and causes a functional inhibition of the transport activity without altering the expression of Pgp.

When the Pgp substrate daunorubicin is added to the system it has to be actively effluxed in order to enable the cell to survive. For effective efflux, however, the cell needs functional Pgp to be expressed in the plasma membrane. Through

treatment with both, antisense ODNs as well as WK-X-34, the activity of surface Pgp is decreased. In the case of antisense treatment, the lack of Pgp activity is caused by a decrease in the number of functional Pgp molecules on the cell surface.

How effective is the *in vitro* treatment using antisense ODN in comparison to a direct Pgp inhibition using WK-X-34? To better compare these two treatments, results from daunorubicin chemosensitivity assays in WK-X-34 and antisense treated cells are summarized in table 5.1.

Table 5.1   EC$_{50}$ values (daunorubicin chemosensitivity) after WK-X-34 and antisense treatments

		EC$_{50}$ (μM)	S.F.		EC$_{50}$ (μM)	S.F.
Controls	A2780/Adr	40,4 ± 9.8				
	A2780/wt	1.29 ± 0.1	**31**			
Treatment (in A2780/Adr)	**WK-X-34 (10 μM)**	4.5 ± 0.7	**9**	**AS (50 nM)**	19.0 ± 0.8	**2.1**
				AS (100 nM)	9.7 ± 0.9	**4.2**
				AS (200 nM)	7.7 ± 0.9	**5.2**

Abbreviations used in the table: S.F. Sensitizing Factor (A2780/Adr Control / Treatment); AS Antisense (*MDR1* AS ODNs).

From the results in table 5.1, it can be concluded that both treatment strategies effectively inhibit the Pgp-mediated MDR phenotype towards daunorubicin. Although the highest sensitizing factor (S.F. 9) was reached for the treaement with WK-X-34 (10 μM), EC$_{50}$ values were considerably reduced after antisense treatments up to a sensitizing factor of 5.2 for a concentration of 200 nM of antisense ODNs. Hence, it does not appear to make a difference whether the activity of Pgp is decreased by a functional inhibition or by a decrease of functional Pgp molecules in the plasma membrane. The effectiveness of both treatments strategies, however, was unequal. The S.F. of 5.2 could only be obtained in A2780/Adr cells after a three-day treatment with the highest tolerated dose of antisense ODNs (200 nM). In contrats, the S.F. of 9 was easily obtained after a

single dose of WK-X-34 at a concentration (10 μM) much lower than the maximum tolerated dose of 200 μM (see table 4.2). Therefore, it can be concluded that WK-X-34 more effectively reverses the Pgp-mediated MDR phenotype *in vitro* in comparison to antisense treatments.

Moreover, the data presented in table 5.1 reveals a discrepancy between the inhibition of Pgp transport function and MDR phenotype. As the EC_{50} value for WK-X-34 was determined to be around of 80 nM in a daunorubicin transport assay (figure 4.22), a concentration 125 times as high (10 μM) is expected to completely inhibit the Pgp-mediated MDR phenotype towards daunorubicin to levels seen in A2780/wt cells. However, the S.F. of 31 as obtained for A2780/wt cells could not be reached even with the treatment of 10 μM of WK-X-34 (S.F. 9).

Thus, a discrepancy between the inhibition of Pgp-mediated transport and MDR phenotype towards daunorubicin has to be noted. The toxicity of daunorubicin in the multidrug resistant tumor cell is most likely determined by a combination of factors, among which the transport capacity of Pgp plays an important role. However, other MDR mechanisms towards daunorubicin as well as the cytotoxicity of the drug itself contribute to the anti-MDR effect. For A2780/Adr cells, several non-transporter-based MDR mechanisms have been described in the literature. In doxorubicin resistant A2780-DX3 cells, for example, an altered localization of p53 in the cytoplasm, rather than the cell nucleus was detected in comparison to wild-type A2780, suggesting an involvement of p53 in resistance mechanisms towards doxorubicin (Vikhanskaya, 1997). Moreover, resistance against the Toposiomerase II enzyme, which is involved in DNA replication processes, has been associated with the overexpression of Pgp (Kunikane, 1990). It is very likely that such additional MDR mechanisms are present in A2780/Adr but not in A2780/wt cells and might contribute to the protection of WK-X-34 treated A2780/Adr cells from daunorubicin. To confirm the contribution of additional MDR mechanisms towards daunorubicin in A2780/Adr cells, however, further experiments have to be undertaken.

Nevertheless, the results indicate that the reversal of the Pgp-mediated MDR phenotype towards a specific cytotoxic drug like daunorubicin can only be predicted by a transport assay in combination with a chemosensitivity assay.

5.3   MDR inhibitors

Results from *in vitro* characterization of the novel multi-targeted MDR inhibitors will be discussed in the following chapter. Particularly, interactions with Pgp as well as with other ABC transporters will be elaborated with regard to the hypothesis formulated in chapter 2.1 (Novel multi-targeted MDR inhibitors (I.)). The most promising candidate for further development will be selected on the basis of *in vitro* results and compared to current third generation MDR inhibitors.

5.3.1   Characterization of novel MDR inhibitors

Novel MDR inhibitors from our laboratory were characterized for their efficacy in reversing the MDR phenotype in several cell lines. Three novel MDR inhibitors, WK-X-34, WK-X-50 and WK-X-84 were developed and selected. One Xenova compound XR9577, formerly described (Roe, 1999) but never characterized *in vitro/in vivo,* was included. As outlined in chapter 2.3.1, the well-established first generation Pgp inhibitor cyclosporin A (Smeets, 2001; List, 2001) was used as a reference compound.

P-glycoprotein inhibition

Consistently, WK-X-34 and XR9577 were the most effective Pgp inhibitors in all three Pgp transport assays: ^{99m}Tc-Sestamibi accumulation, daunorubicin accumulation and daunorubicin efflux (see chapter 4.3.2.4). These compounds significantly increased intracellular accumulation of daunorubicin with EC_{50} values in the nanomolar range (136 and 82 nM, respectively). EC_{50} values of other recently characterized third generation Pgp inhibitors were found to be in a similar range. For example, EC_{50} values of 12-38 nM and 32 nM were measured for Pgp-mediated MDR reversal by XR9576 and OC144-093, respectively (Mistry, 2001; Newman, 2000). Recent analyses of structure-activity relationships of Tariquidar (XR9576) analogs have revealed that the presence of a bulky aromatic ring system with a third position heteroatom in direction to the anthranilamide structure such as found in

XR9576 and WK-X-34 (compare XR9576 in figure 1.7 and WK-X-34 in figure 3.1) are likely to be associated with a strong Pgp inhibitory potency (Globisch, 2006).

In comparison to WK-X-34 and XR9577, EC_{50} values in the lower micromolar range (4.8 and 2.5 μM) were obtained for verapamil and cyclosporin A (chapter 4.3.2.3). Daunorubicin efflux and ^{99m}Tc-Sestamibi accumulation were most strongly affected by WK-X-34 and XR9577. In these two assays, inhibition by WK-X-34 and XR9577 was also superior to that of cyclosporin A and all other inhibitors. EC_{50} values for ^{99m}Tc-Sestamibi accumulation, for instance, were more than 10-fold lower for WK-X-34 and XR9577 as compared to cyclosporin A.

As ^{99m}Tc-Sestamibi is not a substrate of BCRP and only a very weak substrate of MRP1 (Chen, 2000), results from the ^{99m}Tc-Sestamibi transport assay are very specific for Pgp. Yet the threshold of this assay appears to be higher than for daunorubicin-based assays. These differences might result from parameters related to the Pgp substrates used, ^{99m}Tc-Sestamibi and daunorubicin, and variations in the experimental setups of both assays. As outlined in chapter 2.3.4, the substrates ^{99m}Tc-Sestamibi and daunorubicin display differences in their affinity to and selectivity for Pgp (Muzzammil, 2001). Therefore, only consistent results from a combination of these two transport assays provide reliable information about Pgp inhibition. In contrast to the other MDR inhibitors, WK-X-34 and XR9577 demonstrated a consistent and potent Pgp inhibition in assays utilizing either ^{99m}Tc-Sestamibi or daunorubicin as the transported substrate.

Results from transport assays were in accordance with results generated with chemosensitivity assays (See chapter 4.3.5.1). As chemosensitivity assays were conducted in Pgp-expressing A2780/Adr and non-Pgp expressing A2780/wt cells, interactions with other non-Pgp-related MDR mechanisms towards daunorubicin could be detected. In comparison to verapamil and cyclosporin A, WK-X-34 and XR9577 demonstrated a potent and selective reversal of resistance towards daunorubicin in A2780/Adr but not in the wild-type A2780/wt cells (Table 4.4).

Recent characterizations in the literature

Other recently characterized third generation Pgp inhibitors including GF120918 and XR9576 are summarized in table 5.2. WK-X-34 and XR9577 can be compared to these compounds as they comparably inhibited Pgp efflux activity and reversed Pgp-mediated multidrug resistance with EC_{50} values in the nanomolar range. In table 5.2 the targets as well as the experimental setup for the characterization are presented for each novel inhibitor.

Table 5.2   Novel third generation Pgp inhibitors in the literature –*in vitro* characterization

Reference	MDR inhibitor	Target	Cell Model	*In vitro /in vivo*	*in vitro* Experiments
Hyafil, 1993 Laboratoire GLAXO	GF120918	Pgp, later BCRP[1]	3 human MDR cell lines	*In vitro /in vivo*	Efflux R* Ph*-labeling CS (DOX, VCR)
Dantzig, 1996 Lilly Research	LY335979	Pgp[2]	CEM/ VLB100 cells	*In vitro /in vivo*	Ph*-labeling CS (VNB, DOX, ETP, TAX)
Dale, 1998 Xenova Ltd	XR9051	Pgp	Several human + murine MDR cell lines	*In vitro*	CS (DOX, VCR, ETP) Ph*-labeling Efflux R* Binding VNB*
Newman, 2000 Ontogen Corporation	OC144-093	Pgp	Several human MDR cell lines	*In vitro /in vivo*	ATPase assay Ph*-labeling CS (VNB) Uptake R* Efflux DNR
Mistry, 2001 Xenova Ltd	XR9576	Pgp later BCRP[3]	Several human + murine MDR cell lines	*In vitro /in vivo*	CS (DOX, PTX, VCR, ETP) Ph*-labeling Efflux R*/ F*
Jekerle, 2006a University of Bonn/ Toronto	WK-X-34	Pgp + BCRP	human Ppg, BCRP & MRP cell lines	*In vitro /in vivo*	Uptake R*/ DNR Efflux DNR, MITX, 5-CFDA CS (DNR, MITX)

Abbreviations used in this table:

R*: radiolabeled Pgp substrate; Ph*: photoaffinity labeling using [3H]azidopine; CS: Chemosensitivity assay;

DOX: doxorubicin; VCR: vincristine; VNB: vinblastine; ETP: etoposide; PTX: paclitaxel; TAX: taxol; MITX: mitoxantrone

[1] Malipaard, 2001; [2] Shepard, 2003; [3] Robey, 2004

For *in vivo* characterization see table 7.1.

As all of these compounds have been developed with aims to specifically inhibit Pgp, the initial target was Pgp for all compounds. Only later, some compounds were discovered to also target BCRP, while others like LY335979 were confirmed to be selective for Pgp (Shepard, 2003). GF120918 (Malipaard, 2001) and XR9576 (Robey, 2004) are such examples as they have been shown to interact with BCRP. Similarly to GF120918 and XR9576, BCRP inhibition was verified for WK-X-34 and XR9577.

Like WK-X-34, most of these third generation Pgp inhibitors have been characterized using functional *in vitro* and *in vivo* assays. *In vitro* experiments were typically carried out in a number of different multidrug resistant human cell lines. Newman and coworkers, for example, applied a combination of multidrug resistant human cancer cell lines for the characterization of OC144-093. The researchers used human lymphoma (CCRF-CEM) and ovarian carcinoma cells (SKOV3), which they incubated in the presence of vinblastine to obtain the MDR variant. Additionally, they used human breast cancer cells (MCF7) which were challenged with doxorubicin in order to obtain the MDR variant MCF/Adr (Newman, 2000). XR9576 was studied (Mistry, 2001) using the same A280/Adr cell model as for WK-X-34.

Similarly to WK-X-34, other *in vitro* characterizations contained a combination of assays. Pgp transport assays were used with different radiolabeled or non-labeled substrates and combined with chemosensitivity assays using different chemotherapeutic agents. For WK-X-34 one radiolabeled substrate (^{99m}Tc-Sestamibi) and one non-labeled substrate (daunorubicin) were used. Parts of this present thesis, containing the characterization of WK-X-34 and other inhibitors, have been summarized and published (Jekerle, 2006a; Jekerle, 2006b; also see table 5.2 and 5.3). In these reports, WK-X-34 has been examined applying a combination of MDR transport and chemosensitivity assays, comparable to other third generation Pgp inhibitors. Some important techniques, however, including photoaffinity labeling with [3H]azidopine, unfortunately, could not be conducted for WK-X-34 due to the lack of resources and facilities for this technique.

In the photoaffinity labelling experiments, the compound and [3H]azidopine compete for binding to the Pgp molecule. Hence, the technique allows the examination of direct binding between a compound and Pgp. However, as up to

seven different binding sites (Safa, 2004) were identified on the Pgp molecule, it remains to be evaluated whether the investigated compound and [3H]azidopine actually compete for the same binding site. The technique was applied by most groupes for the characterization of novel Pgp inhibitors. It must be kept in mind, however, that most groups applying photoaffinity labelling are based in large pharmaceutical companies such as Lilly Research, Glaxo Laboratories or Xenova Ltd which develop Pgp inhibitors solely with a commercial aim. Obviously, their financial resources, techniques and manpower available for screening experiments are much greater than those of laboratories within an academic setting.

5.3.2   Interactions with other ABC transporters

Thus far, inhibition of a single MDR mechanism like Pgp alone could not successfully reverse MDR in clinical applications. As several other ABC transporters such as BCRP and MRP1-3 have been found to be implicated in the development of multidrug resistant tumors (Sarkadi, 2004; Allen, 2002; Borst, 2002), the interaction profile with these transporters was further characterized.

Breast cancer resistance protein

The breast cancer resistance protein, BCRP, was potently inhibited by all WK-X-compounds and XR9577 with EC_{50} values in the low micromolar range. Indeed, inhibition of BCRP-mediated efflux of mitoxantrone was comparable to that of the well-established BCRP inhibitor novobiocin (Yang, 2003). This is of particular interest as histological studies have identified an extensive overlap between BCRP and Pgp in many tumors. BCRP has been found to be overexpressed in over 40 % of different tumor tissues including colon or melanoma (see chapter 1.2.2). Hence, BCRP is believed to play a more important role in drug resistance than originally thought (Allen, 2002). Only recently, the involvement of BCRP in the development and protection of drug resistant cells was confirmed with the discovery that high levels of BCRP are expressed in leukemic stem cell subpopulations. These stem cells are highly resistant towards chemotherapeutic treatments (Raaijmakers, 2005; Doyle, 2003). Incomplete eradication of cancer stem cells is thought to be a main

cause for tumor relapse. Therefore, treatment strategies designed to target the tumor together with its stem cell subpopulation would considerably improve the clinical outcome. Additional BCRP modulating effects can thus be of great advantage, when choosing an adequate Pgp inhibitor for the treatment of MDR resistant tumors.

Findings from chemosensitivity assays underline the ability of XR9577 and WK-X-34 to target BCRP-protected cells and to reverse their resistance towards BCRP substrates. Chemosensitivity towards the mitoxantrone was strongly increased for XR9577 and WK-X-34 by 200- and 400-fold, respectively (see table 4.5). In comparison, cyclosporin A showed little effects.

Interestingly, WK-X-34 and XR9577 show a strong similarity to the structures of GF120918 and XR9576, both potent BCRP and Pgp inhibitors. Like XR9576 and GF1209188 (see figure 1.7), WK-X-34 and XR9577 (see figure 3.1) consist of a tetrahydroisoquinolin-ethyl-phenyl amine partial structure which is connected to a highly hydrophobic rest via an amide bond. Therefore, it is likely that these common structures within the molecules might contain the BCRP binding domain. This is of particular interest as no BCRP pharmacophore model has been developed to date.

Multidrug resistance associated proteins

MDR-associated proteins MRP1, MRP2 and MRP3 have been shown to be implicated in the development of MDR in many different tumors (Kruh, 2003; Kool, 1999). Moreover, the MRP transporters are widely expressed in different organs and tissues, where they are involved in many physiological functions such as the excretion of xenobiotics and endogenous substrates, protection of tissues and cell signalling (see chapter 1.2.3). Accidental inhibition of the MRP transporters by MDR inhibitors can cause a substantial interference of important protection mechanisms which contributes to clinical toxicities, particularly in the presence of chemotherapeutic agents (see chapter 1.2.3). Thus, it is important to analyze the interaction profile of novel MDR inhibitors with the three transporters MRP1-3.

Interactions with MRP1, MRP2 or MRP3 were not detected for WK-X-34. XR9577 only showed some high dose MRP1 interference. In contrast, the unspecific

MDR inhibitor verapamil displayed various unspecific inhibitions of MRP1-, MRP2- and MRP3-mediated transport. Consistent with previously published reports (Qadir, 2001), cyclosporin A was identified as an MRP1 inhibitor with some additional effects on MRP3.

Cyclosporin A, however, appears to be an unselective broad-spectrum inhibitor with effects in resistant and sensitive cells. Cyclosporin A displayed moderate effects on Pgp and the MRPs, particularly MRP1 (Qadir, 2005). In daunorubicin chemosensitivity assays, for example, it was detected that cyclosporin A increased sensitivity towards daunorubicin by 7-fold in sensitive non-Pgp expressing A2780/wt cells. This observation can only be explained by interaction with MDR mechanism, other than Pgp. The interfering mechanisms appear to be sensitive for daunorubicin, but not for mitoxantrone (Table 4.5). Daunorubicin is a fairly unspecific substrate of Pgp; it is also transported by MRP1 and BCRP (Chauvier, 2002; Jia, 2005). As MRP1, but not Pgp, is expressed in A2780/wt cells, and cyclosporin A is an inhibitor of MRP1 (see chapter 4.3.4.1), it is likely that MRP1 contributes to the increase of sensitivity towards daunorubicin in the presence of cyclosporin A in wild-type A2780/wt cells. The observations above indicate that unselective MDR inhibition by the first generation MDR inhibitor cyclosporin A, for example, may cause highly unpredictable interactions such as with sensitive tumor celllines that do not express the target.

Summary of BCRP and MRP inhibition

The two novel MDR inhibitors, WK-X-34 and XR9577, demonstrated potent and specific inhibition of BCRP- and Pgp-mediated transport and functionality with no effects on wild-type cells like A2780/wt and MCF7/wt. For potential clinical applications, a specificity of the MDR inhibitor for multidrug resistant cells is anticipated in order to prevent interactions and toxicities resulting from unspecific effects in different tissues and organs. The findings suggest that target specificity is considerably improved for WK-X-34 and XR9577 as compared to the first generation inhibitors verapamil and cyclosporin A.

5.3.3   Multi-targeted MDR inhibitors

Recent discoveries have confirmed that many multidrug resistant tumors and important cancer stem cell populations express multiple MDR transporters. These findings have highlighted the importance of MDR inhibitors with broad-spectrum properties (Ross, 2000; Brooks, 2003). For the modulation of multiple MDR mechanisms, a combination of specific MDR inhibitors or one multi-targeted compound can be used.   The use of one effective broad-spectrum inhibitor versus single-spectrum inhibitors in combination may offer some advantages. Cumulative toxicities, for instance resulting from a potential competition for excretion pathways, are easier to prevent when only one compound is administered in combination with the chemotherapy. Moreover, potential interactions with non-cancer related targets are decreased. Finally, the pharmaceutical compliance of the therapy is ameliorated when fewer drugs are administered at the same time.

Among numerous disappointing attempts to use novel MDR inhibitors in clinical investigations, the first generation Pgp inhibitor, cyclosporin A, showed some encouraging results in AML-patients (Smeets, 2001; List, 2001). The recent discovery that cyclosporin A actually is a broad-spectrum inhibitor with effects on Pgp, BCRP, MRP1 and the lung resistance protein (LRP) (Qadir, 2005) underlines the importance of a "broad-spectrum therapeutic approach". In this thesis, these findings could be confirmed for MRP1 and Pgp but only vaguely for BCRP (see chapter 4.3.3 and 4.3.4).   Interactions with LRP were not investigated. Overexpression of MRP1 and LRP could be associated with MDR in AML and other malignancies (Kruh, 2003; List, 1996). Their prognostic relevance, however, remains unclear, as studies have been published showing that there is no correlation between high MRP1 (Filipits, 1997) and LRP (Damiani, 1998) expression and clinical response in AML. As previously discussed, BCRP has been discovered to be a crucial component in the MDR of many tumors and seems to be implicated in the protection of tumor stem cell subpopulations.

Therefore, treatment strategies directed against Pgp and BCRP in combination might target the tumor together with its self-renewing cancer stem cell subpopulation. It therefore appears likely that successful clinical trials in ALM

patients for cyclosporin A were mainly due to its Pgp inhibition in combination with a potentially much lower BCRP inhibition (Ross, 2004).

In comparison to cyclosporin A, our novel WK-X- compounds, particularly WK-X-34 and XR9577 demonstrate stronger BCRP and Pgp modulating properties. They effectively inhibited BCRP-mediated efflux and chemosensitivity towards mitoxantrone in a way that was comparable to novobiocin.

Furthermore, cyclosporin A, despite convincing performance in clinical trials, is associated with many interactions and toxicities, particularly neurotoxicities (Calney, 1979; Gijtenbeek, 1999). As clinical toxicities are a major limitation to the successful therapeutic application of MDR inhibitors, this might present an advantage of the novel WK-X-compounds and XR9577, which demonstrated significantly lower *in vitro* toxicities compared to cyclosporin A. Of note, toxicity studies in mice revealt that WK-X-34 was well tolerated both in wild-type and immunocomprimised mice.

Novel multi-targeted MDR inhibitors

With the latest discoveries about the complexity of MDR mechanisms in mind, our group and other researchers have begun to develop MDR inhibitors with targets other than Pgp. In 2002, Allen and coworkers published a report introducing a novel BCRP inhibitor, Ko143, a non-toxic, synthetic analog of fumitremorgin C. This compound was thoroughly characterized *in vitro* and *in vivo*. Ko143 appears to be the most potent BCRP inhibitor to date and was shown to effectively reverse BCRP-mediated MDR with low activity against Pgp and MRP1. *In vivo*, Ko143 markedly increased the oral bioavailability of topotecan in mice (Allen, 2002).

The characterizations of recently developed compounds are summarized in table 5.3. Minderman and coworkers have concentrated on multi-targeted MDR inhibitors. Two *in vitro* characterizations of the compounds, VX-710 and BAY59-8862, both targeting Pgp, BCRP and MRP1 were published in 2004 (Minderman, 2004a; Minderman, 2004b). VX-710 has already proven clinical safety and efficacy in Phase II clinical studies. VX-710 was investigated in combination with paclitaxel in women with advanced multidrug resistant breast cancer (Toppmeyer, 2002) and in

combination with mitoxantrone and prednisone in men with hormone-refractory prostate cancer (Rago, 2003).

Table 5.3 Novel MDR inhibitors targeting Pgp, BCRP and/or MRP1 in the literature

Reference	MDR inhibitor	Target	Cell Model	*In vitro/ In vivo*	*In vitro* Experiments
Allen, 2002 Netherlands Cancer Institute	Ko143	BCRP	Several human + murine BCRP expressing cell lines	*In vitro/ in vivo*	Uptake MITX CS (MITX, TPC)
Minderman, 2004a Roswell Park Cancer Institute, NY	VX-710 (Biricodar)	Pgp, BCRP, MRP1	Pgp, BCRP and MRP over-expressing human cell lines	*In vitro*	Uptake MITX, DNR CS (DOX, MITX, DNR, TPC)
Minderman, 2004b Roswell Park Cancer Institute, NY	BAY59-8862 (Ortataxel)	Pgp, BCRP, MRP1	Pgp, BCRP and MRP over-expressing human cell lines	*In vitro*	Uptake MITX,DOX, DNR CS (DOX, MITX, DNR, TPC)
Jekerle, 2006b University of Bonn/Toronto	WK-X-34 WK-X-50 WK-X-84 XR9577	Pgp, BCRP, (MRPs)	Pgp, BCRP and over-expressing human cell lines Selectively transfected cell lines with MRP1,2 and 3	*In vitro*	Uptake R*, DNR Efflux MITX, DNR, 5-CFDA CS (DNR, MITX)

Abbreviations used in this table:

R*: Radio-labeled substrate, CS: Chemosensitivity assay;

DOX: doxorubicin; DNR: daunorubicin; MITX: mitoxantrone; PTX: paclitaxel; TPC: topotecan

For *in vivo* characterization see table 7.1

For over 15 years, research in the MDR field has focused on the development of selective Pgp inhibitors to target resistant tumor cells. The recent concentration on multi-targeted MDR inhibitors, however, points at the potential that lies in a

"broad-spectrum approach". In line with these latest developments, the additional BCRP inhibitory properties of WK-X-34 and XR9577, make these two compounds particularly interesting.   Current knowledge in the field indicates that anti-MDR treatments benefit from BCRP inhibition due to the involvement of BCRP in many tumors and cancer stem cell subpopulations. Therefore, WK-X-34 and XR9577 are two promising compounds that warrant further development. XR9577 and WK-X-34 appear to be of equal potency. XR9577 has been formerly described by Roe and coworkers (Roe, 1999). In contrast, WK-X-34 was developed and described solely by our research group.   Therefore, WK-X-34 was selected for further *in vivo* investigations.

6 Results - *in vivo*

Two separate sets of ^{99m}Tc-Sestamibi imaging experiments were performed in order to investigate the *in vivo* effects of WK-X-34 and *MDR1* antisense ODN treatments in Pgp overexpressing and sensitive tumors. The experimental designs of the "WK-X-34 imaging study" and the "WK-X-34 + antisense imaging study" are outlined in chapter 3.4.1.

Imaging experiments were carried out about four weeks following tumor inoculation, when tumor xenografts reached a weight of approximately 0.5 g. In picture 1 (Appendix) the development of the human ovarian cancer xenografts is presented over the span of four weeks.

To begin with, the toxicity of the utilized WK-X-34 Cremophor EL formulation was investigated.

6.1 Toxicity of the WK-X-34 formulation

Based on *in vitro* results, the novel MDR inhibitor WK-X-34 was chosen for *in vivo* characterization as outlined in chapter 5.3.3. The substituted 2-benzamidobenzamide WK-X-34 (for structure see figure 3.1) exhibits very low water solubility; therefore *in vivo* formulations were developed using 10 % Cremophor EL ethanol as solvent.

As Cremophor EL has been associated with some toxic *in vivo* effects (e.g. peripheral neuropathy) (Gelderblom, 2001), potential toxicity of the WK-X-34-Cremophor EL formulation had been studied before ^{99m}Tc-Sestamibi imaging experiments were initiated.

In vivo toxicity experiments were conducted in six-week old female CD1 mice. The animals were injected i.p. daily with a 100 µl dose of 20 or 50 mg/kg of WK-X-34 Cremophor EL formulation for 14 days. Controls received the vehicle only. Mice

were examined every second day for 14 days for any signs of ill effects including weight loss, change in appetite or behavioral changes.

Two days following the first dose of WK-X-34, mice appeared healthy, agile and no weight loss was detectable in all animals (see figure 6.1). These experiments were carried on for 14 days. Likewise, no differences in body weights were detected between all groups.
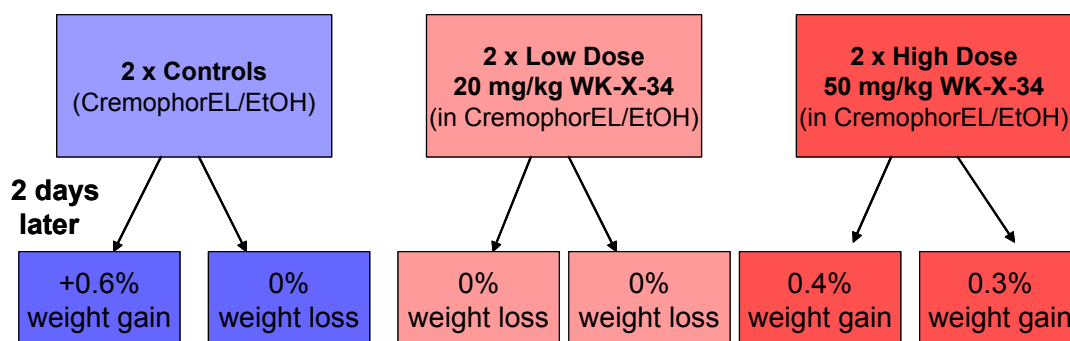
Figure 6.1   Toxicity of WK-X-34/Cremophor EL formulation in CD1 mice

Female CD1 mice were injected with either 20 or 50 mg/kg of WK-X-34 in Cremophor EL or vehicle control and potential weight loss was determined two days later.

Potential hepatotoxicity of WK-X-34 in Cremophor EL was studied using the ALT hepatotoxicity test (see chapter 3.4.4). A substantial loss of absorption was not detected and the slopes of all treated and control animals did not differ significantly from each other. These findings indicate that WK-X-34 is unlikely to have any hepatotoxic effects in mice.

WK-X-34 in the formulation with Cremophor EL ethanol (1:1) appeared to be fairly untoxic in mice. As a precaution, the total amount of Cremophor EL was kept to a minimum of 10 % for all following experiments.

6.2   WK-X-34 imaging studies

6.2.1 ^{99m}Tc-Sestamibi imaging

These studies were designed to investigate the *in vivo* performance of the selected MDR inhibitor WK-X-34.   Human ovarian cancer xenografts bearing a resistant A2780/Adr and a sensitive A2780/wt tumor on each back flank were developed in immunocomprimised mice. ^{99m}Tc-Sestamibi uptake was studied twice in the same animal in the absence and presence of WK-X-34. Thus, effects of WK-X-34 on the accumulation of ^{99m}Tc-Sestamibi in the resistant and sensitive tumor xenograft as well as potential inhibition of physiological Pgp in liver, kidney, brain, intestine and heart could be examined.   Gamma images obtained from ^{99m}Tc-Sestamibi imaging experiments elegantly visualized the *in vivo* distribution of the Pgp substrate ^{99m}Tc-Sestamibi in the presence and absence of WK-X-34.   As each animal was imaged on two consecutive days without and with WK-X-34 pretreatment, accumulation of ^{99m}Tc-Sestamibi could be compared in the same tumor of the same animal.

Changes in the intensity of ^{99m}Tc-Sestamibi within the region of the A2780/Adr tumor upon WK-X-34 administration were detectable for all animals. The 2 h images of a representative animal in the absence (baseline) and presence of 20 mg/kg WK-X-34 are shown in figure 6.2.
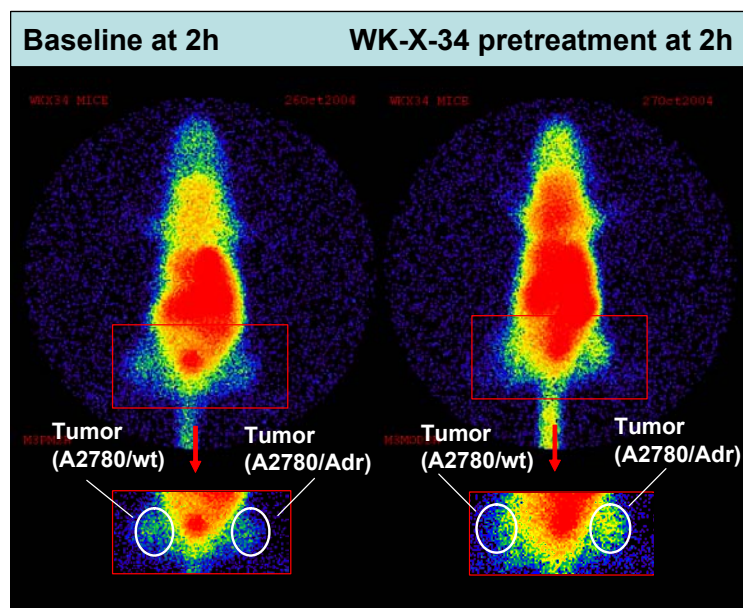
Figure 6.2 ^{99m}Tc-Sestamibi images of A2780/Adr and A2780/wt xenografts at 2 h

Representative dorsal images of the same animal at baseline (left) and after administration of WK-X-34 (right) are depicted as taken 2 h after tail vein injection of ^{99m}Tc-Sestamibi in mice xenografts bearing an A2780/wt tumor on the left flank and an A2780/Adr tumor on the right flank. The two images are normalized to the same color intensity

In these images, A2780/Adr tumors are visible on the right flank and A2780/wt tumors are visible on the left flank, as indicated. The tumor regions are enlarged in the box below and surrounded by a white ring. On the right image (WK-X-34 pretreatment), an increase in radio-intensity is detectable for the A2780/Adr tumor but not for the A2780/wt tumor.

Furthermore, potential changes in the ^{99m}Tc-Sestamibi distribution throughout the body over the span of the imaging experiments were investigated. In figure 6.3, the 15 min, 1 h, 2 h and 4 h gamma-images at baseline and upon WK-X-34 pretreatment are presented for the same animal.
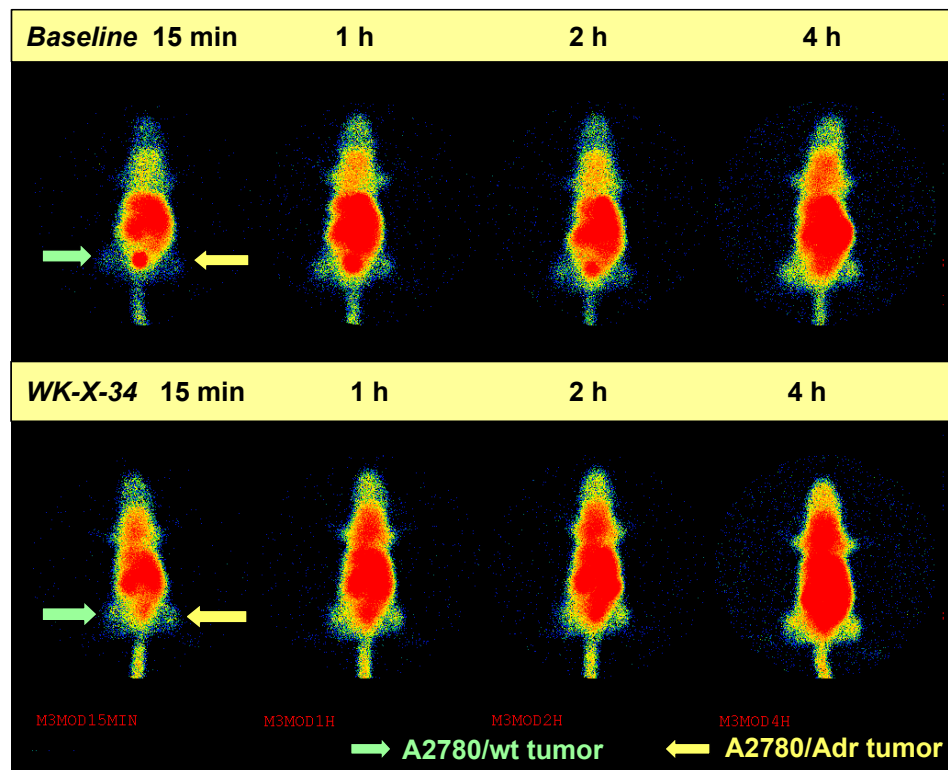
Figure 6.3   Time course of ^{99m}Tc-Sestamibi distribution in tumors and organs

Representative dorsal ^{99m}Tc-Sestamibi images at baseline and after administration of WK-X-34 are depicted as taken 15 min, 1 h, 2 h and 4 h after tail vein injection of ^{99m}Tc-Sestamibi in BalbC nu/nu mice bearing an A2780/wt tumor on the left flank and an A2780/Adr tumor on the right flank (indicated by arrows). All images are normalized to the same color intensity.

Differences in the overall body distribution between baseline and WK-X-34 treatments are easily detectable for all time points. Radio-intensity was particularly increased in the region of the brain. ^{99m}Tc-Sestamibi appeared to accumulate in the brain, as higher levels were detectable at later time points (see figure 6.3: WK-X-34 at 4 h). An increase in the region of the A2780/Adr tumor on the right flank of the animal was furthermore visible on the 1 h, 2 h and 4 h images.

Regions of interest were drawn around the brain, heart, liver, intestine, right kidney, A2780/Adr tumor and A2780/wt tumor (see picture 5, appendix). The radio-intensity (expressed in counts/pixel/second) in these regions was determined for each image and plotted against the imaging time point. Representative radio-intensity-time plots for the region of the whole body, brain and A2780/Adr tumor are shown in figure 6.4. Whereas the radio-intensities in the region of the whole body

were equal between baseline and WK-X-34 pretreatment, radio-intensity was increased in the regions of the brain and the A2780/Adr tumor upon WK-X-34 pretreatment. From radio-intensity-time plots the AUC values were calculated for each organ (for calculation see chapter 3.4.8).
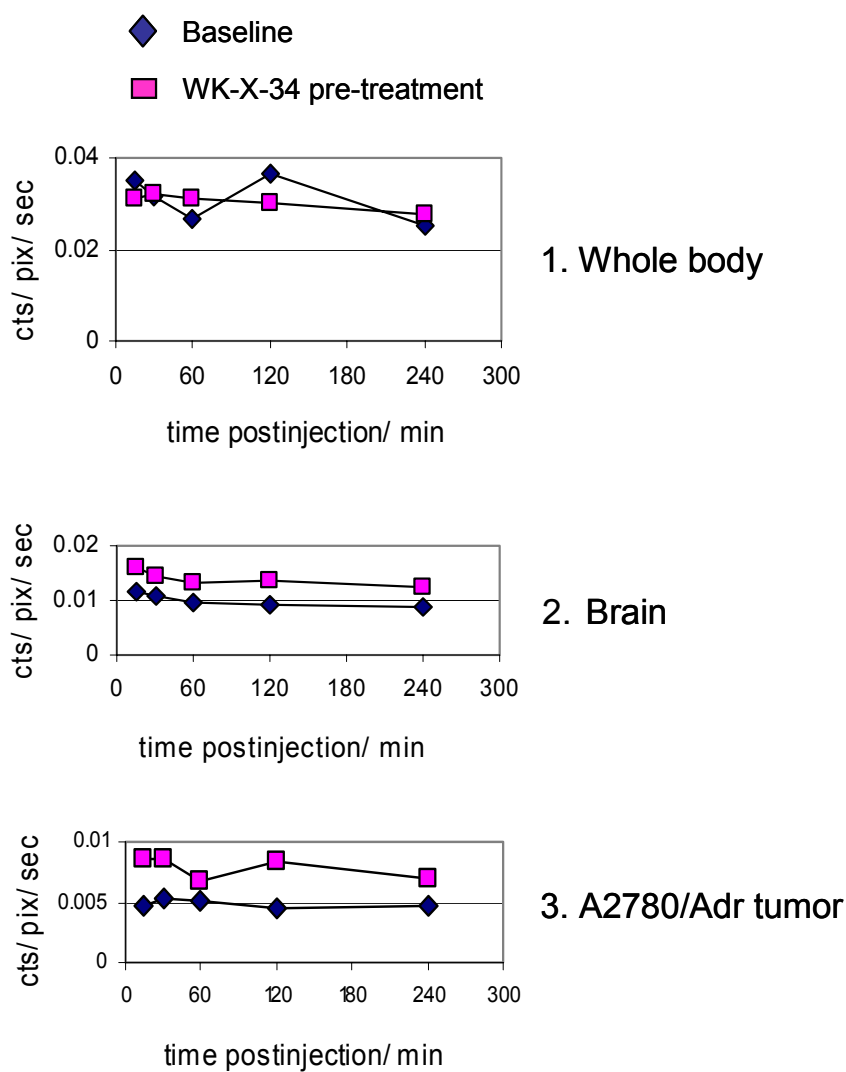
Figure 6.4   Radio-intensity-time plots for whole body, brain and A2780/Adr tumors

The radio-intensity at baseline and upon WK-X-34 pretreatment in the region of the whole body, brain and A2780/Adr tumor is plotted against the time postinjection. Representative plots from one animal are shown. Radio-intensity-time plots were generated for each gamma image and AUC values were calculated using the linear trapezoid method.

In figure 6.5, the AUCs of organs and tumors were compared between baseline and WK-X-34 treatment. The results show changes in ^{99m}Tc-Sestamibi accumulation within the organ region (in % of baseline treatment) in the presence of WK-X-34. Values above 100 % indicate increased accumulation of ^{99m}Tc-Sestamibi in the region.

	Brain	Heart	Liver	Intestine	Kidney	A2780/Adr tumors	A2780/wt
AUCs	147.5	85.3	100.2	137.9	123.2	135.5	119.2
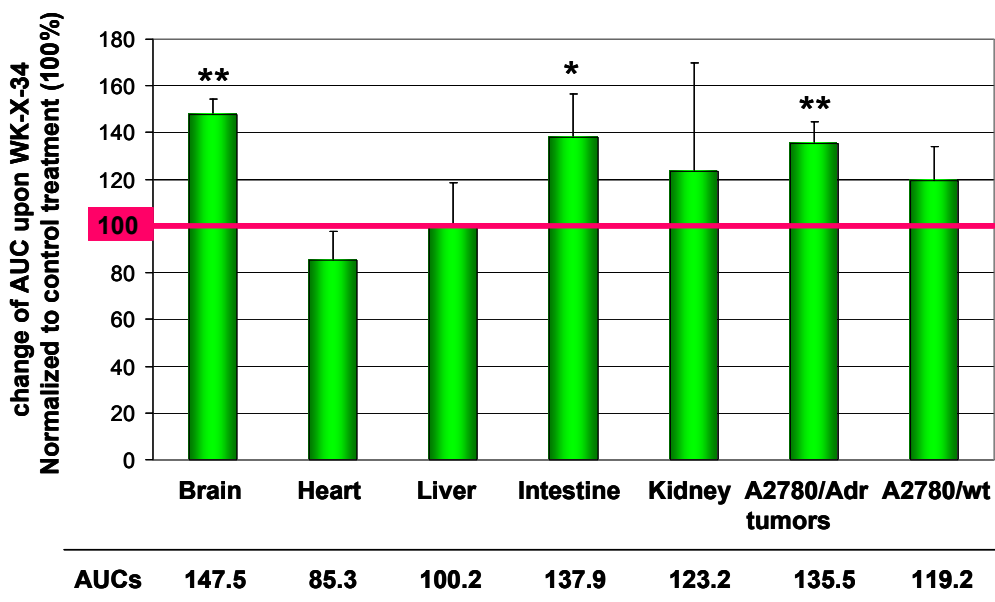
Figure 6.5   AUC analysis of ^{99m}Tc-Sestamibi distribution in tumors and organs

^{99m}Tc-Sestamibi uptake into tumors and tissues on gamma images were analyzed by ROI analysis. The AUC values for individual organs and tumors were calculated for imaging time points between 15 min and 4 h. Results indicate the % change of uptake upon WK-X-34 treatments in comparison to control treatments. Results are expressed as means of n=5 ± S.D. with p-levels of * ≤ 0.05 and ** ≤ 0.01, as determined by a paired two-tailed *t*-test.

Administration of WK-X-34 significantly increased the radio-intensity of ^{99m}Tc-Sestamibi uptake into the Pgp-overexpressing (A2780/Adr) tumor to 136 % of control but did not significantly alter accumulation in the A2780/wt tumor. Furthermore, significantly increased ^{99m}Tc-Sestamibi accumulation was detectable in the brain and intestine (148 % and 138 % of control) of the WK-X-34 treated mice. This indicates a rapid and prolonged *in vivo* inhibition of Pgp in these tissues. ROI analysis of ^{99m}Tc-Sestamibi imaging of central organs such as the liver and the kidney showed considerable variability due to some overlaps in their imaging regions. Therefore,

significant changes could not be detected. WK-X-34 did not significantly affect whole body imaging values.

6.2.2 ^{99m}Tc-Sestamibi biodistribution

To confirm results from ^{99m}Tc-Sestamibi imaging, biodistribution analyses were performed two hours postinjection of the radiopharmaceutical (see chapter 3.4.9). Table 6.1 summarizes the results from the biodistribution study. Organ levels of ^{99m}Tc-Sestamibi are expressed as a % of the injected dose per gram of tissue (%ID/ g tissue). Furthermore, results from tumors were normalized to the non-Pgp expressing tissue muscle and are given as tissue/muscle ratios. As compared to controls, ratios of ^{99m}Tc-Sestamibi concentrations in the A2780/Adr tumors to concentrations found in non-Pgp expressing muscle tissue were significantly increased by 9-fold in WK-X-34 pretreated mice ($p<0.05$). In A2780/wt tumors, a much smaller elevation was seen however, the results were inconsistent and did not reach a level of significance. Elevated levels in A2780/wt tumors, particularly at later time points, can be explained by an inhibition of Pgp-mediated routes of ^{99m}Tc-Sestamibi excretion via the liver and the kidneys (Kabasakal, 2000). ^{99m}Tc-Sestamibi is rapidly cleared from the blood into other organs. Interestingly, relative blood levels in WK-X-34 treated animals are significantly lower compared to non-treated animals. Physiological Pgp is also inhibited in WK-X-34 treated animals. Hence, impaired ^{99m}Tc-Sestamibi efflux from tissues such as heart or brain back into the blood might account for lower blood levels. Furthermore, significantly increased retention of radioactivity was detectable in the brain and liver. In contrast to ^{99m}Tc-Sestamibi imaging data, a significant increase was also detected for the region of the heart.

Table 6.1 Biodistribution of ^{99m}Tc-Sestamibi in control and WK-X-34 treated xenograft mice[§]

Tissue	%ID/ g tissue ± S.D. Control		WK-X-34 treatment		% of control values	
Blood	0.18	± 0.02	0.11*	± 0.02	61	± 11
Heart	5.90	± 1.13	10.09*	± 1.55	**171**	**± 26**
Liver	5.83	± 0.36	11.91*	± 2.44	**204**	**± 42**
Kidney	14.60	± 1.24	15.07	± 1.45	103	± 10
Intestine	6.50	± 2.69	5.09	± 1.47	78	± 23
Muscle	1.63	± 0.13	2.58*	± 0.2	**158**	**± 13**
Brain	0.06	± 0.00	0.10*	± 0.02	**166**	**± 33**
Adr Tumor	0.09	± 0.12	0.95*	± 0.32	**1055**	**± 356**
Wt Tumor	0.13	± 0.04	0.44	± 0.28	338	± 216

Tissue/ muscle ratios

Adr Tumor	0.05	± 0.001	0.45*	± 0.20	**900**	**± 392**
Wt Tumor	0.074	± 0.05	0.284	± 0.31	384	± 419

[§] Values represent means ± S.D. for 5 xenograft mice per group with p-levels of * *p* < 0.05.

6.3   WK-X-34 + antisense imaging studies

6.3.1 ^{99m}Tc-Sestamibi imaging

Mouse xenografts bearing two A2780/Adr tumors on each back flanks were injected with *MDR1* antisense ODNs into one tumor for three days. Animals were divided into a control and a WK-X-34 treatment group, and ^{99m}Tc-Sestamibi imaging was performed on day 4 following the antisense treatments. The experimental setup of the "WK-X-34 + antisense imaging studies" is outlined in chapter 3.4.1.2. Prior to the injection of the radiopharmaceutical ^{99m}Tc-Sestamibi, mice were pretreated either with 20 mg/kg of WK-X-34 or vehicle.

Representative gamma images (Figure 6.6) show the *in vivo* distribution and uptake of ^{99m}Tc-Sestamibi 15 min and 1 h postinjection into both tumors. The location of the control (blue) and antisense (orange) treated A2780/Adr tumor is indicated by arrows. In controls, ^{99m}Tc-Sestamibi uptake was slightly increased in the antisense pretreated tumor as compared to the non treated tumor (see 1 h image of control animals). Administration of WK-X-34 increased the amount of ^{99m}Tc-Sestamibi into both tumors (see orange line).
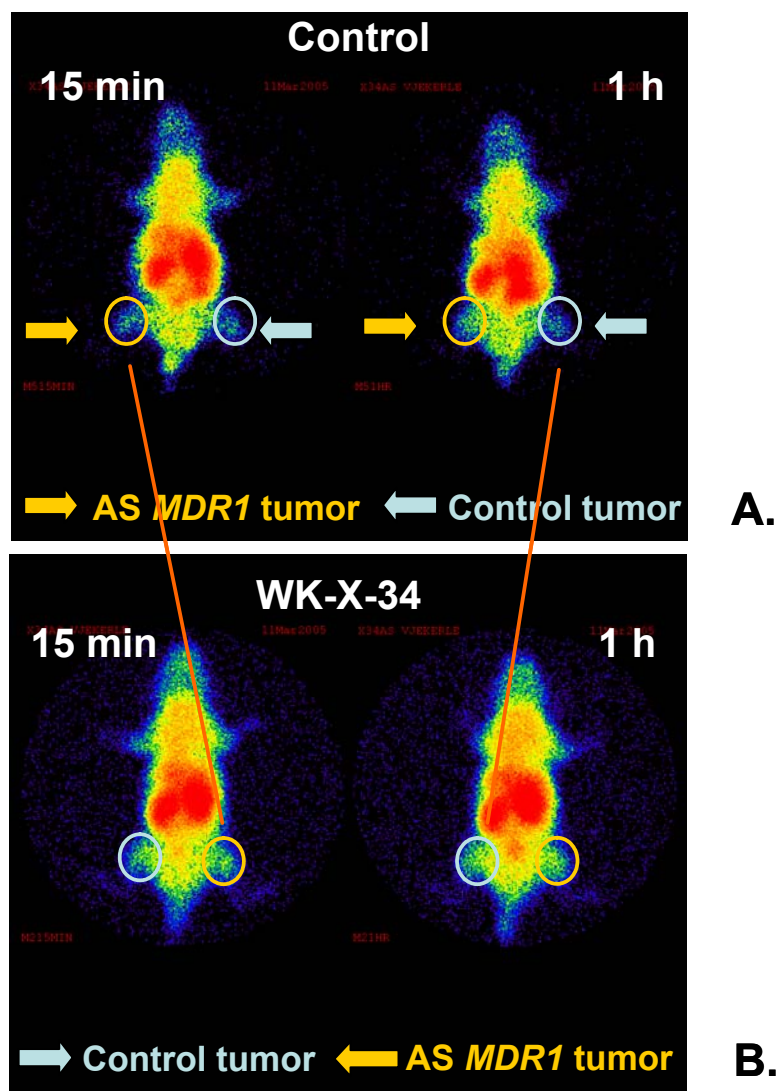
Figure 6.6 ^{99m}Tc-Sestamibi imaging of A2780/Adr xenografts

Representative dorsal images of control **(A)** and WK-X-34 treated **(B)** mice were acquired 15 min and 1 h postinjection of ^{99m}Tc-Sestamibi. Mice xenografts were bearing two A2780/Adr tumors on the right and left flank (see regions), of which one (orange) had been treated intra-tumorally with *MDR1* antisense ODNs. Images are normalized to the same color intensity.

Again, ROI analyses were performed and these data are presented in figure 6.7 for the 1 h imaging time point. Data of four animals per group were analyzed.

Increased ^{99m}Technetium accumulation of about 20 % and 90 % of control was determined within the region of the antisense treated and untreated tumor in WK-X-34 treated mice, respectively. Due to high variability between animals within the same treatment group, the data did not reach a level of significance.
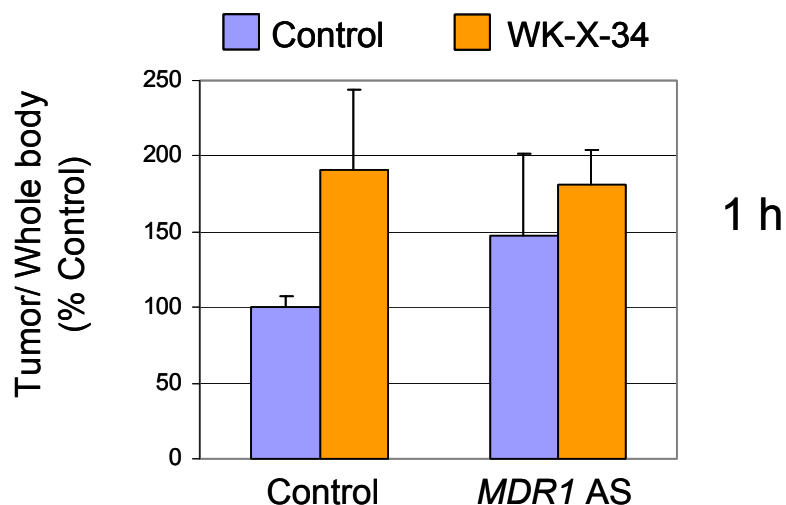
Figure 6.7 ROI analyses of ^{99m}Tc-Sestamibi imaging in A2780/Adr xenografts

^{99m}Tc-Sestamibi uptake into tumors was analyzed by ROI analysis. The AUC values for both tumors were calculated for the 1 h imaging time point and normalized to whole body. Results indicate the % change of uptake upon WK-X-34 and/or *MDR1* AS treatments in comparison to control treatments. Results are expressed as mean values of n=5 ± S.D. Data were analyzed using a two-tailed unpaired t-test; a level of significance ($\alpha <$ 0.05) was not reached.

6.3.2 ^{99m}Tc-Sestamibi biodistribution

Comparably to the WK-X-34 imaging study (see chapter 6.2), biodistribution analyses were performed and the results are presented in table 6.2. Tumor levels of ^{99m}Tc-Sestamibi were initially calculated as a % of injected dose per gram of tissue (%ID/ g tissue) and are normalized to the non-Pgp-expressing tissue "muscle". In the WK-X-34 pretreated mice, ^{99m}Tc-Sestamibi tissue/muscle ratios in untreated and antisense-pretreated tumors were significantly increased by 9- and 2-fold, respectively.

Table 6.2 ^{99m}Tc-Sestamibi biodistribution in A2780/Adr xenografts

Tissue/ muscle	Control mean ± S.D.	WK-X-34 pretreatment mean ± S.D.	
Blood	0.32 ± 0.091	0.09 ± 0.091	
Control Tumor	0.05 ± 0.001	0.45* ± 0.196	(9-fold)
MDR1 AS Tumor	0.18 ± 0.122	0.38* ± 0.065	(2-fold)

Table 6.2 Accumulation of ^{99m}Tc-Sestamibi radioactivity in control and *MDR1* AS treated tumors was determined from isolated tissues. Results are expressed as a % dose/gram of tissue and normalized to muscle**.** Data are expressed as means ± S.D. of 4 animals with p-levels determined by an unpaired two-tailed t-test of $\alpha^{**} < 0.01$ and * <0.05.

6.4   Tumor characterization

6.4.1   Immunohistochemical analyses of tumor tissue

Tumor growth was comparable in A2780/Adr and A2780/wt xenografts as observed by caliper measurements (for tumor development see picture 1 in appendix) and H&E histological analysis (Figure 6.8).
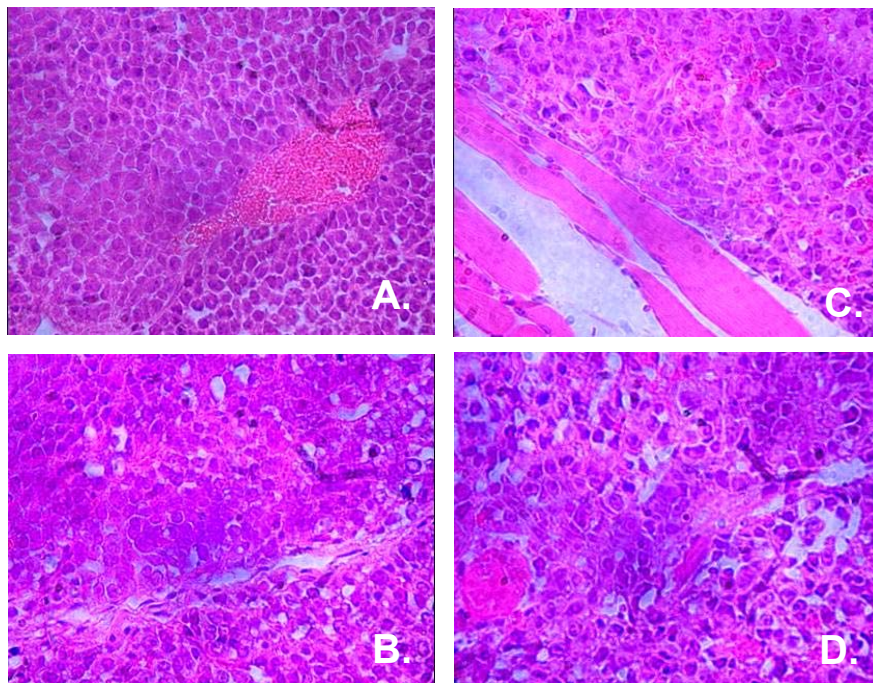
Figure 6.8   H & E staining of tumor tissue

Representative pictures of tumor tissue obtained from A2780/wt **(A, B)** and A2780/Adr **(C, D)** xenografts are shown. Tissue sections were H & E stained and pictures were taken on a light microscope using a 40x/0.65 oil-immersion objective.

In Figure 6.8, picture A and B show tissue sections from A2780/wt tumors and picture C and D are obtained from A2780/Adr tumor sections. A blood vessel incorporated in the tumor tissue can be seen on picture A. Infiltrated blood cells are visible on pictures C and D. In figure C invasive growth of the tumor tissue into remaining muscle tissue can be observed. To summarize, both tumors showed

invasive growth into muscle tissue with high vascularisation. This observation is important as it confirms that detected changes in ^{99m}Tc-Sestamibi accumulation between resistant and sensitive tumors were not due to a difference in tissue formation.

6.4.2   Immunofluorescence examinations of tumor tissue

Additionally, Pgp expression was examined by immunofluorescence analysis using the FITC-labeled anti human Pgp monoclonal antibody according to methods specified in chapter 3.4.10. Tissue sections from A2780/Adr and A2780/wt tumors as well as from antisense treated A2780/Adr tumors were analyzed. Representative fluorescence microscopy pictures are shown in figure 6.9.
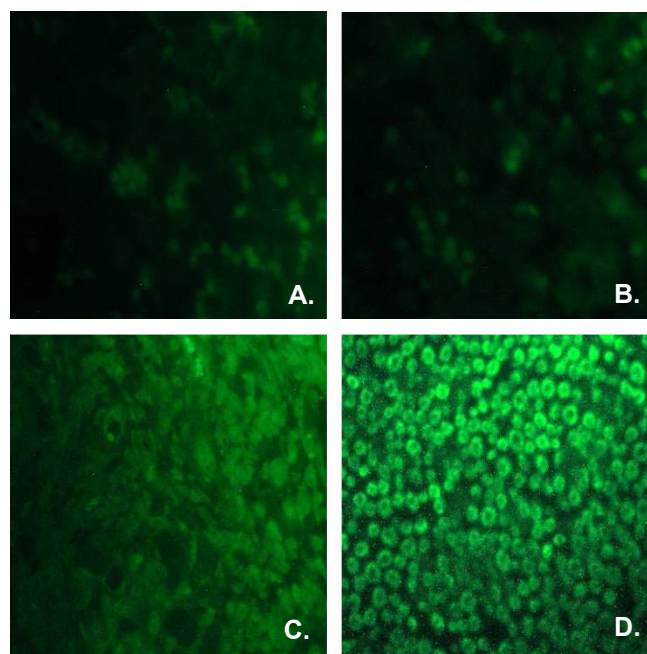
Figure 6.9. Immunofluorescence analysis of tumor tissue

Tissue slides of A2780/Adr xenografts treated intra-tumorally with *MDR1* antisense ODNs were examined by immunofluorescence. Representative tissue pictographs show tumor sections from unstained A2780/Adr controls **(A)** and stained sections from A2780/wt **(B)**, *MDR1* antisense ODNs treated A2780/Adr **(C)**, and A2780/Adr control **(D)** (all pictures taken on an 40x/0.65 objective).

Whereas no Pgp expression was detectable on tumor sections from A2780/wt tumors (picture 6.9-B), strong Pgp overexpression was visible in the A2780/Adr tumors (picture 6.9-D). In *MDR1* antisense pretreated tumors (picture 6.9-C) Pgp protein expression was detectable, but appeared to be lower in comparison to expression levels seen in non treated A2780/Adr tumors. Background fluorescence in A2780/Adr tissue slides in the absence of the antibody (picture 6.9-A) was minimal and comparable to fluorescence detectable in antibody incubated slides of A2780/wt tumors (picture 6.9-B).

6.4.3   *MDR1* antisense treatment of tumors

To confirm whether reductions in Pgp surface expression upon antisense treatments correlated with mRNA expression, levels of *MDR1* were analyzed in A2780/Adr tumors. RNA was isolated from tumor tissue and RT-PCR analysis was performed using primer and conditions as described in chapter 3.3.1. As presented in figure 6.10, *MDR1* levels were downregulated after intra-tumoral antisense treatments. Expression of *MDR1* mRNA was significantly reduced to about 10 % of controls in the antisense treated tumors
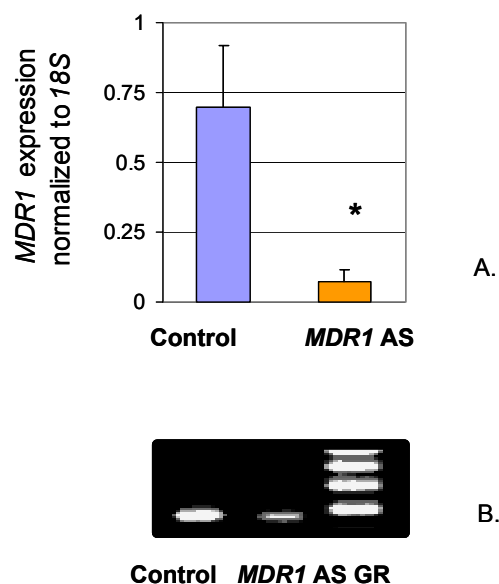
Figure 6.10   RT-PCR analysis of tumor tissue

RNA was isolated from tumor tissue and *MDR1* expression analyzed by RT-PCR analysis. Expression levels were normalized to 18S values and mean values ± S.D. from 4 tumors per group are presented **(A)**. Representative RT-PCR gels with the PCR products from both tumors are depicted **(B)**.

7   Discussion - *in vivo*

In the following chapter, results from ^{99m}Tc-Sestamibi imaging and biodistribution experiments will be discussed. These methods were used to characterize WK-X-34 *in vivo*. In a second set of animal experiments, antisense treatments were compared to treatments with WK-X-34. Some repetition of *in vitro* results will be necessary to correlate *in vivo* to *in vitro* results and to better discuss the *in vivo* findings in the context of this thesis.

7.1   Characterization of WK-X-34

Toxicities

Doses of 20 mg/kg and 50 mg/kg of WK-X-34 in a Cremophor EL ethanol formulation were well tolerated both in healthy and tumor-bearing mice. Likewise, other recently characterized Pgp inhibitors were nontoxic *in vivo*. XR9576 (Mistry, 2001) and OC144-093 (Newman, 2002) were found to be well tolerated in mice at doses of 2-8 mg/kg and 20 mg/kg, respectively. As WK-X-34 was nontoxic in several cell lines (see table 4.2), it is likely that WK-X-34 might be well tolerated in a potential clinical application.

Pgp inhibition in tumor xenografts

The *in vivo* performance of WK-X-34 in sensitive and resistant human xenografts was investigated using the radiopharmaceutical ^{99m}Tc-Sestamibi (Piwnica-Worms, 1993; Del Vecchio, 2004 and Hendrikse, 1999). This technique allows the non-invasive monitoring of Pgp activity and is approved by the FDA for the evaluation of novel Pgp inhibitors in clinical trials (see chapter 2.3.7).

Whereas the cellular uptake of ^{99m}Tc-Sestamibi is mainly due to passive diffusion, Pgp is known to play an important role in its cellular efflux. Indeed, a strongly decreased accumulation of ^{99m}Tc-Sestamibi was seen in the Pgp-overexpressing A2780/Adr cells as compared to the non-Pgp expressing A2780/wt cells. Moreover, treatment of A2780/Adr cells with WK-X-34 increased ^{99m}Tc-Sestamibi accumulation to levels seen in the A2780/wt cells (see figure 4.16).

In vivo, WK-X-34 treatment was found to significantly increase ^{99m}Tc-Sestamibi levels in A2780/Adr resistant but not in sensitive A2780/wt tumor xenografts. This was detected through ^{99m}Tc-Sestamibi imaging and was further verified in ^{99m}Tc-Sestamibi biodistribution experiments. The results indicate that WK-X-34 is capable of reversing the multidrug resistant phenotype *in vivo* in solid tumors.

WK-X-34–mediated changes *in vivo* on the tumor accumulation of ^{99m}Tc-Sestamibi likely occur primarily through Pgp inhibition. It has been reported that ^{99m}Tc-Sestamibi can be transported by MRP1 and MRP2 *in vitro* (Chen, 2000). The affinity of these two transporters to ^{99m}Tc-Sestamibi, however, is much lower than Pgp, and can not be detected *in vivo* (Sharma, 2003). *In vitro,* WK-X-34 did not appear to inhibit MRP-mediated transport in selectively transfected cell lines (see chapter 4.3.4). *In vitro* studies in MCF7/mx cells also demonstrated a lack of interaction between ^{99m}Tc-Sestamibi and BCRP (see figure 4.19).

As *in vitro* studies have identified a dual interaction profile of WK-X-34 with Pgp and BCRP, it would be interesting to investigate *in vivo* effects of BCRP inhibition by WK-X-34. At the time of the experiments, however, no suitable animal model was available for the study. Two animal models of BCRP expressing tumors have only been developed very recently. In 2004, Gefitinib, the epidermal growth factor tyrosine kinase inhibitor, was investigated in immunocomprimised mice inoculated with P388 cells that had been transfected with human BCRP (Yanase, 2004). In 2005, Garimella and coworkers reported a BCRP-overexpressing human ovarian xenograft model, which they used to study the BCRP inhibitor fumitremorgin C (Garimella, 2005). Moreover, no comparable non-invasive imaging model for BCRP has been established to date.

Inhibition of physiological Pgp

In the animals, human Pgp was solely expressed in the xenografts of A2780/Adr tumors. However, mice furthermore express murine Pgp throughout the body particularly in their organs of excretion (i.e. liver, kidney) and barrier tissue (i.e. blood-brain-barrier). Whereas humans only have one Pgp, which is encoded by *MDR1*, mice express two types of Pgp, encoded by *mdr1a* and *mdr1b* (Chen, 1986). Together *mdr1a-* and *mdr1b*-type Pgps fulfil the same function as the single human Pgp (Schinkel, 1997). It was expected that WK-X-34 would interact with murine Pgp and impose changes in the accumulation of ^{99m}Tc-Sestamibi in organs and different tissues. Indeed, ^{99m}Tc-Sestamibi imaging and biodistribution data revealed a significantly increased accumulation of ^{99m}Tc-Sestamibi in the brain, heart, liver and intestine of WK-X-34 treated animals.

Increases in the organ accumulation of ^{99m}Tc-Sestamibi have been reported with other Pgp inhibitors (Rao, 1999; Planting, 2005). Thus, there exists a potential for these agents to impact the distribution, clearance and organ toxicities of anticancer drugs. Pharmacokinetic alterations of coadministered chemotherapeutic agents (e.g. daunorubicin) have been associated with third generation Pgp inhibitors (Dale, 1998; Lê, 2005). Comparably, WK-X-34 caused increased ^{99m}Tc-Sestamibi levels in major organs and deep tissues. These observations point to potential complications in the therapeutic use of third generation Pgp inhibitors. A careful risk-benefit evaluation as well as thorough toxicity monitoring should precede and accompany the therapeutic application of a Pgp inhibitor.

Some pharmacokinetic properties of WK-X-34 could be deduced from the analysis of ^{99m}Tc-Sestamibi images. Imaging data demonstrated a Pgp inhibition in WK-X-34 treated mice as soon as 75 min after administering WK-X-34 (1 h pretreatment with WK-X-34 + 15 min poatinjection of ^{99m}Tc-Sestamibi). This suggests that WK-X-34 is rapidly absorbed from the intraperitoneal cavity into the blood with subsequent distribution to distant organs and tumors. WK-X-34 continued to display effective *in vivo* inhibition of Pgp four hours after administration of ^{99m}Tc-Sestamibi, indicating that the inhibitor was not being rapidly cleared from the system. This seems plausible, as pharmacokinetic investigations of another third generation Pgp inhibitor, XR9051 (Mistry, 1999) with a similar structure to WK-X-34 (compare structure of WK-X-34 in figure 3.1 to structure of XR9051 in figure 1.7) have

indicated rapid uptake with sufficiently long disposition in the system. Mistry and coworkers found an apparent elimination half-life of XR9051 in plasma and liver of around 4 and 5 h, respectively. In tumor xenografts, the maximum concentration of XR9051 was detected 1.5 h following administration of a 20 mg/kg dose i.v. with an apparent elimination half-life of around 8 h.

Recent characterizations in the literature

Most recently characterized third generation Pgp inhibitors included *in vivo* investigations in human or murine tumor xenograft models, which are summarized in table 7.1.

The A2780/Adr xenograft model used in this thesis is a commonly applied tumor model, which was employed to test for MDR reversal of XR9051 and XR9576. Other tumor models include the murine leukemia model P388/Dox (Hyafil, 1993; Dantzig, 1996, Mistry, 1999 and Newman, 2000) and the human small cell lung cancer model SCLC-H69/LX4 (Mistry, 1999 and 2001). Newman and coworkers generated a xenograft model with a selectively transfected human breast cancer cell line, MDA435/ LCC6^{MDR1} (Newman, 2000). The great majority of xenograft models, however, were generated using multidrug resistant cell lines, which have been selected through cytotoxic treatments.

The antitumor efficacy of commercially developed third generation Pgp inhibitors has been extensively studied in several different tumor models using common chemotherapeutic agents (e.g. paclitaxel, doxorubicin, etoposide). Studies of pharmacokinetic parameters and potential alterations in the pharmacokinetic profile of co-administered chemotherapy were usually included. In an academic setting or in the context of a PhD thesis, it is obvious that such a detailed characterization is not possible.

Table 7.1   Novel third generation Pgp inhibitors in the literature –*in vivo* characterization

Reference	MDR inhibitor	Target	Tumor Model	*In vivo* Experiments
Hyafil, 1993 Laboratoire GLAXO	GF120918	Pgp, later BCRP[1]	Mu leukemia and colon xenograft models (MDR P388/Dox; i.p.; C26MDR s.c.)	DOX in xenograft DOX-PK in mice PK/Tox in mice
Dantzig, 1996 Lilly Research	LY335979	Pgp[2]	Mu leukemia (MDR P388/Dox; i.p.) Hu NSCLC xenografts i.p.	DOX/ ETP in leukemia model TAX in xenograft; PK
Mistry, 1999 Xenova Ltd	XR9051	Pgp	Mu leukemia and colon model (MDR P388/ Dox; i.p.; MC26; s.c.) Hu ovarian and SCLC cancer xenograft (A2780/Adr + CH1/Dox; H69/LX4 s.c.)	VCR, DOX in leukemia models and colon xenograft PTX, ETP, VCR, DOX in human xenografts PK in mice and xenografts
Newman, 2000 Ontogen Corporation	OC144-093	Pgp	Mu leukemia (MDR P388/Dox; i.p.) Hu breast and colon xenografts (MDA435/ LCC6[MDR1]* i.p; HCT-15; s.c.)	DOX in xenograft PXT-PK in mice PK in dogs
Mistry, 2001 Xenova Ltd	XR9576	Pgp later BCRP[3]	Mu colon carcinoma (MC26; s.c.) Hu ovarian and SCLC xenograft (A2780/Adr and A2780/wt s.c.; H69/LX4 s.c)	PTX, ETP, VCR in xenografts (A2780/Adr + H69/LX4) DOX in xenografts (MC26) PK of PTX in rats
Jekerle, 2006a University of Bonn/Toronto	WK-X-34	Pgp + BCRP	Hu ovarian cancer xenograft (A2780/Adr and A2780/wt; s.c.)	Tox in mice MIBI* imaging and biodistribution in A2780/Adr & A2780/wt xenografts
Allen, 2002 Netherlands Cancer Institute	Ko143	BCRP	--------------------------------	Tox in mice Modification of oral BA of TPC in mice

Abbreviations used in this table:

BA: bioavailability; PK: Pharmacokinetic investigations; Tox: toxicity; SCLC: small cell lung cancer, Mu: Murine; Hu: Human

DOX: doxorubicin; ETP: etoposide; PTX: paclitaxel; VCR: vincristine; MIBI*: ^{99m}Tc-Sestamibi; TPC: topotecan

* human breast cancer cell line (MDA435/LCC6[MDR1]) is selectively transfected with human *MDR1*

[1] Malipaard, 2001; [3] Shepard, 2003; [3] Robey, 2004; for *in vitro* characterization see table 5.1 and 5.2

Non-invasive ^{99m}Tc-Sestamibi imaging techniques, used for the initial *in vivo* characterization of WK-X-34, elegantly provided proof of *in vivo* efficacy. Comparable to other third generation Pgp inhibitors, WK-X-34 effectively reversed the MDR phenotype in human xenografts of ovarian cancer at a dose of 20 mg/kg. Moreover, some information on the distribution and pharmacological interactions of WK-X-34 with physiological Pgp in relevant tissues such as the blood –brain barrier or excreting organs was obtained.

To investigate WK-X-34 for a potential application in humans, further preclinical studies, such as antitumor efficacy studies and pharmacokinetic investigations, are warranted. Nevertheless, ^{99m}Tc-Sestamibi imaging techniques were particularly suitable for the initial *in vivo* testing of WK-X-34.

7.2   Antisense treatment in comparison to WK-X-34

In a second set of *in vivo* experiments *MDR1* antisense ODNs alone and in combination with WK-X-34 were used to reverse Pgp-mediated MDR in tumor xenograft models.   Likewise, ^{99m}Tc-Sestamibi imaging techniques were applied to assess Pgp inhibition *in vivo*.

Downregulation of Pgp activity

As mice were treated with both, the third generation Pgp inhibitor WK-X-34 and *MDR1* antisense ODNs, *in vivo* efficacy of both treatments could be compared. First, these treatments were evaluated *in vitro* using the chemotherapeutic drug daunorubicin.   Both, *MDR1* antisense ODNs and WK-X-34 increased intracellular daunorubicin levels through functional Pgp inhibition (see figure 4.12 and 4.21).   *In vivo*, intratumoral treatments with *MDR1* antisense ODNs resulted in transcriptional downregulation of *MDR1* mRNA and Pgp expression in the A2780/Adr tumor (see figure 6.10).   *MDR1* mRNA was downregulated to about 10 % of controls.   Likewise, Pgp surface expression was decreased as determined by immunofluorescence analysis techniques.   Yet reductions in protein levels appeared to be less pronounced.   This seems reasonable as results from *in vitro* antisense experiments showed a downregulation by only 50 % for the highest concentration of antisense ODNs (see figure 4.11).   Differences in the degree of downregulation between *MDR1* mRNA and Pgp effects are likely to depend on their dissimilar half lives. Whereas *MDR1* mRNA has a half life of 4 h, the half life of the protein Pgp is 14-16 h (Aleman, 2003).   As a result, transcriptional inhibition can first be detected on the mRNA level.   Translation of these effects into a reduction in Pgp surface expression thus occurs much slower and potentially not in a quantitative way.

Changes in Pgp expression translated into an impaired Pgp-mediated MDR phenotype.   In tumor xenografts, functional Pgp inhibition was detected through altered ^{99m}Tc-Sestamibi accumulation both by imaging and biodistribution analysis with a significant degree of sensitivity.   An increased level of ^{99m}Tc-Sestamibi due to an impaired efflux activity of Pgp was detected in the antisense treated resistant tumor (see chapter 6.3.1 and 6.3.2).   Through additional functional Pgp inhibition by WK-X-34, intratumoral accumulation of ^{99m}Tc-Sestamibi was further increased and

reached a maximum level, which no longer differed between antisense untreated and pretreated tumors. What can be concluded from this observation?

Treatments with *MDR1* antisense ODNs caused increased ^{99m}Tc-Sestamibi levels within the tumors; these differences, however, were nullified when WK-X-34 was added (see figure 6.6 and table 6.2). The results indicate that a single dose of the Pgp inhibitor WK-X-34 more effectively reverses Pgp-mediated MDR than a three-day treatment with *MDR1* antisense ODNs. Moreover, the combination of a Pgp inhibitor and antisense ODNs together does not offer an advantage over the single treatment with WK-X-34 alone. Hence, a potential benefit of antisense ODNs treatment in the therapy of multidrug resistant cancer could not be concluded from these studies (Jekerle, 2006c).

Nevertheless, results from *in vivo* antisense treatments demonstrated effectiveness of antisense ODNs in downregulating *MDR1*/Pgp *in vivo*. For a potential clinical application, however, antisense treatments appear to be less powerful in comparison to small molecule MDR inhibitors such as WK-X-34.

Antisense treatments in the literature

In the antisense field, some studies have confirmed the effectiveness of antisense treatments in reversing the Pgp-mediated MDR phenotype *in vivo*. Ramachandran and coworkers (Ramachandran, 2003) were able to show that a combined four-day treatment of *MDR1* antisense ODNs and doxorubicin significantly controlled tumor growth. The effect was attributed to the addition of *MDR1* antisense ODNs. Unfortunately, such convincing examples are rare and can only be generated with a complicated experimental setup. Ramachandran had to use a combination of two antisense sequences in order to observe efficacy in his *in vivo* experiment.

In another study, Lopes de Menezes and coworkers (Lopes de Menezes, 2003) used a combined treatment of antisense oligonucleotides directed against the antiapoptotic gene bcl-2 and PSC 833, a second generation Pgp inhibitor. *In vivo,* the combination of bcl-2 antisense, PSC 833 and liposomal doxorubicin showed maximal growth suppression of multidrug resistant tumors in comparison to the

individual treatments.   While this study introduces an interesting therapeutic approach through targeting two different MDR mechanisms with a combination of a small molecule inhibitor and antisense treatment, the clinical relevance is questionable. It remains to be seen, whether such complicated treatment strategies can be translated into the clinical practice.

Limitations of antisense-based treatments

Although convincing and rational in theory, therapeutic approaches targeting mRNA have been associated with many unexpected complications. *In vivo* toxicity, stability and delivery-related problems are among the major obstacles in a successful clinical application of antisense ODNs.

Even though some recent Phase I and II clinical trials of antisense-based drugs could demonstrate an acceptable level of safety of phosphorothioated ODNs (Galderisi, 1999), they have frequently been associated with toxicity complications (Kurreck, 2003).

Delivery-related problems are more difficult to circumvent. For good reasons, the body possesses a strong protection mechanism against infection from foreign nucleotides (Robinson, 2004).   Complicated delivery systems or backbone modifications had to be developed to enable antisense molecules to enter the system and persist in the circulation sufficiently long to guarantee a delivery to the site of action. Indeed, after an i.v. or i.p. injection phosphorothioated antisense molecules were shown to remain in the blood circulation for up to 24 h before excretion via the urine (Galderisi, 1999). Moreover, detectable levels of ODNs were found in most tissues up to 48 h postinjection with only 15-50 % of degradation in that period. As most tumor tissue is poorly circulated by the blood (see chapter 1.1.2), this brings about a reduced delivery into the tumor. Even though *in vivo* experiments and initial trials can avoid this problem by direct injection into the target tumor, only a solution for such delivery-related problems can give rise to broad clinical application.

So strikingly simple in theory, yet experts have reservations about the nature of the antisense mechanism (Robinson, 2004). The only antisense-based drug with

FDA approval, Vitravene, is used to treat cytomegalovirus infections in the eyes of HIV patients. Its antisense sequence actually targets viral DNA but not a human mRNA sequence. Therefore, it remains unclear whether Vitravene actually works through the antisense mechanism. To date, no antisense-based drug targeting a sequence within the human genome has demonstrated sufficient efficacy and safety to receive a marketing authorization.

The above-mentioned aspects illustrate just how complicated *in vivo* applications of antisense molecules can be. Some of these limitations were reflected in this thesis. Substantial *in vitro* toxicities detected as significant downregulations in cell proliferation were observed upon antisense treatments. *In vivo*, comparable toxicities were not seen in mice that were dosed intratumorally for three days with antisense ODNs. Yet many reports have indicated *in vivo* toxicities associated with non-specific binding of antisense ODNs to several proteins (Levin, 1999).

Delivery-related problems could mostly be avoided by the intratumoral route of administration. In a clinical setting, however, intratumoral injections will not be feasible in the majority of cases. Moreover, as antisense treatment via the most direct route of application over a treatment period of three consecutive days has not shown a satisfying degree of Pgp inhibition that was comparable to WK-X-34 alone, it remains highly questionable whether antisense treatment will be effective in a therapeutic application. Even the combination of antisense ODNs and WK-X-34, which was originally thought to be effective due to a dual targeting of Pgp and *MDR1* mRNA, did not show a benefit over the single treatment with WK-X-34. Overall, results from ^{99m}Tc-Sestamibi imaging studies demonstrated an inhibition of the Pgp-mediated phenotype with a sufficient, yet much lower efficacy of antisense ODNs in comparison to WK-X-34. The results appear to be in accordance with common experience and support the reservations outlined above. In order to justify such complications associated with antisense-based therapy, their effectiveness needs to exceed other less complicated strategies. Thus, the clinical usefulness of antisense-based therapies in targeting multidrug resistant tumors remains questionable and will always be limited by the presence of potent and nontoxic small molecule inhibitors of Pgp.

8   Conclusion

In this thesis I have characterized novel multi-targeted MDR inhibitors and *MDR1* antisense ODNs using common *in vitro* and *in vivo* experimental techniques. The evaluation of different treatment strategies alone and in combination addressed the hypothesis that the simultaneous targeting of different MDR mechanisms might be advantageous in mastering the complexity of multidrug resistant tumors (See rational; chapter 2.1).

Whereas antisense ODNs were found to be less effective while associated with more complications, some Pgp inhibitors showed effective MDR reversing properties. Among the tested compounds, the most effective, WK-X-34 and XR9577 were found to be potent, specific and non-toxic inhibitors of both, Pgp- and BCRP-mediated MDR in different cell lines. These compounds clearly showed an advantage in potency and cellular tolerance over cyclosporin A, a broad spectrum MDR inhibitor with successful performance in clinical trials in AML patients.

WK-X-34 was chosen for further *in vivo* characterization of toxicity, efficacy and pharmacokinetic alterations. Using ^{99m}Tc-Sestamibi imaging techniques in human ovarian cancer xenografts, WK-X-34 was shown to effectively target MDR *in vivo.* The MDR-reversing potency as well as typical interactions with other Pgp expressing tissues were comparable to those of other third generation Pgp inhibitors. A combined treatment of antisense ODNs and WK-X-34 was found to not be superior to the treatment with WK-X-34 alone.

The selective interaction profile of WK-X-34 with Pgp and BCRP holds a great potential in a broader anti-MDR therapy, particularly with regard to solid tumors with Pgp and BCRP coexpression and highly protected cancer stem cell subpopulations. Therefore, extended preclinical development is anticipated and required to evaluate whether WK-X-34 might potentially be a promising candidate for the successful

therapeutic treatment of *de novo* or acquired Pgp- and BCRP-mediated MDR in human malignancies.

Outlook

Some recently developed potent MDR inhibitors of the third generation including WK-X-34 are effective in reversing the Pgp and BCRP-mediated MDR phenotype. In multidrug resistant tumor cells, they can increase intracellular drug concentrations to levels found in sensitive tumor cells and sensitize the tumor to the chemotherapeutic treatment. Unfortunately, there are many tumors, which lack expression of Pgp and BCRP, yet they do not respond to chemotherapy. In these tumors, Pgp and BCRP targeting MDR inhibitors fail to reverse the MDR phenotype. Does it mean MDR inhibitors are not effective and the development of these compounds should not be pursued?

As the pathology of a tumor cell is such a complex concert of numerous mechanisms, one therapy by itself has only limited potential. Nevertheless, each therapeutic approach adds a weapon to the "arsenal" which is needed to fight the tumor cell. With the development and characterization of the potent, selective and non-toxic MDR inhibitor, WK-X-34, we are on the way to create another tool to target a subpopulation of tumors, namely those tumor cells that are predominantly resistant through the overexpression of Pgp and BCRP. If such a Pgp/BCRP inhibitor was only one "arrow" that could be added to the "arsenal", it could be assembled together with other arrows and weapons. The greater the selection of weapons, the more likely it will be for the therapist to find the right combination of weapons against the individual tumor. Together with other existing and yet to be discovered therapies, MDR inhibitors are of value in the treatment of multidrug resistant cancer.

9   Summary

Purpose: The ATP-binding cassette (ABC) transporters P-glycoprotein (Pgp) and BCRP are implicated in the multidrug resistance (MDR) of many tumors. Pgp-mediated MDR can be functionally inhibited using small molecule inhibitors or transcriptionally downregulated by *MDR1* antisense oligodeoxynucleotides (ODNs). Interestingly, simultaneous inhibition of several ABC transporters including Pgp and BCRP by cyclosporin A has been shown to circumvent MDR in clinical trials. In this thesis, the novel multi-targeted tetrahydroisoquinolin-ethyl-phenyl-amine-based MDR inhibitors XR9577, WK-X-34, WK-X-50 and WK-X-84 were thoroughly *in vitro* and *in vivo* characterized for interaction with Pgp, BCRP and MRP-transporters and compared to treatments with *MDR1* antisense ODNs.

Methods: The novel MDR inhibitors and cyclosporin A were examined for cellular toxicity in several cell lines. Inhibition of BCRP-mediated mitoxantrone efflux was studied in BCRP-overexpressing MCF7/mx cells. Inhibition of Pgp function was assessed in ^{99m}Tc-Sestamibi and daunorubicin transport assays. Reversal of Pgp- and BCRP-mediated resistance towards daunorubicin and mitoxantrone, respectively, were investigated in A2780/Adr and MCF7/mx cells. Potential MRP-interactions were evaluated in 5-CFDA efflux assays using selectively transfected MRP-1, -2 and -3 cell lines.

Daunorubicin transport and Pgp surface expression in resistant A2780/Adr cells treated with *MDR1* antisense ODNs were determined using flow cytometry, fluorescence microscopy and protein staining techniques.

The *in vivo* performance and toxicity of WK-X-34 was evaluated by ^{99m}Tc-Sestamibi imaging experiments using multidrug resistant human ovarian cancer (A2780/Adr) xenograft models. To study antisense treatments *in vivo*, A2780/Adr xenograft models were dosed intratumorally with *MDR1* antisense ODNs for three days followed by either WK-X-34 or vehicle treatment. ^{99m}Tc-Sestamibi distribution and accumulation were analyzed by imaging of the animals and gamma-counting of the isolated tissues. Tumor xenografts were analyzed histologically and Pgp expression was monitored by immunohistochemistry and RT-PCR.

Results: WK-X-34 and XR9577 were the most potent MDR inhibitors and completely reversed ^{99m}Tc-Sestamibi and daunorubicin accumulation at concentrations of 10 and 1 μM. Daunorubicin chemosensitivity was increased by 7-8-fold after 10 μM XR9577 or WK-X-34 pretreatment. All WK-X-compounds showed significant BCRP inhibition comparable to novobiocin in both mitoxantrone transport and chemosensitivity assays. Compared to cyclosporin A, the *in vitro* toxicity was reduced for all WK-X-compounds. Moreover, XR9577 or WK-X-34 showed increased specificity for Pgp and BCRP as only resistant cells were targeted and significant MRP interactions were not detected.

In immunocomprimised mice dosed with WK-X-34 (20 mg/kg; i.p.)*,* uptake of ^{99m}Tc-Sestamibi was significantly increased in A2780/Adr xenograft tumors (AUCs$_{0-4h}$ 136%; $p < 0.05$) but not in sensitive A2780/wt tumors. Moreover, increased levels of ^{99m}Tc-Sestamibi were detected in the brain, liver and intestine of WK-X-34 treated animals.

MDR1 antisense treatments significantly increased daunorubicin levels in A2780/Adr cells. *In vivo,* ^{99m}Tc-Sestamibi retention was significantly increased by over two fold in the antisense pretreated tumors. Upon additional WK-X-34 treatment, tissue/muscle ratios of ^{99m}Tc-Sestamibi were significantly increased by 9-fold in the untreated but only by 2-fold in the antisense pretreated tumors and correlated with results from the 1-hour ^{99m}Tc-Sestamibi images. ^{99m}Tc-Sestamibi levels in the A2780/Adr tumors could not be further increased by a combined treatment with antisense ODNs and WK-X-34 as compared to WK-X-34 alone. *MDR1* mRNA levels and Pgp expression were down-regulated in the antisense treated tumors.

Conclusion: Among the novel MDR inhibitors, WK-X-34 and XR9577 were most effective in modulating Pgp and BCRP and demonstrated an increased *in vitro* tolerance and specificity over cyclosporin A. *In vivo*, WK-X-34 potently inhibited the Pgp-mediated MDR phenotype in resistant human ovarian cancer xenograft models. In comparison to WK-X-34, *MDR1* antisense ODNs were less effective while associated with more complications. Based on these *in vitro* and *in vivo* characterizations, WK-X-34 may have potential utility in the treatment of multidrug resistant tumors

.

10   Literature

Agrawal M, Abraham J, Balis FM, Edgerly M, Stein WD, Bates S, Fojo T, Chen CC. Increased ^{99m}Tc-sestamibi accumulation in normal liver and drug-resistant tumors after the administration of the Glycoprotein inhibitor, XR9576. Clin Cancer Res **2003**;9:650-656

Akiyama S, Cornwell MM, Kuwano M, Pastan I, Gottesman MM. Most drugs that reverse multidrug resistance also inhibit photoaffinity labeling of P-glycoprotein by a vinblastine analog. Mol Pharmacol **1988**;33:144-147

Alahari SK, Dean NM, Fisher MH, DeLong R, Manoharan M, Tivel KL, Juliano RL. Inhibition of expression of the multidrug resistance-associated P-glycoprotein by phosphorothioate and 5'-cholesterol-conjugated phosphorothioate antisense oligonucleotides. Mol Pharmacol **1996**;50:808-19

Alahari SK, DeLong R, Fisher MH, Dean NM, Viliet P, Juliano RL**.** Novel chemically modified oligonucleotides provide potent inhibition of P-glycoprotein expression. JPET **1998**;286:419-428

Aleman C, Annereau JP, Liang XJ, Cardelli CO, Taylor B, Yin JJ, Aszalos A, Gottesman MM. P-Glycoprotein, Expressed in Multidrug Resistant Cells, Is Not Responsible for Alterations in Membrane Fluidity or Membrane Potential. Cancer Res **2003**;63:3084-3091

Allen AD, Schinkel AH. Multidrug Resistance and Pharmacological Protection mediated by the Breast Cancer Resistance Protein (BCRP/ABCG2). Mol Cancer Ther **2002**;1:427-434

Allen JD, van Loevezijn A, Lakhai JM, van der Valk M, van Tellingen O, Reid G, Schellens JH, Koomen GJ, Schinkel AH. Potent and specific inhibition of the breast cancer resistance protein multidrug transporter in vitro and in mouse intestine by a novel analogue of fumitremorgin C. Mol Cancer Ther **2002**;1:417-425

Ambudkar SV, Kimchi-Sarfaty C, Sauna ZE, Gottesman MM. P-glycoprotein: from genomics to mechanisms. Oncogene **2003**;22:7468-85

Axel DI, Spyridopoulos I, Riessen R, Runge H, Viebahn R, Karsch KR. Toxicity, uptake kinetics and efficacy of new transfection reagents: increase of oligonucleotide uptake. J Vasc Res **2000**;37:221-34

Bakos E, Hegedus T, Hollo Z, Welker E, Tusnady GE, Zaman GJ, Flens MJ, Varadi A, Sarkadi B. Membrane topology and glycosylation of the human multidrug resistance-associated protein. J Biol Chem **1996**;271:12322-26

Ballinger JR, LiJH. Sestamibi accumulation in human nasopharyngeal carcinoma cell lines in vitro. Anticancer Res **2000**;20:677-679

Bates SE, Robey R, Miyake K, Ross DD, Litman T. The role of half-transporter in multidrug resistance. J Bioenerg Biomembr **2001**; 33:503-11

Beck T, Grogan TM, Willman CL, Cordon-Cardo C, Parham DM, Kuttesch JF, Andreeff M, Bates SE, Berard CW, Boyett JM, Brophy NA, Broxterman HJ, Chan HS, Dalton WS, Dietel M, Fojo AT, Gascoyne RD, Head D, Houghton PJ, Srivastava DK, Lehnert M, Leith CP, Paietta E, Pavelic ZP, Weinstein R. Methods to detect P-glycoprotein-associated multidrug resistance in patients' tumors: consensus recommendations. Cancer Res **1996**;56:3010-3020

Belinsky MG, Bain LJ, Balsara BB, Testa JR, Kruh GD. Characterization of MOAT-C and MOAT-D, new members of the MRP/cMOAT subfamily of transporter proteins. J Natl Cancer Inst **1998**;90:1735-1741

Bennett CF; Cowsert LM. Antisense Oligonucleotides as a tool for gene functionalization and target validation. Biochim Biophys Acta **1999**;1489:19-30

Beringer PM, Slaughter RL. Transporters and Their Impact on Drug Disposition. Ann Pharmacother **2005**;39:1097-1108

Bernard BF, Krenning EP, Breeman WAP, Ensing G, Benjamins H, Bakker WH, Visser TJ, de Jong M. 99mTc-MIBI, 99mTc-Tetrofosmin and 99mTc-Q12 in vitro and in vivo. Nuc Med Biol **1998**;25:233-240

Black SM, Beggs JD, Hayes JD, Bartoszek A, Muramatsu M, Sakai M, Wolf CR. Expression of human glutathione S-transferases in Saccharomyces cerevisiae confers resistance to the anticancer drugs adriamycin and chlorambucil. Biochem J **1990**;268:309–315

Bodó A, Bakos E, Szeri F, Váradi A, Sarkadi B. The role of multidrug transporters in drug availability, metabolism and toxicity. Tox Letters **2003**;140:133-143

Borst P, Schinkel AH. What we learnt thus far from mice with disrupted P-glycoprotein genes? Eur J Cancer **1996**;32A:985-990

Borst P, Evers R, Kool M, Wijnholds J. A family of drug transporters: the multidrug resistance-associated proteins. J Nat Cancer Inst **2000**;92:1295-1302

Bradley G, Naik M, Ling V. P-glycoprotein expression in multidrug-resistant human ovarian carcinoma cell lines. Cancer Res **1989**;49:2790-6

Brigui I, Djavanbakht-Samani T, Jolles B, Pigaglio S, Laigle A. Minimally modified phosphodiester antisense oligodeoxyribonucleotide directed against the multidrug resistance gene mdr1. Biochem Pharmacol **2003**;65:747-754

Brooks T, Minderman H, O'Loughlin KL, Pera P, Ojima I, Baer MR, Bernacki RJ. Taxane- based reversal agents modulate drug resistance mediated by P-glycoprotein, multidrug resistance protein, and breast cancer resistance protein. Mol Cancer Ther **2003**;2:1195-1205

Caffrey PB, Zhang Y, Frenkel GD. Rapid development of drug resistance in human ovarian tumor xenografts after a single treatment with melphalan in vivo. Anticancer Res **1998**;18:3021-3025

Calne RY, White DJ, Thiru S, Evans DB, McMaster P, Dunn DC, Craddock GN, Rolles K. Cyclosporin A initially as the only immunosuppressant in 34 recipients of cadaveric organs: 32 kidneys, pancreases and 2 livers. Lancet **1979**;2:1033–1036

Chauvier D, Kegelaer G, Morjani H, Manfait M. Reversal of multidrug resistance-associated protein-mediated daunorubicin resistance by camptothecin. J Pharm Sci **2002**;91:1765-75

Chen CJ, Chin JE, Ueda K, Clark DP, Pastan I, Gottesman MM, Roninson IB. Internal duplication and homology with bacterial transport proteins in the mdr1 (P-glycoprotein) gene from multidrug-resistant human cells. Cell **1986**;47:381-389

Chen H, Rossier C, Lalioti MD, Lynn A, Chakravarti A, Perrin G, Antonarakis SE. Cloning of the cDNA for a human homologue of the Drosophila white gene and mapping to chromosome 21q22.3. Am J Hum Genet **1996**;59:66-75

Chen WS, Luker KE, Dahlheimer JL, Pica CM, Luker GD, Piwnica-Worms D. Effects of MDR1 and MDR3 P-glycoproteins, MRP1, and BCRP/MXR/ABCP on the transport of (99m)Tc-tetrofosmin. Biochem Pharmacol **2000**;60:413-426

Chin DJ, Green GA, Zon G, Szoka FC Jr., Straubinger RM. Rapid nuclear accumulation of injected oligodeoxyribonucleotides. New Biol **1990**;2:1091-1100

Ciarmiello A, Del Vecchio S, Silvestro P, Potena MI, Carriero MV, Thomas R, Botti G, D'Aiuto G, Salvatore M. Tumor clearance of technetium 99m-sestamibi as a predictor of response to neoadjuvant chemotherapy for locally advanced breast cancer. J Clin Oncol **1998**;16:1677-1683

Coley HM, Sargent JM, Williamson CJ, Titley J, Scherper RJ, Gregson SE, Elgie AW, Lewandowicz GM, Taylor CG. Assessment of the classical MDR phenotype in epithelial ovarian carcinoma using primary cultures: a feasibility study. Anticancer Res **2002**;22:69-75

Cornwell MM, Safa AR, Felsted RI, Gottesman MM, Pastan I. Membrane vesicles from multidrug-resistant human cancer cells contain a specific 150-170-kDa protein detected by photoaffinity labeling. Proc Natl Acad Sci USA **1986**;83:3847-3850

Croy BA, Linder KE, Yager JA. Primer for non-immunologists on immuno-deficient mice and their applications in research. Comp Med **2001**;51:300-313

Cullen KV, Davey RA, Davey MW. Verapamil-stimulated glutathione transport by the multidrug resistance-associated protein (MRP1) in leukaemia cells. Biochem Pharmacol **2001**;62:417-24

Dale IL, Tuffley W, Callaghan R, Holmes JA, Martin K, Luscombe M, Mistry P, Ryder H, Stewart AJ, Charlton P, Twentyman PR, Bevan P. Reversal of P-glycoprotein -mediated multidrug resistance by XR9051, a novel diketopiperazine derivative. Br J Cancer **1998**;78:885-892

Dalton WS, Grogan TM, Meltzer PS, Scheper RJ, Durie BG, Taylor CW, Miller TP, Salmon SE. Drug-resistance in a multiple myeloma and non-Hodgkin's lymphoma: detection of p-glycoprotein and potential circumvention by addition of verapamil to chemotherapy. J Clin Oncol **1989**;7:415-424

Damiani D, Michieli M, Ermacora A, Candoni A, Raspadori D, Geromin A, Stocchi R, Grimaz S, Masolini P, Michelutti A, Scheper RJ, Baccarani M. P-glycoprotein (PGP) and not lung resistance-related protein (LRP), is a negative prognostic factor in secondary leukemias. Haematologica **1998**;83:290-297

Dantzig AH, Shepard RL, Cao J, Law KL, Ehlhardt WJ, Baughman TM, Bumol TF, Starling JJ. Reversal of P-glycoprotein-mediated multidrug resistance by a potent cyclopropyldibenzosuberane modulator, LY335979. Cancer Res **1996**; 56:4171-4179

Dassow H. Modulation of multidrug resistance gene (hmdr1) with antisense oligodeoxynucleotides Int J Clin Pharm Ther **2000**;38:209-16

De Cesare M, Pratesi G, Perego P, Carenini N, Tinelli S, Merlini L, Penco S, Pisano C, Bucci F, Vesci L, Pace S, Capocasa F, Carminati P, Zunino F. Potent antitumor activity and improved pharmacological profile of ST1481, a novel 7-substituted camptothecin. Cancer Res **2001**;61:7189-95

Delaney B, Carlson T, Frazer S, Zheng T, Hess R, Ostergren K, Kierzek K, Haworth J, Knutson N, Junker K, Jonker D. Evaluation of the toxicity of concentrated barley glucan in a 28-day feeding study in Wistar rats. Food Chem Toxicol **2003**;41:477-487

Del Vecchio S, Salvatore M. ^{99m}Tc-MIBI in the evaluation of breast cancer biology. Eur J Nuc Med Mol Imaging **2004**;31:88-96

Demant EJ, Sehested M, Jensen PB. A model for computer simulation of P-glycoprotein and transmembrane delta pH-mediated anthracycline transport in multidrug-resistant tumor cells. Biochim Biophys Acta **1990**;1055:117–125

De Smet MD, Meenken CJ, van den Horn GJ. Fomivirsen – a phosphorothioate oligonucleotide for the treatment of CMV retinitis. Ocul Immunol Onflamm **1999**; 7:189-198

Diestra JE, Scheffer GL, Catala I, Maliepaard M, Schellens JH, Scheper RJ, Germa-Lluch JR, Izquierdo MA. Frequent expression of the multi-drug resistance-associated protein BCRP/MXR/ABCP/ABCG2 in human tumours detected by the BXP-21 monoclonal antibody in paraffin-embedded material. J Pathol **2002**;198:213-219

Doyle LA, Yang W, Abruzzo LV, Krogmann T, Gao Y, Rishi AK, Ross DD. A multidrug resistance transporter from human MCF-7 breast cancer cells. Proc Natl Acad Sci USA **1998**;95:15665-15670

Doyle LA, Ross DD. Multidrug resistance mediated by the breast cancer resistance protein BCRP (ABCG2). Oncogene **2003**;22:7340-7358

Drake FH, Zimmerman JP, McCabe FL, Bartus HF, Per SR, Sullivan DM, Ross WE, Mattern MR, Johnson RK, Crooke ST, Mirabelli CK. Purification of topoisomerase II from amsacrine-resistant p388 leukemia cells: Evidence for two forms of the enzyme. J Biol Chem **1987**;262:16739–16747

Draper MP, Martell RL, Levy SB. Indomethacin-mediated reversal of multidrug resistance and drug efflux in human and murine cell lines overexpressing MRP, but not P-glycoprotein. Br J Cancer **1997**;75:810-815

Dubin IN, Johnson FB. Chronic idiopathic jaundice with unidentified pigment in liver cells; a new clinicopathologic entity with a report of 12 cases. Medicine **1954**;33:155-197

Eckstein F. Phosphorothioate oligodeoxynucleotides: what is their origin and what is unique about them? Antisense Nucleic Acid Drig Dev **2000**;10:117-21

El-Deiry WS. The role of p53 in chemosensitivity and radiosensitivity. Oncogene **2003**;22:7486-7495

Elkas JC, Baldwin RL, Pegram M, Tseng Y, Slamon D, Karlan BY. A human ovarian carcinoma murine xenograft model useful for preclinical trials. Gynecol Oncol **2002**;87:200-6

Evers R, Zaman GJ, van Deemter L, Jansen H, Calafat J, Oomen LC, Oude Elferink RP, Borst P, Schinkel AH. Basolateral localization and export activity of the human multidrug resistance-associated protein in polarized pig kidney cells. J Clin Invest **1996**;97:1211-1218

Filipits M, Suchomel RW, Zochbauer S, Brunner R, Lechner K, Pirker R. Multidrug resistance-associated protein in acute myeloid leukemia: no impact on treatment outcome. Clin Cancer Res **1997**;3:1419-1425

Fisher GA, Lum BL, Hausdorff J, Sikic BI. Pharmacological Considerations in the Modulation of Multidrug Resistance. Eur J of Cancer **1996**; 32A: 1082-1088

Fisher TL, Terhorst T, Cao X, Wagner RW. Intracellular disposition and metabolism of fluorescently-labeled unmodified and modified oligonucleotides microinjected into mammalian cells. Nucleic Acids Res **1993**;21:3857-3865

Fojo AT, Ueda K, Slamon DJ, Poplack DG, Gottesman MM, Pastan I. Expression of a multidrug-resistance gene in human tumors and tissues. Proc Natl Acad Sci USA **1987**;84:265-269

Fojo T, Bates S. Strategies for reversing drug resistance. Oncogene **2003**;22:7512-7523

Ford JM, Hait WN. Pharmacology of drugs that alter multidrug resistance in cancer. Pharmacol Rev **1990**;42:155-199

Fracasso P, Westervelt P, Fears C, Rosen DM, Zuhowski EG, Cazenave LA, Litchman M, Egorin MJ. Phase I study of Paclitaxel in combination with a multidrug resistance modulator PSC 833 (Valspodar), in refractory malignancies. J Clin Oncol **2000**;18:1124-1134

Galderisi U, Cascino A, Giordano A. Antisense Oligonucleotides as therapeutic agents. J Cell Physiol **1999**;181:251-257

Garimella TS, Ross DD; Eiseman JL, Mondick JT, Joseph E, Nakanishi T, Bates SE, Bauer KS. Plasma pharmacokinetics and tissue distribution of the breast cancer resistance protein (BCRP/ABCG2) inhibitor fumitremorgin C in SCID mice bearing T8 tumors. Cancer Chemother Pharmacol **2005**;55:101-109

Giaccone G, Linn S, Welink J, Catimel G, Stieltjes H, van der Vijgh WJ, Eeltink C, Vermorken JB, Pinedo HM.. A dose-finding and pharmacokinetic study of revearsal of multidrug resistance with SDZ PSC 833 in combination with doxorubicin in patients with solid tumors. Clin Cancer Res **1997**;3:2005-2015

Gijtenbeek JM, Van den Bent MJ, Vecht CJ. Cyclosporine neurotoxicity: A review. J Neurol **1999**;246:339-34

Globisch C, Pajeva IK, Wiese M. Structure-activity relationships of a series of tariquidar analogs as multidrug resistance modulators. Bioorg Med Chem **2006**;14:1588-1598

Gottesman MM. How cancer cells evade chemotherapy: Sixteenth Richard and Hinda Rosenthal Foundation award lecture. Cancer Res **1993**;53:747-754

Gottesman MM, Pastan I. Biochemistry of multidrug resistance mediated by the multidrug transporter. Annu Rev Biochem **1993**;62:385-427

Gelderblom H, Verweij J, Nooter K, Sparreboom A. Cremophore EL: the drawbacks and advantages of vehicle selection for drug formulation. European J of Cancer **2001**;37:1590-1598

Hartmann G, Kim H, Piquette-Miller G. Regulation of the hepatic multidrug resistance gene expression by endotoxin and inflammatory cytokines in mice. Int Immunopharmacol **2001**;1:189-199

Hendrikse NH, Franssen EJF, Van der Graaf WTA, Vaalburg W, De Vries EGE. Visualization of Multidrug resistance in vivo. Eur J Nuc Med **1999**;25:283-293

Higgins CF, Gottesman MM. Is the multidrug transporter a flippase? Trend Biochem **1992**;17:18-21

Hirohashi T, Suzuki H, Ito K, Ogawa K, Kume K, Shimizu T, Sugiyama Y. Hepatic expression of multidrug resistance-associated protein-like proteins maintained in eisai hyperbilirubinemic rats. Mol Pharmacol **1998**;53:1068-1075

Holland IB, Blight MA. ABC-ATPases, adaptable energy generators fueling transmembrane movement of a variety of molecules in organisms from bacteria to humans. J Mol Biol **1999**;293:381-399

Hyafil F, Vergely C, Du Vignaud P, Grand-Perret T. In vitro and in vivo reversal of multidrug resistance by GF120918, an acridonecarboxamide derivative. Cancer Res **1993**;53:4595-4602

Ishikawa T. The ATP-dependent glutathione S-conjugate export pump. Trends Biochem Sci **1992**;17:463-468

Jain RK. Transport of molecules in the tumour interstitium: a review. Cancer Res **1987**;47:3039–3051

Jedlitschky G, Leier I, Buchholz U, Hummel-Eisenbeiss J, Burchell B, Keppler D. ATP-dependent transport of bilirubin glucuronides by the multidrug resistance protein MRP1 and its hepatocyte canalicular isoform MRP2. Biochem J **1997**;327:305-310

Jekerle V, Kassack MU, Reilly RM, Wiese M, Piquette-Miller M. Functional comparison of single- and double-stranded *mdr1* antisense oligodeoxynucleotides in human ovarian cancer cell lines. JPPS **2005**;8:516-527

Jekerle V, Klinkhammer W, Scollard DA, Breitbach K, Reilly RM, Piquette-Miller M, Wiese M. *In vitro* and *in vivo* evaluation of WK-X-34, a novel inhibitor of P-glycoprotein and BCRP using radio imaging techniques. Int J Cancer **2006a**;119:414-422

Jekerle V, Klinkhammer W, Reilly RM, Piquette-Miller M, Wiese M. Novel tetrahydroisoquinolin-ethyl-phenylamine based multidrug resistance inhibitors with broad-spectrum modulating properties. **2006b**; Cancer Chemother Pharmacol, in press

Jekerle V, Wang JH, Scollard DA, Reilly RM, Wiese M, Piquette-Miller M. ^{99m}Tc-Sestamibi, a sensitive probe for *in vivo* imaging of P-glycoprotein inhibition by modulators and *mdr1* antisense oligodeoxynucleotides. **2006c**; Molecular Imaging and Biology, in press

Jensen KD, Kopečková P, Bridge JHB, Kopeček J. The cytopasmic escape and nuclear accumulation of endocytosed and microinjected HPMA copolymers and a basic kinetic study in Hep G2 cells. AAPS Pharm Sci **2001**;3:32

Jensen KD, Kopečková P, Kopeček J, "Antisense oligonucleotides delivered to the lysosome escape and actively inhibit the hepatitis B virus", Bioconjug Chem **2002**;13:975-984

Jensen KD, Nori A, Tijerina M, Kopečková P, Kopeček J, Cytoplasmic delivery and nuclear targeting of synthetic macromolecules. J Control Release **2003**;87:89-105

Jie P, Venkatraman SS, Min F, Freddy BY, Huat GL. Micelle-like nanoparticles of star-branched PEO-PLA copolymers as chemotherapeutic carrier. J Control Release **2005**;110:20-33

Jia P, Wu S, Li F, Xu Q, Wu M, Chen G, Liao G, Wang S, Zhou J, Lu Y, Ma D. Breast cancer resistance protein-mediated topotecan resistance in ovarian cancer cells. Int J Gynecol Cancer **2005**;15:1042-8

Jones AG, Abrams MJ, Davison A, Brodack JW, ToothakerAK, Adeistein SJ, Kassis AI. Biological studies of a new class of technetium complexes: the hexakis(alkylisonitrile)technetium(I) cations. Int J Nuc Med Biol **1984**;11:225-234

Jonker JW, Smit JW, Brinkhuis RF, Maliepaard M, Beijnen JH, Schellens JH, Schinkel AH. Role of breast cancer resistance protein in the bioavailability and fetal penetration of topotecan. J Natl Cancer Inst **2000**;62:1651-1656

Johnson JI, Decker S, Zaharevity D, Rubinstein LV, Veditti JM, Schepartz S, Kalyandrug S, Christin M, Arbuck S, Hollingshead M, Sausville EA. Relationships between drug activity in NCI preclinical *in vitro* and *in vivo* models and early clinical trials. Br J Cancer **2001**;84:1424-1431

Juliano RL, Ling V. A surface glycoprotein modulating drug permeability in Chinese hamster ovary cell mutations. Biochim biophys Acta **1976**;455:152-162

Kabasakal L, Halac M, Nisli C, Ogiz O, Önsel C, Civi G, Uslu I. The Effect of P-Glycoprotein Function Inhibition With Cyclosporine A on the Biodistribution of Tc-99m Sestamibi. Clin Nuc Med **2000**;1:20-23

Kaufmann SH, Vaux DL. Alterations in the apoptotic machinery and their potential role in anticancer drug resistance. Oncogene **2003**;22:7414-7430

Kemper EM, Cleypool C, Boogerd W, Beijnen JH, van Tellinger O. The influence of the P-glycoprotein inhibitor zosuquidar trihydrochloride (LY335979) on the brain penetration of paclitaxel in mice. Cancer Chemother Pharmacol **2004**;53:173-178

Ketterer B, Meyer DJ, TaylorJB, Pemble S, Coles B and Fraser G. Glutathione S-transferases and protection against oxidative stress. In: Haye, J.D., Pickett, C.B. and Mantle, T.J., Editors, **1990**. Glutathione S-Transferases and Drug Resistance, Taylor and Francis, London.

Klein I, Sarkadi B, Váradi A. An inventory of the human ABC proteins. Biochim Biophys Acta **1999**;1461:237-62

Kool M, van der Linden M, de Haas M, Scheffer GL, de Vree JM, Smith AJ, Jansen G, Peters GJ, Ponne N, Scheper RJ, Elferink RP, Baas F, Borst P. MRP3, an organic anion transporter able to transport anti-cancer drugs. Proc Natl Acad Sci USA **1999**;96:6914-6919

Krishnamurthy P, Ross DD, Nakanishi T, Bailey-Dell K, Zhou S, Mercer KE, Sarkadi B, Sorrentino BP, Schuetz JG. The stem cell marker Bcrp/ABCG2 enhances hypoxic cell survival through interactions with heme. JBC **2004**;279:24218-24225

Krishna R, De Jong, G, Mayer L. Pulsed exposure of SDZ PSC 833 to multidrug resistant P388/Adr and MCF7/Adr cells in the absence of anticancer drugs can fully restore sensitivity to doxorubicine. Anticancer Res **1997**;17:3329-3334

Krishna R, Mayer LD. Multidrug resistance (MDR) in cancer Mechanisms, reversal using modulators of MDR and the role of modulators in influencing the pharmacokinetics of anticancer drugs. Eur J Pharm Sci **2000**;11:265-283

Kruh GD, Gaughan KT, Godwin A, Chan A. Expression pattern of MRP in human tissues and adult solid tumor cell lines. J Natl Cancer Inst **1995**;87:1256-1258

Kruh GD, Belinsky MG. The MRP family of drug efflux pumps. Oncogene **2003**;22:7537-7552

Kunimoto T, Nitta K, Tanaka T, Uehara N, Baba H, Takeuchi M, Yokokura T, Sawada S, Miyasaka T, Mutai M. Antitumor activity of 7-Ethyl-10-[4-(1-piperidino)-1-piperidino]carbonyloxy-c amptothecin, a novel water soluble derivative of camptothecin, against murine tumors. Cancer Res **1987**;47:5944–5947

Kurreck J. Antisense technologies: Improvement through novel chemical modifications. Eur J Biochem **2003**;270:1628-1644

Kuss BJ, Corbo M, Min Lau W, Fennell DA, Dean NM, Cotter FE. In vitro and in vivo downregulation of MRP1 by antisense oligonucleotides: a potential role in neuroblastoma therapy. Int J Cancer **2002**;98:128-133

Kuzmich S, Tew KD. Detoxification mechanisms and tumor cell resistance to anticancer drugs. Medic Res Rev **1991**;11:185–217

Lê LH, Moore MJ, Siu LL, Oza AM, MacLean M, Fisher B, Chaudhary A, de Alwis DP, Slapak C, Seymour L. Phase I study of the multidrug resistance inhibitor yosuquidar administered in combination with vinorelbine in patients with advanced solid tumours. Cancer Chemother Pharmacol **2005**;56:154-160

Lee G, Piquette-Miller M. Influence of IL-6 on MDR- and MRP-mediated multidrug resistance in human hepatoma cells. Can J Physiol Pharmacol **2001**;79:876-884

Le Garrec D, Gori S, Luo L, Lessard D, Smith DC, Yessine MA, Ranger M, Leroux JC. Poly(*N*-vinylpyrrolidone)-block-poly(d,l-lactide) as a new polymeric solubilizer for hydrophobic anticancer drugs: in vitro and in vivo evaluation. J Control Release **2004**;72:83-101

Lehnert M, de Giuli R, Kunke K, Emerson S, Dalton WS, Salmo SE. Serum can inhibit reversal of multidrug resistance by chemosensitizers. Eur J Cancer **1996**;32A:862-867

Leith CP, Kopecky KJ, Chen IM, Eijdems L, Slovak ML, McConnell TS, Head DR, Weick J, Grever MR, Appelbaum FR, Willmann CL. Frequency and clinical significance of the expression of the multidrug resistance proteins MDR1/P-glycoprotein, MRP1, and LRP in acute myeloid leukemia: a Southwest Oncology Group Study. Blood **1999**;94:1086-1099

Levin AA. A review of the issues in the pharmacokinetics and toxicology of phosphorothioate antisense oligonucleotides. Biochim Biophys Acta **1999**;1489:69-84

Lewis AD, Forrester LM, Hayes JD, Wareing CJ, Carmichael J, Harris AL, Mooghen M, Wolf CR. Glutathione S-transferase isoenzymes in human tumours and tumour derived cell lines. Br J Cancer **1989**;60:327–331

Ling V, Thompson LH. Reduced permeability in CHO cells as a mechanism of resistance to colchicin. J Cell Physiol **1974**;83:103-116

Ling V. P-glycoprotein: its role in drug resistance. Am J Med **1995**;99:31-34

List AF, List AF, Spier CS, Grogan TM, Johnson C, Roe DJ, Greer JP, Wolff SN, Broxterman HJ, Scheffer GL, Scheper RJ, Dalton WS. Overexpression of the major vault transporter protein lung-resistance protein predicts treatment outcome in acute myeloid leukemia. Blood **1996**;87:2464-9

List AF, Kopecky KJ, Willman CL, Head DR, Persons DL, Slovak ML, Dorr R, Karanes C, Hynes HE, Doroshow JH, Shurafa M, Appelbaum FR. Benefit of cyclosporine modulation of drug resistance in patients with poor-risk acute myeloid leukemia: a Southwest Oncology Group study. Blood **2001**;98:3212-3220

Loke SL, Stein CA, Zhang XH, Mori K, Nakanishi M, Subasinghe C, Cohen JS, Neckers LM. Characterization of oligonucleotides transport into living cells. Proc Natl Acad Sci **1989**;86:3473-3478

Loo TW, Clarke DM. Location of the rhodamine-binding site in the human multidrug resistance P-glycoprotein. J Biol Chem **2002**; 277:44332-44338

Lopes de Menezes DE, Hu Y, Mayer LD. Combined treatment of bcl-2 antisense oligodeoxynucleotides (G3139), p-glycoprotein inhibitor (PSC 833), and sterically stabilized liposomal doxorubicin suppresses growth of drug-resistant breast cancer in severely combined immunodeficient mice. J Exp Ther Oncol **2003**;3:72-82

Lorenz P, Baker BF, Bennett CF, Spector DL. Phosphorothioate antisense oligonucleotides induce the formation of nuclear bodies. Mol Biol Cell **1998**; 9:1007-1023

Lorke DE, Krueger M, Buchert R, Bohuslavizki KH, Clausen M, Schumacher U. In vitro and in vivo trancer characteristics of an established multidrug-resistant human colon cancer cell line. J Nuc Med **2001**;42:646-654

Louie KG, Hamilton TC, Winker MA, Behrens BC, Tsuruo T, Klecker RW Jr, McKoy WM, Grotyinger KR, Myers CE, Young RC, et al. Adriamycin accumulation and metabolism in adriamycin-sensitive and –resistant human ovarian cancer cell lines. Biochem Pharmacol **1986**;35:467-72

Lowe SW, Schmitt EM, Smith SW, Osborne BA, Jacks T. p53 is required for radiation-induced apoptosis in mouse thymocytes. Nature **1993a**;362:847–849

Lowe SW, Ruley HE, Jacks T, Houseman DE. p53-dependent apoptosis modulates the cytotoxicity of anticancer agents. Cell **1993b**;74:957–967

Maliepaard M, van Gastelen MA, Tohgo A, Hausheer FH, van Waardenburg RC, de Jong LA, Pluim D, Beijnen JH, Schellens JH. Circumvention of breast cancer resistance protein (BCRP)-mediated resistance to camptothecins in vitro using non-substrate drugs or the BCRP inhibitor GF120918. Clin Cancer Res **2001**;7:935-941

Márián T, Szabo G, Goda K, Nagy H, Szincsak N, Juhasz I, Galuska L, Balkay L, Mikecz P, Tron L, Krasznai Z. In vivo and in vitro multitracer analysis of P-glycoprotein expression-related multidrug-resistance. Eur J Nuc Med Mol Imaging **2003**;30:1147-1154

Marks DC, Belov L, Davey MW, Davey RA, Kidman AD. The MTT cell viability assay for cytotoxicity testing in multidrug-resistant human leukemic cells. Leuk Res **1992**;16:1165-73

Massazza G, Tomasoni A, Lucchini V, Allavena P, Erba E, Colombo N, Mantovani A, D'Incalci M, Mangioni C, Giavazzi R. Intraperitoneal and subcutaneous xenografts of human ovarian carcinoma in nude mice and their potential in experimental therapy. Int J Cancer **1989**;44:494-500

Martin C, Berridge G, Higgins CF, Mistry P, Charlton P, Callaghan R. Communication between multiple drug binding sites on P-glycoprotein. Mol Pharmacol **2000**;58:624-632

Menefee ME, Fan C, Edgerly M, Draper D, Chen C, Robey R, Balis F, Figg WD, Bates S, Fojo AT. Tariquidar (XR9576) is a potent and effective P-glycoprotein (Pgp) inhibitor that can be administered safely with chemotherapy. J Clin Oncol, 2005 ASCO Annual Meeting Proceedings **2001**;23:3093

Minderman H, Suvannasankha A, O'Loughlin KL, Scheffer GL, Scheper RJ, Robey RW, Baer MR. Flow Cytometry Analysis of Breast Cancer Resistance Protein Expression and Function. Cytometry **2002**;48:59-65

Minderman H, O'Loughlin KL, Pendyala L, Baer MR. VX-710 (Biricodar) increases drug retention and enhances chemosensitivity in resistant cells overexpressing P-glycoprotein, Multidrug Resistance Protein and Breast Cancer Resistance Protein. Clin Cancer Res **2004a**;10:1826-1834

Minderman H, Brooks TA, O'Loughlin KL, Ojima I, Bernacki RJ, Baer MR. Broad-spectrum modulation of ATP-binding cassette transport protein by taxane dericatives ortataxel (IDN-5109, BAY 59-8862) and tRA96023. Cancer Chemother Pharmacol **2004b**;53:363-369

Mistry P, Plumb J, Eccles S, Watson S, Dale I, Ryder H, Box G, Charlton P, Templeton D, Bevan PB. *In vivo* efficacy of XR9051, a potent modulator of P-glycoprotein mediated multidrug resistance. Br J Cancer **1999**;79:1672-1678

Moscow JA, Townsend AJ, Cowan KH. Elevation of pi class glutathione S-transferase activity in human breast cancer cells by transfection of the GST pi gene and its effect on sensitivity to toxins. Mol. Pharmacol **1989**;36:22–28

Mueller H, Kassack MU, Wiese M. Comparison of the usefulness of the MTT; ATP, and calcein assay to predict the potency of cytotoxic agents in various human cancer cell lines. J Biomol Screen **2004**;9:506-15

Muzzammil T, Ballinger JR, Moore MJ. 99mTc-sestamibi imaging of the multidrug resistance transporter in a mouse xenograft model of human breat cancer. Nucl Med Commun **1999**;20:115-122

Muzzammil T, Moore MJ, Hedley D, Ballinger JR. Comparison of 99mTc-Sestamibi and doxorubicin to monitor inhibition of P-glycoprotein function. Brit J Cancer **2001**;84:367-373

Naesens L, De Clercq E. Recent developments in herpesvirus therapy. Herpes **2001**;8:12-16

Newman MJ, Rodarte JC, Benbatoul KD, Romano SJ, Zhang C, Krane S, Moran EJ, Uyeda RT, Dixon R, Guns ES, Mayer LD. Discovery and characterization of OC144-093, a novel inhibitor of P-glycoprotein-mediated multidrug resistance. Cancer Res **2000**;60:2964-2972

Nishida T, Sugiyama T, Kataoka A, Ushijima K, Yakushiji M. Histologic characterization of rat ovarian carcinoma induced by intraovarian instertion of a 7,12-dimethyl-benz[a]anthracene-coated suture: common epithelial tumors of the ovary in rats? Cancer **1998**;83:965-970

Orsulic S, Li Y, Soslow RA, Vitale-Cross LA, Gutkind JS, Varmus HE. Induction of ovarian cancer by defined multiple genetic changes in a mouse model system. Cancer Cell **2002**;1:53-62

Oza AM. Clinical development of P-glycoprotein modulators in oncology. Novartis Found Symp **2002**;243:103-15

Ozols R, Cunnion R, Klecker R, Hamilton TC, Ostchega Y, Parrillo JE, Young RC. Verapamil and adriamycin in the treatment of drug-resistant ovarian cancer patients. J Clin Oncol **1987**;5:641-647

Pajeva IK, Wiese M. Pharmacophore model of drugs involved in P-glycoprotein multidrug resistance: Explanation of structural variety (Hypothesis). J Med Chem **2002**;45: 5671-5686

Pajeva IK, Globisch C, Wiese M. Structure-function relationships of multidrug resistance P-glycoprotein. J Med Chem **2004**;47: 2523-2533

Piwnica-Worms D, Chiu M, Budding M, Kronauge JF, Kramer RA, Croop JM. Functional imaging of multidrug-resistant P-glycoprotein with an organotechnetium complex. Cancer Res **1993**;53:977-984

Planting AS, Sonneveld P, van der Gaast A, Sparreboom A, van der Burg MEI, Luyten GPM, de Leeuw K, de Boer-Dennert M, Wissel PS, Jewell RC, Paul EM, Purvis NB, et al. A phase I and pharmacologic study of MDR converter GF120918 in combination with doxorubicin in patients with advanced solid tumors. Cancer Chemother Pharmacol **2005**;55:91-99

Plumb JA, Milroy R, Kaye SB. The activity of verapamil as a resistance modifier in vitro in drug resistant human tumour cell lines is not stereospecific. Biochem Pharmacol **1990**;39:787-92

Qadir M, O'Loughlin KL, Fricke SM, et al. Cyclosporin A is a broad-spectrum multidrug resistance modular Clin Cancer Res **2005**;11:2320-2326

Raaijmakers MHGP, De Grouw EPLM, Heuver LHH. Breast cancer resistance protein in drug resistance of primitive CD34+38- cells in acute myeloid leukemia. Clin Cancer Res **2005**;11:2436-2444

Rago RP, Einstein A Jr, Lush R, Beer TM, Ko YJ, Henner WD, Bubley G, Merica EA, Garg V, Ette E, Harding MW, Dalton WS. Safety and efficacy of the MDR inhibitor Incel (biricodar, VX-710) in combination with mitoxantrone and prednisone in hormone-refractory prostate cancer. Cancer Chemother Pharmacol **2003**;51:287-305

Ramachandran C, Wellham LL. Effect of MDR1 phosphorothioate antisense oligodeoxynucleotides in multidrug-resistant human tumor cell lines and xenografts. Anticancer Res **2003**;23:2681-90

Ramnath N, Hamm J, Schwartz G, Holden S, Eckhardt SG, Vredenburg MR, Bernacki RJ, Lathia C, Kanter P, Creaven PJ. A phase I and pharmacokinetic study of BAY59: a novel taxane. Oncology **2004**;67:123-9

Rao VV, Dahlheimer JL, Bardgett ME, Snyder AZ, Finch RA, Sartorelli AC, Piwnica-Worms D. Choroid plexus epithelial expression of MDR1 P-glycoprotein and multidrug resistance associated protein contribute to the blood-cerebrospinal fluid drug-permeability barrier. Proc Natl Acad Sci USA **1999**;96:3900-05

Reed JC. Regulation of apoptosis by bcl-2 family proteins and its role in cancer and chemoresistance. Curr Opin Oncol **1995**;7:541–546

Robey RW, Steadman K, Polgar O, Morisaki O, Blayney M, Mistry P, Bates SE. Phenophorbide a is a specifc probe for ABCG2 function and inhibition. Cancer Res **2004**;64:1242-1246

Roe M, Folkes A, Ashworth P, Brumwell J, Chima L, Hunjan S, Pretswell I, Dangerfield W, Ryder H, Charlton P. Reversal of P-glycoprotein mediated multidrug resistance by novel anthranilamide derivatives. Bioorg & Med Chem Let **1999**;9:595-600

Ros JE, Libbrecht L, Geuken M, Jansen PL, Roskams TA. High expression of MDR1, MRP1, and MRP3 in the hepatic progenitor cell compartment and hepatocytes in severe human liver disease. J Pathol **2003**;200:553-560

Rose GS, Tocco LM, Granger GA, DiSaia PJ, Hamilton TC, Santin AD, Hiserodt JC. Development and characterization of a clinically useful model of epithelial ovarian cancer in Fisher 344 rats. Am J Obstet Gynecol **1996**;175:593-9

Ross DD. Novel mechanisms of drug-resistance in leukemia. Leukemia **2000**;14:467-473.

Ross W, Rowe T, Glisson B, Yalowich J, Liu LF. Role of topoisomerase II in mediating epipodophyllotoxin-induced DNA cleavage. Cancer Res **1984**;44:5857–5860

Roy C, Brown DL, Little JE, Valentine BK, Walker PR, Sikorska M, LeBlanc J, Chaly N. The topoisomerase II inhibitor teniposide (VM-26) induces apoptosis in unstimulated mature murine lymphocytes. Exp. Cell Res **1992**;200:416–424

Safa AR. Identification and characterization of the binding sites of P-glycoprotein for multidrug resistance related drugs and modulators. Curr Med Chem–Anti-Cancer Agents **2004**,4,1-17

Sarkadi B, Özvegy-Laczka C, Nemet K, Varadi A. ABCG2 – a transporter for all seasons. FEBS Letters **2004**;567:116-120

Sasaki H, Takada K, Terashima Y, Ekimoto H, Takahashi K, Tsuruo T, Fukushima M. Human ovarian cancer cell lines resistant to cisplatin, doxorubicin, and L-phenylalanine mustard are sensitive to delta 7-prostaglandin A1 and delta 12-prostaglandin J2. Gynecol Oncol **1991**;41:36-40

Scharenberg CW, Harkey MA, Torok-Storb B. The ABCG2 transporter is an efficient Hoechst 33342 efflux pump and is preferentially expressed by immature human hematopoietic progenitors. Blood **2002**;99:507-512

Schinkel AH, Mayer U, Wagenaar E, Mol CA, van Deemter L, Smit J, van der Valk MA, Voordouw AC, Spits H, van Tellingen O, Yijlmans JM, Fibbe WE, Borst P. Normal viability and altered pharmacokinetics in mice lacking mdr 1-type (drug-transporting) P-glycoproteins. Proc Natl Acad Sci USA **1997**;94:4028-4033

Schneider E, Yamazaki H, Sinha BK, Cowan KH. Buthionine sulphoximine-mediated sensitisation of etoposide-resistant human breast cancer MCF7 cells overexpressing the multidrug resistance-associated protein involves increased drug accumulation. Br J Cancer **1995**;71:738-743

Shapiro AB, Ling V. Reconstitution of drug transport by purified P-glycoprotein. J Biol Chem **1995**;270:16167-16175

Shapiro AB, Ling V. Positively cooperative sites for drug transport by P-glycoprotein with distinct drug specificities. Eur J Biochem **1997**;250:130-137

Sharma V, Luker G, Piwnica-Worms D. Molecular Imaging of gene expression and protein function in vivo with PET and SPECT. J Magn Reson Imaging **2002**;16:336-351

Shiozawa K, Oka M, Soda H, Yoshikawa M, Ikegami Y, Tsurutani J, Nakatomi K, Nakamura Y, Doi S, Kitazaki T, Mizuta Y, Murase K, Yoshida H, Ross DD, Kohno S. Reversal of breast cancer resistance protein (BCRP/ABCG2)-mediated drug resistance by novobiocin, a coumermycin antibiotic. Int J Cancer **2004**;108:146-151

Shepard RL, Cao J, Starling JJ, Dantzig AH. Modulation of P-glycoprotein but not MRP1- or BCRP-mediated drug resistance by LY335979. Int J Cancer **2003**;103:121-125

Silva EG, Tornos C, Fritsche HA Jr, El-Naggar A, Gray K, Ordonez NG, Luna M, Gershenson D. The induction of benign epithelial neoplasms of the ovaries of guinea pigs by testosterone stimulation: a potential animal model. Mod Pathol **1997**;10:879-883

Sloan Stakleff KD, Von Gruenigen VE. Rodent models for ovarian cancer research. Int J Gynecol Cancer **2003**;13:405-412

Smeets M, Raymakers R, Muus P, Vierwinden G, Linssen P, Masereeuw R, de Witte T. Cyclosporin increases cellular idarubicin and idarubicinol concentrations in relapsed or refractory AML mainly due to reduced systemic clearance. Leukemia **2001**;15:80-88

Smit J, Huisman M, van Tellingen O, Wiltshire HR, Schinkel AH. Absence or pharmacological blocking of placental P-glycoprotein profoundly increases fetal drug exposure. J Clin Invest **1999**;104:1441-1447

Stein CA, Cohen JS. Oligodeoxynucleotides: as inhibitors of gene expression: a review. Cancer Res **1988**;48:2659-68

Sukhai M, Yong A, Pak A, Piquette-Miller M. Decreased expression of P-glycoprotein in interleukin-1beta and interleukin-6 treated rat hepatocytes. Inflamm Res **2001**;50:362-70

Taetle R, Rosen F, Abramson I, Venditti J, Howell S. Use of nude mouse xenografts as preclinical drug screen: *in vivo* activity of established chemotherapeutic agents against melanoma and ovarian carcinoma xenograft. Cancer Treat Rep **1987**;71:297-304

Takei Y, Kadomatsu K, Itoh H, Sato W, Nakazawa K, Kubota S, Muramatsu T. 5"-,3'-Inverted Thymidine-modified Antisense Oligodeoxynucleotide Targeting Midkine. JBC **2002**;26:23800-23806

Tan B, Piwnica-Worms D, Ratner L. Discovery of Multidrug resistance transporters and modulation. Curr Opi in Oncology **2000**;12:450-458

Taniguchi K, Wada M, Kohno K, Nakamura T, Kawabe T, Kawakami M, Kagotani K, Okumura K, Akiyama S, Kuwano M. A human canalicular multispecific organic anion transporter (cMOAT) gene is overexpressed in cisplatin-resistant human cancer cell lines with decreased drug accumulation. Cancer Res **1996**;56:4124-4129

Toppmeyer D, Seidman AD, Pollak M, Russell C, Tkaczuk K, Verma S, Overmoyer B, Garg V, Ette E, Harding MW, Demetri GD. Safety and efficacy of the multidrug resistance inhibitor Incel (biricodar; VX-710) in combination with paclitaxel for advanced breast cancer refractory to paclitaxel. Clin Cancer Res **2002**;8:633-5

Tsuruo T, Iida H, Nojiri M, Tsukagoshi S, Sakurai Z. Overcoming of vincristine resistance in P388 leukemia in vivo and in vitro through enhanced cytotoxicity of vincristine and vinblastine by verapamil. Cancer Res **1981**;41:1967-1972

Urasaki Y, Urasaki Y, Ueda T, Yoshida A, Fukushima T, Takeuchi N, Tsuruo T, Nakamura T. Establishment of daunorubicin-resistant cell line which shows multi-drug resistance by multifactorial mechanisms. Anticancer Res **1996**;16:709-14.

Utsunomiya K, Ballinger JR, Piquette-Miller M, Rauth AM, Tang W, Su ZF, Ichise M. Comparison of the accumulation and efflux kinetics of technetium-99m sestamibi and technetium-99m tetrofosmin in an MRP-expressing tumour cell line. Eur J Nucl Med **2000**;27:1786-92

Van Veen HW, Callaghan R, Soceneantu L, Sardini A, Konings WN, Higgins CF. A bacterial antibiotic-resistance gene that complements the human multidrug-resistance P-glycoprotein gene. Nature **1998a**;391:291-295

Van Veen HW, Konings WN. The ABC family of multidrug transporters in microorganisms. Biochim Biophys Acta **1998b**;1365:31-36

Van Zuylen L, Verweij J, Sparreboom A. Role of formulation vehicles in taxane pharmacology. Invest New Drugs **2001**;19:125-141

Voskoglou-Nomikos T, Pater JL, Seymour L. Clinical predicitive value of the in vitro cell line, human xenograft, and mouse allograft preclinical cancer models. Clin Cancer Res **2003**;15:4227-4239

Wang JH, Scollard DA, Teng S, Reilly RM, Piquette-Miller M. Detection of P-glycoprotein activity in endotoxemic rats by ^{99m}Tc-Sestamibi imaging. J Nucl Med **2005**;46:1537-1545

Wang ZR, Liu W, Smith ST, Parrish RS, Young SR. C-myc and chromosome 8 centromere studies of ovarian cancer by interphase FISH. Exp Mol Pathol **1999**;66:140-8

Wilfinger WW, Mackey K, Chomczynski P. Effect of pH and ionic strength on the spectrophotometric assessment of nucleic acid purity. Biotechniques **1997**;22:474-6

Yanase K, Tsukahara S, Asada S, Ishikawa E, Imai Y, Sugimoto Y. Gefitinib reverses breast cancer resistance protein-mediated drug resistance. Mol Cancer Ther **2004**;3:1119-1125

Yang CH, Chen YC, Kuo ML. Novobiocin sensitizes BCRP/MXR/ABCG2 overexpressing topotecan-resistant human breast carcinoma cells to topotecan and mitoxantrone. Anticancer Res **2003**;23:2519-23

Zelcer N, Saeki T, Reid G, Beijnen JH, Borst P. Characterization of drug transport by the human multidrug resistance protein 3 (ABCC3). J Biol Chem **2001**;276:46400-46407

Zhou J, Higashi K, Ueda Y, Kodama Y, Guo D, Jisaki F, Sakurai A, Takegami T, Katsuda S, Yamamoto I. Expression of multidrug resistance protein and messenger RNA correlated with (99m)Tc-MIBI imaging in patients with lung cancer. J Nuc Med **2001**;42:1476-83

Zhou S, Schuetz JD, Bunting KD, Colapietro AM, Sampath J, Morris JJ, Lagutina I, Grosveld GC, Osawa M, Nakauchi H, Sorrentino BP. The ABC transporter Bcrp1/ABCG2 is expressed in a wide variety of stem cells and is a molecular determinant of the side-population phenotype. Nat Med **2001**;7:1028-1034
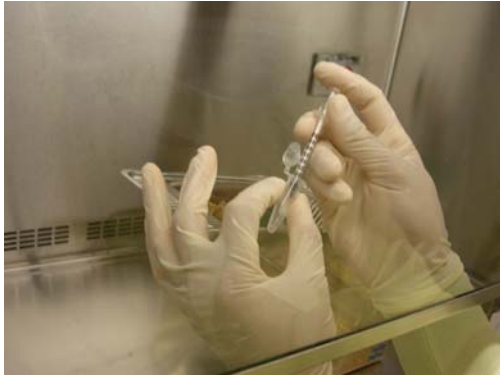
A.
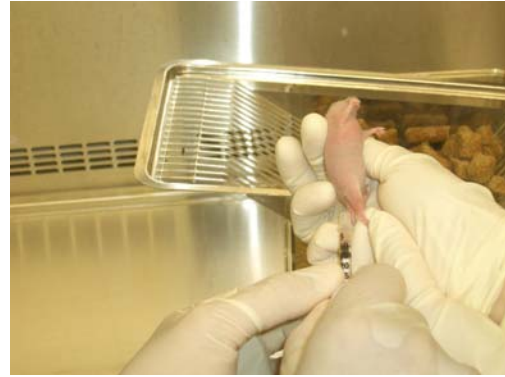
B.

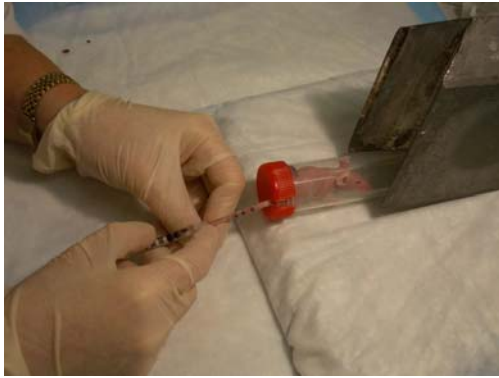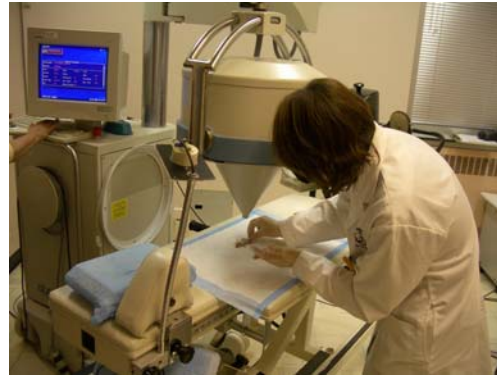1 week   2 weeks   3 weeks   4 weeks

C.

Picture 1. Development of human ovarian cancer xenograft model

5 x 10^6 A2780/Adr or A2780/wt cells in a 100 μl cell suspension (**A**) were injected s.c. into the back flank of immunocomprimised nude mice (**B**). Tumor formation was visible after one week and tumor volume rapidly increased per week as depicted in **C**.

A.

B.

C.

D.

Picture 2. ^{99m}Tc-Sestamibi imaging studies

Mice were injected with 5 MBq of ^{99m}Tc-Sestamibi into one of the lateral vein (**A**) anesthetised and placed on the imaging counter (**B**). The injection spot on the tail was shielded with a led shield (**C**) Images were acquired using a small field-of-view gamma-camera ADAC TransCam™ equipped with a pinhole collimator (4 mm aperture) and processed using Pegasys™ X, Version 4.2 software (**D**).
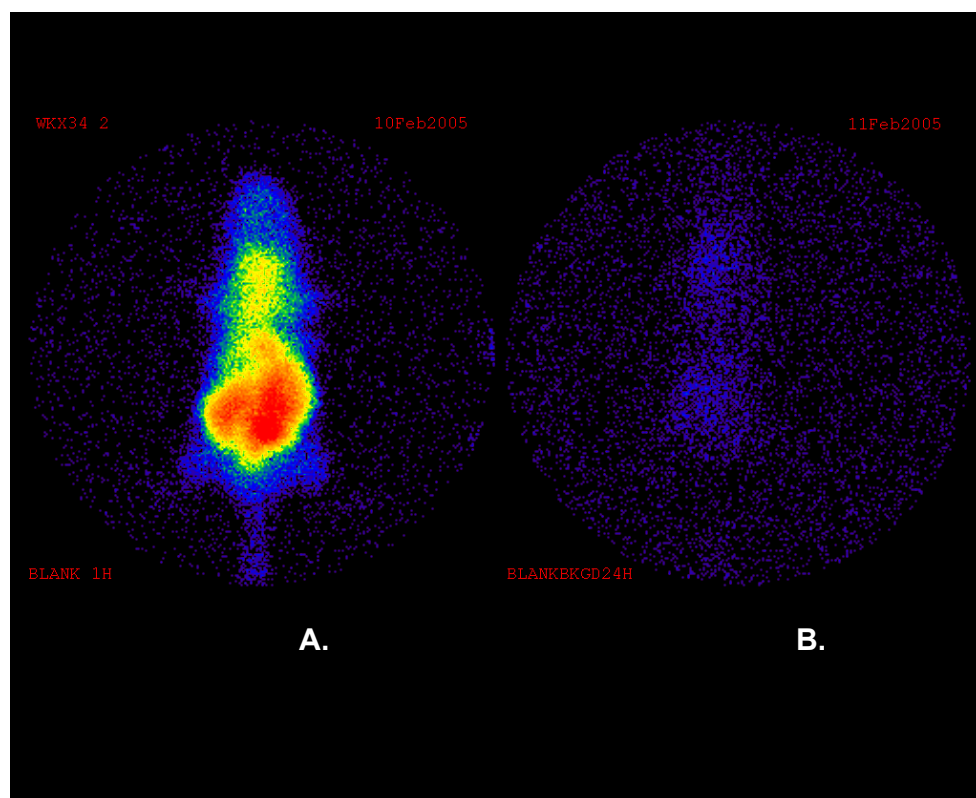
A.

B.

C.

D.

Picture 3. ^{99m}Tc-Sestamibi biodistribution studies

After ^{99m}Tc-Sestamibi imaging experiments were terminated, mice were sacrificed and tumors (**A**) as well as blood and remaining tissues (**B**) were isolated. Tissues were weighted and placed into glass tubes (**C**) for gamma-counting using the Packard Cobra II Series Auto-Gamma ® Counting System (**D**).

Picture 4. Residual ^{99m}Tc-Sestamibi activity 24 postinjection

The same animal was imaged 15 min **(A)** and 24 h **(B)** following i.v. injection of 5 mBq ^{99m}Tc-Sestamibi. Residual ^{99m}Tc-Sestamibi activity decreased to less than 2 % after 24 h.
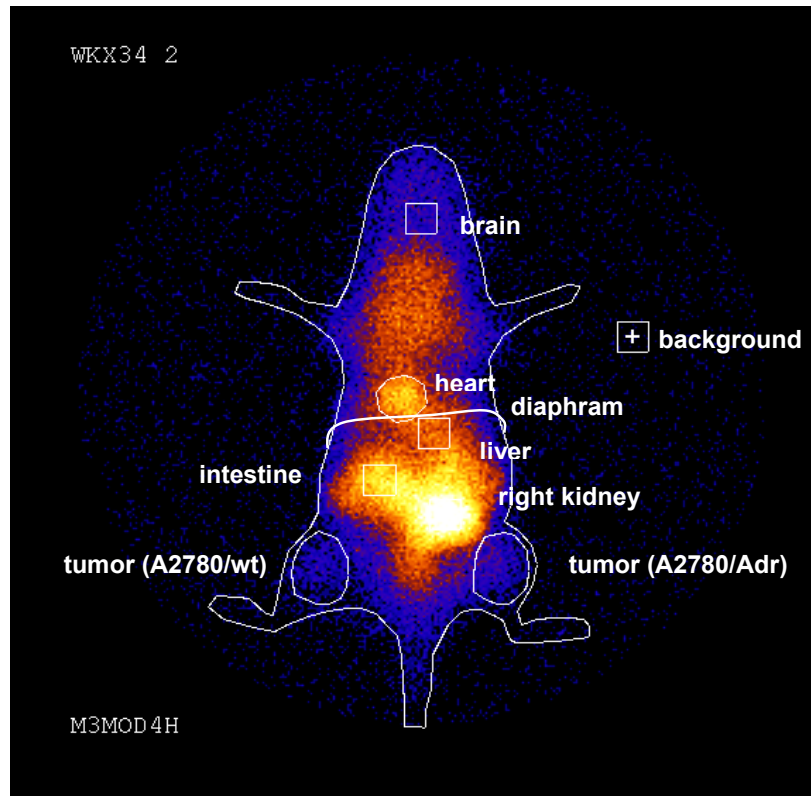
Picture 5. Regions of interest analysis

Regions of interest were drawn around the whole body, central organs and tumors as depicted. Radio-intensity of ^{99m}Tc-Sestamibi uptake was determined for each organ and expressed in counts/pixel/second of acquisition time.

Lebenslauf

Akademische Ausbildung

Februar 2003 - April 2006	Dissertation im Fach Pharmazeutische Chemie unter der Leitung von Herrn Prof. Dr. M. Wiese an der Universität Bonn, DFG-Stipendiatin im Graduiertenkolleg 804
Mai 2004 - April 2005	Forschungsaufenthalt im Labor von Prof. Dr. M. Piquette-Miller an der University of Toronto, Kanada
Januar 2003	Approbation als Apotheker
Januar 2003	3. Staatsexamen
Oktober 2001	2. Staatsexamen
September 2000 - Februar 2001	ERASMUS Austauschsemester an der Université de Paris 11, Châtenay-Malabry, Paris, France
September 1999	1. Staatsexamen
Oktober 1997 - Oktober 2001	Studium der Pharmazie and der Philipps-Universität Marburg
Juni 1997	Allgemeine Hochschulreife
August-Dezember 1994	St. Clement's School, Toronto, Kanada
1988 - 1997	Wilhelmsgymnasium, Kassel
1984 - 1988	Friedrich-Ebert Grundschule, Baunatal

Praktische Ausbildung

Seit April 2006	Trainee bei der European Medicines Agency, London, UK
April 2003 - April 2006	Weiterbildung zum Fachapotheker für Arzneimittelinformation
Mai 2002 - Dezember 2001	2. Halbjahr der praktische Ausbildung im Labor von Prof. Dr. M. Piquette-Miller an der University of Toronto, Kanada
November 2001 - April 2001	1. Halbjahr der praktische Ausbildung in der Birken Apotheke, Köln
Februar 2001	Forschungspraktikum im Labor von Prof. Dr. P. Tschoreloff, Université de Paris 11, Châtenay-Malabry, Paris, France
Februar 2000	Forschungspraktikum im Labor von Prof. K. Kuschinsky und Dr. Ferger, Pharmakologie, Philipps-Universität Marburg
März und September 1998	Famulaturen in der St. Georg Apotheke, Baunatal und in der Krankenhausapotheke der Städtische Kliniken, Kassel

Publikationen

Manuskripte:

Shirley Teng, **Veronika Jekerle**, Micheline Piquette-Miller. Induction of ABCC3 (MRP3) by Pregnane X Receptor Activators. DMD 2003;31:1296-1299

Veronika Jekerle, Matthias U. Kassack, Raymond M. Reilly, Michael Wiese, Micheline Piquette-Miller. Functional comparison of single- and double-stranded *mdr1* antisense oligodeoxy-nucleotides in P-glycoprotein overexpressing ovarian cancer cells. JPPS 2005;31:1296-1299

Veronika Jekerle, Werner Klinkhammer, Deborah A. Scollard, Kerstin Breitbach, Raymond M. Reilly, Micheline Piquette-Miller, Michael Wiese. *In vitro* and *in vivo* evaluation of WK-X-34, a novel inhibitor of P-glycoprotein and BCRP using radio imaging techniques. Int J Cancer 2006;119:414-422

Veronika Jekerle, Werner Klinkhammer, Raymond M. Reilly, Micheline Piquette-Miller, Michael Wiese. Novel tetrahydroisoquinolin-ethyl-phenylamine based multidrug resistance inhibitors with broad-spectrum modulating properties. Cancer Chemother Pharmacol 2006, in press

Veronika Jekerle, Jing-Hung Wang, Deborah A. Scollard, Raymond M. Reilly, Michael Wiese, Micheline Piquette-Miller. ^{99m}Tc-Sestamibi, a sensitive probe for *in vivo* imaging of P-glycoprotein inhibition by modulators and *mdr1* antisense oligodeoxynucleotides. Molecular Imaging and Biology 2006, in press

Konferenzbeiträge:

V. Jekerle, G. Hartmann, M. Piquette-Miller. Hepatic Expression of PXR is suppressed in LPS and IL-6 treated mice. Selected as one of the top 40 abstracts submitted to the 2003 ASCPT meeting. Presented at select poster- discussion session. *Clin. Pharmacol. Ther.* 73(2):p60(2003).

V. Jekerle, G. Hartmann, S. Teng, M. Piquette-Miller. Interleukin-6 Downregulates the Expression of Pregnane X Receptor in Mice. *JPPS,* 6 (2): p56 (2003). Presented at the 2003 CSPS Annual Meeting, May 2003, Montréal, QC.

V. Jekerle, M.U. Kassack, M. Piquette-Miller, M. Wiese. Antisense MDR1 oligonucleotides and PGP modulators in combination are effective in reducing P-GP overexpression in A2780Adr. *AAPS Journal* 2004; 6(S1). Presented at the 2004 AAPS Annual Meeting, November 2004, Baltimore, MD.

V. Jekerle, W. Klinkhammer, M. Wiese, R.M. Reilly, M. Piquette-Miller. *In Vitro* and *in vivo* Evaluation of a Novel PGP Modulator in Human Ovarian Cancer Xenografts using Radionuclide Imaging Techniques. *Proc Amer Assoc Cancer Res* 2005;46:526. Presented at the 2005 AACR Annual Meeting, April 2005, Anaheim, CA.

V. Jekerle, J-H. Wang, D.A. Scollard, M. Wiese, R.M. Reilly, M. Piquette-Miller. ^{99m}Tc-MIBI is a Senstive Probe for Imaging the Effectiveness of the Novel Pgp Modulator WK-X-34 in Mice. Presented at the Society of Nuclear Medicine 52nd Annual meeting, Mai 2005, Toronto, ON.

V. Jekerle, J-H. Wang, D.A. Scollard, R.M. Reilly, M. Wiese and M. Piquette-Miller. ^{99m}Tc-Sestamibi, a sensitive probe for imaging P-glycoprotein inhibition by modulators and *mdr1* antisense oligodeoxynucleotides in human ovarian cancer xenografts. Presented at the Society of Molecular Imaging 4th Annual meeting, September 2005, Cologne, Germany.

V. Jekerle, M. Christlieb, S. Leyers, W. Klinkhammer, M. Piquette-Miller, M. Wiese. Novel anthranilic-acid-based multidrug resistance modulators with different effects on P-glycoprotein, BCRP and MRPs. Presented at the 2006 ABC-Transporter Meeting, March 2006, Innsbruck, Austria.